



Dynamic computational modeling of fatty acid *de novo* synthesis in the liver and qualitative analysis of fatty acid metabolism

Inaugural dissertation

for the attainment of the title of doctor in the Faculty of Mathematics and Natural Sciences at the Heinrich Heine University Düsseldorf

presented by

Chilperic Armel Foko Kuate

from Bandjoun, Cameroon

Düsseldorf, January 2023

from the institute for Quantitative and Theoretical Biology
at Heinrich Heine University Düsseldorf

Published by the permission of the
Faculty of Mathematics and Natural Sciences at
Heinrich Heine University Düsseldorf

Supervisor: Prof. Dr. Oliver Ebenhöf

Co-supervisor:

Date of examination: 07.03.2023

Erklärung

Ich versichere an Eides statt, dass die Dissertation von mir selbstständig und ohne unzulässige fremde Hilfe unter Beachtung der "Grundsätze zur Sicherung guter wissenschaftlicher Praxis an der Heinrich- Heine Universität Düsseldorf" erstellt worden ist. Die Dissertation habe ich in dieser oder in ähnlicher Form noch bei keiner anderen Institution eingereicht. Ich habe bisher keine erfolglosen oder erfolgreichen Promotionsversuche unternommen.

Düsseldorf, den 10. Januar 2023

Chilperic Armel Foko Kuate

The research detailed in this thesis was conducted from August 2019 until August 2022 in Düsseldorf at the Heinrich Heine University Düsseldorf in the Institute for Quantitative and Theoretical Biology under the supervision of Prof. Dr. Oliver Ebenhöf.

Summary

Mathematical modeling has nowadays become a cornerstone in the study of metabolic pathways. Mathematical models provide a framework for predicting and explaining observations made in experiments. In this work, mathematical modeling is used at two scales of detail to represent, on the one hand, the metabolism of fatty acids (FAs) in the liver and, on the other hand, the *de novo* synthesis of FAs in animals.

Fatty acids are essential in metabolism as they play a crucial role in energy conversion and storage. Furthermore, they are involved in many other cellular functions, such as signaling and immune response, and are material for the cell wall. They are associated with metabolic syndromes, including mitochondrial fatty acid oxidation disorders (mFAODs). The recent investigation of some mFAODs suggests that the disorder impacts oxidation, synthesis, and pathways. However, the studies of mFAODs using dynamical mathematical modeling have been mainly focused on the β -oxidation. To explore mFAODS in a more global framework, one needs models of fatty acid metabolism that combine FA oxidation, synthesis, and degradation pathways. Additionally, I suspect FA metabolism must be a bistable system to satisfy both the safety and rapid response to energy constraints (switching from fed to fasted state and reciprocally).

I start by reviewing the biochemistry of enzymes involved in FA synthesis and summarize the kinetic information of the corresponding enzymes. This step allows me to gather sufficient knowledge to develop the two models.

The first model is a coarse-grained open model of fatty acid metabolism based on lumped enzyme kinetics and inhibitory mechanisms. The model includes four variables: acetyl-CoA, malonyl-CoA, fatty acids, and triglycerides, and eight reactions and eighteen parameters. I show that the model could exhibit bi-stability through fatty acids pool. I also derive the conditions to be fulfilled by the parameterization of the system for it to be bi-stable.

The second model is a semi-mechanistic model of the elongation part of FA *de novo* synthesis. I reduced its complex mechanism into four types of reactions modeled as elementary reactions associated with mass action kinetics. The model uses acetyl-CoA, malonyl-CoA, and NADPH to produce three FAs (myristic acid, palmitic acid, and stearic acid) and free CoA. The model is fitted

to the time course data of three FAs. Under the resulting parametrization, each FA's production rate as a function of acetyl-CoA can be approximated by Michaelis-Menten rate equations as long as the malonyl-CoA in the system is at a low concentration. Under the latter consideration, the palmitic acid production rates as a function of malonyl-CoA or NADPH can also be approximated with Michaelis-Menten rate laws.

Contents

Abstract	iv
1 Introduction	1
1.1 Energy metabolism in the liver	2
1.1.1 Carbohydrate metabolism	3
1.1.2 Amino acid metabolism	3
1.1.3 Fatty acid metabolism	4
1.2 Inborn errors of metabolism	8
1.2.1 Mitochondria fatty acid oxidation disorders	8
1.3 Modeling	9
1.3.1 Steps of mathematical modeling	10
1.3.2 The framework for modeling metabolic pathway	10
1.3.3 Kinetic rate laws	11
1.3.4 Aims of dynamic modeling	12
1.3.5 Experimental data in kinetic modeling	13
1.4 Aims of the thesis	14
1.5 Outline of the thesis	16
2 Material and methods	18
2.1 Descartes' rule of signs	18
2.2 Structural stability of a dynamical system	19
2.2.3 Linearization and structural stability	20
2.3 Kinetic rate laws	21
2.3.1 Elementary reactions and Mass actions rate laws	21
2.3.3 Michaelis-Menten derived kinetics	23
2.4 Fitting method: Lavenberg-Marquart algorithm	29
2.4.1 The Gradient descent method	30
2.4.3 The Gauss-Newton method	31
2.4.4 Lavenberg-Marquart algorithm	32

2.4.6	Sensitivity analysis	35
3	Biochemistry and kinetics of enzymes involved in animal fatty acid synthesis	44
3.1	Basic biochemistry of enzymes of fatty acid <i>de novo</i> synthesis	45
3.1.1	Fatty acid <i>de novo</i> synthesis	45
3.1.2	Microsomal modifications of fatty acids	47
3.2	Kinetic of enzymes of fatty acid synthesis	50
3.2.1	Fatty acid <i>de novo</i> synthesis	50
3.2.2	Microsomal modifications of fatty acids	53
4	Fatty acid metabolism: conditions for bi-stability	57
4.1	Coarse-grained model of fatty acids metabolism	58
4.2	Conditions for having three steady-states	61
4.2.1	Necessary condition	61
4.2.2	Sufficient conditions	66
4.2.3	Summary of the conditions for having three steady-states	68
4.3	Stability analysis of the steady-states	68
4.3.1	Conditions for a steady-state to be stable	71
4.3.2	Condition for a steady-state to be unstable	74
4.4	Summary of bi-stability conditions	83
4.5	Discussion and conclusion	84
5	A semi mechanistic model of fatty acid <i>de novo</i> synthesis	87
5.1	Model construction: hypotheses and dynamics	91
5.1.1	Summary of the assumptions	92
5.1.2	Summary of the compounds in the models and their initial concentrations	93
5.1.3	Model schemes, ODEs and parameters	93
5.1.5	Experimental data to support model validation	97
5.2	Results	99
5.2.1	Vanilla model	99
5.2.2	Fitting the models to data	108
5.3	Discussion and Conclusion	124
	Conclusion	127
	Appendix	133
	Acknowledgements	169
	Dedication	171

Portfolio	172
List of publications	174

List of Acronyms

ACADs	Acyl-CoA dehydrogenases
ACC	Acetyl-CoA carboxylase
ATP	Adenosine triphosphate
CACT	Carnitine acyl translocase
CPT	Carnitine palmitoyl transferase
CTDs	Carnitine transporter defects
DH	Dehydratase
DNL	<i>De novo</i> lipogenesis
ELOVL	Elongation of very long chain fatty acids enzyme
ER	Endoplasmic reticulum
FA	Fatty acid
FADNS	fatty acid <i>de novo</i> synthesis
FAOD	Fatty acid oxidation disorder
FAODs	Fatty acid oxidation disorders
FAS	Fatty acid synthase
GPAT	Glycerol-3-phosphate-acyltransferase
GSA	Global sensitivity analysis
GSD	Glycogen storage disease
IEM	Inborn errors of metabolism
KAS	Keto-acyl-synthase
KR	Keto-acyl-reductase
LCAD	Long-chain fatty acylCoA dehydrogenase
LCSFA	Long-chain saturated fatty acid
LPL	Lipoprotein lipase
LSA	Local sensitivity analysis

MAT	Malonyl-acetyl-transferase
MCAD	Medium-chain fatty acyl CoA dehydrogenase
MCADD	Medium-chain acyl-CoA dehydrogenase deficiency
MCKAT	Medium-chain ketoacyl-CoA thiolase
mFAOD	Mitochondria fatty acid oxidation disorder
mFAODs	Mitochondria fatty acid oxidation disorders
MMFAs	Microsomal modifications of fatty acids
MSCHAD	Medium/short-chain hydroxy-acyl-CoA dehydrogenase
MTP	Mitochondrial trifunctional proteins
MUFA	Mono-unsaturated fatty acid
NADPH	Nicotinamide adenine dinucleotide phosphate
ODE	Ordinary differential equations
PUFA	Poly-unsaturated fatty acid
QSSA	Quasi-steady state assumption
RMSE	Root-mean-square error
SCAD	Short-chain fatty acyl CoA dehydrogenase
SCADD	Short-chain acyl-CoA dehydrogenase deficiency
SCD	Systemic carnitine deficiency
SSD	Sum of the square of differences
TCA	Tricarboxylic acid
TE	Thioesterase
TG	Triglyceride
VLCAD	Very long-chain fatty acyl CoA dehydrogenase
VLCADD	Very-long-chain acyl-CoA dehydrogenase deficiency
VLDL	Very low-density lipoprotein

List of symbols per chapter

Lists of symbols per chapter

Chapter 1

Symbols	Definition
M_i	i^{th} compound in the system
v_j	Rate law terms of the j^{th} reaction
α_{ij}	Stoichiometric coefficients

Chapter 2

Symbols	Definition
P	Polynomial
$N_p(P)$	The number of positive roots of a polynomial P with real coefficients
$V_p(P)$	The number of sign-changing of the coefficients of the expression $P(x)$
$N_n(P)$	The number of negative roots of a polynomial P with real coefficients
$V_n(P)$	The number of sign-changing of the coefficients of the expression $P(-x)$
J	Jacobian matrix

E_T	Total concentration of enzyme participating in a reaction
v	rate of kinetic reaction
k	Kinetic rate constant
k_f	The kinetic rate constant for the forward reaction
k_b	The kinetic rate constant for the backward reaction
v_f	The rate of the forward reaction
v_b	The rate of the backward reaction
K_{eq}	Equilibrium constant
K_m	Michaelis-Menten constant
K_d	Dissociation constant
K_m^{app}	Apparent Michaelis-Menten constant
V_{max}	Maximum velocity of the reaction
V_{max}^{app}	Apparent maximum velocity of the reaction
k_i	Kinetic rate constants for the forward inhibition reaction
k_{-i}	Kinetic rate constants for the backward inhibition reaction
$\ \cdot\ $	L^2 norm
∇	Gradient
∇^2	Hessian

Chapter 3

Symbols	Definition
k_{cat}	Turnover number
V_{max}	Maximum velocity of the reaction
K_m	Michaelis-Menten constant
K_a	Activation constant

K_a	Inhibition constant
-------	---------------------

Chapter 4

Symbols	Definition
sg	function that give the sign of an expression
s^*	value of s at the steady state
V_{in}	Rate law of Constant Influx
V_{out}	Rate law of Proportional out-flux
r_1	Rate law of Non-competitive inhibition
r_2	Rate law of Michaelis-Menten Kinetic
r_3	Rate law of Michaelis-Menten Kinetic
r_4	Rate law of Non-competitive inhibition
r_5	Rate law of Michaelis-Menten Kinetic
P_i	Polynomial indexed by i
A_i, B_i, C_i, D_i	Coefficients of the polynomial P_i
$\Gamma_k(\lambda)$	Characteristic polynomial associated with the matrix J_k
$\Gamma'_k(\lambda)$	First derivative of the polynomial $\Gamma_k(\lambda)$
$\Gamma''_k(\lambda)$	Second derivative of the polynomial $\Gamma_k(\lambda)$
A_k, B_k, C_k, D_k	Coefficients of the polynomial $\Gamma_k(\lambda)$
$\text{tr}(J_k)$	Trace of a square matrix J_k
$\det(J_k)$	determinant square matrix J_k

Chapter 5

Symbols	Definition
k_{cat}	Turnover number
K_m	Michaelis-Menten constants
K_i	Inhibition constants
<i>AcetCoA</i>	Acetyl-CoA
<i>MalCoA</i>	Malonyl-CoA
<i>NADPH</i>	Nicotinamide adenine dinucleotide phosphate
<i>E</i>	Free enzyme (fatty acid synthase)
EC_2	Complex enzyme substrates with two carbons
EC_4	Complex enzyme substrates with four carbons
EC_6	Complex enzyme substrates with six carbons
EC_8	Complex enzyme substrates with eight carbons
EC_{10}	Complex enzyme substrates with ten carbons
EC_{12}	Complex enzyme substrates with twelve carbons
EC_{14}	Complex enzyme substrates with fourteen carbons
EC_{16}	Complex enzyme substrates with sixteen carbons
EC_{18}	Complex enzyme substrates with eighteen carbons
<i>ECoA</i>	Complex enzyme-Coenzyme A
<i>C14:0</i>	Myristic acid
<i>C16:0</i>	Palmitic acid
<i>C18:0</i>	Stearic acid
<i>CoA</i>	Free Coenzyme A
$V_{x \rightarrow y}$	rate of transformation of x into y
<i>E</i>	Enzyme

S_i	Substrates
ES_i	Complex enzyme-substrate
P	Rate of formation of the main Product
k_{cat}^{NADPH}	Turnover number when using NADPH as unique substrate in Michaelis-Menten rate equations
K_m^{NADPH}	Michaelis-Menten constant when using NADPH as unique substrate in Michaelis-Menten rate equations
θ	Parameter vector
\mathcal{L}	Objective function

Chapter 1

Introduction

Part of this chapter is adapted from the following published article:

Foko Kuate CA, Ebenhöh O, Bakker BM, Raguin A. Kinetic data for modeling the dynamics of the enzymes involved in animal fatty acid synthesis. *Biosci Rep.* 2023 Jul 26;43(7):BSR20222496. DOI: [10.1042/BSR20222496](https://doi.org/10.1042/BSR20222496).

The author of this thesis contributed to the conceptualization, the methodology, the investigation and the writing of the above article. Hence, the author retains the right to include the article in this thesis since it is not published commercially.

Biochemical reactions occurring within living beings' cells are the core of life. They ensure that organisms can meet their vital challenges such as growth, reproduction, and health. To meet these challenges, cells must process macronutrients obtained from external sources to get carbons and free energy. These macronutrients are mainly carbohydrates, amino acids, and fat, which can be broken down (catabolism) or used to synthesize other compounds (anabolism). Catabolism and anabolism are the two components of metabolism, and they are carried out in several steps involving several enzymes responsible for ensuring the relevant fluxes for the involved reactions. Understanding how, where, and when these biochemical reactions occur is not often enough to develop clinical solutions for associated diseases or to optimize those reactions for industrial or commercial purposes.

It is also important to put side-by-side the enzymatic mechanisms of these reactions and their kinetics for their studies at the macroscopic scale (in the form of pathways). In case of a defect of one or several enzymes intervening in the metabolism, the optimal fluxes within the pathways cannot longer be achieved, resulting in an impairment of several functionalities. In the specific cases

of pathways involved in energy homeostasis, numerous disorders of metabolism have been identified that can be divided into two categories depending on whether it is involved in the metabolism of carbohydrates or lipids.

In this work, I am interested in the dynamic understanding of fatty acid metabolism in the liver, describing their dynamic using a mathematical modeling framework. This description is my contribution to the development of tools to understand how disorder in fatty acid β -oxidation impacts lipid metabolism and the whole body's energy homeostasis.

1.1 Energy metabolism in the liver

The central hub of metabolism in the body is the liver, as it plays a crucial role in regulating the synthesis, degradation, and storage of the essential building blocks for macromolecules, including glucose derived from carbohydrates, fatty acids derived from lipids, and amino acids derived from proteins. It is associated with the synthesis, degradation, and storage of these. In addition, it ensures the regulation of these macromolecules through hormonal processes.

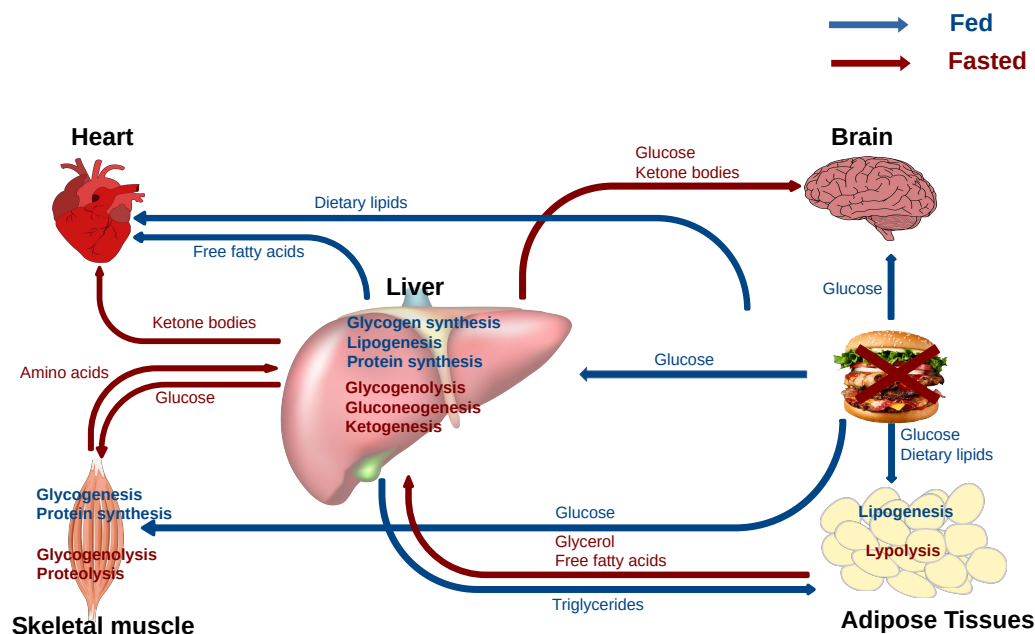


Figure 1.1: **Summary of energy homeostasis of the body:** The liver's vital function is emphasized, as it degrades internal and peripheral organ-derived molecules during fasting to supply other organs with the necessary nutrients. Conversely, during the fed state, the liver converts and stores macronutrients in the peripheral organs.

1.1.1 Carbohydrate metabolism

The liver ensures the maintenance of the plasma glucose concentration (5 *mmol/L*) [1]. Given the high carbohydrate content of the foods we eat, the liver stores the excess as glycogen (up to 10% of its mass) [1]. It can also convert this excess into lipids via glycolysis and *de novo* lipogenesis (DNL). Indeed through glycolysis, the liver converts glucose to pyruvate, which can be converted into acetyl-CoA. The latter will be used as fuel for the generation of ATP through the tricarboxylic acid (TCA) cycle and oxidative phosphorylation or as a precursor for hepatic DNL, which is characterized by three steps: *de novo* fatty acid synthesis (FADNS), microsomal modifications of fatty acids (MMFA) and formation of triglycerides (TGs) and phospholipids. TGs resulting from DNL are stored in the liver as lipid droplets.

In the case of fasting or physical exercise, the concentration of plasma glucose drops. To compensate for this drop, the liver mobilizes the glycogen reserve to produce glucose through glycogenolysis. In the case of glycogen depletion, which usually occurs after 24 h of fasting, the liver can produce glucose from non-carbohydrates sources. This process is known as gluconeogenesis. Through a derivative of glucose, notably the glucose-6-phosphates, the liver synthesizes NADPH via the pentose phosphate pathway. NADPH plays an essential role in FA synthesis (see chapter 4). The liver carbohydrates metabolism is mainly regulated by two pancreatic hormones: insulin and glucagon. If insulin prevents hyperglycemia by activating glycogenesis and DNL, glucagon prevents hypoglycemia by activating the degradation of glycogen and gluconeogenesis. Besides hormonal regulation, glucose metabolism in the liver is subject to allosteric regulation through intermediates of these pathways, and post-translational modification of intervening enzymes [2, 3].

1.1.2 Amino acid metabolism

Amino acids are mainly obtained from dietary proteins and are further metabolized in the liver. They can be divided into essential and non-essential amino acids. Non-essential amino acids are those that can be synthesized *de novo* in the liver in contrast to essential ones that cannot be synthesized in the human body and, therefore, must be acquired from external sources. The liver mainly uses the acquired amino acids for protein synthesis needed by peripheral tissues. In the case of excess amino acids, the body is unable to store the excess. Therefore the liver will break the excess into ammonia and pyruvate. The ammonia will be processed by the urea cycle into urea, while the pyruvate can be used either for gluconeogenesis or for producing acetyl-CoA. The latter can go directly into the TCA cycle or be used for DNL or ketogenesis. Similar to the metabolism of carbohydrates, amino acid metabolism is subjected to hormonal and allosteric regulations. Compared to other macromolecules, amino acids contribute less to the cell's energy, between 10-15 % of the total energy yield [2].

1.1.3 Fatty acid metabolism

As for carbohydrates and amino acids, the liver is also at the center of lipid metabolism. Apart from ensuring the contribution of lipids to energy homeostasis, it also warrants the synthesis of all the classes of lipids necessary for other physiological processes. Although this work is dedicated to lipids' contribution to energy homeostasis through fatty acid (FA) metabolism, I will also mention lipids' structural and functional role occasionally. Lipids can be classified into two categories: simple and complex lipids. Simple lipids are those composed only of atoms of carbon, hydrogen, and oxygen. Complex lipids, in addition to these three components, also include other elements such as nitrogen, phosphate, sulfur, or sugars. The standard criterion for all lipids is their insolubility in water and that they all contain FAs. Therefore the description of the metabolism of lipids in the liver will focus on that of fatty acids. In animals, specifically mammals, FAs can be obtained from dietary sources; however, as we have seen above, the liver and other tissues can synthesize *de novo* FAs from the products resulting from the breakdown of carbohydrates and amino acids. Lipids ingested as TGs or cholesterol esters are hydrolyzed into FA, which is not subsequently absorbed by the intestine and re-esterified into TGs. These are released into the bloodstream in the form of chylomicrons (lipoprotein particles consisting of about triglycerides (85–92%), phospholipids (6–12%), cholesterol (1–3%), and proteins (1–2%)) and very low-density lipoproteins (VLDL). Lipoprotein lipase (LPL) releases FAs and 2-monoacylglycerol, which are then captured by peripheral tissues, including the liver. Once in liver cells, depending on the energy state, FAs can be directly oxidized or remodeled and stored in adipose tissue in the form TGs.

Nomenclature of fatty acids

FAs are long linear hydrocarbon chains, comporting a methyl group (CH_3) at one end and a carboxyl group ($COOH$) at the other. They can be saturated, that is to say, not having a carbon-carbon double bond; otherwise, they are stated to be unsaturated. Natural FAs are generally made of chains with an even number of carbons, although some have an odd number of carbons. The FAs have a molecular formula $C_nH_{2n}O_2$ for the saturated and $C_nH_{(2n-k)}O_2$, where n represents the number of carbon and k the number of double bonds. According to the recommended nomenclature of organic chemistry [4], there are several ways to represent FAs, among which the most popular are the Δ and ω representations. In both representations, the numbers of carbons and double bonds are specified. The difference arises in the position of the double bond and its configuration (*cis* or *trans*). In the Δ representation, the positions of all the double bonds counted from the carboxyl end are indicated by a superscript of the symbol Δ , which itself is preceded by the *cis* or *trans* representing the double bond configuration. For example for arachidonic acid, $(CH_3(CH_2)_4CH=CHCH_2CH=CHCH_2CH=CHCH_2CH=CH(CH_2)_3COOH)$ its Δ representation is 20:4(*cis, cis, cis, cis* - $\Delta^5, \Delta^8, \Delta^{11}, \Delta^{14}$). The ω representation only gives the position of the first double bond counted from the methyl end. Hence, for arachidonic acid, the correspond-

ing representation is $20:4n - 6$, where 20 is the number of carbons, 4 represents the number of the double bonds, and $n - 6$ is the position of the first double bond.

In the following, I will be using the ω convention for the nomenclature of FA as shown in the example, Figure 1.2.

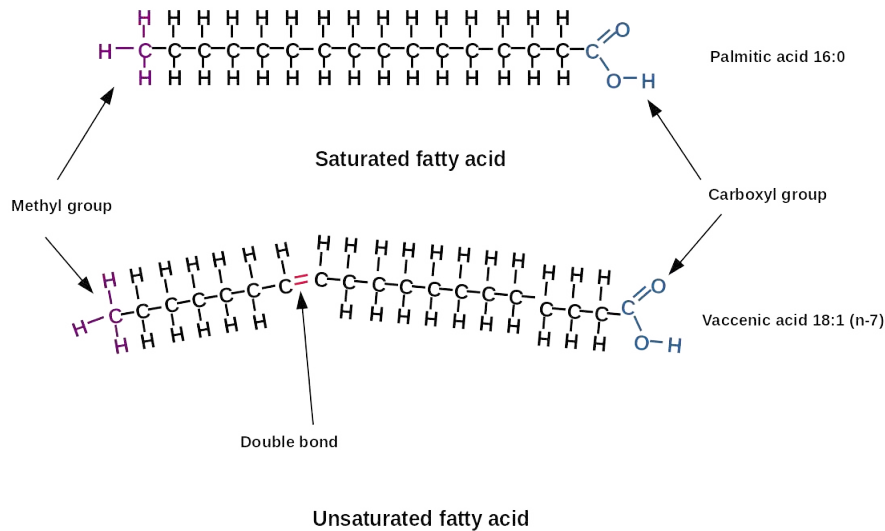


Figure 1.2: **Example of structural formula of saturated and unsaturated FAs**

Fatty acid catabolism: mitochondria β -oxidation

Long-chain saturated fatty acids (LCSFAs) are the favored energy source for the heart and skeletal muscle during exercise [6]. They are mobilized from the lipogenic tissue, mainly adipose tissue, and processed in the liver to provide the acetyl-CoA required for gluconeogenesis, ureagenesis, and ketogenesis. Independently of the source, free FAs, are first released into the cytoplasm. Their fate is determined by the enzyme in charge of their activation. To undergo mitochondria β -oxidation, they are activated by acyl-CoA synthetases located in the outer membrane of the mitochondria [7]. The activation process takes place in the presence of 2 ATP, resulting in the formation of acyl-CoAs ready to be oxidized. The resulting acyl-CoAs can directly cross the mitochondria or be shuttled by the carnitine shuttle, a system composed of three enzymes. Short and medium-chain acyl-CoAs cross the mitochondria membranes, whereas long-chain fatty acyl CoA requires the carnitine shuttle system [8].

In the carnitine shuttle system (purple square boxes in Figure 1.3), the carnitine palmitoyl transferase 1 (CPT1), located within the outer membrane of the mitochondria, exchange the CoA group of the acyl-CoA with the free carnitine resulting in an acyl-carnitine transferred in the intermembrane space. The carnitine acyl translocase (CACT) locate within the inner membrane transfers the acyl-carnitine into the mitochondrial matrix, where the carnitine palmitoyl transferase 2 (CPT2)

will exchange the carnitine group of the acyl-carnitine with the CoA. The resulting acyl-CoA, which is ready to enter the β -oxidation cycle, is the same as the one at the beginning of the shuttling reactions. The carnitine freed uses the shuttle system to be recycled back into the cytosol.

The oxidation cycle comprises seven in humans and eight enzymes in rodents [9] (see dark green square boxes Figure 1.3). The difference arises in the set of substrate-specific enzymes acyl-CoA dehydrogenases (ACADs), responsible for the first step of the oxidation cycle. The ACADs discriminate the substrate according to its chain length. In rodents, very long-chain fatty acyl CoA dehydrogenase (VLCAD) acts on FAs with chains greater than 12, long-chain fatty acyl CoA dehydrogenase (LCAD) processes FAs with chains between 8 and 16, medium-chain fatty acyl CoA dehydrogenase (MCAD) acts on FAs with chains ranging from 6 to 12. Short-chain fatty acyl CoA dehydrogenase (SCAD) works on FAs with chains of 4 and 6. In humans, LCAD is not expressed and therefore MCAD and VLCAD cover a wider range of substrates. Although ACADs are considered as substrate-specific, they display a degree of flexibility when it comes to the length of the substrate's carbon chain. The other enzymes of the β -oxidation cycle are mitochondrial trifunctional proteins (MTP) which in one step can process in the presence of the free CoA and NAD^+ an enoyl-CoA with a chain greater or equal to 8, resulting from the dehydrogenation by ACADs. The MTP competes with the crotonase, which processes any chain length of enoyl-CoA through a hydration reaction, resulting in a hydroxy-acyl-CoA. The hydroxy-acyl-CoA then goes into a dehydrogenation reaction carried by medium/short-chain hydroxy-acyl-CoA dehydrogenase

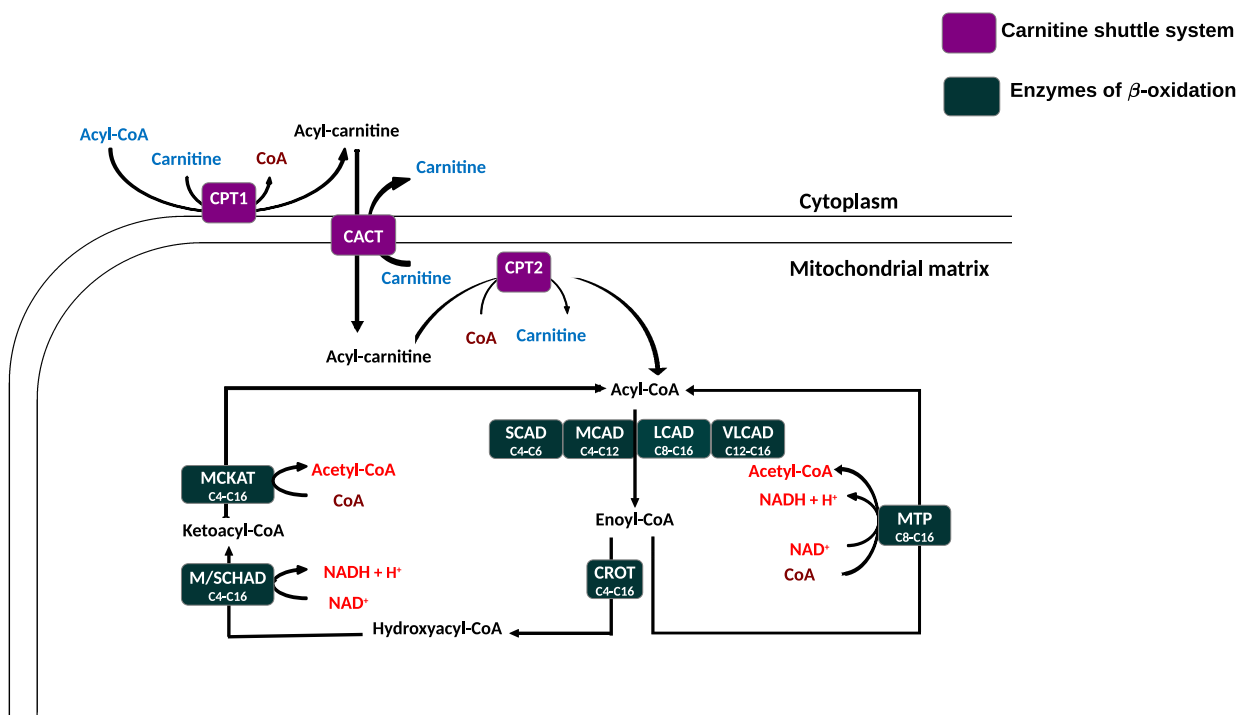


Figure 1.3: **Summary of mitochondrial β -oxidation reactions in rodents:** the purple square boxes represent the enzymes of the carnitine shuttle system, while the green square boxes represent the enzymes of the β -oxidation cycle. (Adapted from [5])

(MSCHAD) in the presence of NAD^+ . The obtained Keto-acyl-CoA goes through the last reaction of the cycle, producing acetyl-CoA and acyl-CoA, two carbons shorter or two acetyl-CoA. This last reaction is catalyzed by medium-chain ketoacyl-CoA thiolase (MCKAT) in the presence of the free CoA. Regarding the oxidation of unsaturated fatty acids, specifically when the carbons containing double bonds are encountered, instead of being acted upon by an ACAD enzyme, we observe an isomerization reaction catalyzed by Δ^3, Δ^2 -enoyl-CoA isomerase [10]. Figure 1.4 depicts the isomerization mechanism of Δ^3, Δ^2 -enoyl-CoA isomerase on a $12:2n - 3$ allowing its double bond to relocate and resulting in the formation of the $12:2n - 2$ enoyl-CoA which could be further processed by the MTP or the crotonase (see Figure 1.3).

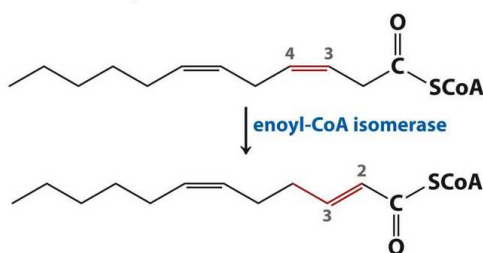


Figure 1.4: **Mechanism of Δ^3, Δ^2 -enoyl-CoA Isomerase:** The enzyme relocates the double bond from between carbons 3 and 4 to between carbons 2 and 3. (Adapted from <https://www.slideserve.com/hang/lecture-notes-for-chapter-17-lipid-metabolism>)

The mitochondria β -oxidation is subject to hormonal and allosteric regulation. As discussed above, insulin activates oxidative enzymes while glucagon represses these enzymes. With respect to allosteric regulation, the flux of each enzyme in the oxidation cycle is inhibited by the acyl-CoA intermediate it produces [11, 12]. It is also important to note that malonyl-CoA, which is essential in DNL, inhibits CPT1[13].

Fatty acid anabolism

In the fed state, where the blood glucose concentration is high, the liver, via fatty acid *de novo* synthesis (FADNS), will process in two steps the acetyl-CoA resulting from the degradation of glucose into fatty acids. For FADNS to take place, the mitochondria acetyl-CoA is exported in the cytoplasm via the citrate shuttle system. Indeed, the citrate synthase combines acetyl-CoA with oxaloacetate to form the citrate that freely crosses the mitochondria membranes. Once in the cytoplasm, the citrate is processed back into acetyl-CoA and oxaloacetate by the citrate lyase using one ATP. The resulting acetyl-CoA can now be used for FADNS. The first steps of FADNS consist in synthesizing malonyl-CoA from acetyl-CoA via a carboxylation reaction catalyzed by acetyl-CoA carboxylase. The second step utilizes the acetyl-CoA, malonyl-CoA, and NADPH in a series of channeling elongation reactions to produce LCSFAs. The latter, with exogenous FAs, will contribute to cholesterol synthesis and phospholipids synthesis or be stored as triglycerides. The

FADNS is subjected to hormonal regulation by glucagon and insulin. The glucagon inhibits FADNS by repressing allosterically acetyl-CoA carboxylase, while insulin stimulates by dephosphorylation. Since this work focuses on the synthesis of FAS, I dedicated a part to reviewing the literature on the biochemical mechanisms and the kinetics of enzymes associated with the synthesis of FAs. Refer to Chapter 3 for a more in-depth discussion of FA synthesis.

1.2 Inborn errors of metabolism

Inborn errors of metabolism (IEM) are a set of rare hereditary diseases of metabolism resulting from enzyme or transporter deficiencies [14]. This results in the inefficiency of the pathway involving the corresponding enzymes or transporters. They affect the metabolism of carbohydrates, amino acids, and lipids. A compilation of worldwide data reported by Campeau et al. [15] reveals IEMs had an incidence of about 1:1000 in 2008 [15]. To date, more than 500 IEMs have been identified and can be classified depending on whether they are involved in the metabolism of carbohydrates, lipids, or amino acids [14]. Among IEMs, while some can have a mild impact on the metabolism, others could severely impact the energy homeostasis of the cell. Among others, glycogen storage diseases (GSDs) that affect either glycogen synthesis or its breakdown into glucose are notable examples. More than sixteen GSDs are known to date and can be clustered depending on the organ that they impact primarily. For example, GSD type 1a and type 1b affect the liver, whereas GSD type 2a and type 2b primarily affect muscles. Besides GSDs, mitochondria fatty acid oxidation disorders (mFAODs) are associated either with a defect with carnitine transporters or oxidative enzymes. A popular class of mFAODs associated with the oxidative enzymes is acyl-CoA dehydrogenase deficiencies resulting from the defect of one of the acyl-CoA dehydrogenase (ACAD) enzymes catalyzing the first step of the β oxidation cycle [16].

1.2.1 Mitochondria fatty acid oxidation disorders

Fatty acid oxidation disorders (FAODs) are autosomal recessive inborn errors of metabolism associated with the defects in the enzyme or transporter in the degradation of fatty acyl-CoA [17]. The defect in one of these enzymes of the carnitine shuttle system results in the class of disorders known as carnitine transporter defects (CTDs). CTDs mainly affect the heart and are characterized by cardiac failure and generalized muscle weakness [18]. For a detailed description of CTDs, the reader is encouraged to read [19, 16, 20]. As for the case of the carnitine shuttle, if one of these enzymes is deficient, mitochondrion fatty acid oxidation disorders (mFAODs) occur, in which ACAD deficiency disorders are the most encountered [21]. ACAD deficiencies are inherited and autosomal recessive genetic diseases resulting in low production of an ACAD enzyme. They consist of short-chain acyl-CoA dehydrogenase deficiency (SCADD), medium-chain acyl-CoA dehydrogenase deficiency (MCADD), and very-long-chain acyl-CoA dehydrogenase deficiency (VLCADD). This

class of deficiencies shares common symptoms such as muscle soreness, hypoglycemia, vomiting, and lethargy and can worsen with fasting or stress exposure. In some extreme cases, these diseases can lead to sudden death, as is the case with MCADD [22]. The current treatment strategy consists primarily in avoiding fasting, feeding with high carbohydrate diets, replacing LCFAs fat diets with MCFAs fat diets for the case of VLCADD, carnitine supplementation, and uncooked corn starch for overnight fasting [23, 16]. Some of these treatments do not always bring the expected effect. For example, in the case of VLCADD, carnitine supplementation aimed at increasing the plasma carnitine content negatively impacts the range of toxic acylcarnitines [24].

The most prominent ACADD is medium-chain acyl-CoA dehydrogenase deficiency (MCADD) which is more prevalent in the caucasian population [25, 16]. The average incidence resulting from compiling newborn screening studies from Germany, England, Australia, the United States, and Japan suggests an average incidence of 1:10000 and 1:27000 [25]. The disease is a consequence of the mutation of the ACADM gene that code the MCAD [14]. Since the MCAD enzyme is affected, the cell can no longer break down medium-chain acyl-CoA leading to the accumulation of carnitine in the blood. Another disorder of fatty acid metabolism is systemic carnitine deficiency (SCD), characterized by the limitation of carnitine required for the carnitine shuttle. This autosomal recessive disorder results from the mutation of the gene SLC22A5 coding for carnitine transporter OCTN2 [25], which recover the carnitine in the kidney and ensure the availability of the carnitine for fatty oxidation. The current treatment is carnitine supplementation and avoiding fasting [16].

1.3 Modeling

A model is a more or less simplified representation at a particular scale of a system under study in terms of its components, their interactions, and how they come together for the system to work. In this representation, only the relevant features of the system to allow for answering particular or particular questions are included. Therefore, it never gives an accurate description of the system. However, it will enable me to study the system to a certain instance, explain observations, derive new insights, make predictions, and test various scenarios. Modeling, which is the process of creating a representation of a system to infer knowledge from it, is a growing and popular discipline applied in almost all fields. In biology, mathematical modeling is one of the main components of Systems Biology and Systems Medicine, regrouping experimental and theoretical approaches. Biological systems are complex and dynamic, involving thousands of metabolites and reactions occurring at different time scales. To have a proxy of such complexity, it is estimated that a single eukaryotic cell performs about ten billion reactions per second. One needs a rigorous and rule-based framework representing the system at the microscopic and macroscopic levels to decipher such complexity. Mathematical modeling coupled with computer simulation offers such a framework, as mathematics provides rigor, and computers allow high-level computations and

simulations and analyze the results.

Mathematical modeling is a vast field that includes many approaches. Depending on the aspect of the models being studied, one approach could be more interesting than another. Fischer [26], Voit [27], and Motta and Pappalardo [28] give a brief description of how to choose the modeling method. No matter which modeling method is chosen, the modeling process will include the following five fundamental steps, as described by Voit [27]

1.3.1 Steps of mathematical modeling

- **Defining the scope, the goal, and the objective of the model.** In this part, one should define the question(s) to be addressed with the model and decide what aspect of the system under study should be included. Besides, it is essential to check the data available for testing or validating the model.
- **Selecting the modeling approach and the level of details to be incorporated.**
- **Model construction.** It consists in i) selecting the model's components (metabolites, enzymes, conserved quantities); ii) define the interaction between the component of the system (reactions, rate equations, and parameters); iii) The calibration of the model, either by extracting the parameter value from the literature, fitting the model to experimental data, or comparing the model to existing validated models.
- **Diagnosis and analysis of the model.** Check for consistency, sensitivity and robustness, and interpretation of the model's results.
- **Use of the model and applications.** In this step, the model can be used for validating the hypothesis, explaining observations, making predictions, or for other purposes

In the following, I will focus on the mathematical modeling framework based on ordinary differential equations (ODE) used to study qualitatively and quantitatively the dynamics of several types of biological systems and, in my case, biochemical pathways.

1.3.2 The framework for modeling metabolic pathway

Metabolism comprises many reactions, most of which are coupled and interconnected. This network of reactions may seem insurmountable and inexplicable at first sight when regarded as a whole. However, once dissected into subsets known as metabolic pathways, its understanding and study become affordable. For instance, one can define a metabolic pathway as the ensemble of reactions leading to either the degradation or the synthesis of particular compounds. Pathways can be studied from a static or a dynamic point of view, which is chosen depending on the size of the pathway, the questions to be addressed, the pre-existing information, and the assumptions. Static

modeling, such as stoichiometric models and constraint-based models, allows studying the distinct metabolic routes and the associated fluxes at the steady states [29, 30]. They are particularly relevant for large-scale models (e.g., genome-scale) that involve up to thousands of reactions and metabolites. However, if one is interested in tracking metabolites change over time, dynamical models are required. Furthermore, access to the concentration of the system's metabolites over time allows to discriminate optimal fluxes predicted by static models that may pass through biologically unrealistic transient states. Among dynamic models, one could differentiate between deterministic and stochastic ones. The latter specifically allows the study of systems made of a small number of entities and their fluctuations and to represent *in silico* large and complex substrates for which kinetic rate laws cannot be derived (e.g., glycogen). Knowing what type of model to use reside in the time scale, the assumptions, and the question to be addressed by the model. For instance, for studying the time evolution, either quantitatively or qualitatively, of the particular metabolites (state variables), kinetic modeling is suitable. However, if one is interested in studying steady-state metabolites concentrations or/and steady states fluxes, one should consider static models.

1.3.3 Kinetic rate laws

The rate of change over time of individual chemical entities (noted M_i) is expressed as the sum and difference of kinetic rate law terms (noted v_j), weighted by their stoichiometric coefficients (noted α_{ij}), following:

$$\frac{dM_i}{dt} = \sum_j \alpha_{ij} v_j. \quad (1.3.1)$$

A good overview of some simple and commonly used kinetic rate laws has been published by Saa and Nielsen [31], as well as Kim et al. [29]. However, the ones that I use in this piece of work are reviewed in the Chapter 2. The closer a reaction is to the equilibrium, the least details are needed to model it. Kinetic rate laws require parameters that can be estimated from experimental data using methods such as Lineweaver-Burk plots [32, 33, 34], Hanes-Woolf plots [35], and non-linear regressions [36]. Still, when missing kinetic parameters, the typical approach consists in either using those from a related organism or implementing simplistic rate laws such as mass-action kinetics or its generalization. Although these types of rate laws are easy to analyze, they have the disadvantage of not capturing substrate saturation [37]. To circumvent this limitation, more complex kinetics can be used, such as Michaelis-Menten [38], multi-substrate (sequential or ping-pong) [39], "convenience" [37] or "universal" [40] kinetics. They account for the order of addition of the substrates, the order of formation of the products, the different types of inhibition, the activations, the competitions, etc. Aside from these strengths, the potentially large number of parameters is usually an obstacle for further analysis. Besides, the King and Altman method is a generic approach to derive kinetic rate laws, step-by-step, from the underlying specific enzymatic mechanism [41, 42, 43]. It allows determining the kinetic rate laws of complex mechanisms involving

one or more reactants, products, inhibitors, etc. The steps of the method have been fully described by Cleland et al. [39] and Ulusu et al. [44]. Simpler kinetics such as Michaelis-Menten can also be retrieved by this means. In addition, the Haldane relationship can be used to relate the kinetic parameters and the thermodynamics of the reaction *via* the equilibrium constant.

Generally, the mathematical representation of the dynamics of the pathway leads to large systems of non-linear differential equations that are difficult or impossible to solve and interpret analytically. Therefore, dedicated software tools have been developed to solve them numerically. Among others, one can mention Modelbase [45], COPASI [46], PySCeS [47], and Berkeley Madonna [48].

1.3.4 Aims of dynamic modeling

Kinetic models can help with testing hypotheses, designing and assisting experiments, discriminating between possible regulatory mechanisms, identifying drug targets, and making sense of genomic, proteomic, and metabolic data [49, 50, 31, 51]. They allow for predicting how the system responds to perturbations or identifying the existence of rescuing pathway routes, for example, towards understanding disease phenotypes. They also can be used to predict the time course of metabolite concentrations and fluxes, for instance, towards optimizing the latter. For illustration, I report here a typical example where theory derived hypotheses have been verified experimentally and led to major progress in understanding the associated metabolic pathway. It is known that hypoglycemia observed in acyl-CoA dehydrogenase deficiencies is the result of the inability of β -oxidation to deal with substrate influx, because one of the first enzymes involved in this cyclic pathway is defective. Remarkably, using a detailed kinetic model, based on a bottom-up approach and a set of mice experiments, Martines et al. [12] have been able to predict that intermediate metabolites accumulate within the pathway, causing the reverse reactions to be more thermodynamically favorable than the forward ones. Using metabolic control analysis, they also showed that medium-chain ketoacyl-CoA thiolase (MCKAT) can restore the pathway fluxes, revealing its potential for being a drug target. As an incentive, I additionally present two specific cases of experimental observations that would typically benefit from a complementary kinetic modeling investigation. First, experimental results by Santos and Schulze [52], and de Cedrón and de Molina [53], showed that targeting acetyl-CoA carboxylase (ACC) and fatty acid synthase (FAS), or adopting appropriate diet habits, holds the potential to reduce tumor growth, since long chain saturated fatty acids (LCSFAs) are considered as a risk factor for tumor proliferation. Beyond this qualitative observation, the quantitative details of these therapeutic approaches are not specified, nor their consequences on the whole lipid metabolism. A kinetic model could help to quantitatively characterize the respective contribution of each enzyme to the overall LCSFAs *de novo* production, thereby unveiling their potential as drug targets. Second, Lelliott and Vidal-Puig [54] observed lipotoxicity caused by an imbalance between the synthesis and the breakdown of FA in fatty acid oxidation disorders. To counteract this effect, they suggested that the exceeding fluxes from the oxidative tissues could be

redirected towards lipogenic tissues such as white adipose tissue. To test this hypothesis, one would need to develop a large model that includes the whole lipid metabolism at the organ level. For this re-routing strategy to be quantified in a time-dependent manner and avoid unfeasible solutions, as a first-line strategy, a kinetic model appears most appropriate.

1.3.5 Experimental data in kinetic modeling

Experimental data play a crucial role in the kinetic modeling of biological processes. They are typically used following two fundamental modeling approaches: top-down and bottom-up. The top-down, or data-driven approach, starts with data, whose quality and quantity guide the complexity of the kinetic rate laws to be chosen. Indeed, it is not worth using complex kinetic rate laws that include several parameters if only little amount of data is available. In contrast to the top-down approach, the bottom-up uses data at the last modeling stage for model validation and refinement. The bottom-up approach relies on prior knowledge of the enzymatic mechanism, kinetic rate laws, and parameter values. The parameter values are usually extracted from literature or databases (e.g., Brenda[55] and SABIO-RK [56]). It is important to keep in mind that the two methods are not mutually exclusive. Combining them can be very powerful if data (needed for top-down) and knowledge (needed for bottom-up) are unequally available for the distinct parts of the system under study. The bottom-up approach requires more prior knowledge but less data for model validation than the top-down does for model construction. Still, in both cases, time course data of metabolite concentrations with high temporal resolution are ideal to validate kinetic models. In case time course data are not available, one can also use fluxes to validate their model results at the steady state, but those will not inform on the dynamics.

Metabolic data for building kinetic models are generated using targeted metabolomic techniques. The method differs from its non-targeted counterpart in that it is calibrated for the absolute quantification of specific metabolites. Targeted metabolomics can be combined with enzymatic assays to measure enzyme activity or their kinetic parameters (e.g., catalytic, Michaelis-Menten, or inhibition constants). It can also be applied to monitor the production of metabolites over time. The most popular techniques in the field are mass spectrometry, nuclear magnetic resonance, and liquid chromatography [57]. Most often, these methods are combined depending on the chemical properties of the compounds to be measured, as well as that of the matrix in which the measurements are performed [57]. The field of mass spectrometry is undergoing quick expansion, that is boosted by the technique of stable isotope tracer labeling [58, 59, 60]. The latter allows to track both *in vivo* and *in vitro* the incorporation of the labeled isotope to specific products, and thus, to determine the fluxes of distinct biochemical routes in complex metabolic pathways [61]. For example, Topolska et al. [59] use ^{13}C -labeled malonyl-CoA in combination with high-resolution mass spectrometry, to measure the activity of fatty acid synthase (FAS) and the total fatty acid production *in vitro*. Similarly, Yoo et al. [60] use ^{13}C -labeled acetyl-CoA in combination with

gas chromatography and mass spectrometry to measure the contribution of fluxes from different sources, to the *de novo* fatty acid synthesis, in cultured brown adipose tissue.

Despite the rapid evolution of the field of targeted metabolomics with high-resolution techniques, kinetic modeling is still limited by the quantity and quality of the available data. Regarding the data quality, the values of the kinetic parameters associated with rate laws are most often measured *in vitro* and differ from one source to another. Those do not only fail to reflect the situation *in vivo*, but it is also challenging to decide what source is most suitable for modeling. Furthermore, kinetic parameters highly depend on measurement conditions and protocols. For instance, pH and temperature can have drastic effects, as shown by Cox and Hammes [36] for FAS. One should also note that the amount of data produced by targeted metabolomics techniques can become insufficient [26]. That is, for instance, the case of parameterizing complex models that include several parameters. Depending on the time resolution of the data, it can also be challenging to interpret the dynamics of the process, and identify kinetic parameters [62, 44].

1.4 Aims of the thesis

The metabolism of fatty acids, and thus those of lipids, is essential for the energy homeostasis of the cell. Many metabolic disorders are related to the abnormal metabolism of FAs. Among these disorders, mitochondrial fatty acid oxidation disorders (mFAODs) are among the most significant due to their health care burden. To understand and provide the most appropriate clinical solutions, extensive clinical, experimental, and computational efforts have been made, including studies by Bentler et al. [63], Martines et al. [64, 12], and T Tucci et al. [65]. These efforts have led to the development of treatments such as medical diets, cofactor treatments, enzyme replacement, small molecule therapies, solid organ transplantation, carnitine supplementation, and cell gene-based therapies [66]. However, the effectiveness of these treatments varies due to the wide range of phenotypes observed for the same condition, necessitating further research for a deeper understanding of these diseases. Particularly for MCAD deficiency, which motivates this work, mathematical modeling has primarily focused on the dynamics of oxidation pathways [12, 67, 68]. Yet, lipidomics studies in mFAODs, such as MCAD and VLCAD deficiencies [5, 65], indicate significant changes in the FA profiles of liver triglycerides (TGs) under these conditions, suggesting an impact on both FA oxidation and synthesis pathways. This observation leads to our research questions:

1. Which metabolic routes lead to the disruption of triglyceride distribution in the liver in the context of MCAD deficiency?
2. What is the magnitude of the shift in steady-state concentration values of key metabolites (acetyl-CoA, malonyl-CoA, and FAs) in MCAD deficiency?

To address these questions comprehensively, an examination of the entire FA metabolism is essential. To my knowledge, no existing mathematical models investigating mFAODs incorporate FA synthesis dynamics, possibly due to the lack of a mechanistic model for a crucial part of FA metabolism, namely fatty acid *de novo* synthesis (FADNS), and the scarcity of kinetic parameters for FA synthesis. This work aims to make a pioneering step towards answering the posed research questions. My contribution is primarily theoretical, focusing on a mathematical modeling approach. Initially, I identify the main challenges in modeling FA synthesis (Chapter 3) through a literature review and identification of existing gaps. Subsequently, I propose two mathematical models: the first addresses selected questions in FA metabolism (4), and the second provides a semi-mechanistic model of the elongation process in fatty acid *de novo* synthesis (Chapter 5).

Studies on mFAODs using mathematical modeling have primarily focused on FA degradation pathways, partly due to the lack of kinetic parameters for enzymes involved in FA synthesis. Through Chapter 3, I conduct a thorough literature review on these enzymes' kinetic parameters, aiming to highlight gaps and direct where efforts should be concentrated to facilitate the development of mathematical models for FA synthesis dynamics. Despite the lack of specific parameter values, constructing a mathematical model of FA metabolism and analyzing it qualitatively remains feasible.

Given the limited parameters and experimental data for constructing a detailed mechanistic mathematical model of FA metabolism, my initial focus was on qualitative understanding. Depending on nutritional, environmental, or metabolic conditions, FAs are either synthesized or degraded, with both processes representing stable, steady states within the FA metabolism dynamical system. An initial step towards addressing the main research questions includes answering the following:

1. Which biochemical mechanisms explain the existence of two distinct metabolic steady-states (synthesis and degradation)?
2. Under what scenarios do we observe these steady-states?

To tackle these questions, I developed a coarse-grained model of fatty acid metabolism that includes acetyl-CoA, malonyl-CoA, FAs, and TGs. This model allows deriving sufficient and necessary conditions for the parameterization to exhibit bistability in FA metabolism. The two steady states represent those for FA synthesis and degradation. Furthermore, these steady-states are guaranteed by the utilization of liver FAs for non-energetic purposes. These insights provide a better understanding of how conditions like hypoglycemia or hyperglycemia influence the breakdown and synthesis of FAs and the transition between steady states based on glucose or dietary fat influx.

Addressing the research questions also involves confronting the need for a detailed mechanistic model for FADNS. I, therefore, have developed a semi-mechanistic model for FADNS, a pathway directly linking FA synthesis and oxidation and deserving of detailed study due to its complexity

and the multiplicity of reactions performed by a single enzyme. Besides, this model can predict fluxes and dynamics of LCFA synthesis in any lipogenic tissue under specific conditions and deduce kinetic parameters like k_{cat} and K_m values for FADNS in different tissues and mammalian species, addressing the kinetic parameter scarcity.

1.5 Outline of the thesis

This thesis aims to contribute to the understanding of fatty acid (FA) metabolism, particularly in the context of mitochondrial fatty acid oxidation disorders (mFAODs), by developing and analyzing mathematical models. The research questions outlined in the previous section guide the structure and content of this thesis as follows:

1. Which metabolic routes lead to the disruption of triglyceride distribution in the liver in the context of MCAD deficiency?
2. What is the magnitude of the shift in steady-state concentration values of key metabolites (acetyl-CoA, malonyl-CoA, and FAs) in MCAD deficiency?

The thesis is organized into five chapters, each building upon the last to systematically address these questions through theoretical modeling and analysis.

Chapter 1: Introduction provides a comprehensive background on FA metabolism, highlighting its importance in cellular energy homeostasis and the liver's role. This chapter introduces key metabolic disorders, with a focus on mFAODs, and outlines the modeling frameworks employed to simulate metabolic pathways, emphasizing kinetic rate laws.

Chapter 2: Materials and methods details the mathematical tools and kinetic rate laws utilized throughout the thesis. This chapter serves as a foundation for the modeling work, explaining the methodologies employed in subsequent chapters.

Chapter 3: Biochemistry and kinetics of enzymes involved in animal fatty acid synthesis reviews the current knowledge on FA synthesis biochemistry and the kinetics of involved enzymes. It identifies gaps in the literature, particularly concerning kinetic parameters, and suggests directions for future research to facilitate model development.

Chapter 4: Fatty acid metabolism: conditions for bi-stability presents a coarse-grained model of FA metabolism in the liver. It establishes conditions under which bi-stability occurs, offering insights into the metabolic transitions between FA synthesis and oxidation. This chapter employs Descartes' rules of signs and dynamic system theory to establish the necessary and sufficient conditions for FA metabolism to be a bi-stable system, where the steady-states correspond to two regimes, FA oxidation and FA synthesis.

Chapter 5: A semi mechanistic model of fatty acid de novo synthesis introduces a semi-mechanistic model of fatty acid *de novo* synthesis (FADNS), validated against experimental datasets. It links model parameters with experimental data and prioritizes parameters based on sensitivity analysis. The chapter concludes with a discussion on model limitations and future research directions.

The **General conclusion** evaluates the thesis's contributions to the field of FA metabolism modeling, discusses limitations, and suggests avenues for future work. This final section reflects on the implications of the findings for understanding mFAODs and potential clinical applications.

This structure not only gives a beginning of an answer to the proposed research questions but also contributes to the theoretical modeling of FA metabolism, offering insights into the complex dynamics of FA synthesis and oxidation.

Chapter 2

Material and methods

2.1 Descartes' rule of signs

Descartes' rule of signs is an approach used to determine the number of possible positive and negative roots of a polynomial with real coefficients, regardless of its degree. The rule is based on analyzing the number of sign changes among the coefficients of the polynomial. This technique, when combined with the study of the polynomial's maxima, can be employed to describe the roots of a polynomial or establish constraints on its behavior. In Chapter 4, I will demonstrate the powerful application of Descartes' rule of signs in studying the structural stability of a dynamical system.

In the following, I will provide a concise explanation of Descartes' rule of signs by presenting two fundamental propositions that serve as the foundation of this rule. Subsequently, I will provide an example to illustrate how the rule is applied. For a more thorough understanding, extension, and practical implementation of this concept, I encourage readers to refer to the comprehensive summary by Anderson et al. [69].

Proposition 1 (Descartes' rule of signs for positive roots). *The number of positive roots $N_p(P)$ of a polynomial P with real coefficients is equal to the number of sign-changing $V_p(P)$ of the coefficients of the expression $P(x)$ minus an even number.*

$$V_p(P) - N_p(P) = 2k, \quad k \in \mathbb{N}$$

Proposition 2 (Descartes' rule of signs for negative roots). *The number of negative roots $N_n(P)$ of a polynomial P with real coefficients is equal to the number of sign-changing $V_n(P)$ of the coefficients of the expression $P(-x)$ minus an even number.*

$$V_n(P) - N_n(P) = 2k, \quad k \in \mathbb{N}$$

Example 1. Let us consider the polynomial P defined by

$$P(x) = -2x^5 + x^4 - 3x^3 - 7x^2 + 6x - 3,$$

the coefficients are $-2, 1, -3, -7, 6, -3$. The number of sign-changing, $V_p(P)$, in the polynomial $P(x)$ is represented by the number of color changes. In this case, since $V_p(P) = 4$, it suggests that the polynomial P could potentially have four, two, or zero positive roots.

We have

$$P(-x) = 2x^5 + x^4 + 3x^3 - 7x^2 - 6x - 3,$$

the coefficients are $2, 1, 3, -7, -6, -3$, which suggests number of sign-changing $V_n(P)$ of the polynomial P is 1. Therefore the polynomial P has one negative root.

2.2 Structural stability of a dynamical system

The study of deterministic dynamic systems, such as metabolic pathways, consists in determining the future of a system in which one has limited information of its history; still, its dynamic is determined by a physical law of evolution. This study can be done quantitatively or qualitatively. In the quantitative approach, one solves analytically or numerically the differential equation associated with the system and infers the numerical values of certain aspects of the system, such as fluxes and concentrations, as a function of time. This first approach will be used in Chapter 5. The qualitative approach involves obtaining information on the trajectories without solving the differential equation. More precisely, it allows for characterizing the system's nature and predicting its asymptotic behavior based on a particular initial condition. For example, it enables knowing if a system presents oscillatory behaviors and determining the number of fixed points of a system and their respective stability. This second approach is the subject of this section and will be used in Chapter 4 to determine the bi-stability conditions of FA metabolism. My intention is not to present the theory of dynamical systems exhaustively, but rather to give the theoretical foundations of the tools that I use in the chapter 4 to determine the structural stability of the dynamical system that represents FA metabolism.

Definition 2.2.1. (steady state) Consider the autonomous non-linear system described by the equation

$$\frac{dx}{dt} = f(x), \quad (2.2.1)$$

a point x^* is a fixed point (steady-state) of the system if it is a solution of the algebraic equation

$$f(x) = 0. \quad (2.2.2)$$

Definition 2.2.2. (stability of steady-state)

A steady-state x^* is stable if and only if

$$\forall \epsilon > 0, \exists \delta(\epsilon) > 0, s.t. \|x(t_0) - x^*\| < \delta \implies \|x(t) - x^*\| < \epsilon, \forall t \geq t_0.$$

In other words, it says that there is a neighborhood of x^* such that any trajectory representing the solution of (2.2.1) entering that neighborhood will end in x^* .

A steady state is said to be unstable if it is not stable.

2.2.3 Linearization and structural stability

Studying the non-linear global and asymptotical stability of the fixed points of a non-linear dynamical system is quite complex as it is difficult to predict the effect of nonlinearity. The classical approach consists in finding the Lyapunov function to apply the Lyapunov theorem [70] that guarantees global and asymptotical stability. However, in practice, it is challenging to find a Lyapunov function, and the difficulty increases with the system's dimensionality. Nevertheless, it is always possible to study the structural stability of the fixed points, that is to say, study the trajectories of the solutions in the neighborhood of the fixed point. The Hartman-Grobman theorem allows us to say that the linearized system has the same qualitative structures near hyperbolic fixed points. Thus, the analysis of the stability of a fixed point of a non-linear system can be restricted to studying the behavior of the trajectories of the linearized system in the neighborhood of this fixed point.

Definition 2.2.4. (Linearized system) Considering the system (2.2.1), Taylor expansion allows rewriting (2.2.1) as follow

$$\frac{dx}{dt} = Df(x) + \mathcal{O}(\|x^2\|). \quad (2.2.3)$$

The ODE

$$\frac{dx}{dt} = Df(x) \quad (2.2.4)$$

will be called the linearized system associated with (2.2.1).

Definition 2.2.5. (Hyperbolic steady-state) Let us set

$$J = Df(x^*) \quad (2.2.5)$$

and x^* is a hyperbolic fixed point of (2.2.1) if and only if all the eigenvalues of J has non zeros real parts.

Remark 2.2.6. J is also known as the Jacobian matrix for the system (2.2.1) associated with the steady-state S^* .

Theorem 1. (Stable hyperbolic steady-state) *If all the eigenvalues of J have a strictly negative real part, then x^* is an asymptotically stable steady-state.*

Theorem 2. (Unstable hyperbolic steady-state) *If J has at least one eigenvalue with strictly positive real part, then the equilibrium x^* is unstable*

In the case of linear systems, theorems 1 and 2 give sufficient and necessary conditions for the stability or the non-stability of a non-hyperbolic equilibrium. However, in the case of a non-linear system, these conditions are only sufficient.

Theorem 3. (The Hartman-Grobman theorem) *Let x^* be a hyperbolic fixed point of the system (2.2.1). If f is continuously differentiable on its domain, then there exists a small open neighborhood \mathcal{U} of x^* so that the system (2.2.1) is topologically equivalent to its linearization (2.2.3) on \mathcal{U} .*

Given that in this Chapter 4, I am only interested in the stability of the steady-states, I will apply the above-mentioned theorem to determine the conditions for the metabolism of FAs to exhibit bi-stability.

2.3 Kinetic rate laws

This section gives a general overview of kinetic rate laws that I use in Chapters 4 and 5.

2.3.1 Elementary reactions and Mass actions rate laws

Elementary reactions are either reactions of spontaneous change of a molecule A to a molecule B (uni-molecular) or resulting from the collision between two molecules (bi-molecular) and, very rarely, of several molecules (multi-molecular). Uni-molecular elementary reactions are better known as decay processes, in which a molecule changes its nature to give another molecule (e.g., isomerization) or dissociates to give two molecules. Unimolecular reactions are first-order reactions because the product(s) formation rate is proportional to the reaction compound's concentration (reactant). Let us consider the two scenarios. In the first case, the compound A reacts to give B , and in the second case, A reacts to give B and C that is



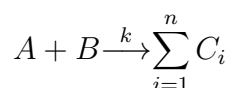
In both cases, the rate of disappearance of A over time v is

$$-v = \frac{dA}{dt} = -k[A],$$

and the rate of formation of product(s) in the two scenario are

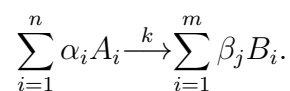
$$v = \frac{dB}{dt} = k[A], \quad v = \frac{dC}{dt} = k[A].$$

For bimolecular reactions, two reactants, A and B , react to give one or more products. The rate of disappearance of reactants and formation of product(s) follow the second-order kinetics, as they are proportional to the concentration of reactants. Hence, we have



$$-v = \frac{dA}{dt} = \frac{dB}{dt} = -k[A][B] \quad \text{and} \quad v = \frac{dC_i}{dt} = k[A][B], \quad 1 \leq i \leq n.$$

More generally, consider reactant A_1, A_2, \dots, A_n reacting to give m products B_1, B_2, \dots, B_m . To account for how many molecules of reactants and products are consumed and produced in a single reaction, we introduce the stoichiometry coefficients α_i and β_j . The reaction can be described with the following scheme,



The rate of disappearance of reactants and formation of products will is,

$$-v = \frac{dA_i}{dt} = -k \prod_{i=1}^n [A_i]^{\alpha_i} \quad \text{and} \quad v = \frac{dB_j}{dt} = \prod_{i=1}^n [A_i]^{\alpha_i}, \quad 1 \leq i \leq n, \quad 1 \leq j \leq m.$$

The constant k is the kinetic rate constant relating the reactants' concentrations and the reaction rate. It describes how fast the reaction occurs and is related to the temperature. The larger k is, the faster the reaction is.

So far, we have only considered reactions going in one direction (irreversible), yet almost all reactions proceed in both directions (reversible). And the corresponding net rate of the overall reaction is equal to the difference between the rate of the forward and the backward reaction. The choice of the forward and backward reactions can be made arbitrarily. However, in practice, The forward reaction is the one that is thermodynamically favorable. To give a better illustration, consider the following reversible with n reactants and m products reaction. The kinetic rate constants are k_f for the forward reaction and k_b for the backward reaction.



The rate of the forward reaction

$$v_f = k_f \prod_{i=1}^n [A_i]^{\alpha_i}, \quad (2.3.2)$$

and that of the backward reaction is

$$v_b = k_b \prod_{j=1}^n [B_j]^{\beta_j}. \quad (2.3.3)$$

Hence the net rate of the reaction is given by

$$v = v_f - v_b = k_f \prod_{i=1}^n [A_i]^{\alpha_i} - k_b \prod_{j=1}^n [B_j]^{\beta_j}. \quad (2.3.4)$$

At the equilibrium, the rates of the forward and the backward reactions are equal and one can derive the equilibrium constant

$$K_{eq} = \frac{k_f}{k_b} = \frac{\prod_{j=1}^n [B_j]_{eq}^{\beta_j}}{\prod_{i=1}^n [A_i]_{eq}^{\alpha_i}}, \quad (2.3.5)$$

where $[A_i]_{eq}$ and $[B_j]_{eq}$ are the concentrations of n reactants and m products, respectively.

The equilibrium constant is related to the thermodynamics of the reaction through the Gibbs' free energy of the reaction by the following relationship,

$$\Delta G = \Delta G^0 + RT \ln Q, \quad \text{with} \quad \Delta G^0 = -RT \ln K_{eq}.$$

ΔG defines the spontaneity of a reaction. Indeed, if $\Delta G < 0$, the reaction proceeds spontaneously; otherwise, the reaction will need external energy.

Remark 2.3.2. It is important to note that no matter how complex a chemical reaction is, it is always possible to break it down into elementary reactions. It is this observation that inspires us in the development of the model of Chapter 5.

2.3.3 Michaelis-Menten derived kinetics

We have seen earlier that it is possible that certain reactions are not taking place spontaneously and will need external intervention. Indeed, enzymes, through their catalytic action, can bring such an intervention. They are capable of reducing Gibbs' free energy. They have a catalytic site (active site) and an allosteric site (see Figure 2.1). The substrate(s) bind to the catalytic site, while other molecules not participating directly in the reaction can attach to the allosteric site. In this section, we are interested in some kinetic rate laws of one substrate enzyme-catalyzed reactions, particularly "Michaelian" kinetics. I used these kinetics, notably Michaelis-Menten kinetics and

non-competitive inhibition, to build the model studied in Chapter 4. Furthermore, in Chapter 5, I consider the description mechanism of competitive inhibition to represent the inhibition of FADNS by the free CoA.

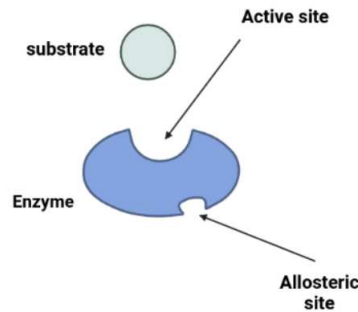


Figure 2.1: **Basic description of an enzyme** (Adapted from “Enzymes, Substrates, and Inhibitors”, by BioRender.com (2022). Retrieved from <https://app.biorender.com/biorender-templates>)

Michaelis-Menten Kinetics

The Michaelis-Menten equation [38, 71], for describing the kinetics of enzymatic reactions, might be the most famous in the field of enzyme kinetics. It allows describing the rate v of formation of the product as a function of the concentration of the substrate and two parameters reflecting the efficiency of the enzyme. In this paragraph, we present the derivation of Michaelis-Menten equations from the elementary reactions and key assumptions.

Consider the enzymatic reaction with one substrate (S), where the enzyme is denoted by E . In the first step, the enzyme binds with the substrate to form the complex enzyme-substrate ES , which in the second step reacts to form the product P and the enzyme E (see diagram 2.3.7). For the most recent derivation of the equation, the following assumptions are made:

- The backward reaction of dissociation of the complex ES into E and P negligible.
- The total concentration of enzyme participating in the reaction is conserved:

$$E_T = E + ES \quad (2.3.6)$$

- The concentrations of ES remains constant, although those of S and P are changing. This last consideration, known as the quasi-steady state assumption (QSSA) proposed by Briggs and Haldane [71], is crucial for deriving the equation.



From elementary reactions, the dynamic of the components of the system is described by the system of ODEs

$$\frac{d[S]}{dt} = -k_1[E][S] + k_{-1}[ES] \quad (2.3.8)$$

$$\frac{d[E]}{dt} = -k_1[E][S] + (k_{-1} + k_2)[ES] \quad (2.3.9)$$

$$\frac{d[ES]}{dt} = k_1[E][S] - (k_{-1} + k_2)[ES] \quad (2.3.10)$$

$$\frac{d[P]}{dt} = k_2[ES], \quad (2.3.11)$$

The overall rate of product formation is given by,

$$v = \frac{d[P]}{dt} = k_2[ES], \quad (2.3.12)$$

which is the same equation as (2.3.10). The idea is to express $[ES]$ in terms of known or tractable quantities. The last two assumptions will be applied for this purpose.

From the QSSA, we have:

$$\frac{d[ES]}{dt} = 0 \iff (k_{-1} + k_2)[ES] = k_1[E][S], \quad (2.3.13)$$

From the conservation of the enzyme species, one can express E in terms of $[E_T]$ and $[ES]$, and the above equation becomes

$$(k_{-1} + k_2)[ES] = k_1([E_T] - [ES])[S], \quad (2.3.14)$$

hence

$$[ES] = \frac{k_1[E_T][S]}{(k_{-1} + k_2) + k_1[S]} = \frac{[E_T][S]}{\frac{(k_{-1} + k_2)}{k_1} + [S]}. \quad (2.3.15)$$

By replacing ES , by its expression in (2.3.12) one obtains

$$v = \frac{k_2[E_T][S]}{\frac{(k_{-1} + k_2)}{k_1} + [S]}. \quad (2.3.16)$$

Let

$$V_{max} = k_2[E_T], \quad \text{and} \quad K_m = \frac{k_{-1} + k_2}{k_1}.$$

Thus the Michaelis-Menten equation can be written as

$$v = \frac{V_{max}[S]}{K_m + [S]}. \quad (2.3.17)$$

The equation displays a hyperbolic relation between the substrate concentration and the rate of formation of the product (see 2.2).

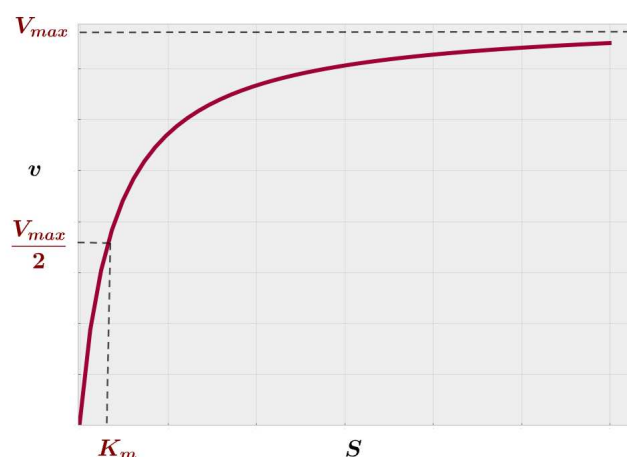


Figure 2.2: **Michaelis-Menten kinetics curve**

The graphical representation allows giving physical meaning to the equation parameter: V_{max} is the maximal rate of the reaction, and K_m is the substrate concentration that gives half of the maximum rate. For a particular reaction, these parameters can be estimated by using a Lineweaver-Burk plot if one has experimental data before hands (see 2.3). The Lineweaver-Burk plot is also known as the inverse plot because it results from expressing $\frac{1}{v}$ as a function of $\frac{1}{S}$ as follows

$$\frac{1}{v} = \frac{K_m}{V_{max}} \frac{1}{[S]} + \frac{1}{V_{max}}, \quad (2.3.18)$$

by using linear regression one can estimate K_m and V_{max} .

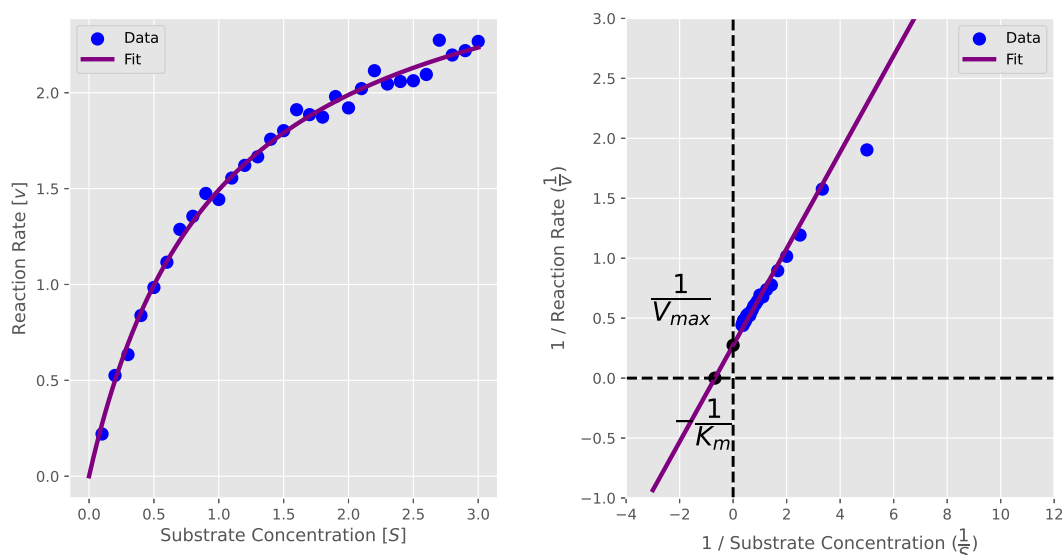


Figure 2.3: **How to extract the parameter of Michaelis-Menten equation using Lineweaver-Burk plot**

Remark 2.3.4. There is an earlier derivation of the Michaelis-Menten equation by Michaelis et al. [38] based on rapid equilibrium assumption instead of the QSSA. This derivation assumes that

the rate at which the equilibrium for the formation of the $[ES]$ complex is faster than the rate of formation of P . Hence, toward the course of the reaction, the formation of $[ES]$ is the chemical equilibrium, and one can define the dissociation constant

$$K_d = \frac{[E][S]}{[ES]} = \frac{k_{-1}}{k_1}$$

and express $[ES]$ in terms of $[E_T]$, K_d and $[S]$. using the same reasoning as for QSSA, one obtains the following formulation of Michaelis-Menten equations

$$v = \frac{V_{max}[S]}{K_d + [S]} \quad (2.3.19)$$

K_m defines the enzyme's affinity with the substrate. A lower K_m shows a high affinity, while a large K_m shows a low affinity.

In some cases, we may have compounds that do not directly participate in the reaction but influence its kinetics, as is the case for many biochemical reactions. A good example is the *in vivo* malonyl-CoA synthesis, where LCFAs inhibit the response. Generally, a compound external to a reaction can influence its kinetics in two ways. In the first case, it can enhance the kinetics; in this case, it is called an activator. In the second case, it can inhibit the reaction, and it is said to be an inhibitor. Given that I am only working with inhibition mechanisms in this thesis, I will briefly describe some of them and their influence on the Michaelis-Menten equation. Above all, note that in the presence of an inhibitor, the Michaelis-Menten equation remains valid, but with the parameters V_{max}^{app} and K_m^{app} . The superscript "app" means that they are apparent parameters due to the effect of the inhibitor.

In the following, we denote I any inhibitor, k_i , and k_{-i} kinetic rate constants for the forward and backward inhibition reaction, respectively.

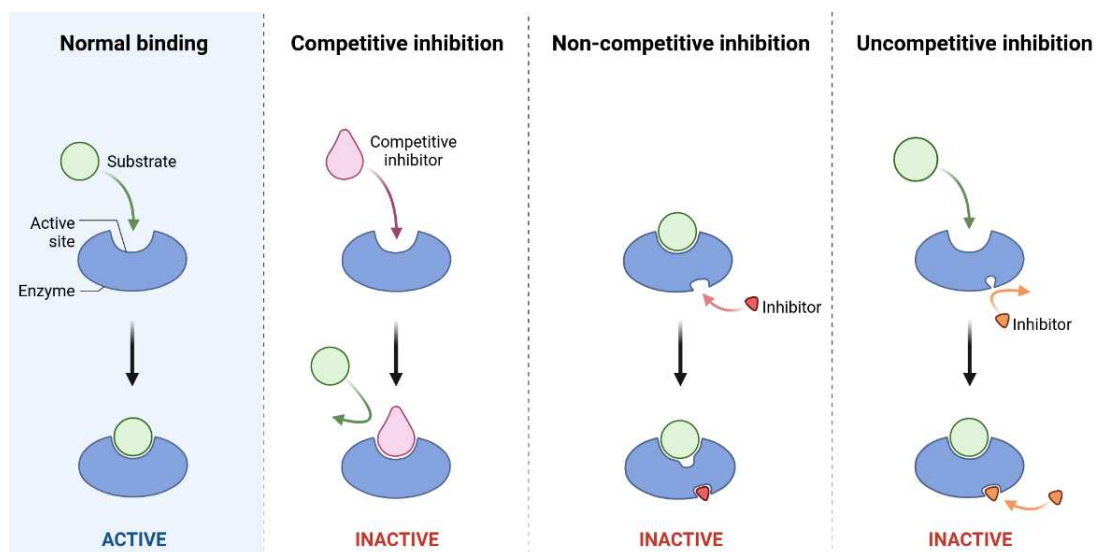


Figure 2.4: **Different type of inhibition** (Adapted from "Enzymes, Substrates, and Inhibitors", by BioRender.com (2022). Retrieved from <https://app.biorender.com/biorender-templates>)

Competitive inhibition

In the case of competitive inhibition, the inhibitor occupies the enzyme's active site, thus preventing the substrate from binding to the enzyme. Therefore, it reduces the enzyme's affinity for the substrate (increases the value of K_m). The competitive inhibition mechanism is described by Figure 2.4 and the equations (2.3.20) and (2.3.21).



The kinetic rate law is given by

$$v = \frac{V_{max}^{app}[S]}{K_m^{app} + [S]} = \frac{V_{max}[S]}{K_m(1 + \frac{[I]}{K_i}) + [S]}, \quad \text{with} \quad K_i = \frac{k_{-i}}{k_i}. \quad (2.3.22)$$

Thus, in the Michaelis-Menten formulation, we have

$$V_{max}^{app} = V_{max} \quad \text{and} \quad K_m^{app} = K_m(1 + \frac{I}{K_i}).$$

Uncompetitive inhibition

In the case of uncompetitive inhibition, the inhibitor occupies the allosteric site after the enzyme has already bound to the substrate, thus preventing the reaction to proceed. As a result, it reduces the enzyme's affinity for the substrate (increases the value of K_m) and the enzyme's capacity to release the product (V_{max}). The uncompetitive inhibition mechanism is described in Figure 2.4 and by equations (2.3.23) and (2.3.24).



The kinetic rate law is given by:

$$v = \frac{V_{max}^{app}[S]}{K_m^{app} + [S]} = \frac{V_{max}[S]}{K_m + [S](1 + \frac{[I]}{K_i})}, \quad \text{with} \quad K_i = \frac{k_{-i}}{k_i}. \quad (2.3.25)$$

Hence

$$V_{max}^{app} = V_{max}(1 + \frac{I}{K_i}) \quad \text{and} \quad K_m^{app} = K_m(1 + \frac{I}{K_i}).$$

Non-competitive inhibition

In non-competitive inhibition, the inhibitor occupies the allosteric site of the free enzyme, modifying its active site and preventing the substrate from binding. Equally, it can bind to the allosteric site after the complex enzyme substrate is formed, thus preventing the reaction from proceeding. As a result, it reduces the V_{max} . The non-competitive inhibition mechanism is described in Figure 2.4 and by equations (2.3.26)-(2.3.29).



The kinetic rate law is given by

$$v = \frac{V_{max}^{app}[S]}{K_m^{app} + [S]} = \frac{V_{max}[S]}{(K_m + [S])(1 + \frac{[I]}{K_i})}, \quad \text{with } K_i = \frac{k_{-i}}{k_i}. \quad (2.3.30)$$

Hence

$$V_{max}^{app} = \frac{V_{max}}{1 + \frac{[I]}{K_i}} \quad \text{and} \quad K_m^{app} = K_m.$$

In Chapter 4.1, I use only the Michaelis-Menten equation and non-competitive inhibition to describe the kinetics of processes associated with FA metabolism. We decided to mention the other types of inhibition as a basis for comparison, and also to question the choice of the mechanism of inhibition.

2.4 Fitting method: Lavenberg-Marquart algorithm

Once a mathematical model representing a biological system is constructed, experimental data (observable) are essential in measuring how accurately the model describes the system and its predictive value. As part of the answer to these questions, it is to find the best parameterization such that the model is close enough to the system. Finding such a parameterization is known as fitting the model to data by continuously adjusting the parameterization until the model displays the behavior of the data. The fitting relies on optimization techniques that minimize an objective function describing the distance between the output of the model and the data. For example, one can choose to minimize the sum of the square of differences (SSD) between the model output and the data under a set of constraints or not. They are mainly two classes of optimization techniques: linear and non-linear optimization. The linear optimization techniques are used when the objective

function and all the constraints are linear (affine is considered linear) with the parameters to be optimized. If that is not the case, as in Chapter 5, one should use the non-linear optimization techniques. This section intends to briefly describe the Lavenberg-Marquart algorithm, which will be used to fit the model developed in Chapter 5 to experimental data. To introduce the Lavenberg-Marquart method, one needs the Gradient descent method and Gauss newton method that I present in the following.

To simplify the description, we assume that the model output and the data are one dimension and that the system under study is a time-dependent process. Let us consider a model f that depends on the parameterization θ describe by the following diagram

$$\begin{aligned} f: \mathbb{R}^p &\rightarrow \mathbb{R} \\ \theta &\mapsto y, \end{aligned} \tag{2.4.1}$$

let suppose that we have m observable $\bar{y}(t_1), \bar{y}(t_2), \dots, \bar{y}(t_m)$. We would like to find a parameterization $\tilde{\theta}$ that minimizes the distance between the output of the model and the observable. In order words

$$\tilde{\theta} = \operatorname{argmin} \chi(\theta), \tag{2.4.2}$$

where

$$\chi(\theta) = \sum_{i=1}^m \left(\frac{f(t_i, \theta) - \bar{y}(t_i)}{\sigma_i} \right)^2 = \sum_{i=1}^m r_i(\theta). \tag{2.4.3}$$

2.4.1 The Gradient descent method

The method requires the objective function χ to be differentiable and convex, as the differentiability ensures the existence of the gradient that allows finding the steepest descent, and the convexity ensures the presence of the global minimum. The method is iterative and consists in starting from an arbitrary value of the parameter vector θ_0 , at each iteration k , updating the parameter in the direction of the steepest descent ($-\nabla\chi(\theta_k)$, the negative of the gradient), with the step α_k . The iteration scheme is given by

$$\theta_{k+1} = \theta_k - \alpha_k \nabla\chi(\theta_k). \tag{2.4.4}$$

Notice that at each iteration, one must compute the gradient of χ at θ_k , $\nabla\chi(\theta_k)$ and α_k . α_k is computed by solving the one dimension optimization problem

$$\alpha_k = \operatorname{argmin}_{\alpha \in \mathbb{R}} \chi(\theta_k - \alpha \nabla\chi(\theta_k)) \tag{2.4.5}$$

The algorithm stops when the minimum (θ_{min}) is reached. Indeed, θ_{min} is the solution of the equation

$$\|\nabla\chi(\boldsymbol{\theta})\| = 0. \quad (2.4.6)$$

Remark 2.4.2. In practice, the equation (2.4.6) is not set as a stopping condition. Rather, an acceptable tolerance value $\varepsilon > 0$ is chosen, and the stopping condition is

$$\|\nabla\chi(\boldsymbol{\theta})\| < \varepsilon. \quad (2.4.7)$$

When far away from θ_{min} , α_k is big, and the method converges faster. However, when close to θ_{min} , α_k becomes slower, resulting in slow convergence. The cost for computing for α_k at each iteration can be very expensive, especially when getting close to θ_{min} . Indeed, the step sizes α_k become very small, resulting in slow convergence. The Gauss-Newton Method has the power to correct this last limitation.

2.4.3 The Gauss-Newton method

The Gauss-Newton methods is specific for solving the least square optimization problem (the objective function is written as the sum of squared residuals).

One can notice that the equation (2.4.3) is written as a sum of squares of residuals, therefore suitable to describe the Gauss-Newton method.

Like the gradient descent gradient method, this method is iterative based on the general Newton method to find the minimum θ_{min} of any function starting from an arbitrary initial guess θ_0 . In the case studied in this section, the Newton iteration scheme is written as follows

$$\boldsymbol{\theta}_{k+1} = \boldsymbol{\theta}_k - (\nabla^2\chi(\boldsymbol{\theta}_k))^{-1}\nabla\chi(\boldsymbol{\theta}_k). \quad (2.4.8)$$

It is often expensive to compute the Hessian term $\nabla^2\chi(\boldsymbol{\theta}_k)$. To solve this issue, one can approximate the Hessian term with an expression including only the gradient, which is less expensive to compute. Indeed

$$\nabla^2\chi(\boldsymbol{\theta}_k) = \nabla\chi(\boldsymbol{\theta}_k)\nabla\chi(\boldsymbol{\theta}_k)^T + \sum_{i=1}^m r_i(\boldsymbol{\theta}_k)\nabla^2 r_i(\boldsymbol{\theta}_k). \quad (2.4.9)$$

By neglecting the second term of the right-hand side of (2.4.9), one obtains the following approximation of the Hessian matrix

$$\nabla^2\chi(\boldsymbol{\theta}_k) \approx \nabla\chi(\boldsymbol{\theta}_k)\nabla\chi(\boldsymbol{\theta}_k)^T, \quad (2.4.10)$$

replacing the Hessian in the equation (2.4.8), one obtains the iteration scheme of the Gauss-Newton method

$$\boldsymbol{\theta}_{k+1} = \boldsymbol{\theta}_k - (\nabla\chi(\boldsymbol{\theta}_k)\nabla\chi(\boldsymbol{\theta}_k)^T)^{-1}\nabla\chi(\boldsymbol{\theta}_k). \quad (2.4.11)$$

The stopping condition can be set by choosing two positive reals ε and δ , and the iteration will terminate when either

$$\|\nabla\chi(\boldsymbol{\theta})\| < \varepsilon \quad (2.4.12)$$

or

$$|\boldsymbol{\theta}_k - \boldsymbol{\theta}_{k-1}| < \delta. \quad (2.4.13)$$

The Gauss-newton method converges but only quadratically around the $\boldsymbol{\theta}_{min}$, which was not the case with gradient descent methods.

2.4.4 Lavenberg-Marquart algorithm

Earlier, we noted the limitations of the gradient descent and Gauss-Newton methods. In particular, the weak convergence around $\boldsymbol{\theta}_{min}$ for that of gradient descent and a weak convergence far from $\boldsymbol{\theta}_{min}$ for the Gauss-Newton method. The Lavenberg-Marquardt algorithm combines the two methods to take advantage of their strength. Indeed, it behaves like the gradient descent method when far from $\boldsymbol{\theta}_{min}$ and like the Gauss-Newton method when close.

By noting that in the case of the gradient descent and Gauss-Newton methods, the iterative scheme can be written as

$$\boldsymbol{\theta}_{k+1} = \boldsymbol{\theta}_k - \omega \nabla\chi(\boldsymbol{\theta}_k)$$

with

$$\omega = \alpha_k$$

in the case of the gradient descent and

$$\omega = (\nabla\chi(\boldsymbol{\theta}_k)\nabla\chi(\boldsymbol{\theta}_k)^T)^{-1}$$

in the case of Gauss-Newton, Lavenberg proposes the following scheme

$$\boldsymbol{\theta}_{k+1} = \boldsymbol{\theta}_k - (\nabla\chi(\boldsymbol{\theta}_k)\nabla\chi(\boldsymbol{\theta}_k)^T + \alpha_k\mathbf{I})^{-1}\nabla\chi(\boldsymbol{\theta}_k) \quad (2.4.14)$$

that include the features of the two methods. However, when evaluated far from $\boldsymbol{\theta}_{min}$, the $\alpha_k\mathbf{I}$ is dominant compared to the contribution of the Hessian matrix, and therefore the Hessian term is almost not used. By remarking that the Hessian matrix is proportional to the curvature, Marquardt

later suggests replacing the identity matrix with the diagonal matrix made of diagonal entry of the Hessian. Hence, we obtain the Lavenberg-Marquart scheme:

$$\boldsymbol{\theta}_{k+1} = \boldsymbol{\theta}_k - (\nabla\chi(\boldsymbol{\theta}_k)\nabla\chi(\boldsymbol{\theta}_k)^T + \alpha_k \text{diag}(\boldsymbol{\theta}_k)\nabla\chi(\boldsymbol{\theta}_k)^T)^{-1}\nabla\chi(\boldsymbol{\theta}_k). \quad (2.4.15)$$

The Lavenberg-Marquardt algorithm generally converges quadratically and uses the same stopping condition as the Gauss-Newton method. The literature presents numerous directions to improve these techniques. Good starting points are the books by Nocedal and Wright [72] and Boyd et al. [73] that I used for writing this section. I will present an example where I used `lmfit` [74] *Python* package to show how the Lavenberg-Marquardt is an excellent fitting algorithm for non-linear least square problems.

lmfit package

`lmfit` is a *Python* package that allows solving the non-linear optimization problem. Initially, the package was developed only to apply the Levenberg-Marquardt algorithm (default method) to solve non-linear least square optimization problems, but it has been extended to various forms. A quick search on Google Scholar shows that the package has been used approximately a thousand times in different disciplines. The package has the advantage of returning several pieces of information, such as the confidence interval, and Akaike info criterion, the Bayesian info criterion as shown in the example below.

Example 2.4.5. In this example, I would like to show how the Python-based library `lmfit` [74] is powerful for non-linear optimization.

Consider the following mathematical function

$$f: \mathbb{R} \rightarrow \mathbb{R}^3 \\ (\mathbf{x}) \mapsto (f_1(x), f_2(x), f_3(x)),$$

where

$$\begin{cases} f_1(x) = \frac{ax + c}{x^2 + 1} + \frac{dx}{\exp(x + 1)} \\ f_2(x) = a\sqrt{x} + d \sin x + b \cos x \\ f_3(x) = -bx + \frac{c}{ax^4 + 1} + d \cos x. \end{cases}$$

To generate the data, the values of a , b , c , and d were set to 2, 0.2, 10, and 3, respectively. Then the standardized normally distributed noise around the function output were added. Then `lmfit` was used to estimate the value of the parameters a , b , c , and d that allow to best reproduce the data.

I start with three initial guesses for the parameter vector (a, b, c, d) to be $(0.1, 0.01, 0.7, 0.3)$, $(10, 21, 27, 50)$, and $(0.006, 33, 2.7, 0.08)$. The three fits equally produce the same estimate of the vector $(\hat{a}, \hat{b}, \hat{c}, \hat{d}) = (2.007, 0.198, 9.855, 2.98)$. Figure 2.5 shows the visualization of the fitting results.

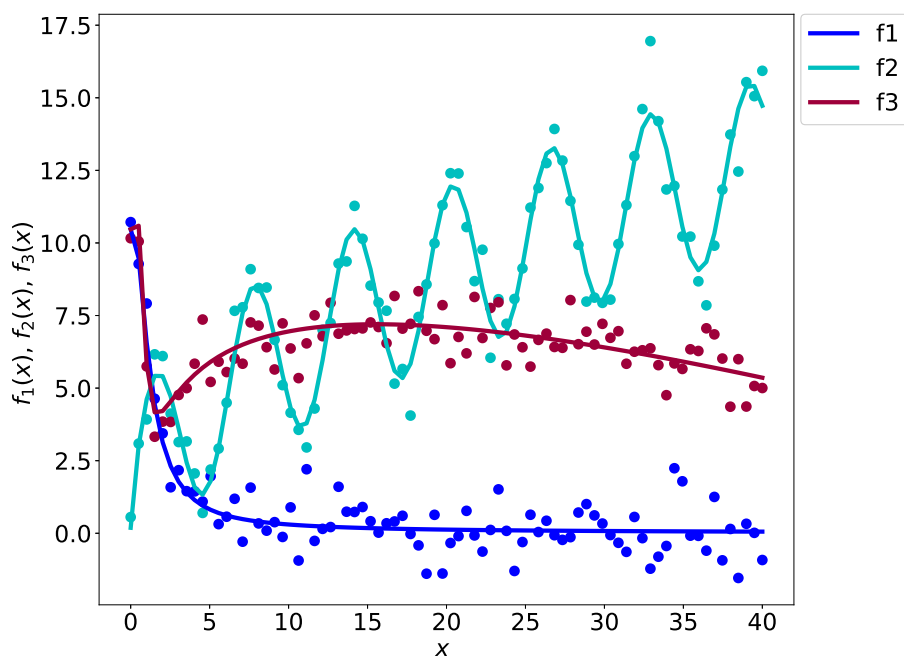


Figure 2.5: Fitting result with lmfit library

```
[[Fit Statistics]]
# fitting method = leastsq
# function evals = 36
# data points = 240
# variables = 4
chi-square = 122.415157
reduced chi-square = 0.51870829
Akaike info crit = -153.572975
Bayesian info crit = -139.650419
[[Variables]]
a: 2.00766892 +/- 0.01799346 (0.90%) (init = 10)
b: 0.19769103 +/- 0.00975653 (4.94%) (init = 21)
c: 9.85508511 +/- 0.36302912 (3.68%) (init = 27)
d: 2.98016729 +/- 0.06296143 (2.11%) (init = 12)
[[Correlations]] (unreported correlations are < 0.100)
C(b, d) = 0.934
```

2.4.6 Sensitivity analysis

Creating parsimonious models representing physical processes presents many difficulties in design and validation. Regarding the design, the question of the model's size and the detail level are not questions that can be addressed straightforwardly. As for the validation of the model, it often consists of the estimation of the parameters, which can be costly. It becomes crucial to study the model's parameterization to tackle the issues mentioned above. i.e., measuring the contribution of each parameter to the output of the model. Thus one can classify the parameters according to their importance and prioritize those that significantly contribute to the model. Sensitivity Analysis (SA) is the mathematical formalism that allows such study not only from a qualitative point of view, but also quantitatively. It allows for checking whether the model faithfully describes the phenomenon under study. For instance, If an input parameter that *a priori* is known to have less importance turns to exert a significant contribution to the model's output, then the model does not reflect the process under study and should be improved. Furthermore, identifying the influential parameters permits reducing the volatility by enhancing the quality of the model's parameterization or modifying its structure to attenuate. Identifying the less significant parameters reduces the model size, complexity, or parameterization, for example, by deleting the part of the model inherent to those parameters. SA enables the measurement of the interaction between the parameters of the model. There are three classes of sensitivity analysis. 1) the screening method whose best-known approach is that of Morris [75]. It allows qualitatively classifying the model's input parameters according to their importance. 2) The local approach measure quantitatively the variation of the model's output in response to a perturbation of the parameter vector around a particular nominal value [76, 77]. 3) The global approach, which is also quantitative, measures the model's response following variation of the parameter vector over its variability domain. The best-known method for studying global sensitivity analysis (GSA) is based on the calculation of Sobol indices [78]. Here I present a description of the GSA used to classify model parameters of *de novo* fatty acid synthesis according to their contributions to model uncertainty (see Chapter 5).

Let us consider the abstract deterministic model describing a physical process represented by

$$\mathbf{y} = f(\mathbf{x}, \boldsymbol{\theta}), \quad (2.4.16)$$

where

$$\begin{aligned} f: \mathbb{R}^n \times \mathbb{R}^p &\rightarrow \mathbb{R}^m \\ (\mathbf{x}, \boldsymbol{\theta}) &\mapsto \mathbf{y}, \end{aligned}$$

- $\boldsymbol{\theta} = (\theta_1, \theta_2, \dots, \theta_p)$ is the vector of parameter input of the model
- $\mathbf{x} = (x_1, x_2, \dots, x_n)$ is the vector input variables of the system. In our case, it could represent the vector of different metabolites of the pathways.

- $\mathbf{y} = (y_1, y_1, \dots, y_m)$ is the vector output of the model. in our case, it could be some selected metabolites produced by the model.

Since our SA focuses on the parameterization of the system, to ease the notation, I will ignore \mathbf{x} in the definition of f . Hence, f will be defined as follows

$$\begin{aligned} f: \mathbb{R}^p &\rightarrow \mathbb{R}^m \\ \boldsymbol{\theta} &\mapsto \mathbf{y}, \end{aligned} \quad (2.4.17)$$

Local sensitivity analysis (LSA)

A multi-index $\boldsymbol{\alpha}$ is a p -tuple of positive integer $(\alpha_1, \dots, \alpha_p)$. Multi-indices are very useful in differential calculus as it allows a rigorous definition of the differential in high-dimension spaces. Let $\boldsymbol{\alpha} = (\alpha_1, \alpha_2, \dots, \alpha_p)$ be a multi index, and define

$$\begin{aligned} |\boldsymbol{\alpha}| &= \sum_{i=1}^p \alpha_i, \quad \boldsymbol{\alpha}! = \prod_{i=1}^p \alpha_i!, \quad \forall \boldsymbol{\theta} \in \mathbb{R}^p, \quad \boldsymbol{\theta}^\alpha = \prod_{i=1}^p \theta_i^{\alpha_i} \\ \partial^\alpha f &= \left(\prod_{i=1}^p \partial_i^{\alpha_i} \right) f = \frac{\partial^{|\boldsymbol{\alpha}|} f}{\partial \theta_1^{\alpha_1} \partial \theta_2^{\alpha_2} \dots \partial \theta_p^{\alpha_p}} \end{aligned}$$

Let $\boldsymbol{\theta}^0 = (\theta_1^0, \theta_2^0, \dots, \theta_p^0)$ a nominal value of the parameter vector $\boldsymbol{\theta}$. Using Taylor's expansion the order k one can express the variation of the \mathbf{y} due to a small change $\boldsymbol{\zeta} = (\zeta_1, \dots, \zeta_p)$ of $\boldsymbol{\theta}$ by

$$\Delta \mathbf{y}(\boldsymbol{\theta}^0) = f(\boldsymbol{\theta}^0 + \boldsymbol{\zeta}) - f(\boldsymbol{\theta}^0) = Df(\boldsymbol{\theta}^0)(\boldsymbol{\zeta}) + \dots + D^k f(\boldsymbol{\theta}^0)(\boldsymbol{\zeta})^k + o(\|\boldsymbol{\zeta}\|^k), \quad (2.4.18)$$

with

$$D^k f(\boldsymbol{\theta}^0)(\boldsymbol{\zeta})^k = \sum_{|\boldsymbol{\alpha}|=k} \frac{\partial^\alpha f}{\boldsymbol{\alpha}!}(\boldsymbol{\theta}^0) \boldsymbol{\zeta}^\alpha.$$

For $k > 1$, the terms $D^k f(\boldsymbol{\theta}^0)(\boldsymbol{\zeta})^k$ represent the non-linear response due to the interaction of the different combination of the parameters $p_i \in \boldsymbol{\theta}$. In the local sensitivity analysis, one ignore higher interaction and only consider the Taylor expansion to the order 1 as $o(\|\boldsymbol{\zeta}\|^1)$ tends to 0 as $\boldsymbol{\zeta}$ tends 0. Thus (2.4.18) can be written after expansion of the term $Df(\boldsymbol{\theta}^0)(\boldsymbol{\zeta})$ as follows

$$f(\boldsymbol{\theta}^0 + \boldsymbol{\zeta}) - f(\boldsymbol{\theta}^0) = \sum_{j=1}^p \zeta_j \frac{\partial f}{\partial \theta_j}(\boldsymbol{\theta}^0) + o(\|\boldsymbol{\zeta}\|). \quad (2.4.19)$$

Let

$$S_j = \frac{\partial f}{\partial \theta_j}(\boldsymbol{\theta}^0) = \left(\frac{\partial f_1}{\partial \theta_j}(\boldsymbol{\theta}^0), \frac{\partial f_2}{\partial \theta_j}(\boldsymbol{\theta}^0), \dots, \frac{\partial f_m}{\partial \theta_j}(\boldsymbol{\theta}^0) \right) \quad (2.4.20)$$

As defined, the sensitivity index S_j is not a standardized quantity, which makes it impossible to compare other sensitivity indices that are not expressed by the same units. For the specific case

of $m = 1$ in the definition (2.4.17) It is then advisable to favor a standardized sensitivity index defined by

$$S_j^* = \frac{\theta_j^0}{f(\boldsymbol{\theta}^0)} \frac{\partial f}{\partial \theta_j}(\boldsymbol{\theta}^0) \quad (2.4.21)$$

S_j measures the response of \mathbf{y} due to a small change in the j entry θ_j^0 of $\boldsymbol{\theta}^0$. In practice, local sensitivity is studied by calculating each S_j separately. This justifies the designation of one factor at the time (OAT) given to the method. The LSA can be expensive for a relatively large model, as its computation often uses brute-force methods based on "trial and error," which is expensive [76]. Furthermore, for a non-linear model, the input and the output are often in different orders of magnitude, and the inter-dependence between the parameters is difficult to identify.

Global sensitivity analysis (GSA): Sobol indices

We have pointed out the limitations of LSA, especially in the case of nonlinear models. For a more reliable analysis, it is necessary to use a more global approach to evaluate the model's response in its entire parameterization range. In addition, the analysis must consider the correlation between the parameters of the model. As mentioned earlier, the S_j calculated in the LSA case does not provide information on how changing one parameter p_j of the model affects the other parameters. The Sobol method can be used to solve the above problems. The method is based on decomposing the variance of the model output into terms representing the contributions of each parameter taken separately, as well as the contributions of different combinations of these parameters. Without loss of generality, and to facilitate the presentation of Sobol's method, we will assume that $m = 1$ in the definition of the function f in (2.4.17). Hence

$$\begin{aligned} f: \mathbb{R}^p &\rightarrow \mathbb{R} \\ \boldsymbol{\theta} &\mapsto \mathbf{y}. \end{aligned} \quad (2.4.22)$$

In general, the analytical form of the function f that the model represents is not accessible. However, the variance $V(\mathbf{y})$ of its output values \mathbf{y} can be evaluated. To ensure the existence of the variance of \mathbf{y} , suppose that the f is L^2 a square-integrable function, that is to say

$$\int \|f\|^2 < \infty,$$

then in its work to define the sensitivity index, Sobol [79] introduces the following decomposition of f known as Sobol-Hoeffding decomposition:

$$\mathbf{y} = f_0 + \sum_{i=1}^p f_i(\theta_i) + \sum_{1 \leq i < j \leq p} f_{i,j}(\theta_i, \theta_j) + \cdots + \sum_{1 \leq i_1 < i_2 < \cdots < i_{p-1} \leq p} f_{i_1, i_2, \dots, i_{p-1}}(\theta_{i_1}, \dots, \theta_{i_{p-1}}) + f_{1, \dots, p}(\theta_1, \dots, \theta_p), \quad (2.4.23)$$

where

$$\begin{aligned}
f_0 &= \mathbb{E}(y), \\
f_i(\theta_i) &= \mathbb{E}(y|\theta_i) - f_0, \\
f_{i,j}(\theta_i, \theta_j) &= \mathbb{E}(y|\theta_i, \theta_j) - f_i - f_j - f_0, \\
f_{i,j,k}(\theta_i, \theta_j, \theta_k) &= \mathbb{E}(y|\theta_i, \theta_j, \theta_k) - f_{i,j} - f_{i,k} - f_{j,k} - f_i - f_j - f_k - f_0 \\
&\vdots
\end{aligned}$$

Taking the variance of both sides of the equation (2.4.23) one gets

$$V = + \sum_{i=1}^p V_i + \sum_{1 \leq i < j \leq p} V_{i,j} + \cdots + \sum_{1 \leq i_1 < i_2 < \cdots < i_{p-1} \leq p} V_{i_1, i_2, \dots, i_{p-1}} + V_{1, \dots, p}, \quad (2.4.24)$$

with

$$\begin{aligned}
V &= \text{Var}(\mathbf{y}) \\
V_i &= V(\mathbb{E}(y|\theta_i)) \\
V_{i,j} &= V(\mathbb{E}(y|\theta_i, \theta_j)) - V_i - V_j \\
V_{i,j,k} &= V(\mathbb{E}(y|\theta_i, \theta_j, \theta_k)) - V_{i,j} - V_{i,k} - V_{j,k} - V_i - V_j - V_k \\
&\vdots \\
V_{1,2, \dots, p} &= V - \sum_{i=1}^p V_i - \sum_{1 \leq i < j \leq p} V_{i,j} - \cdots - \sum_{1 \leq i_1 < i_2 < \cdots < i_{p-1} \leq p} V_{i_1, i_2, \dots, i_{p-1}}.
\end{aligned}$$

Sobol defines the following sequence of indices

$$\begin{aligned}
S_i &= \frac{V_i}{V}, \\
S_{i,j} &= \frac{V_{i,j}}{V}, \\
S_{i,j,k} &= \frac{V_{i,j,k}}{V}, \\
&\vdots \\
S_{1,2, \dots, p} &= \frac{V_{1,2, \dots, p}}{V}.
\end{aligned} \quad (2.4.25)$$

S_i represents the contribution of θ_i to the variance of \mathbf{y} , $S_{i,j}$ represents the contribution of the interaction of θ_i, θ_j to the variance of \mathbf{y} , $S_{i,j,k}$ is the contribution of the interaction of θ_i, θ_j and θ_k to the variance of \mathbf{y} , and so on.

One should note that

$$\sum_{i=1}^p S_i + \sum_{1 \leq i < j \leq p} S_{i,j} + \cdots + \sum_{1 \leq i_1 < i_2 < \cdots < i_{p-1} \leq p} S_{i_1, i_2, \dots, i_{p-1}} + S_{1, \dots, p} = 1, \quad (2.4.26)$$

this means that the closer the value of an index is to 1, the greater the influence of the corresponding parameter or the interactions of the corresponding group of parameters on the model result.

Finally, Sobol [79] defines the total index of a parameter θ_i as

$$S_{T_i} = S_i + \sum_{\substack{j=1 \\ j \neq i}}^p S_{i,j} + \sum_{\substack{j=1 \\ j \neq i}} + \sum_{\substack{k>j \\ k \neq j \\ k \neq i}} S_{i,j,k} + \cdots + S_{i,j,k,\dots,p}, \quad (2.4.27)$$

representing the contributions θ_i and its interactions with other parameters. S_{T_i} can also be written as

$$S_{T_i} = 1 - \frac{\text{Var}(E(\mathbf{y}|\theta_{\sim i}))}{V} = 1 - \frac{V_{\sim i}}{V}, \quad (2.4.28)$$

where $V_{\sim i}$ represents the variance of the conditional expectation \mathbf{y} given all the other parameters θ_j parameters except θ_i . In practice, the equation (2.4.28) is used to compute S_{T_i} .

For example, if $p = 3$,

$$S_{T_1} = S_1 + S_{1,2} + S_{1,3} + S_{1,3,3} \quad \text{and} \quad S_{T_2} = S_2 + S_{1,2} + S_{2,3} + S_{1,3,3}.$$

One should notice that the calculation of one of the Sobol's total index S_{T_i} requires the calculation of the indices of order 1 to p defined in the equation (2.4.25), which are $2^p - 1$ indices. For p large, the computation of the total index will be very expensive. In practice, Monte Carlo methods are used. In the following, I describe the sampling methods for estimating the indices defined in (2.4.25).

Suppose $\boldsymbol{\theta}$ is a random vector following an arbitrary distribution, and let us sample N times $\boldsymbol{\theta}$. Hence, the estimation of the $f_0 = \mathbb{E}(\mathbf{y})$ and the variance V over the sample of size N are

$$\hat{f}_0 = \frac{1}{N} \sum_{k=1}^N f(\boldsymbol{\theta}^k), \quad \text{and} \quad \hat{V} = \frac{1}{N} \sum_{k=1}^N f^2(\boldsymbol{\theta}^k) - \hat{f}_0^2, \quad (2.4.29)$$

where $\boldsymbol{\theta}^i$ is the i th sample of $\boldsymbol{\theta}$.

Estimate \hat{S}_i of S_i

We have

$$V_i = U_i - f_0^2, \quad \text{where} \quad U_i = \mathbb{E}[(\mathbb{E}(\mathbf{y}|\theta_i))^2],$$

hence the estimate of the V_i is

$$\hat{V}_i = \hat{U}_i - \hat{f}_0^2. \quad (2.4.30)$$

To compute \hat{U}_i one needs two samples of size N , $\boldsymbol{\theta}_{(N)}^{(1)}$ and $\boldsymbol{\theta}_{(N)}^{(2)}$ of $\boldsymbol{\theta}$.

$$\hat{U}_i = \frac{1}{N} \sum_{k=1}^N f(\theta_{k1}^{(1)}, \dots, \theta_{k(i-1)}^{(1)}, \theta_{ki}^{(1)}, \theta_{k(i+1)}^{(1)}, \dots, \theta_{kp}^{(1)}) \times f(\theta_{k1}^{(2)}, \dots, \theta_{k(i-1)}^{(2)}, \theta_{ki}^{(1)}, \theta_{k(i+1)}^{(2)}, \dots, \theta_{kp}^{(2)}), \quad (2.4.31)$$

Hence

$$\hat{S}_i = \frac{\hat{V}_i}{\hat{V}}. \quad (2.4.32)$$

Estimate $\hat{S}_{i,j}$ of $S_{i,j}$ By proceeding similarly to the estimation of S_i , one obtains

$$\hat{S}_{i,j} = \frac{\hat{V}_{i,j}}{\hat{V}}, \quad (2.4.33)$$

with the estimate of $V_{i,j}$,

$$\hat{V}_{i,j} = \hat{U}_{i,j} - \hat{f}_0^2 - \hat{V}_i - \hat{V}_j, \quad (2.4.34)$$

where

$$\hat{U}_{i,j} = \frac{1}{N} \sum_{k=1}^N f(\theta_{k1}^{(1)}, \dots, \theta_{k(i-1)}^{(1)}, \theta_{ki}^{(1)}, \theta_{k(i+1)}^{(1)}, \dots, \theta_{kj}^{(1)}, \theta_{k(j+1)}^{(1)}, \dots, \theta_{kp}^{(1)}) \times f(\theta_{k1}^{(2)}, \dots, \theta_{k(i-1)}^{(2)}, \theta_{ki}^{(1)}, \theta_{k(i+1)}^{(2)}, \dots, \theta_{kj}^{(1)}, \theta_{k(j+1)}^{(2)}, \dots, \theta_{kp}^{(2)}). \quad (2.4.35)$$

Estimate \hat{S}_{T_i} of ST_i

Proceeding similarly to the previous cases, one obtains

$$\hat{S}_{T_i} = 1 - \frac{\hat{V}_{\sim i}}{\hat{V}}, \quad (2.4.36)$$

with

$$\hat{V}_{\sim i} = \mathbb{E}(\widehat{\mathbf{Y}}|\theta_{\sim i})^2 - (\mathbb{E}(\widehat{\mathbf{Y}}|\theta_{\sim i}))^2 = \hat{U}_{\sim i} - \hat{f}_0^2, \quad (2.4.37)$$

and estimate of $U_{\sim i}$

$$\hat{U}_{\sim i} = \frac{1}{N} \sum_{k=1}^N f(\theta_{k1}^{(1)}, \dots, \theta_{k(i-1)}^{(1)}, \theta_{ki}^{(1)}, \theta_{k(i+1)}^{(1)}, \dots, \theta_{kp}^{(1)}) \times f(\theta_{k1}^{(1)}, \dots, \theta_{k(i-1)}^{(1)}, \theta_{ki}^{(2)}, \theta_{k(i+1)}^{(1)}, \dots, \theta_{kp}^{(1)}). \quad (2.4.38)$$

Since the number of simulations necessary to calculate the Sobol's indices for a sample of size N is $2N$, to compute the index of all orders up to p , the function f will be called $N \times 2^p$ times, which is very expensive for N large. However, to estimate the first-order and total indices, f is called only $N \times (2p + 1)$. Therefore, it is advisable to first compute the first-order index and the total indices before looking at the higher-order indices.

In practice, θ is not extracted from an arbitrary random distribution but from a quasi-random distribution known as Sobol's sequence (Sobol sampling) [80, 81]. The processes that generate quasi-random numbers, such as the Sobol sequence, are not truly random but are designed to distribute the numbers evenly over the range of numbers in a sequence. Unlike purely random numbers, which are generated using stochastic processes, quasi-random numbers are deterministic and repeatable. They exhibit improved distribution properties and aim to reduce clustering and clumping of points.

However, it is important to note that Sobol's sequence is not random in the traditional sense. Each number in the sequence is determined by a specific algorithmic calculation based on the previous numbers in the sequence. As a result, the sequence is not subject to the same level of randomness as truly random numbers generated by stochastic processes. Figure 2.6 illustrates the difference between Sobol sampling and random sampling, highlighting the more evenly distributed nature of Sobol's sequence compared to purely random numbers.

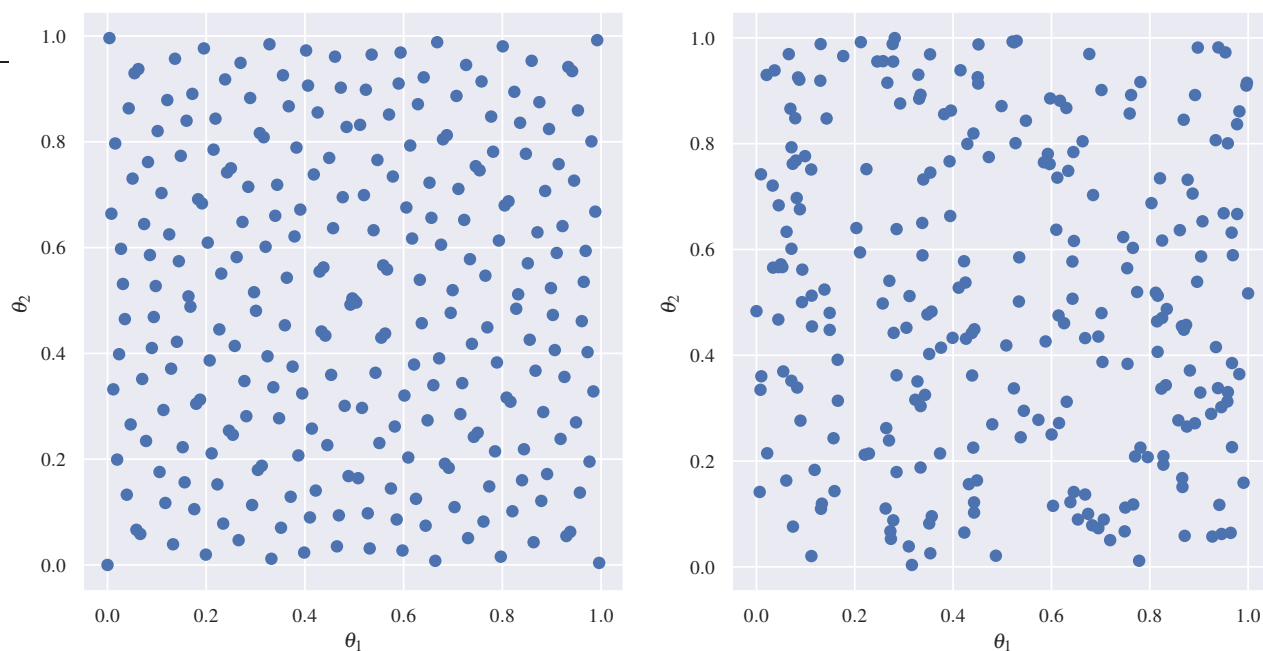


Figure 2.6: **Sobol sampling vs. random sampling**: In the left panel, we have a Sobol sample of 256 points couples of points (θ_1, θ_2) between 0 and 1, and the right panel random sample of 256 couples of points (θ_1, θ_2) between 0 and 1. The Sobol sample is evenly distributed in the sample space, whereas the random sample does not uniformly cover the sample space uniformly.

Example 2.4.7. In this example, I present a system made of a linear opened model composed of the compounds A and B . The influx in the system via the compound A is constant and associated with the parameter k_1 . The internal reactions follow the mass action kinetics with the kinetic rate constant k_2 . The outflux is proportional to the concentration of the compounds B . I apply Sobol's sensitivity analysis to evaluate the contribution of each parameter to the uncertainty of the time course of the system.

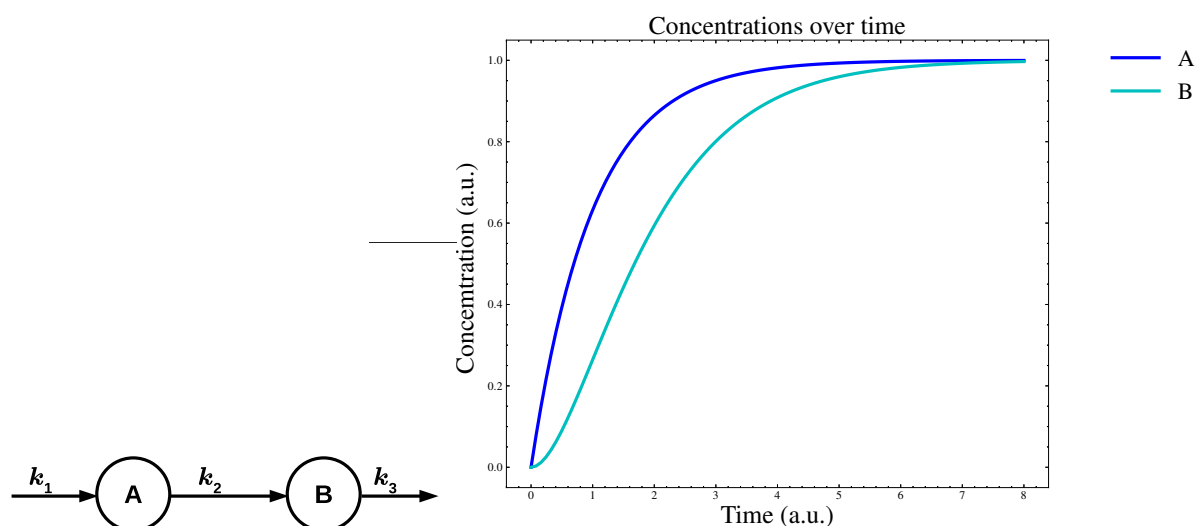


Figure 2.7: Scheme and time course of a linear open system made of two compounds and three reactions

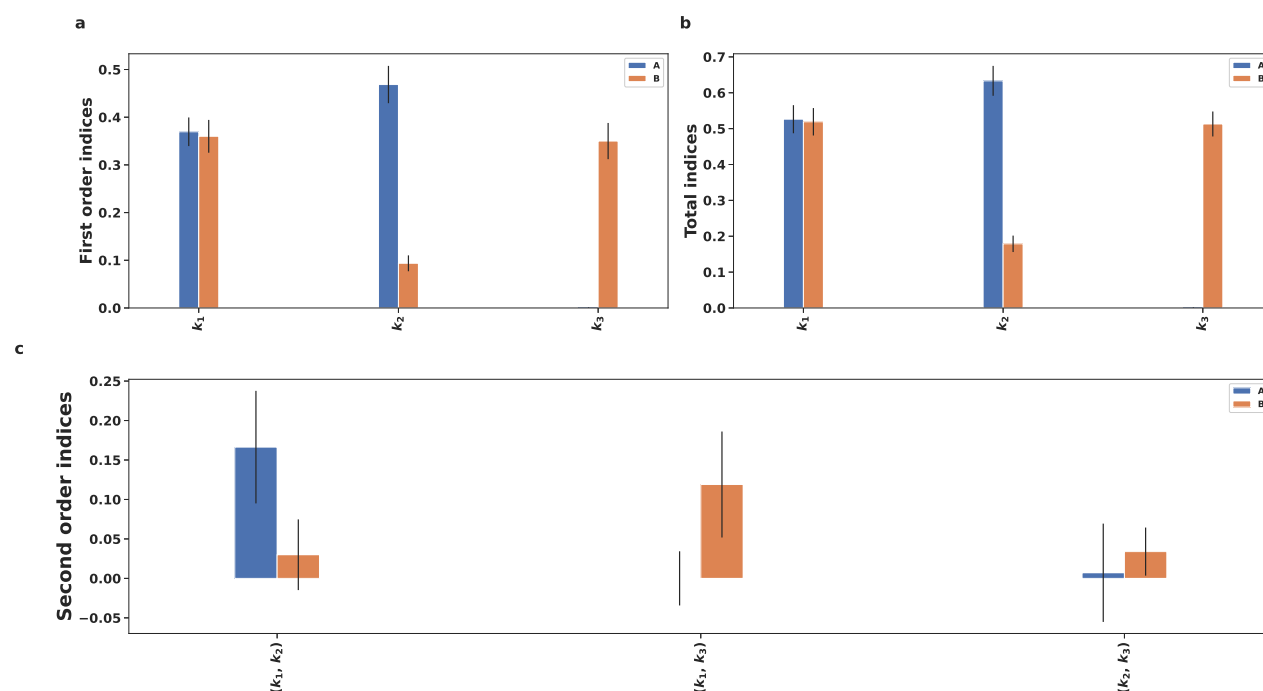


Figure 2.8: Sobol's sensitivity analysis for the linear model with two compounds: As expected, k_1 and k_2 are the only parameters controlling the variance of the compound A, whereas k_3 exclusively control the variance of B.

Example 2.4.8. In this example, I present a system made of a branched opened model composed of the compounds A, B, C, and D. The influx in the system via the compound A is constant and associated with the parameter k_1 . The internal reactions follow the mass action kinetics with the related kinetic rate constants k_2 , k_3 , k_4 , and k_5 . The system has two outfluxes proportional to the concentration of the compounds C and D. I apply Sobol's sensitivity analysis to evaluate the contribution of each parameter to the uncertainty of the time course of the system.

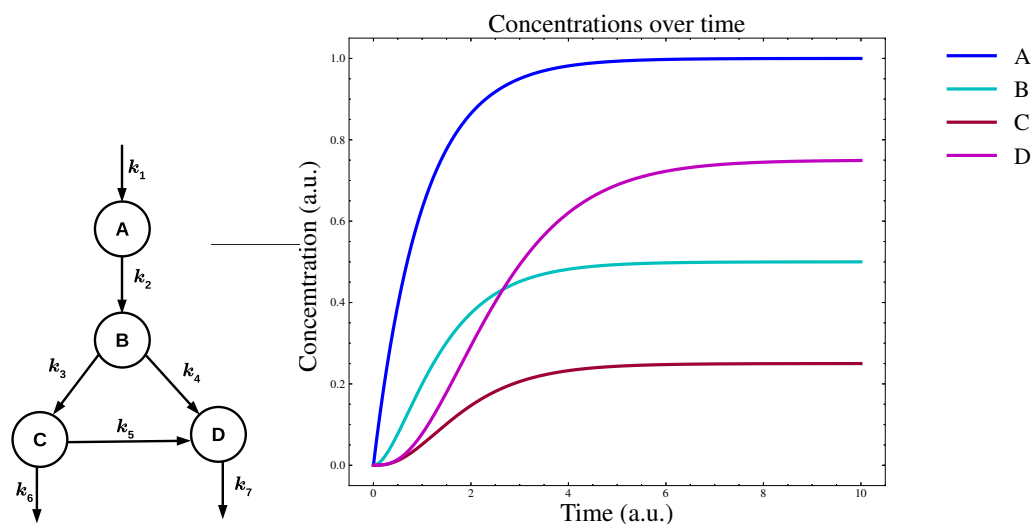


Figure 2.9: **Scheme and time course of a branched open system made of four compounds and seven reactions**

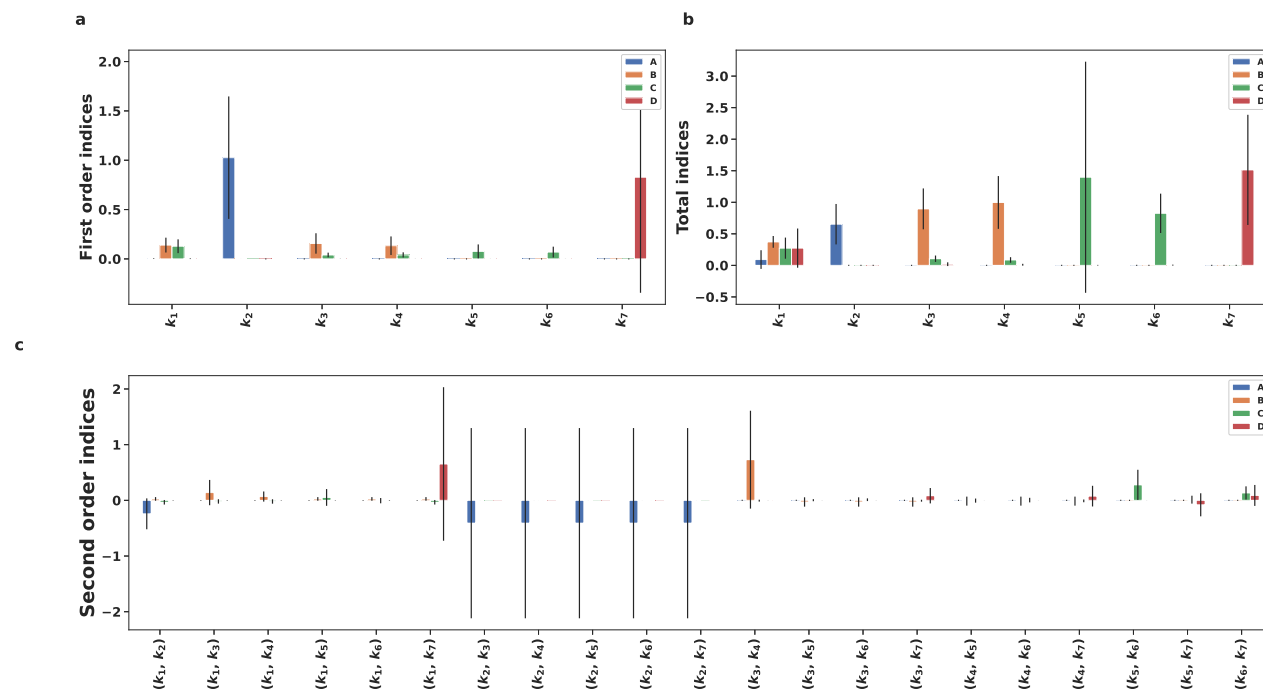


Figure 2.10: **Sobol's sensitivity analysis for the branched open model with four compounds:** By looking at the total indices, one can note that k_1 has a substantial control on the concentrations of all compounds. The other parameters have less global influences, although their effect on the concentration of a particular compound can be more considerable, as shown by the first-order, second-order, and total indices.

Chapter 3

Biochemistry and kinetics of enzymes involved in animal fatty acid synthesis

Part of this chapter is adapted from the following published article:

Foko Kuate CA, Ebenhöf O, Bakker BM, Raguin A. Kinetic data for modeling the dynamics of the enzymes involved in animal fatty acid synthesis. *Biosci Rep.* 2023 Jul 26;43(7):BSR20222496. DOI: [10.1042/BSR20222496](https://doi.org/10.1042/BSR20222496).

The author of this thesis contributed to the conceptualization, the methodology, the investigation and the writing of the above article. Hence, the author retains the right to include the article in this thesis since it is not published commercially.

To quantitatively model the dynamics of a metabolic pathway with ODEs, it is not enough to know the system's constituent elements and the list of reactions that characterize the metabolic pathway. It is also essential to have the evolution laws of the reactions associated with the metabolite changes in the system. These laws of evolution, known in particular by the name of kinetic rate laws, are represented in the form of mathematical formulas comprising the metabolites involved in and the parameters encoding the information specific to these reactions and, more precisely, on the enzymes in the case of enzymatic reactions. In this chapter, I collect and concisely present the necessary information to develop computational models of animal fatty acid synthesis dynamics with a particular focus on mammals. It includes information on FADNS and microsomal modification (elongation and desaturation) for both endogenous and exogenous FAs. We first focus on the basic biochemistry of the associated enzymes and then review their kinetics.

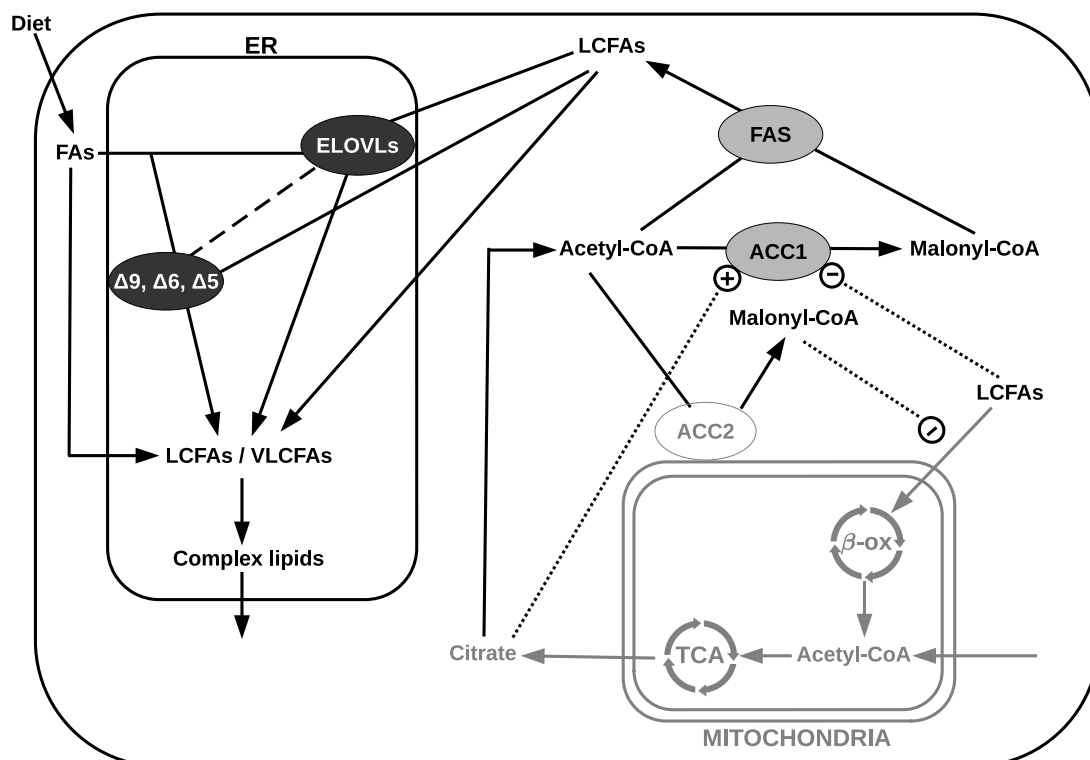


Figure 3.1: **Schematic representation of the biochemistry of fatty acid biosynthesis.** The process is organized in two main parts. Enzymes involved in the fatty acid *de novo* synthesis (FAS and ACC1) are color-coded with a gray background. They are responsible for the production of long chain saturated fatty acids (LCSFAs). This process takes place in the cytoplasm. Enzymes involved in the microsomal modifications of fatty acids (ELOVLs, Δ -desaturases) are color-coded with a black background. They are responsible for elongating and desaturating long-chain fatty acids (LCFAs) and very long-chain fatty acids (VLCFAs). This process takes place in the endoplasmic reticulum (ER) where these enzymes are membrane-bound. In the ER, LCFAs and VLCFAs, represented in the figure, include long-chain saturated fatty acids (LCSFAs), mono-unsaturated FAs (MUFAs), and poly-unsaturated FAs (PUFAs). The β -oxidation that takes place in the mitochondria is not part of fatty acid synthesis. Still, it is represented because it influences the overall synthesis process.

3.1 Basic biochemistry of enzymes of fatty acid *de novo* synthesis

3.1.1 Fatty acid *de novo* synthesis

The fatty acid *de novo* synthesis, also known as the endogenous synthesis of fatty acids, produces long-chain saturated fatty acids from Acetyl-CoA in presence of ATP, bicarbonate, and NADPH. This involves two enzymes, namely the biotin enzyme acetyl-CoA carboxylase (ACC) and the multi-complex enzyme fatty acid synthase (FASN). The process can be divided into two parts: i) the synthesis of malonyl-CoA from acetyl-CoA, and ii) the step-wise elongation of the acyl-CoA chain. The main resulting product is palmitic acid (16:0), together with some myristic (14:0) and stearic (18:0) acid, and very low amounts of medium chain FAs (e.g.: (12:0)) [59, 82, 83].

Acetyl-CoA carboxylase

ACC is a key enzyme for lipid homeostasis [84]. It synthesizes malonyl-CoA which is central for fatty acid synthesis and oxidation. To date, two isoforms of ACC are known. The ACC1 isoform, which is found in all tissues, is specifically highly expressed in lipogenic tissues such as the liver, adipose tissues and mammary glands. The second isoform, ACC2 is mostly present in oxidative tissues such as the heart and the skeletal muscles. It is also expressed to a lesser extent in lipogenic tissues [85, 86, 87, 88]. ACC1 is located in the cytosol while ACC2 is located at the outer surface of the mitochondria [89, 90, 13] (see Figure 3.1). The two isoforms are encoded by two distinct genes, which share 80 % of similarities when comparing their amino acid sequences. One of the major differences between the two isoforms resides in their N-terminal amino acid sequences [86]. The N-terminal amino acid sequence of ACC2 starts with hydrophobic residues, which is responsible for its location at the surface of the mitochondrial membrane [86, 13]. The different locations of ACC1 and ACC2 reflect their specific metabolic role. Malonyl-CoA produced by ACC1 is utilized for elongation in FADNS, while malonyl-CoA from ACC2 inhibits the carnitine palmitoyl transferase 1 and thereby β -oxidation [90].

For both ACC isoforms, the synthesis of malonyl-CoA from acetyl-CoA takes place in three steps. In the first step, the ACC is carboxylated, using bicarbonate in presence of ATP. In the second step, the carboxyl group is transferred between the catalytic sites of the enzyme. In the third step, the carboxyl group reacts with acetyl-CoA to form malonyl-CoA [91]. The overall reaction is activated by citrate, which is the precursor for cytosolic acetyl-CoA, and thereby the precursor for cytosolic FADNS (see Figure 3.1) [85]. Besides, the overall reaction is allosterically repressed by malonyl-CoA, long-chain fatty acyl-CoA, and free CoA [91, 92, 93]. Both ACC isoforms are also subject to diet and hormonal regulations [85, 89, 94, 95].

Fatty acid synthase

FASN is the cytosolic homodimeric multi-functional enzyme responsible for the channeled elongation reactions in the FADNS [96, 97] (see Figure 3.1). This enzyme comprises two sub-units that each contain three domains and seven catalytic sites. The initialization step is catalyzed by the malonyl-acetyl-transferase site. It cleaves the CoA moieties of the acetyl-CoA and malonyl-CoA, and transfers both the malonyl and acetyl groups to the acyl carrier protein (ACP) domain. This leads to the formation of acetyl-ACP and malonyl-ACP. Then, in each elongation cycle, the addition of two carbons in the growing acyl-chain takes place in four steps: condensation, reduction, dehydration, and reduction [98]. In the condensation step, the β -ketoacyl synthase site condenses the malonyl-ACP with the growing chain of acyl-ACP/ acetyl-ACP to form the β -ketoacyl-ACP. In this step, a molecule of CO_2 is released. At the β -ketoacyl reductase site, the β -ketoacyl-ACP is reduced by NADPH in a first reduction step to form β -hydroxyacyl-ACP, which is dehydrated by the dehydratase

site to form the trans-enoyl-ACP. A second reduction step (again involving NADPH) then forms the end product of the elongation cycle, an acyl-ACP with two extra carbons. This acyl-ACP either serves as substrate for a new elongation cycle, or is released by the thioesterase site after the incorporation of a CoA moiety. The thioesterase site is regarded as the termination site since it releases the final product of the FADNS. The main product of the FADNS is 16:0. This suggests a high selectivity of the thioesterase domain for the 16:0 intermediate, which was confirmed by Chakravarty et al. [99] in *in vitro* experiments.

3.1.2 Microsomal modifications of fatty acids

Biological functions require specific FA profiles [100, 101]. Among these profiles, there are FAs that cannot be synthesized *de novo* (essential FAs) and, therefore, must be obtained from external sources. The FAs produced *de novo* (endogenous) and those from the diet (exogenous) are not always suitable and must be modified accordingly. This modification takes place in the ER and involves two processes, elongation and desaturation. Elongation produces very-long-chain fatty acids (VLCFAs). They are essential precursors for various classes of lipids, such as phospholipids, sphingolipids, triglycerides, cholesterol esters, and wax esters, whose syntheses are beyond the scope of this mini-review [102]. Desaturation tunes FA properties [103]. For instance, the cellular and organellar membrane permeability and fluidity depend on the level of unsaturation of their constitutive FAs [104]. Below, I introduce the biochemistry of each enzyme. For the sake of brevity, I also provide tables that summarize the main biochemical characteristics of elongases (see Table A4) and desaturases (see Table A5).

Elongases

The microsomal elongation of fatty acids is the major pathway to produce very-long-chain fatty acids (VLCFAs) [105]. Similarly to the *de novo* synthesis, it utilizes malonyl-CoA and NADPH as carbon donors and reducing agents, respectively. The microsomal elongation process consists of four steps: condensation, reduction, dehydration, and reduction. Unlike the *de novo* synthesis, each step is catalyzed by a distinct enzyme. In the condensation step, the 3-acyl-CoA synthetase links the acyl-CoA chain with the malonyl-CoA to form the 3-keto-acyl-CoA. The latter is reduced by the 3-keto-acyl-CoA reductase during the reduction step, to produce the 3-hydroxy-acyl-CoA. In the dehydration step, the 3-hydroxy-acyl-CoA dehydratase removes a molecule of H₂O from the 3-hydroxy-acyl-CoA, leading to the 2,3-trans-enoyl-CoA. The enoyl-CoA reductase subsequently reduces the latter to form the end product of the elongation, an acyl-CoA with two extra carbons.

The 3-acyl-CoA synthetase catalyzing the condensation step plays a central role in determining the tissue specific distribution of VLCFAs [106]. Its expression varies from one tissue to another and its action is substrate specific [102, 107, 108, 109, 110].

To date, seven so-called elongation of very long chain fatty acids (ELOVLs) enzymes that belong to the 3-acyl-CoA synthetase family have been identified in humans and rodents [107]. They are membrane bound and located at the surface of the ER (see Figure 3.1). ELOVL1 is expressed in almost all tissues, and favors the elongation of saturated and mono-unsaturated FAs with chain lengths ranging from 18 to 26 carbons [102, 111]. ELOVL2 elongates poly-unsaturated FAs with 20 or 22 carbons. In mice, it plays a predominant role in the elongation of non-essential FAs [102, 111, 112]. ELOVL3 elongates saturated and unsaturated FAs with chain lengths ranging from 16 to 22 carbons [102, 113]. ELOVL4 is mostly involved in the elongation of both saturated and unsaturated FAs with at least 24 carbons [102]. ELOVL5 has a high affinity for poly-unsaturated FAs with 18 or 20 carbons, with a particular preference for essential FAs [102, 114]. ELOVL6 acts on FAs with chain lengths ranging from 12 to 18 carbons [115], with a high affinity for saturated FAs with chain lengths between 12 and 16 carbons [102, 115]. This enzyme is preponderant in the lipogenic tissues and is repressed by poly-unsaturated FAs [116]. An *in vivo* study conducted with knock-out mice showed a high penchant for 16:0 and 16:1n7 [117]. ELOVL7 elongates FAs with chain lengths ranging from 16 to 20 carbons, with a high affinity for chains of 18 carbons [102]. Investigations of its substrate specificity revealed a high affinity for non-essential FAs as compared to other FAs of the same length [118].

Desaturases

The desaturase enzymes are responsible for the introduction of double bonds at specific positions along FA chains. Like the ELOVLs, they are membrane-bound enzymes and are located in the ER (see Figure 3.1). They are substrate and tissue-specific [109]. Desaturation tailors FA properties (e.g., melting point, rancidity, and flexibility) which ensures their suitability for various biological processes [103]. In mammals, three desaturases have been identified, namely the $\Delta 5$ desaturase, the $\Delta 6$ desaturase, and the $\Delta 9$ desaturase [103, 119]. The three desaturations follow the same mechanism. The ΔX desaturation consists in introducing a *cis* double bond between the carbons X and $X + 1$, counted from the carboxyl end. Via a series of reactions, the ΔX desaturase consecutively removes two hydrogen atoms, the first one at the X th position, and the second one at the $X + 1$ th position [119, 120, 121, 21]. These two hydrogens are combined with molecular oxygen and released as water [122]. The electrons required for this reduction are derived from cytochrome b_5 [120, 121, 21]. One should note that for unsaturated FAs, a further desaturation does not change the nY family to which the FA belongs, Y being the position of the first double bond, counted from the methyl-end. Further biochemistry details of the ΔX enzymes are summarized in Table A5, i.e., their isoforms, substrates, tissue specificity, regulators, and biological functions. As for their kinetic features, very little information and data are available. This may be due to particularly challenging experimental tractability. Specifically, here we are dealing with membrane-bound enzymes, whose purification requires several complicated steps. Furthermore, the desaturation reactions involve an

intermediate step catalyzed by an extra enzyme (i.e., cytochrome b_5 reductase), making the design of kinetics assays difficult.

$\Delta 9$ Desaturase The mono-unsaturated FAs are essential for producing different lipids, including phospholipids, triglycerides, cholesterol esters and wax esters. Therefore, they play a crucial role in lipid homeostasis and the physiological functions of lipids [122, 123, 124]. To ensure their presence in an adequate proportion, they are endogenously produced from saturated FAs by the $\Delta 9$ desaturase, also known as stearoyl-CoA desaturase (SCD). The mechanism of $\Delta 9$ desaturation consists in introducing a *cis* double bond between the carbons 9 and 10, counted from the carboxyl end. Via a series of reactions, the $\Delta 9$ desaturase consecutively removes two hydrogen atoms, firstly at the 9th position, secondly at the 10th position [119, 120]. These two hydrogens are combined with molecular oxygen and released as water [122]. The electrons required for this reduction are derived from cytochrome b_5 [120]. The preferred substrates of the $\Delta 9$ desaturase are 14:0, 16:0, and 18:0, with 14:1n5, 16:1n7, and 18:1n9 as respective products [123, 120, 125]. Among them, 18:1n9 is the most abundant one, and is consistently found as dominant in adipose tissues [103]. Furthermore, Ntambi et al. [126] and Miyazaki et al. [127] reported that SCD-deficient mice show an increase in insulin sensitivity and are protected against diet-induced adiposity. This suggests that the $\Delta 9$ desaturase could be a good therapeutic candidate for obesity and metabolic syndromes.

Four isoforms of the *SCD* gene have been identified in mouse (*SCD1-4*) and two in human (*SCD1* and *SCD5*) [122, 128, 129, 130, 131, 132]. Mouse and human *SCD1* are the most abundant and expressed in the lipogenic tissues such as liver and adipose tissues [133]. Human *SCD5* and mouse *SCD2* are both predominantly expressed in the brain and the pancreas [133]. Mouse *SCD3* is mainly expressed in harderian, preputial glands, and sebocytes [134], while mouse *SCD4* is only expressed in the heart [132]. All *SCD* isoforms (except mouse *SCD3*) act on 16:0 and 18:0, with a strong preference for 18:0 [135]. Opposite, the mouse *SCD3* can only desaturate the 16:0 [133]. The $\Delta 9$ desaturases, in particular *SCD1*, which is the most studied isoform, are subject to various regulations, ranging from diet to hormones, as summarized by Ntambi and Miyazaki [123]. High carbohydrate diets, saturated fat, insulin, estrogen, peroxisome proliferator-activated receptor α (*PPAR α*), and liver X receptors enhance the expression of the $\Delta 9$ desaturases, whereas glucagon, poly-unsaturated fatty acids (PUFAs) and leptin repress it.

$\Delta 6$ and $\Delta 5$ desaturases The n3 and n6 FA families (also known as $\omega 3$ and $\omega 6$) are essential for building highly unsaturated fatty acids. Those are necessary for cell membrane, signaling processes, brain and retina development, and cognition and inflammatory responses [103, 119]. Animals cannot synthesize *de novo* $\omega 3$ and $\omega 6$ FAs, but can modify essential FAs (18:2n6 and 18:3n3) acquired from external sources to fit the adequate lipid profiles. The $\Delta 5$ and $\Delta 6$ desaturases are required for this modification [103, 121, 21]. Like the ELOVLs and $\Delta 9$ desaturases, the $\Delta 5$ and $\Delta 6$

desaturases are membrane-bound enzymes. They introduce a *cis* double bond between the carbons 5 and 6, and the carbons 6 and 7, respectively, counted from the carboxyl end. The mechanism by which the double bonds are introduced is similar to that of the $\Delta 9$ desaturases [121, 21]. The predominant substrates are 18:2 n -6, 18:3 n -3, and 24:5 n -3 for the $\Delta 6$ desaturase, and 20:3 n -6 and 20:4 n -3 for the $\Delta 5$ desaturase, respectively leading to the products 18:3 n -6, 18:4 n -3, and 24:6 n -3, and 20:4 n -6 and 20:5 n -3. [103]. Both enzymes are mainly regulated by PUFAs [103].

The $\Delta 5$ and $\Delta 6$ desaturases are encoded by the *FASD1* and *FASD2* genes respectively, yet their distinct isoforms have so far not been identified. They are highly expressed in the liver and the brain, moderately expressed in the heart and lungs, and lowly expressed in the kidney, spleen, and muscles [121, 21, 136]. A study by Ge et al. [136] shows a high expression of the $\Delta 6$ desaturase in the skin. Interestingly, the $\Delta 6$ desaturase, highly expressed in the skin, has been shown to act on the saturated FA 16:0, resulting in the mono-unsaturated FA 16:1 n -10. This special case is highlighted by the symbol # in Table A5. This finding is consistent with the fact that 16:1 n -10 is the major FA found in human sebum [136].

3.2 Kinetic of enzymes of fatty acid synthesis

A bottleneck in constructing kinetic models is often the experimentally determined enzymatic parameters [137, 27, 138]. This is not surprising because enzyme kinetic parameters are difficult and tedious to measure with high accuracy, which is in particular the case for membrane-associated enzymes [139]. Moreover, the kinetic parameters strongly depend on external parameters, such as pH and temperature. This section discusses experimental findings that give insight into kinetic mechanisms and parameters of enzymes involved in the fatty acid synthesis.

3.2.1 Fatty acid *de novo* synthesis

The particularity of FADNS is the difficulty of building kinetic rate laws from the detailed enzymatic mechanism. If the overall kinetic of malonyl-CoA synthesis by acetyl-CoA carboxylase is known to follow the random Ter Ter mechanism, this is not the case for the elongation phase carried out by FAS. It is rather complex as it includes several channeling reactions which follow either Ping Pong or a random sequential mechanism. However, it is always possible to make simplifications, for example, by lumping several reactions and deducing a less complex yet meaningful kinetic law. Regardless of the level of detail or abstraction in representing the kinetics of FADNS, the literature abounds with important information that I believe to be a good starting point to build models of the dynamics of FADNS reactions.

Although some of the kinetic features discussed here are not from mammals, they can still be used as a starting point for modeling. They typically share a similar enzymatic mechanism, as well as

high amino acid sequence identity. For instance, chicken and rat FAS sequences are 63% and 79% identical to that of human, respectively [140]. Also, murine FAS sequence is 81%, 78%, and 94% identical to that of human, pig, and rat, respectively [35].

Acetyl-CoA carboxylase

Wright et al. [141] showed using metabolic control analysis that 63 % of the fluxes of FADNS is controlled by the ACC1. The conversion of acetyl-CoA to malonyl-CoA is often considered as the rate-limiting step in the *de novo* synthesis of LCFAs [142, 143, 141]. Therefore, understanding its kinetics is essential for any modeling approach aiming to simulate FA metabolism and related disorders.

The current understanding of the ACC mechanism is based on several studies, that have been reviewed by Numa and Tanabe [144]. Using isotope labeling, the three steps of the mechanism could be characterized. Also, Hashimoto et al. [145], and Hashimoto and Numa [146] suggested an ordered Bi Bi Uni Uni Ping Pong mechanism with an activation by citrate. The order of attachment of the substrates to the enzyme is, ATP, HCO_3^- , and acetyl-CoA for the forward reaction, and malonyl-CoA, Pi, and ADP for the reverse reaction [146]. The reaction is subject to product regulation, notably by malonyl-CoA and ADP. The mathematical expression of the rate law, including numerical values of the kinetic parameters, has been reported by Hashimoto and Numa [146]. With 16 parameters, it is quite complex, although it does not include inhibition by long-chain acyl-CoAs. The reaction mechanism was later questioned by Beaty and Lane [147], and Kaushik et al. [148], who instead proposed the random Ter Ter mechanism. Both articles provide detailed kinetic parameter values, useful for the construction of models. Liquid chromatography/mass spectrometry/mass spectrometry (LC/MS/MS) data of malonyl-CoA formation were fitted to the proposed rate law, allowing characterizing the human recombinant ACC2 [148]. The resulting kinetic parameters resemble those reported for rat skeletal muscle [149] and human recombinant enzymes [91]. Besides, Ogiwara et al. [92] and Tanabe et al. [150] focused on the inhibition constants of natural inhibitors (both substrate and product inhibitions) in rat liver. For example, Tanabe et al. [150] reported the inhibition constants of LCFAs and analogs. Inhibition constants for malonyl-CoA and palmitoyl-CoA were also determined [149]. In Table A2, I summarize some kinetic information, notably those extracted from the work of Cheng et al. [91], Kaushik et al. [148], and Trumble et al. [149].

Fatty acid synthase

The kinetics of FA synthesis is quite complex since the same enzyme synthesizes LCFAs through channeling [151]. Two main strategies are reported in the literature for the derivation of the corresponding rate law: i) considering each elementary reaction till the production of an LCFA [36, 152]; or ii) lumping all the steps up to the production of an LCFA as a single reaction [153, 154].

The common feature of the studies using either approach is that acetyl-CoA and malonyl-CoA compete for the same enzyme binding site.

Studying the mechanism of elongation by focusing on each of the seven enzymatic sites, Katiyar et al. [152] concluded that all individual reactions follow a Ping Pong mechanism except the reduction steps [152]. The latter was suggested to instead follow random sequential or ordered sequential mechanisms, with NADPH added first and the proton added second [154]. From these individual steps, the overall kinetic rate law of FADNS was derived using King and Altman method [41]. The resulting detailed rate law has eleven parameters. This complexity may make it difficult to fit the kinetic parameters and to relate them to their biological meaning. In chicken liver, Cox and Hammes [36] proposed a simpler rate law for the overall reaction, following a three substrates Michaelis-Menten kinetics, with competition of acetyl-CoA and malonyl-CoA. They described the associated mechanism with eight elementary steps. The first two correspond to the attachment of acetyl-CoA to the enzyme. Steps 3 to 7 repeat at each elongation cycle, while step 8 is the release of the final product, here chosen as palmitic acid (16:0). In this approach, all complex formation involving CoA or NADPH are reversible, characterized by their dissociation constant. Moreover, the authors highlighted the explicit relation between the mechanistic parameters (kinetic rate constants and dissociation constants), and the k_{cat} and K_{m_i} (i is either acetyl-CoA, malonyl-CoA, or NADPH) of the overall kinetics. k_{cat} and K_{m_i} were measured at various pH-values, thereby highlighting the impact of this experimental condition on the efficiency of the enzyme (k_{cat}/K_{m_i}).

Other studies employ a twofold approach, to first lump the reactions and derive the rate law, and second measure detailed kinetic parameters for specific reaction steps. For instance, Carlisle-Moore et al. [154] considered a lumped reaction for the production of 16:0 in human, and measured the k_{cat} and K_{m_i} -values (i is either acetyl-CoA, malonyl-CoA, or NADPH). Then, the same parameters were determined for the reduction and dehydration steps, when considered separately. In particular, those of the enoyl-CoA reductase site (last one of the elongation cycle) were assessed as a function of the substrate chain length (4:0, 8:0, and 12:0) (see Table A3). A similar approach was followed in chicken liver using tracer experiments in order to determine V_{max} and K_m -values for various substrates [153].

In vitro measurements of the FAS kinetics suffer from limitations, e.g., the malonyl-CoA decarboxylation into acetyl-coA, and the natural abundance of the ^{13}C carbons that introduce extra noise in the measurement of the products of the pathway. Their impact was observed in kinetic assays by OHASHI et al. [155] and Topolska et al. [59], using enzymes from guinea pig harderian gland and cow, respectively.

3.2.2 Microsomal modifications of fatty acids

The kinetics of the enzymes of MMFA are poorly studied in the literature. This can be explained by the fact that we deal with membrane-bound enzymes, so their purification is quite complex. Furthermore, in the specific case of elongases, they were discovered less than two decades ago. Nevertheless, I collected some kinetic information relevant to construct their respective kinetic rate laws (see Table A6 for ELOVLs, and Tables A7, A8 for desaturases).

Elongases

The analysis of the kinetics of the microsomal elongation began with the pioneering work by Nugteren [156] in the rat liver microsomes. This work focused on the overall elongation cycle using tracer data. They investigated the normalized rate of elongation as a function of the chain length and degree of unsaturation of substrates. They also reported detailed time-course data for the overall elongation of 14:0 to 16:0. Similar approaches were carried out in porcine neutrophil microsomes, assuming that the elongation follows a Michaelis-Menten rate law. It was possible to determine V_{max} and K_m -values for malonyl-CoA and NADPH for 16:0 and 20:0, and to determine the overall enzyme activity for elongation [157]. Although during this time, ELOVLs were not yet identified, these studies paved the way for investigating the kinetics of the overall elongation cycle. Surprisingly, little has been done to characterize the kinetics of the ELOVLs since they have been identified in the early 2000s. The most popular studies are by Naganuma et al. [118], and Naganuma and Kihara [158] on ELOVL7 and ELOVL6, respectively. In both, the kinetic parameters of ELOVL7 [118] and ELOVL6 [158] were determined using HEK 293T cells. For the ELOVL7, these were V_{max} and K_m -values for malonyl-CoA and 18:3n-3, for ELOVL6 the corresponding values for the malonyl-CoA and 16:0. Neither ELOVL7 nor ELOVL6 are subject to allosteric inhibition. Besides, Naganuma and Kihara [158] showed that NADPH and 3-ketoacyl-CoA reductase enhance the activity of ELOVL7. The underlying mechanism is unknown, but they speculated that the presence of the 3-ketoacyl-CoA reductase might cause a conformational change of the enzyme, thereby increasing its activity. This hypothesis could, for instance, be tested using fluorescent nano-antennas that allow monitoring of small and large protein conformational changes [159].

Desaturases

The complexity of the desaturase mechanism (see section 3.1.2) might explain why little efforts have been dedicated to unravel the associated kinetics. However, kinetic parameters were measured by assuming Michaelis-Menten rate law, for instance in human or rat [160, 161, 162, 163, 164, 165, 166, 167].

$\Delta 9$ Desaturase As mentioned earlier, the literature turns out to be less furnished with respect to the kinetic features of the $\Delta 9$ desaturase compared to those of the FADNS enzymes. Specifically,

the kinetics associated with the detailed mechanism of the enzyme is not discussed. Thus, as a first intention, most studies assume a Michaelis-Menten rate law. Three studies following this approach in mammals can be stressed. They respectively use rat liver microsomes [167], bovine mammary microsomes [160], and purified rat liver enzyme [161], and provide a starting point for kinetic modeling. Since the first two studies do not use purified enzymes, the k_{cat} values cannot be determined. As an alternative, one can use the Lineweaver-Burk plot of the kinetic data, together with the mass of the protein, to infer the V_{max} values. For example, from the data of Soulard et al. [167], I can estimate the V_{max} values to be about $2 \mu M \cdot min^{-1} \cdot mg^{-1}$ protein and $1.17 \mu M \cdot min^{-1} \cdot mg^{-1}$ protein, for 18:0 and NADH, respectively. When considering the study by Strittmatter and Enoch [161], it appears that its purpose is not to measure the kinetic parameters but to present in detail the procedure of purification of the enzyme. Hence, in that case, neither the k_{cat} nor the V_{max} values can be inferred from the reported data. Despite the limited information available in the literature, the reader can take into account the K_m values tabulated in order to begin developing a kinetic model (see Table A7). I believe that a subsequent effort should be placed into measuring the kinetic parameters of the $\Delta 9$ desaturase, notably the k_{cat} and K_m -values for the different substrates and the parameters associated with potential regulatory mechanisms.

$\Delta 6$ and $\Delta 5$ desaturases Like for the $\Delta 9$ desaturase, the kinetics of animal $\Delta 5$ and $\Delta 6$ desaturases is under-studied. Furthermore, only a few studies use purified enzymes. For instance, Okayasu et al. [163] used the purified $\Delta 6$ desaturase from rat liver to measure K_m and V_{max} values for 18:2n-6-CoA. Opposite, Rodriguez et al. [166] focused on the kinetics of both $\Delta 5$ and $\Delta 6$ desaturases using human fetal microsomes. The K_m and V_{max} values were measured for 20:3n-6-CoA for $\Delta 5$, and 18:2n-6-CoA and 18:3n-3-CoA for $\Delta 6$. In addition, Irazú et al. [165], measured the K_m and V_{max} values of $\Delta 5$ using rat kidney microsomes. For these three studies, a summary of the parameter values, as well as the conditions of measurement, are provided in Table A8. In the table, the kinetic parameters are only reported for essential fatty acids. One should also note that, although in all these *in vitro* studies, the authors report substrate inhibition when the substrates are above a certain threshold, I choose not to tabulate them since this phenomenon is unlikely to be observed *in vivo*. Finally, nothing is known about the kinetics of desaturation of 16:0 by the $\Delta 6$ desaturase.

Discussion and conclusions

FAs are the precursors of lipid synthesis, and therefore fundamental building blocks in every living cell. It is thus not surprising that many metabolic disorders are associated with defects in FA metabolism [85, 168]. Mathematical modeling has become an increasingly popular approach for the investigation of biochemical pathways. Model simulations can guide experiments and support the identification of potential drug targets. Their construction relies on the availability of exper-

imental data concerning the detailed enzymatic mechanisms, the enzyme kinetics, the associated mathematical rate laws, and the values of the corresponding parameters. In this review, I focused on animal fatty acid synthesis with a particular emphasis on mammals. I aimed to summarize the information necessary for constructing dynamic mathematical models describing this complex enzymatic process using rate laws. I first gave an overview of the framework, and then reviewed the kinetic information of the enzymes involved, including both the fatty acid *de novo* synthesis and the microsomal modification pathways. We also provided tables summarizing the kinetic information, as well as the basic biochemistry, of the enzymes involved (Tables A2-A8).

We find that, despite enormous amount of information and available data, our knowledge is still limited. Most of the enzymes involved in animal fatty acid synthesis are membrane bound, which makes it extremely challenging to systematically analyze their kinetics in controlled *in vitro* experiments. For instance, the purification of such enzymes requires their solubilization, which may lead to an alteration or even a complete loss of their activity [118]. Furthermore, this step is particularly tedious, which possibly explains why most studies that I reviewed instead use recombinant proteins or cell extracts. Remarkably, recent approaches have shown successes in characterizing membrane-bound enzymes by embedding them into liposomes, mimicking their natural environments [118, 169]. Even if these techniques are further developed to allow for systematic determination of kinetic parameters, it still has to be considered that an *in vitro* system never precisely reflects the situation *in vivo*. The conditions of *in vitro* assays, both physical (e.g., pH, temperature) and chemical (e.g., buffer) can influence the measured kinetic parameter values, due to sub-optimal enzymatic conformation changes during the reaction. Besides, the complexity of the enzymatic process itself can limit the development of new assays. That is for instance the case of the ΔX desaturation process that includes a reduction step involving an extra enzyme, cytochrome b_5 reductase. Furthermore, the unavailability of the purified native enzyme may lead to *in vitro* experiments based on either truncated or recombinant enzymes, or cell extracts. Still, it is unclear whether any of these substitutes can be considered a good proxy for their native counterpart. When kinetic data are unavailable, in order to develop a mathematical model, an alternative is to use information from a distinct tissue or isoform, or an orthologous protein from a closely related organism. It is then important to carefully consider the limits of these approximations. For instance, even if ACC1 and ACC2 share analogous enzymatic mechanisms and high similarity in amino acid sequences [143], the latter is a membrane-bound enzyme, such that one can expect distinct kinetic parameter values. Similarly, although Cox and Hammes [36] provided detailed kinetic information on FAS from chicken liver, one can question whether the derived parameter values reflect those in mammals. Naturally, ethical concerns restrict the possibility to perform *in vivo* experiments in humans. Therefore, alternative methods focusing on simpler systems appear as promising technologies to better mimic *in vivo* conditions. They for instance consist in cultivating specific cell lines (e.g., adipocytes and hepatocytes) or growing organs on chips [170, 171].

It is currently feasible to build mathematical and computational models of animal fatty acid synthesis based on available kinetic information. However, literature gaps present a major obstacle for developing a more fundamental understanding of these pathways, which may considerably impair research progress, and its implications in the medical domain. To overcome these limitations, it will not be sufficient to simply perform more experiments, but it will also be necessary to find unifying standards to test, report, and store this important wealth of data in a findable and reusable manner. Additionally, one must take advantage of the growing field of targeted metabolomics, utilizing techniques such as stable isotope labeling, for measuring the kinetic parameters both *in vitro* and *in vivo*.

Chapter 4

Fatty acid metabolism: conditions for bi-stability

Short description of fatty acids metabolism. As mentioned in the introduction, the maintenance of cellular energy homeostasis largely depends on FA metabolism. In excess glucose, the primary energy source, FAs are built from acetyl-CoA resulting from glucose degradation. The produced FAs are stored in the liver and adipose tissues as TGs. Conversely, in the absence of carbohydrates, cells must rely on lipid sources. As a result, FAs are degraded to fulfill the energy requirements. In this process, the TGs are hydrolyzed into FAs, which are then oxidized into acetyl-CoA. The latter will be used to generate ATPs in the TCA cycle and synthesize ketone bodies. Acetyl-CoA serves as a central metabolite, bridging both the catabolic and anabolic pathways of FAs. Furthermore, it functions as an indicator of cellular energy status, with the cytosolic concentration of acetyl-CoA reflecting the overall energetic state of the cell [172]. In fact, a high level of acetyl-CoA typically correlates with a postprandial state, promoting lipogenesis. In contrast, a reduced concentration is associated with fasting conditions, instigating FA catabolism. Given this, a keen understanding of acetyl-CoA fluctuations is pivotal in shedding light on the integral role of lipids in maintaining cellular energy balance.

Acetyl-CoA also participates in various metabolic processes either as a substrate or product, influencing its cellular concentration. It becomes clear that any supply or consumption from the acetyl-CoA pool must be accounted for in any minimal computational model of FA metabolism. The liver TGs are hydrolyzed into FAs and glycerol in case of a carbohydrate deficit. Like acetyl-CoA, liver TGs are subjected to external influences, such as their conversion into very low-density lipoproteins (VLDL) to be exported to other organs and their supply from adipose tissue [173]. Such processes influence the TGs' pool size. The cytosolic synthesis of long-chain saturated fatty acids (LCSFAs) from acetyl-CoA incorporates an intermediary stage wherein malonyl-CoA is derived from acetyl-CoA. This compound functions as a carbon donor for FA elongation and concurrently inhibits FA β -oxidation. The FA pool consists of LCSFAs produced endogenously and various types of FAs sourced from the diet. FAs are also used to synthesize other lipid classes, such as phos-

pholipids, sphingolipids, and waxes. Both fluxes in and out may significantly influence the pool size.

Objectives. The above description presents FAs metabolism as a complex dynamical system that functions in two separate regimes: the degradation and the synthesis of FAs. The two regimes appear not to be active simultaneously, and the acetyl-CoA concentration might control the switch from one regime to another, as postulated by Shi and Tu [172]. These observations allow me to hypothesize that the metabolism of FAs is a bi-stable system. Therefore, I want to suggest an approach that could enable verifying the above hypothesis and understanding how the switch from one regime to another occurs or design a bi-stable system.

This chapter aims to lay the groundwork for answering the following questions related to hepatic FA acid metabolism:

1. Can hepatic FA acid metabolism exhibit bi-stability?
2. Which metabolites or physiological parameters govern the transition between steady-states?
3. In the context of metabolic diseases, how are these steady-states altered, and is it possible to revert them?

To address these questions, I introduce a coarse-grained model of FA metabolism and subsequently conduct a qualitative analysis of its dynamics. This analysis assists in identifying both the necessary and sufficient conditions for the proposed ODE model to exhibit bi-stability. The model's kinetic rate laws, based on "Michaelian" principles, are further elaborated in Section 2. Here, multi-enzymatic reactions are consolidated into a singular reaction through a process termed "lumping". A primary criterion for bi-stability is established: the existence of at least three steady-states. I specify the conditions that ensure the presence of two stable steady-states and an adjacent unstable steady-state. To pinpoint these conditions, I utilize two direct mathematical methods based on intuitive reasoning:

1. Utilizing Descartes' rule of signs and the analysis of turning points of a polynomial, it's possible to establish conditions under which a polynomial has a designated number of positive or negative roots.
2. I analyze the sign of the Jacobian matrix's eigenvalues at the steady-state under the assumption that these steady-states are hyperbolic.

4.1 Coarse-grained model of fatty acids metabolism

I present here what I consider as minimal model of FA metabolism. It consists only of the critical metabolites that influence the FA dynamics. Notably, acetyl-CoA (S_1), malonyl-CoA (S_2),

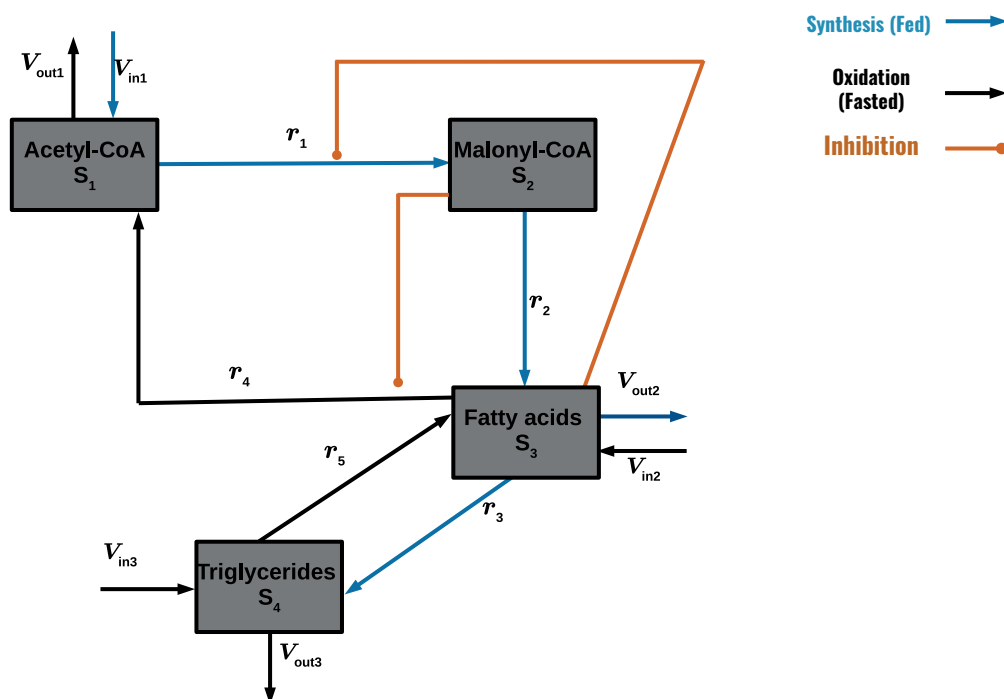


Figure 4.1: **Illustration of interactions among key metabolites in lipid homeostasis:** Square boxes denote the concentrations of distinct metabolites of the system, while triangular-shaped arrows signify reaction fluxes. Reaction fluxes associated with FA synthesis are color-coded in blue, whereas those involved in FA degradation are depicted in black. Circular arrowheads do not represent fluxes but instead indicate inhibition of the target reaction by the originating metabolite. For instance, malonyl-CoA suppresses the flux from the FA pool to acetyl-CoA. V_{ini} and V_{outi} (where $i \in \{1, 2, 3\}$) signify the respective influxes and outfluxes of the attached metabolites.

FAs (S_3), and TGs (S_4). My strategy consists in lumping the reactions resulting in the production or consumption of a metabolite in the model as a single enzymatic reaction. I also include the regulation processes, notably the feedback inhibition of the FAs toward malonyl-CoA synthesis [174, 175, 142] and the inhibition of the FA β -oxidation by malonyl-CoA [90]. These inhibition reactions are assumed to be non-competitive. All the influxes into the different pools are assumed to be constant, while the outfluxes are considered to be proportional to the concentration of the metabolite subjected to outfluxes.

The acetyl-CoA pool (S_1) receives an influx resulting from the degradation of the product of glycolysis or other processes. The rate of this influx is represented by V_{in1} . Other processes, such as ketogenesis, acetylation, and ATP production in the TCA cycle, use acetyl-CoA as a precursor. I represent such utilization of acetyl-CoA by the outflux, V_{out1} . The acetyl-CoA is the substrate for malonyl-CoA synthesis. ACC, the enzyme synthesizing malonyl-CoA from acetyl-CoA, is regulated by two metabolites. While LCFAs allosterically repress its activity [174, 175, 142], citrate enhances it [36]. For the sake of simplicity, I ignore the contribution of citrate and the other hormonal regulations by insulin, glucagon, and epinephrine. Indeed, these processes are considered to be outside the system. Therefore, I only consider the allosteric inhibition by FAs. I model the rate r_1 of malonyl-CoA synthesis as a non-competitive inhibition, in which the acetyl-CoA is the substrate

and FAs the inhibitors. Acetyl-CoA is also a substrate of FADNS. To avoid having a rate law with many parameters, I assume that the net contribution of acetyl-CoA to FADNS is through the malonyl-CoA formation. Malonyl-CoA, together with acetyl-CoA, are used to synthesize FAs via FADNS. This reaction is considered not to be directly regulated by internal metabolites, although it is known that acetyl-CoA and malonyl-CoA compete for a site of the FAS enzyme [176, 36]. With these considerations, I concluded that the rate r_2 of FA synthesis follows Michaelis-Menten kinetics with malonyl-CoA as a unique substrate. The FA pool can receive external influxes, for example, from the diet or the degradation of complex lipids. These influxes are represented by V_{in2} . FAs are also subject to internal reactions. They are used for TG synthesis and β -oxidation. I note the respective rates of these reactions as r_3 and r_4 . FAs are precursors for other processes, such as synthesizing complex lipids noted by the outflux V_{out2} . To account for the allosteric inhibition of the β -oxidation by malonyl-CoA, the rate r_4 is considered to follow a non-competitive inhibition with FAs as substrate and malonyl-CoA as the inhibitor.

As none of the metabolites of the system inhibit TG synthesis, its rate r_5 follows the Michaelis-Menten rate law. The outflux V_{out3} represents the exportation of TGs outside the liver as very low-density lipoproteins (VLDLs) to be stored in adipose tissues. I consider V_{out3} to be proportional to the size of its pool. The TG pool receives an influx noted V_{in3} resulting from the mobilization of fat from adipose tissue, which occurs during prolonged fasting. In case of long fasting, liver TGs are hydrolyzed into FAs to supply the β -oxidation. This reaction is represented by the rate r_5 and follows Michaelis-Menten's kinetics.

A scheme is essential to visualize the interactions among the different metabolites in the pathway (see Figure 4.1). Figure 4.1 enables one to easily express the dynamics of the elements of the pathway as a system of coupled ODEs. They are the equations (4.1.1), (4.1.2), (4.1.3), and (4.1.4). The different rate equations with their corresponding parameters are summarized in Table 4.1.

$$\frac{dS_1}{dt} = V_{in1} - r_1 + r_4 - V_{out1} \quad (4.1.1)$$

$$\frac{dS_2}{dt} = r_1 - r_2 \quad (4.1.2)$$

$$\frac{dS_3}{dt} = V_{in2} + r_2 - r_3 - r_4 + r_5 - V_{out2} \quad (4.1.3)$$

$$\frac{dS_4}{dt} = V_{in3} + r_3 - r_5 - V_{out3}, \quad (4.1.4)$$

which is equivalent to

$$\frac{dS_1}{dt} = k_1 - \frac{V_1 S_1}{(K m_1 + S_1)(1 + q_1 S_3)} + \frac{V_4 S_3}{(K m_4 + S_3)(1 + q_4 S_2)} - \alpha S_1 \quad (4.1.5)$$

$$\frac{dS_2}{dt} = \frac{V_1 S_1}{(K m_1 + S_1)(1 + q_1 S_3)} - \frac{V_2 S_2}{K m_2 + S_2} \quad (4.1.6)$$

Table 4.1: **Rate laws with the corresponding parameters:** the k_i , $i = 1, 2, 3$ are constants and with the dimension of a rate. α , β , and γ are first order rate kinetic constants. V_i , $i = 1, 2, 3, 4, 5$ are the maximum rate of each reaction. K_{mi} , $i = 1, 2, 3, 4, 5$ are the Michaelis-Menten constants. q_1 and q_4 are the inverse of the inhibition constants. S_i , $i = 1, 2, 3, 4$ are the metabolites of the system.

Rate	Kinetic rate law	Formula	Parameters
V_{in1}	Constant influx	k_1	k_1
V_{in2}	Constant influx	k_2	k_2
V_{in3}	Constant influx	k_3	k_3
V_{out1}	Proportional outflux	αS_1	α
V_{out2}	Proportional outflux	βS_3	β
V_{out3}	Proportional outflux	γS_4	γ
r_1	Non-competitive inhibition	$\frac{V_1 S_1}{(K_{m1} + S_1)(1 + q_1 S_3)}$	V_1, K_{m1}, q_1
r_2	Michaelis-Menten kinetics	$\frac{V_2 S_2}{K_{m2} + S_2}$	V_2, K_{m2}
r_3	Michaelis-Menten kinetics	$\frac{V_3 S_3}{K_{m3} + S_3}$	V_3, K_{m3}
r_4	Non-competitive inhibition	$\frac{V_4 S_3}{(K_{m4} + S_3)(1 + q_4 S_2)}$	V_4, K_{m4}, q_4
r_5	Michaelis-Menten kinetics	$\frac{V_5 S_4}{K_{m5} + S_4}$	V_5, K_{m5}

$$\frac{dS_3}{dt} = k_2 + \frac{V_2 S_2}{K_{m2} + S_2} - \frac{V_3 S_3}{K_{m3} + S_3} - \frac{V_4 S_3}{(K_{m4} + S_3)(1 + q_4 S_2)} + \frac{V_5 S_4}{K_{m5} + S_4} - \beta S_3 \quad (4.1.7)$$

$$\frac{dS_4}{dt} = k_3 + \frac{V_3 S_3}{K_{m3} + S_3} - \frac{V_5 S_4}{K_{m5} + S_4} - \gamma S_4. \quad (4.1.8)$$

4.2 Conditions for having three steady-states

4.2.1 Necessary condition

The space of admissible solutions for the system represented by the equations (4.1.5) to (4.1.8) is \mathbb{R}_+^4 , where

$$\mathbb{R}_+^4 = \{(S_1, S_2, S_3, S_4); \text{ such that } S_1, S_2, S_3, S_4 \geq 0\} \quad (4.2.1)$$

The value S_i^* of each metabolite S_i , $i \in \{1, 2, 3, 4\}$ at the steady-state is solution of the equation

$$\frac{dS_i}{dt} = 0. \quad (4.2.2)$$

Given that this is a coupled system, the solution S_i^* of (4.2.2) will be expressed as a function of S_j^* ($j \neq i$). For example, S_1^* will be expressed in terms of S_2^* , S_3^* , and S_4^* . I will omit the symbol "*" in the calculations to avoid overloading the notations and only specify it when needed.

Evaluation of S_1^*

At the steady-state, one has

$$\begin{aligned} \frac{dS_1}{dt} = 0 &\iff k_1 - \frac{V_1 S_1}{(K m_1 + S_1)(1 + q_1 S_3)} + \frac{V_4 S_3}{(K m_4 + S_3)(1 + q_4 S_2)} - \alpha S_1 = 0 \\ &\iff \left(K m_4 S_2 S_3 \alpha q_1^2 + K m_4 S_2 \alpha q_1 + K m_4 S_3 \alpha q_1 + K m_4 \alpha + S_2 S_3^2 \alpha q_1^2 \right. \\ &\quad + S_2 S_3 \alpha q_1 + S_3^2 \alpha q_1 + S_3 \alpha \left. \right) S_1^2 + \left(K m_1 K m_4 S_2 S_3 \alpha q_1^2 + K m_1 K m_4 S_2 \alpha q_1 \right. \\ &\quad + K m_1 K m_4 S_3 \alpha q_1 + K m_1 K m_4 \alpha + K m_1 S_2 S_3^2 \alpha q_1^2 + K m_1 S_2 S_3 \alpha q_1 + K m_1 S_3^2 \alpha q_1 \\ &\quad + K m_1 S_3 \alpha - K m_4 S_2 S_3 k_1 q_1^2 + K m_4 S_2 V_1 q_1 - K m_4 S_2 k_1 q_1 - K m_4 S_3 k_1 q_1 + K m_4 V_1 \\ &\quad - K m_4 k_1 - S_2 S_3^2 k_1 q_1^2 + S_2 S_3 V_1 q_1 - S_2 S_3 k_1 q_1 - S_3^2 V_4 q_1 - S_3^2 k_1 q_1 + S_3 V_1 - S_3 V_4 \\ &\quad \left. - S_3 k_1 \right) S_1 \\ &\quad - K m_1 K m_4 S_2 S_3 k_1 q_1^2 - K m_1 K m_4 S_2 k_1 q_1 - K m_1 K m_4 S_3 k_1 q_1 - K m_1 K m_4 k_1 \\ &\quad - K m_1 S_2 S_3^2 k_1 q_1^2 - K m_1 S_2 S_3 k_1 q_1 - K m_1 S_3^2 V_4 q_1 - K m_1 S_3^2 k_1 q_1 - K m_1 S_3 V_4 \\ &\quad - K m_1 S_3 k_1 = 0 \\ &\iff P_1(S_1) = 0. \end{aligned}$$

$P_1(S_1)$ is a second-degree polynomial in S_1 that one can write in the condensed form as follows:

$$P_1(S_1) = A_1 S_1^2 + B_1 S_1 + C_1,$$

with

$$A_1 = K m_4 S_2 S_3 \alpha q_1^2 + K m_4 S_2 \alpha q_1 + K m_4 S_3 \alpha q_1 + K m_4 \alpha + S_2 S_3^2 \alpha q_1^2 + S_2 S_3 \alpha q_1 + S_3^2 \alpha q_1 + S_3 \alpha,$$

$$\begin{aligned} B_1 = &K m_1 K m_4 S_2 S_3 \alpha q_1^2 + K m_1 K m_4 S_2 \alpha q_1 + K m_1 K m_4 S_3 \alpha q_1 + K m_1 K m_4 \alpha + K m_1 S_2 S_3^2 \alpha q_1^2 \\ &+ K m_1 S_2 S_3 \alpha q_1 + K m_1 S_3^2 \alpha q_1 + K m_1 S_3 \alpha - K m_4 S_2 S_3 k_1 q_1^2 + K m_4 S_2 V_1 q_1 - K m_4 S_2 k_1 q_1 \\ &- K m_4 S_3 k_1 q_1 + K m_4 V_1 - K m_4 k_1 - S_2 S_3^2 k_1 q_1^2 + S_2 S_3 V_1 q_1 - S_2 S_3 k_1 q_1 - S_3^2 V_4 q_1 - S_3^2 k_1 q_1 + S_3 V_1 - \\ &S_3 V_4 - S_3 k_1 \end{aligned}$$

and

$$\begin{aligned} C_1 = &-K m_1 K m_4 S_2 S_3 k_1 q_1^2 - K m_1 K m_4 S_2 k_1 q_1 - K m_1 K m_4 S_3 k_1 q_1 - K m_1 K m_4 k_1 - K m_1 S_2 S_3^2 k_1 q_1^2 \\ &- K m_1 S_2 S_3 k_1 q_1 - K m_1 S_3^2 V_4 q_1 - K m_1 S_3^2 k_1 q_1 - K m_1 S_3 V_4 - K m_1 S_3 k_1. \end{aligned}$$

One has $A_1 > 0$, $C_1 < 0$, which means that regardless of the sign of B_1 , there is only one possible sign-changing of the coefficients of the polynomial $P_1(S_1)$ ($V_p(P_1) = 1$, see Descartes's rule of

signs Chapter 2). It follows from Descartes' rule of signs that P_1 has precisely one positive root, which is

$$S_1^* = \frac{-B_1 + \sqrt{\Delta_{P_1}}}{2A_1}, \quad (4.2.3)$$

where

$$\Delta_{P_1} = B_1^2 - 4A_1C_1, \quad (4.2.4)$$

which is the discriminant of the polynomial P_1 .

Evaluation of S_2^*

$$\begin{aligned} \frac{dS_2}{dt} = 0 &\iff r_1 - r_2 = 0 \\ &\iff \frac{V_2S_2}{Km_2 + S_2} - \frac{V_1S_1}{(Km_1 + S_1)(1 + q_1S_3)} = 0 \\ &\implies S_2^* = \frac{V_1Km_2S_1}{V_2Km_1q_1S_3 + V_2Km_1 + V_2q_1S_1S_3 + (V_2 - V_1)S_1}. \end{aligned} \quad (4.2.5)$$

S_2^* is positive if,

$$V_2Km_1q_1S_3 + V_2Km_1 + V_2q_1S_1S_3 + (V_2 - V_1)S_1 > 0. \quad (4.2.6)$$

From (4.2.6), one can derive a sufficient condition for S_2^* to be positive. That is

$$V_2 \geq V_1. \quad (4.2.7)$$

The inequality (4.2.7) says that if the maximum rate of synthesis of FAs is greater than that of malonyl-CoA, then the positiveness of S_2^* is guaranteed.

Evaluation of S_3^*

$$\begin{aligned} \frac{dS_3}{dt} = 0 &\iff V_{in2} + r_2 - r_3 - r_4 + r_5 - V_{out2} = 0 \\ &\iff k_2 + \frac{V_2S_2}{Km_2 + S_2} - \frac{V_3S_3}{Km_3 + S_3} - \frac{V_4S_3}{(Km_4 + S_3)(1 + q_4S_2)} + \frac{V_5S_4}{Km_5 + S_4} \\ &\quad - \beta S_3 = 0 \\ &\implies P_2(S_3) = 0, \end{aligned}$$

where $P_2(S_3)$ is a third-degree polynomial in S_3 that one can write as follows

$$P_2(S_3) = A_2S_3^3 + B_2S_3^2 + C_2S_3 + D_2, \quad (4.2.8)$$

with

$$\begin{aligned} A_2 &= -Km_2Km_5S_2\beta q_4 - Km_2Km_5\beta - Km_2S_2S_4\beta q_4 \\ &\quad - Km_2S_4\beta - Km_5S_2^2\beta q_4 - Km_5S_2\beta - S_2^2S_4\beta q_4 - S_2S_4\beta, \end{aligned} \quad (4.2.9)$$

$$\begin{aligned}
B_2 = & -Km_2Km_3Km_5S_2\beta q_4 - Km_2Km_3Km_5\beta - Km_2Km_3S_2S_4\beta q_4 - Km_2Km_3S_4\beta \\
& - Km_2Km_4Km_5S_2\beta q_4 - Km_2Km_4Km_5\beta - Km_2Km_4S_2S_4\beta q_4 - Km_2Km_4S_4\beta \\
& - Km_2Km_5S_2V_3q_4 + Km_2Km_5S_2k_2q_4 - 2Km_2Km_5V_3 + Km_2Km_5k_2 \\
& - Km_2S_2S_4V_3q_4 + Km_2S_2S_4V_5q_4 + Km_2S_2S_4k_2q_4 - 2Km_2S_4V_3 + Km_2S_4V_5 \\
& + Km_2S_4k_2 - Km_3Km_5S_2^2\beta q_4 - Km_3Km_5S_2\beta - Km_3S_2^2S_4\beta q_4 - Km_3S_2S_4\beta \\
& - Km_4Km_5S_2^2\beta q_4 - Km_4Km_5S_2\beta - Km_4S_2^2S_4\beta q_4 - Km_4S_2S_4\beta + Km_5S_2^2V_2q_4 \\
& - Km_5S_2^2V_3q_4 + Km_5S_2^2k_2q_4 + Km_5S_2V_2 - 2Km_5S_2V_3 + Km_5S_2k_2 + S_2^2S_4V_2q_4 \\
& - S_2^2S_4V_3q_4 + S_2^2S_4V_5q_4 + S_2^2S_4k_2q_4 + S_2S_4V_2 - 2S_2S_4V_3 + S_2S_4V_5 + S_2S_4k_2,
\end{aligned} \tag{4.2.10}$$

$$\begin{aligned}
C_2 = & -Km_2Km_3Km_4Km_5S_2\beta q_4 - Km_2Km_3Km_4Km_5\beta - Km_2Km_3Km_4S_2S_4\beta q_4 \\
& - Km_2Km_3Km_4S_4\beta + Km_2Km_3Km_5S_2k_2q_4 - Km_2Km_3Km_5V_3 + Km_2Km_3Km_5k_2 \\
& + Km_2Km_3S_2S_4V_5q_4 + Km_2Km_3S_2S_4k_2q_4 - Km_2Km_3S_4V_3 + Km_2Km_3S_4V_5 \\
& + Km_2Km_3S_4k_2 - Km_2Km_4Km_5S_2V_3q_4 + Km_2Km_4Km_5S_2k_2q_4 - Km_2Km_4Km_5V_3 \\
& + Km_2Km_4Km_5k_2 - Km_2Km_4S_2S_4V_3q_4 + Km_2Km_4S_2S_4V_5q_4 + Km_2Km_4S_2S_4k_2q_4 \\
& - Km_2Km_4S_4V_3 + Km_2Km_4S_4V_5 + Km_2Km_4S_4k_2 - Km_3Km_4Km_5S_2^2\beta q_4 \\
& - Km_3Km_4Km_5S_2\beta - Km_3Km_4S_2^2S_4\beta q_4 - Km_3Km_4S_2S_4\beta + Km_3Km_5S_2^2V_2q_4 \\
& + Km_3Km_5S_2^2k_2q_4 + Km_3Km_5S_2V_2 - Km_3Km_5S_2V_3 + Km_3Km_5S_2k_2 + Km_3S_2^2S_4V_2q_4 \\
& + Km_3S_2^2S_4V_5q_4 + Km_3S_2^2S_4k_2q_4 + Km_3S_2S_4V_2 - Km_3S_2S_4V_3 + Km_3S_2S_4V_5 \\
& + Km_3S_2S_4k_2 + Km_4Km_5S_2^2V_2q_4 - Km_4Km_5S_2^2V_3q_4 + Km_4Km_5S_2^2k_2q_4 + Km_4Km_5S_2V_2 \\
& - Km_4Km_5S_2V_3 + Km_4Km_5S_2k_2 + Km_4S_2^2S_4V_2q_4 - Km_4S_2^2S_4V_3q_4 + Km_4S_2^2S_4V_5q_4 \\
& + Km_4S_2^2S_4k_2q_4 + Km_4S_2S_4V_2 - Km_4S_2S_4V_3 + Km_4S_2S_4V_5 + Km_4S_2S_4k_2,
\end{aligned} \tag{4.2.11}$$

and

$$\begin{aligned}
D_2 = & Km_2Km_3Km_4Km_5S_2k_2q_4 + Km_2Km_3Km_4Km_5k_2 + Km_2Km_3Km_4S_2S_4V_5q_4 \\
& + Km_2Km_3Km_4S_2S_4k_2q_4 + Km_2Km_3Km_4S_4V_5 + Km_2Km_3Km_4S_4k_2 \\
& + Km_3Km_4Km_5S_2^2V_2q_4 + Km_3Km_4Km_5S_2^2k_2q_4 + Km_3Km_4Km_5S_2V_2 \\
& + Km_3Km_4Km_5S_2k_2 + Km_3Km_4S_2^2S_4V_2q_4 + Km_3Km_4S_2^2S_4V_5q_4 \\
& + Km_3Km_4S_2^2S_4k_2q_4 + Km_3Km_4S_2S_4V_2 + Km_3Km_4S_2S_4V_5 + Km_3Km_4S_2S_4k_2.
\end{aligned} \tag{4.2.12}$$

Given that $P_2(S_3)$ is a third-degree polynomial, if it admits three distinct roots S_{31}^* , S_{32}^* , and S_{33}^* , then with each of them, one can construct a quadruplet $(S_1^*, S_2^*, S_{3i}^*, S_4^*)$ representing a steady-state. I already demonstrated above that there is only one possible expression for S_1^* and S_2^* . I will show later that this is also the case for S_4^* .

Let us use Descartes' rule of signs to set conditions for any steady-state S_3^* solution of the polynomial $P_2(S_3)$ to be positive. From (4.2.9) and (4.2.12), A_2 is negative while D_2 is positive. However, B_2 and C_2 can be positive, negative, or null. I exclude the situation where S_3^* is null, as that will mean no FA in the liver at the steady-state, which is physiologically impossible. According to Proposition 1 and Proposition 2 (see Chapter 2), the number of the positive roots S_3^* of the

polynomial $P_2(S)$ depends only on the possible signs of B_2 and C_2 . If $B_2 > 0$ and $C_2 < 0$, there are three sign-changing in the coefficients of $P_2(S_3)$, implying that there can be either three or one positive root(s) of S_3^* . This is only the necessary condition for the polynomial $P_2(S_3)$ to have three positive roots. One needs to study the sign of the turning points¹ to have sufficient conditions. I summarize the study of the possible number of positive values of S_3^* using Descartes' rule of signs in Table 4.2.

Table 4.2: **Summary of the possible number of roots for $P_2(S_3)$ by applying Descartes' rule of signs for positive roots:** the highlighted row represents the case where one can have either one positive root or three positive roots. $V_p(P_2)$ is the number of sign-changes in the polynomial $P_2(S_3)$ and $N_p(P_2)$ is the corresponding number of positive roots.

A_2	B_2	C_2	D_2	$V_p(P_2)$	$N_p(P_2)$
-	0	0	+	1	1
-	0	-	+	1	1
-	0	+	+	1	1
-	-	0	+	1	1
-	+	0	+	1	1
-	-	-	+	1	1
-	-	+	+	1	1
-	+	-	+	3	3 or 1
-	+	+	+	1	1

Evaluation of S_4^*

$$\begin{aligned}
 \frac{dS_4}{dt} = 0 &\iff V_{in3} + r_3 - r_5 - V_{out3} = 0 \\
 &\iff k_3 + \frac{V_3 S_3}{K m_3 + S_3} - \frac{V_5 S_4}{K m_5 + S_4} - \gamma S_4 = 0 \\
 &\iff (-K m_3 \gamma - S_3 \gamma) S_4^2 + (-K m_3 K m_5 \gamma - K m_3 V_5 + K m_3 k_3 \\
 &\quad - K m_5 S_3 \gamma + S_3 V_3 - S_3 V_5 + S_3 k_3) S_4 + K m_3 K m_5 k_3 \\
 &\quad + K m_5 S_3 V_3 + K m_5 S_3 k_3 = 0
 \end{aligned}$$

¹A turning point of a function f is any value x_0 of its domain where the function's derivative vanishes with a change of sign.

$$\iff P_3(S_4) = 0.$$

$P_3(S_4)$ is the second-degree polynomial in S_4 that one can write as follows

$$P_3(S_4) = A_3S_4^2 + B_3S_3 + C_3,$$

$$A_3 = -Km_3\gamma - S_3\gamma \quad (4.2.13)$$

$$B_3 = -Km_3Km_5\gamma - Km_3V_5 + Km_3k_3 - Km_5S_3\gamma + S_3V_3 - S_3V_5 + S_3k_3 \quad (4.2.14)$$

$$C_3 = Km_3Km_5k_3 + Km_5S_3V_3 + Km_5S_3k_3. \quad (4.2.15)$$

Using the same analysis as for the case S_1^* , it appears that $P_3(S_4)$ has exactly one positive root, that is

$$S_4^* = \frac{-B_3 - \sqrt{\Delta_{P_3}}}{2A_3} \quad (4.2.16)$$

where

$$\Delta_{P_3} = B_3^2 - 4A_3C_3. \quad (4.2.17)$$

Note that $A_3 < 0$ and $C_3 > 0$ which ensure that

$$\Delta_{P_3} = B_3^2 - 4A_3C_3 > 0. \quad (4.2.18)$$

From the above, the FA dynamics equation (S_3) guarantees a possibility of having three distinct steady-state values S_3^* . In contrast, the other metabolites each have a single steady-state value. So by changing the value of S_3^* , one can have three combinations $(S_1^*, S_2^*, S_3^*, S_4^*)$ of steady-states of system stationary.

4.2.2 Sufficient conditions

In 4.2.1, one can see that the system could only have three steady-states through S_3^* . The conclusion is that for such a realization, it is necessary that the coefficients B_2 and C_2 of the polynomial $P_2(S_3)$ be respectively positive and negative. Furthermore, Descartes' rule of signs guarantees the existence of at least one positive root and no negative root for P_2 . To ensure the existence of the two other positive roots, I will derive additional conditions by studying the turning points of $P_2(S_3)$.

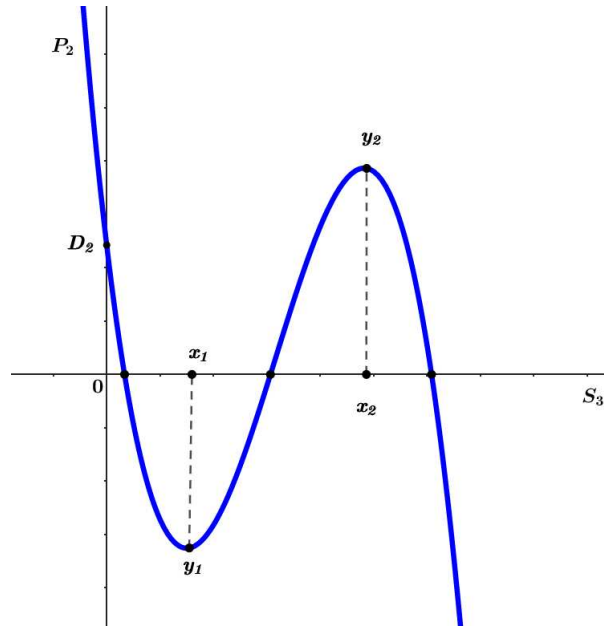


Figure 4.2: Illustration of the scenario where one could have three positive values of S_3^* at the steady-state.

- Given that $A_2 < 0$, then

$$\begin{cases} \lim_{S_3 \rightarrow -\infty} P_2(S_3) = +\infty \\ \lim_{S_3 \rightarrow +\infty} P_2(S_3) = -\infty, \end{cases}$$

which implies that there exists $x_0 \in]-\infty, +\infty[$ such that the curve of $P_2(S_3)$ decreases in $] -\infty, x_0[$. Furthermore, Descartes' rule of signs guarantees at least one positive root.

- If the derivative $P_2'(S_3)$ of $P_2(S_3)$ has two positive roots x_1, x_2 (with $x_1 < x_2$) and $y_1 = P_2(x_1) < 0$, $y_2 = P_2(x_2) > 0$ then P_2 has 3 positives roots. Figure 4.2 illustrates this scenario.

Indeed, one has

$$P_2'(S_3) = 3A_2S_3^2 + 2B_2S_3 + C_2, \quad (4.2.19)$$

with $3A_2 < 0$, $2B_2 > 0$, and $C_2 < 0$. By applying Descartes' rule of signs, it turns out that $P_2'(S_3)$ has either two positive roots or none. Furthermore, if the discriminant $\Delta_{P_2'}$ is strictly positive, then $P_2'(S_3)$ has two positive roots. One should note that having a positive discriminant is a crucial condition.

One obtains

$$\begin{aligned} \Delta_{P_2'} > 0 &\iff 4B_2^2 - 12A_2C_2 > 0 \\ &\iff B_2^2 > 3A_2C_2. \end{aligned} \quad (4.2.20)$$

Hence,

$$\begin{cases} x_1 = \frac{-B_2 + \sqrt{B_2^2 - 3A_2C_2}}{3A_2} \\ x_2 = \frac{-B_2 - \sqrt{B_2^2 - 3A_2C_2}}{3A_2}. \end{cases}$$

One has

$$\begin{aligned} P_2(x_1) &= \frac{1}{27A_2^2}(-B_2 + \sqrt{B_2^2 - 3A_2C_2})^3 + \frac{B_2}{9A_2^2}(-B_2 + \sqrt{B_2^2 - 3A_2C_2})^2 \\ &\quad + \frac{C_2}{A_2}(-B_2 + \sqrt{B_2^2 - 3A_2C_2}) + D_2 \\ &= D_2 - \frac{B_2C_2}{3A_2} + \frac{2C_2\sqrt{B_2^2 - 3A_2C_2}}{9A_2} + \frac{2B_2^3}{27A_2^2} - \frac{2B_2^2\sqrt{B_2^2 - 3A_2C_2}}{27A_2^2} \end{aligned} \quad (4.2.21)$$

$$\begin{aligned} P_2(x_2) &= \frac{1}{27A_2^2}(-B_2 - \sqrt{B_2^2 - 3A_2C_2})^3 + \frac{B_2}{9A_2^2}(-B_2 - \sqrt{B_2^2 - 3A_2C_2})^2 \\ &\quad + \frac{C_2}{A_2}(-B_2 - \sqrt{B_2^2 - 3A_2C_2}) + D_2 \\ &= D_2 - \frac{B_2C_2}{3A_2} - \frac{2C_2\sqrt{B_2^2 - 3A_2C_2}}{9A_2} + \frac{2B_2^3}{27A_2^2} + \frac{2B_2^2\sqrt{B_2^2 - 3A_2C_2}}{27A_2^2} \end{aligned} \quad (4.2.22)$$

4.2.3 Summary of the conditions for having three steady-states

For the system to have three steady-states, it is necessary that S_3^* takes three distinct values, and for this to be achieved, the following conditions must be fulfilled simultaneously:

- 1) B_2 must be positive
- 4) C_2 must be negative
- 3) $B_2^2 > 3A_2C_2$
- 4) $P_2(x_1)$ must be negative
- 5) $P_2(x_2)$ must be positive.

4.3 Stability analysis of the steady-states

Assuming that conditions 1) to 5). ensuring the existence of three steady-states are satisfied, let us denote by S_{31}^* , S_{32}^* , and S_{33}^* the three possible values of S_3^* (with $0 < S_{31}^* < S_{32}^* < S_{33}^*$). The

associated steady-states are

$$\begin{cases} \mathbf{S}^*_1 = (S_1^*, S_2^*, S_{31}^*, S_4^*) \\ \mathbf{S}^*_2 = (S_1^*, S_2^*, S_{32}^*, S_4^*) \\ \mathbf{S}^*_3 = (S_1^*, S_2^*, S_{33}^*, S_4^*). \end{cases} \quad (4.3.1)$$

To achieve bi-stability, it is necessary to have two stable steady-states and one unstable one. Without loss of generality, consider \mathbf{S}^*_1 and \mathbf{S}^*_3 to be stable, and \mathbf{S}^*_2 unstable.

Let us denote by $f_1(\mathbf{S})$, $f_2(\mathbf{S})$, $f_3(\mathbf{S})$, and $f_4(\mathbf{S})$ the right-hand sides of the equation (4.1.1), (4.1.2), (4.1.3), and (4.1.4), respectively, where $\mathbf{S} = (S_1, S_2, S_3, S_4)$. The Jacobian matrix of the system (2.2.1) associated with the steady-state \mathbf{S}^*_k , $k = 1, 2, 3$ is given by:

$$J_k = \left(D_{ij}^k \right)_{\substack{1 \leq i, j \leq 4, \\ 1 \leq k \leq 3}}, \quad (4.3.2)$$

where

$$D_{ij}^k = \frac{\partial f_i}{\partial S_j}(\mathbf{S}^*_k). \quad (4.3.3)$$

Here, k is the index of the steady-states, whereas i and j are used to label the four metabolites in the system and the right-hand side of the ODEs describing their dynamics, respectively.

More precisely, the entries of J_k are:

$$D_{11}^k = -\alpha - \frac{V_1 K m_1}{(1 + q_1 S_{3k}^*)(K m_1 + S_1^*)^2} \quad (4.3.4)$$

$$D_{12}^k = -\frac{V_4 q_4 S_{3k}^*}{(K m_4 + S_{3k}^*)(1 + q_4 S_2^*)^2} \quad (4.3.5)$$

$$D_{13}^k = \frac{V_1 q_1 S_1^*}{(K m_1 + S_1^*)(1 + q_1 S_{3k}^*)^2} + \frac{V_4 K m_4}{(1 + q_4 S_2^*)(K m_4 + S_{3k}^*)^2} \quad (4.3.6)$$

$$D_{14}^k = 0 \quad (4.3.7)$$

$$D_{21}^k = \frac{V_1 K m_1}{(1 + q_1 S_{3k}^*)(K m_1 + S_1^*)^2} \quad (4.3.8)$$

$$D_{22}^k = -\frac{V_2 K m_2}{(K m_2 + S_2^*)^2} \quad (4.3.9)$$

$$D_{23}^k = -\frac{V_1 q_1 S_1^*}{(K m_1 + S_1^*)(1 + q_1 S_{3k}^*)^2} \quad (4.3.10)$$

$$D_{24}^k = 0 \quad (4.3.11)$$

$$D_{31}^k = 0 \quad (4.3.12)$$

$$D_{32}^k = \frac{V_2 K m_2}{(K m_2 + S_2^*)^2} + \frac{V_4 q_4}{(K m_4 + S_{3k}^*)(1 + q_4 S_4^*)^2} \quad (4.3.13)$$

$$D_{33}^k = -\beta - \frac{V_3 K m_3}{(K m_3 + S_{3k}^*)^2} - \frac{V_4 K m_4}{(1 + q_4 S_2^*)(K m_4 + S_{3k}^*)^2} \quad (4.3.14)$$

$$D_{34}^k = \frac{V_5 K m_5}{(K m_5 + S_4^*)^2} \quad (4.3.15)$$

$$D_{41}^k = 0 \quad (4.3.16)$$

$$D_{42}^k = 0 \quad (4.3.17)$$

$$D_{43}^k = \frac{V_3 K m_3}{(K m_3 + S_{3k}^*)^2} \quad (4.3.18)$$

$$D_{44}^k = -\gamma - \frac{V_5 K m_5}{(K m_5 + S_4^*)^2}. \quad (4.3.19)$$

Then,

$$J_k = \begin{pmatrix} D_{11}^k & D_{12}^k & D_{13}^k & D_{14}^k \\ D_{21}^k & D_{22}^k & D_{23}^k & D_{24}^k \\ D_{31}^k & D_{32}^k & D_{33}^k & D_{34}^k \\ D_{41}^k & D_{42}^k & D_{43}^k & D_{44}^k \end{pmatrix} \quad (4.3.20)$$

To facilitate the calculations that will follow, I replace the entries in (4.3.20), which beforehand are 0 by their values. Hence, one has

$$J_k = \begin{pmatrix} D_{11}^k & D_{12}^k & D_{13}^k & 0 \\ D_{21}^k & D_{22}^k & D_{23}^k & 0 \\ 0 & D_{32}^k & D_{33}^k & D_{34}^k \\ 0 & 0 & D_{43}^k & D_{44}^k \end{pmatrix} \quad (4.3.21)$$

The eigenvalues of J_k are the zeros of the polynomial

$$\Gamma_k(\lambda) = \det(J_k - \lambda I_4), \quad (4.3.22)$$

where \det and I_4 stand for the determinant and 4×4 identity matrix, respectively. After some algebra, one obtain

$$\Gamma_k(\lambda) = \lambda^4 + A_k \lambda^3 + B_k \lambda^2 + C_k \lambda + D_k, \quad (4.3.23)$$

with

$$A_k = - (D_{11}^k + D_{22}^k + D_{33}^k + D_{44}^k) = -\text{tr}(J_k) \quad (4.3.24)$$

$$B_k = D_{11}^k D_{22}^k + D_{11}^k D_{33}^k + D_{11}^k D_{44}^k - D_{12}^k D_{21}^k + D_{22}^k D_{33}^k + D_{22}^k D_{44}^k - D_{23}^k D_{32}^k + D_{33}^k D_{44}^k \quad (4.3.25)$$

$$\begin{aligned}
& - D_{34}^k D_{43}^k \\
C_k = & - D_{11}^k D_{22}^k D_{33}^k - D_{11}^k D_{22}^k D_{44}^k + D_{11}^k D_{23}^k D_{32}^k - D_{11}^k D_{33}^k D_{44}^k + D_{11}^k D_{34}^k D_{43}^k \\
& + D_{12}^k D_{21}^k D_{33}^k + D_{12}^k D_{21}^k D_{44}^k - D_{13}^k D_{21}^k D_{32}^k - D_{22}^k D_{33}^k D_{44}^k + D_{22}^k D_{34}^k D_{43}^k + D_{23}^k D_{32}^k D_{44}^k
\end{aligned} \tag{4.3.26}$$

$$\begin{aligned}
D_k = & D_{11}^k D_{22}^k D_{33}^k D_{44}^k - D_{11}^k D_{22}^k D_{34}^k D_{43}^k - D_{11}^k D_{23}^k D_{32}^k D_{44}^k - D_{12}^k D_{21}^k D_{33}^k D_{44}^k \\
& + D_{12}^k D_{21}^k D_{34}^k D_{43}^k + D_{13}^k D_{21}^k D_{32}^k D_{44}^k.
\end{aligned} \tag{4.3.27}$$

tr in equation (4.3.24) stand for trace of the matrix.

If it is obvious that the sign of A_k is positive, one cannot decide *a priori* on the signs of the other coefficients. Indeed, their signs will depend on the values of the parameters in the expression of the steady-state concentration vector \mathcal{S}_k^* .

4.3.1 Conditions for a steady-state to be stable

For \mathcal{S}_k^* to be stable, its corresponding characteristic polynomial $\Gamma_k(\lambda)$ must have four distinct and negative roots. I will use Descartes' rule of signs for negative roots and derive the conditions under which $\Gamma_k(\lambda)$ has all its roots distinct and negative.

Considering

$$\Gamma_k(-\lambda) = \lambda^4 - A_k \lambda^3 + B_k \lambda^2 - C_k \lambda + D_k, \tag{4.3.28}$$

the analysis of the possible number of negative roots of $\Gamma_k(\lambda)$ is summarized in Table 4.3,

Table 4.3: **The possible number of negative roots of $\Gamma_k(\lambda)$ by applying Descartes' rule of signs for negative roots:** the highlighted represents the scenario of interest. $V_n(\Gamma_k)$ is the number of sign-changes in the polynomial $\Gamma_k(-\lambda)$ and $N_n(\Gamma_k)$ is the corresponding number of negative roots.

1	$-A_k$	B_k	$-C_k$	D_k	$V_n(\Gamma_k)$	$N_n(\Gamma_k)$
+	-	-	-	-	1	1
+	-	-	-	+	2	2 or 0
+	-	-	+	-	3	3 or 1
+	-	-	+	+	2	2 or 0
+	-	+	-	-	3	3 or 1
+	-	+	-	+	4	4 or 2 or 0
+	-	+	+	-	3	3 or 1
+	-	+	+	+	2	2 or 0

Based on Table 4.3, one can understand that for $\Gamma_k(\lambda)$ to have four negatives roots, it is necessary that

$$\begin{cases} B_k > 0 \\ C_k > 0 \\ D_k > 0. \end{cases} \quad (4.3.29)$$

Combining (4.3.29) with the positiveness of A_k , a necessary condition for \mathcal{S}_k^* to be stable is that the characteristic polynomial $\Gamma_k(\lambda)$ of J_k must have only positive coefficients. To guarantee the existence of the four negative roots, $\Gamma_k(\lambda)$ must have three negative turning points m_1^k, m_2^k, m_3^k (without loss of generality, I consider $m_1^k < m_2^k < m_3^k$). Furthermore, one must have

$$\begin{cases} \Gamma_k(m_1^k) < 0 \\ \Gamma_k(m_2^k) > 0 \\ \Gamma_k(m_3^k) < 0. \end{cases} \quad (4.3.30)$$

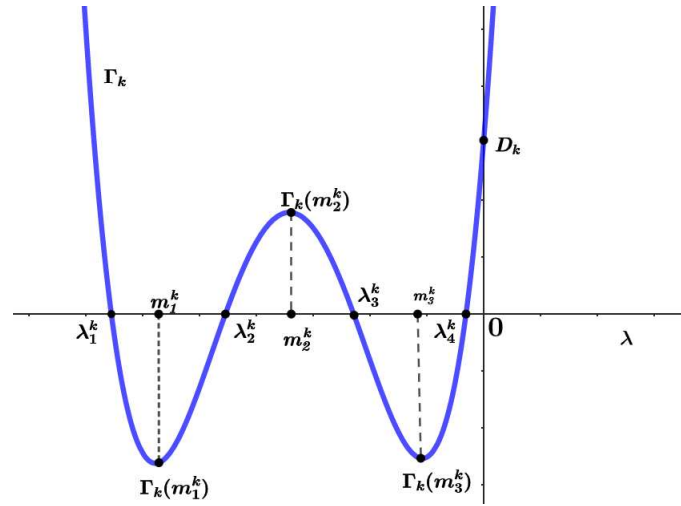


Figure 4.3: **Conditions for the Jacobian matrix J_k to have three negative eigenvalues.**

The turning points of $\Gamma_k(\lambda)$ are the zeros of the polynomial $\Gamma'_k(\lambda)$, where $\Gamma'_k(\lambda)$ is the derivative polynomial of $\Gamma_k(\lambda)$. For $\Gamma'_k(\lambda)$ to have three negative roots, it is necessary to have three changes of sign in the coefficients of $\Gamma'_k(-\lambda)$, which is already satisfied. Thus the sufficient condition is $\Gamma'_k(\lambda)$ having two negative turning points n_1^k and n_2^k . Suppose $n_1^k < n_2^k$, one should have

$$\begin{cases} \Gamma'_k(n_1^k) > 0 \\ \Gamma'_k(n_2^k) < 0. \end{cases} \quad (4.3.31)$$

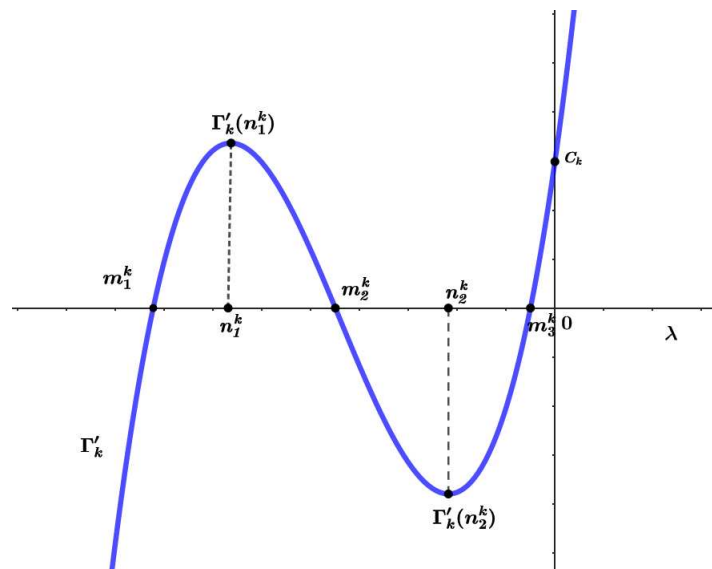


Figure 4.4: **Analysis of the scenario where $\Gamma'_k(\lambda)$ has two turning points.**

Using the same reasoning as in the case of $\Gamma_k(\lambda)$, the turning points of $\Gamma'_k(\lambda)$ are the zeros of $\Gamma''_k(\lambda)$. One already has two sign changes in the expression $\Gamma''_k(-\lambda)$, which is a necessary condition

to have two negative roots. The sufficient condition is that the discriminant $\Delta_{\Gamma_k''}$ should be positive. One has

$$\Gamma_k''(\lambda) = 12\lambda^2 + 6A_k\lambda + 2B_k, \quad (4.3.32)$$

and

$$\Delta_{\Gamma_k''} = 36A_k^2 - 96B_k. \quad (4.3.33)$$

$$\Delta_{\Gamma_k''} > 0 \iff \frac{A_k^2}{B_k} > \frac{8}{3} \quad (4.3.34)$$

Once the condition (4.3.34) is satisfied, one can determine n_1^k and n_2^k as follows

$$n_1^k = -\frac{3A_k + \sqrt{3(3A_k^2 - 8B_k)}}{12} \quad (4.3.35)$$

$$n_2^k = \frac{-3A_k + \sqrt{3(3A_k^2 - 8B_k)}}{12}. \quad (4.3.36)$$

To summarize, for a steady-state \mathbf{S}_k^* to be stable, the following conditions on the parameterization must be fulfilled:

$$(Stab\ Cond) \quad \left\{ \begin{array}{l} B_k > 0 \\ C_k > 0 \\ D_k > 0 \\ \frac{A_k^2}{B_k} > \frac{8}{3} \\ \Gamma_k'(n_1^k) > 0 \\ \Gamma_k'(n_2^k) < 0 \\ \Gamma_k(m_1^k) < 0 \\ \Gamma_k(m_2^k) > 0 \\ \Gamma_k(m_3^k) < 0 \end{array} \right. .$$

4.3.2 Condition for a steady-state to be unstable

To achieve bi-stability, we saw 4.2.1 that at least one steady-state must be unstable; i.e., $\Gamma_k(\lambda)$ must have at least one positive root. This condition leads to different cases depending on the sign of the coefficients B_k , C_k , and D_k . Table 4.4 summarizes the possible situations.

Table 4.4: The possible number of positive roots of $\Gamma_k(\lambda)$ by applying Descartes' rule of signs for positive roots.

1	A_k	B_k	C_k	D_k	$V_p(\Gamma_k)$	$N_p(\Gamma_k)$
+	+	-	-	-	1	1
+	+	-	-	+	2	2 or 0
+	+	-	+	-	3	3 or 1
+	+	-	+	+	2	2 or 0
+	+	+	-	-	1	1
+	+	+	-	+	2	2 or 0
+	+	+	+	-	1	1
+	+	+	+	+	0	0

From Table 4.4, one can already see that it is impossible to have four positive eigenvalues, which eliminates the possibility of an unstable node. Furthermore, I can also eliminate the case of zero negative roots, which corresponds to the case of the unique steady-state (uni-stability). I consider only cases where the eigenvalues are real to avoid getting complex dynamics such as oscillations and limit cycles. Therefore, the possible scenarios are either:

- one positive and three negative eigenvalues
- two positive and two negative eigenvalues
- three positive and one negative eigenvalues.

Given that the signs of the two leading coefficients (1 and A_k) of the characteristic polynomial Γ_k are independent of the values of the parameters, Descartes' rule of signs allows us to summarize the possible combination based on the signs of B_k , C_k , and D_k . Table 4.5 allows summarizes the possibilities possibilities.

Table 4.5 gives the possible combinations of the signs of the real roots of $\Gamma_k(\lambda)$ without guaranteeing their existence. Therefore, one needs to derive further conditions to be fulfilled by S_k^* to be a saddle (unstable in one, two, or three directions). These conditions depend only on the combinations of signs of the coefficients B_k , C_k , and D_k . To represent the combination of sign-changing of those coefficients and the corresponding fixed points, I introduce the following vector notation

$$(\text{sg}(B_k), \text{sg}(C_k), \text{sg}(D_k)), \quad (4.3.37)$$

Table 4.5: The possible number of positive and negative roots $\Gamma_k(\lambda)$ by applying Descartes' rule of signs

1	A_k	B_k	C_k	D_k	$-A_k$	$-C_k$	$V_p(\Gamma_k)$	$V_n(\Gamma_k)$
+	+	-	-	-	-	+	1	3
+	+	-	-	+	-	+	2	2
+	+	-	+	-	-	-	3	1
+	+	-	+	+	-	-	2	2
+	+	+	-	-	-	+	1	3
+	+	+	-	+	-	+	2	2
+	+	+	+	-	-	-	1	3
+	+	+	+	+	-	-	0	4

where the function sg is defined by

$$\text{sg}(x) = \begin{cases} - & \text{if } x \text{ is negative} \\ + & \text{if } x \text{ is positive} \end{cases} . \quad (4.3.38)$$

- i) Saddle with one unstable direction, that is to say, with one positive eigenvalue. For the unstable fixed point to be a saddle with an unstable direction, the vector of signs $(\text{sg}(B_k), \text{sg}(C_k), \text{sg}(D_k))$ should take one of the following combinations of signs $(-, -, -)$, $(+, -, -)$ or $(+, +, -)$.
- ii) Saddle with two unstable directions, that is, two positive eigenvalues. In this case, the vector of signs $(\text{sg}(B_k), \text{sg}(C_k), \text{sg}(D_k))$ should take one of the following combination of signs $(-, -, +)$, $(-, +, +)$ and $(+, -, +)$.
- iii) Saddle with three unstable directions: three positive eigenvalues. in this case the vector of signs $(\text{sg}(B_k), \text{sg}(C_k), \text{sg}(D_k))$ should take the following combination of signs $(-, +, -)$.

For a steady \mathcal{S}_k^* to be any of the saddle I), ii), or iii), one has to derive the further specific conditions. Additionally, after deriving those conditions, it is important to check that they do not contradict the earlier derived necessary conditions in 4.2.1. Remark that $\Gamma_k(\lambda)$ has four real roots and can only have a maximum of three positive roots. Under this remark, $\Gamma_k(\lambda)$ must have three turning points that I denote by x_{k_1} , x_{k_2} , and x_{k_3} (with $x_{k_1} < x_{k_2} < x_{k_3}$). The existence of the four real eigenvalues would be guaranteed by the change of sign of $y_{k_i} = \Gamma_k(x_{k_i})$, $i \in \{1, 2, 3\}$. As illustrated in Figure 4.5 y_{k_1} should be negative, while y_{k_2} positive, and y_{k_3} negative. In the following, I will derive sufficient conditions for each case of saddle-node.

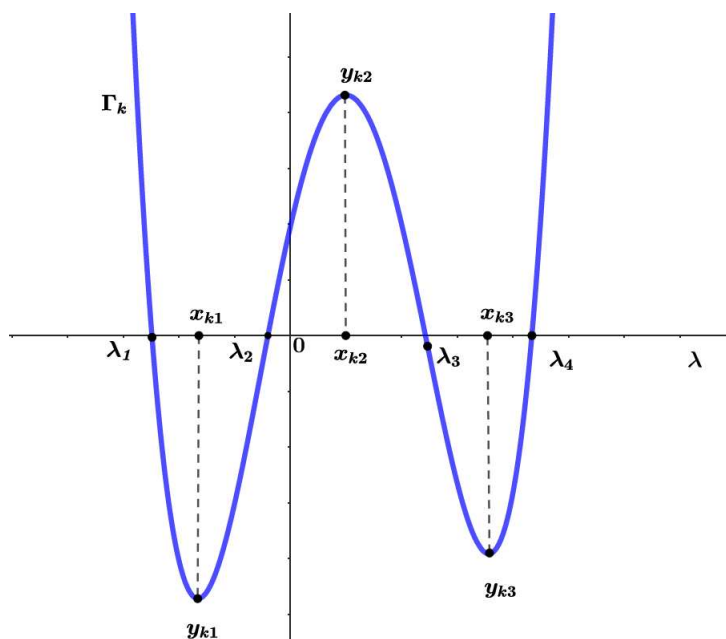


Figure 4.5: **Illustration of the conditions for $\Gamma_k(\lambda)$ to have four roots.**

It is important to remember that Figure 4.5 is only drawn to illustrate the general case and, therefore, can overlap with a particular case of a saddle with two unstable directions.

Saddle with one unstable direction.

As shown in Table 4.5, \mathcal{S}_k^* can be a saddle with one unstable direction only when D_k is negative. Based on the possible combination of B_k and C_k , I will derive further conditions to satisfy such a behavior.

Case 1: The three turning points of $\Gamma_k(\lambda)$ are all negatives.

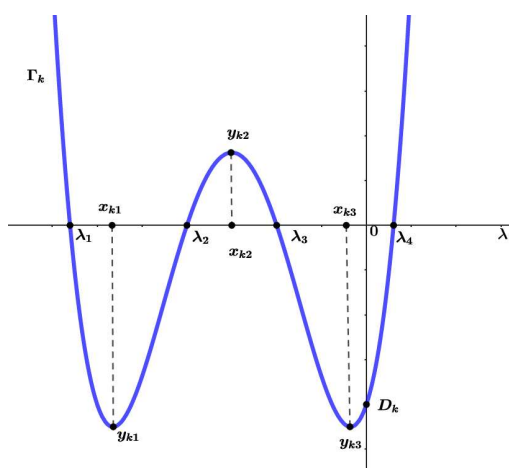


Figure 4.6: **Illustration of the case where $\Gamma_k(\lambda)$ has four distinct roots (three negative and one positive), and all its turning points are negative.**

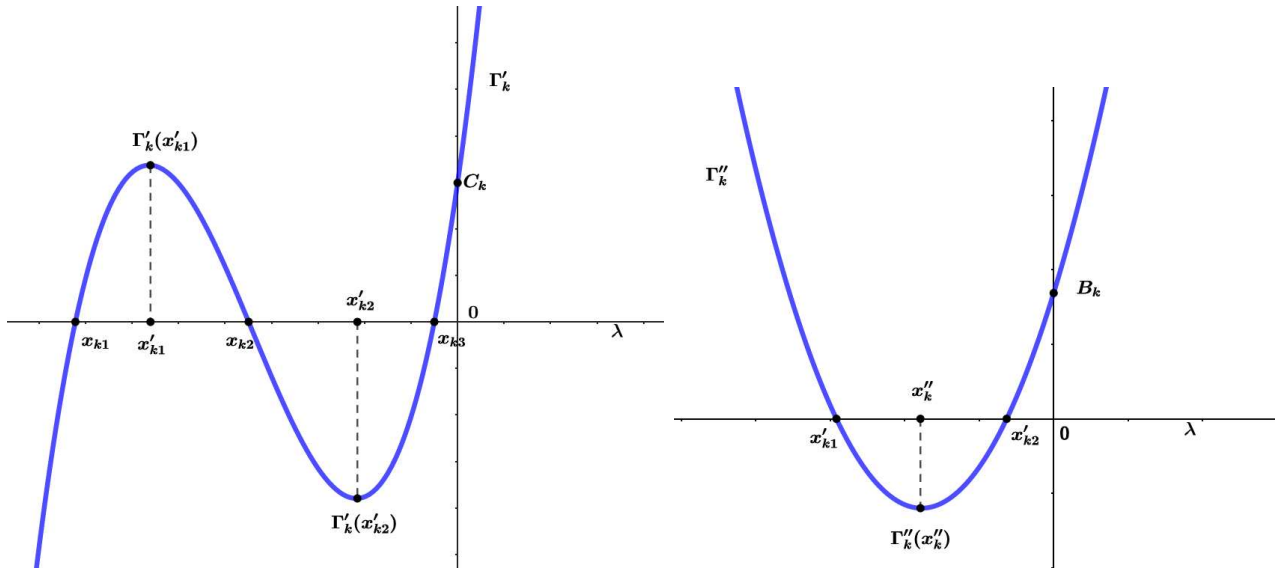


Figure 4.7: Illustration of the curves of the first (left) and second (right) derivatives ensuring that $\Gamma_k(\lambda)$ has four distinct roots (three negative and one positive), and all its turning points are negative.

Given that x_{k1} , x_{k2} , and x_{k3} are the roots of $\Gamma'_k(\lambda)$, they are all negative. The saddle with one unstable will occur if $\Gamma'_k(\lambda)$ has two negative tuning points x'_{k1} , x'_{k2} (with $x'_{k1} < x'_{k2}$) and $\Gamma'_k(x_{k1})$ positive while $\Gamma'_k(x_{k2})$ negative as illustrated by the left panel of Figure 4.7. Furthermore, x'_{k1} and x'_{k2} must verify the following inequation derive from right panel Figure 4.7

$$x'_{k1} < -\frac{1}{4}A_k < x'_{k2}.$$

For this case where the three turning points x_{k1} , x_{k2} , and x_{k3} are negative ($x_{k1} < x_{k2} < x_{k3}$), the saddle with one unstable direction is achieved if $\Gamma_k(x_{k1})$ and $\Gamma_k(x_{k3})$ negative and $\Gamma_k(x_{k2})$ positive. For $\Gamma_k(\lambda)$ to have three turning points that fulfill the aforementioned conditions, Γ'_k must have two turning points x'_{k1} , x'_{k2} ($x'_{k1} < x'_{k2}$) with x'_{k1} and x'_{k2} negative, $\Gamma'_k(x'_{k1}) > 0$, and $\Gamma'_k(x'_{k2}) < 0$.

Similarly, for $\Gamma'_k(\lambda)$ to have two turning points, the discriminant $\Delta_{\Gamma''_k}$ of the second derivative $\Gamma''_k(\lambda)$ of $\Gamma'_k(\lambda)$ must be positive.

$$\begin{cases} B_k > 0 \\ \Delta_{\Gamma''_k} = 36A_k^2 - 96B_k > 0 \end{cases} \iff \begin{cases} B_k > 0 \\ 3A_k^2 - 8B_k > 0 \end{cases}. \quad (4.3.39)$$

This case corresponds to $(\text{sg}(B_k), \text{sg}(C_k), \text{sg}(D_k)) = (+, +, -)$. The conditions can be summarized as follows,

$$(\text{unstab cond 1}) \left\{ \begin{array}{l} B_k > 0 \\ 3A_k^2 - 8B_k > 0 \\ C_k > 0 \\ \Gamma'_k(x'_{k1}) > 0 \\ \Gamma'_k(x'_{k2}) < 0 \\ D_k < 0 \\ \Gamma_k(x_{k1}) < 0 \\ \Gamma_k(x_{k2}) > 0 \\ \Gamma_k(x_{k3}) < 0 \end{array} \right. \quad (4.3.40)$$

Case 2: Two turning points of $\Gamma_k(\lambda)$ are negative and one is positive.

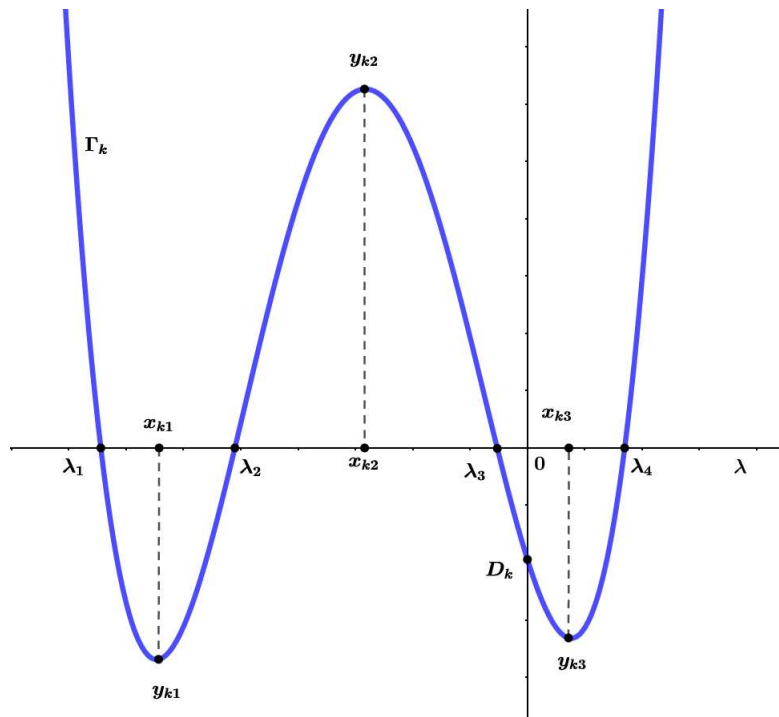


Figure 4.8: Illustration of a case where $\Gamma_k(\lambda)$ has four distinct roots (including three negative ones). Among the three turning points, two are negative, and one is positive.

This situation occurs if C_k is negative, leading to two sub-cases based on the sign of B_k . They are illustrated in the Figures 4.9 and 4.10. The first sub-case corresponds to the situation where the two turning points of $\Gamma'_k(\lambda)$ are negative and B_k is positive. The second sub-case is when the turning points of $\Gamma'_k(\lambda)$ have distinct signs, and B_k is negative. By using the same approach as in Case 4.3.2, one can conclude that for having two turning points of $\Gamma_k(\lambda)$ (one negative and the other positive), the following conditions must be satisfied.

For $(\text{sg}(B_k), \text{sg}(C_k), \text{sg}(D_k)) = (+, -, -)$, the condition for having a saddle in one direction can be summarized as follows:

$$(\text{unstab cond 2}) \quad \left\{ \begin{array}{l} B_k > 0 \\ 3A_k^2 - 8B_k > 0 \\ C_k < 0 \\ \Gamma'_k(x'_{k1}) > 0 \\ \Gamma'_k(x'_{k2}) < 0 \\ D_k < 0 \\ \Gamma_k(x_{k1}) < 0 \\ \Gamma_k(x_{k2}) > 0 \\ \Gamma_k(x_{k3}) < 0. \end{array} \right. \quad (4.3.41)$$

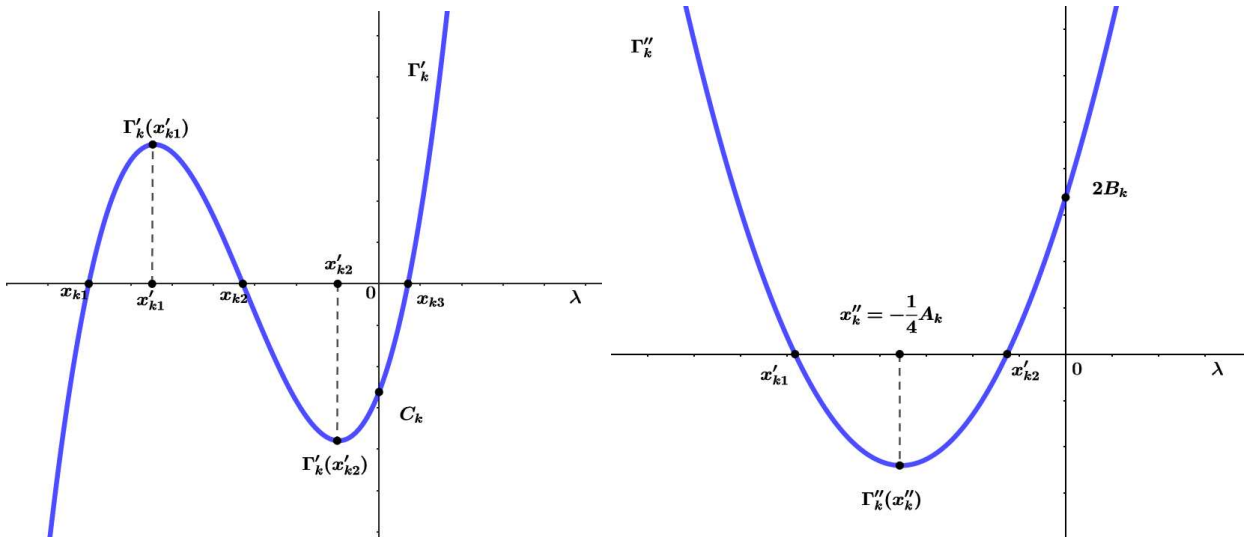


Figure 4.9: **Sub-case 1:** x'_{k1} and x'_{k2} are both negative and B_k is positive.

For $(\text{sg}(B_k), \text{sg}(C_k), \text{sg}(D_k)) = (-, -, -)$, one can summarize the conditions for having a saddle in one direction as follows:

$$\left\{ \begin{array}{l} B_k < 0 \\ 3A_k^2 - 8B_k > 0 \\ C_k < 0 \\ \Gamma'_k(x'_{k1}) > 0 \\ \Gamma'_k(x'_{k2}) < 0 \\ D_k < 0 \\ \Gamma_k(x_{k1}) < 0 \\ \Gamma_k(x_{k2}) > 0 \\ \Gamma_k(x_{k3}) < 0 \end{array} \right. \quad (4.3.42)$$

It is important to underline here that when B_k is negative, the condition $A_k^2 - 8B_k > 0$ is automatically satisfied, which leads to more relaxed conditions

$$(unstab\ cond\ 3) \quad \left\{ \begin{array}{l} B_k < 0 \\ C_k < 0 \\ \Gamma'_k(x'_{k1}) > 0 \\ \Gamma'_k(x'_{k2}) < 0 \\ D_k < 0 \\ \Gamma_k(x_{k1}) < 0 \\ \Gamma_k(x_{k2}) > 0 \\ \Gamma_k(x_{k3}) < 0 \end{array} \right. \quad (4.3.43)$$

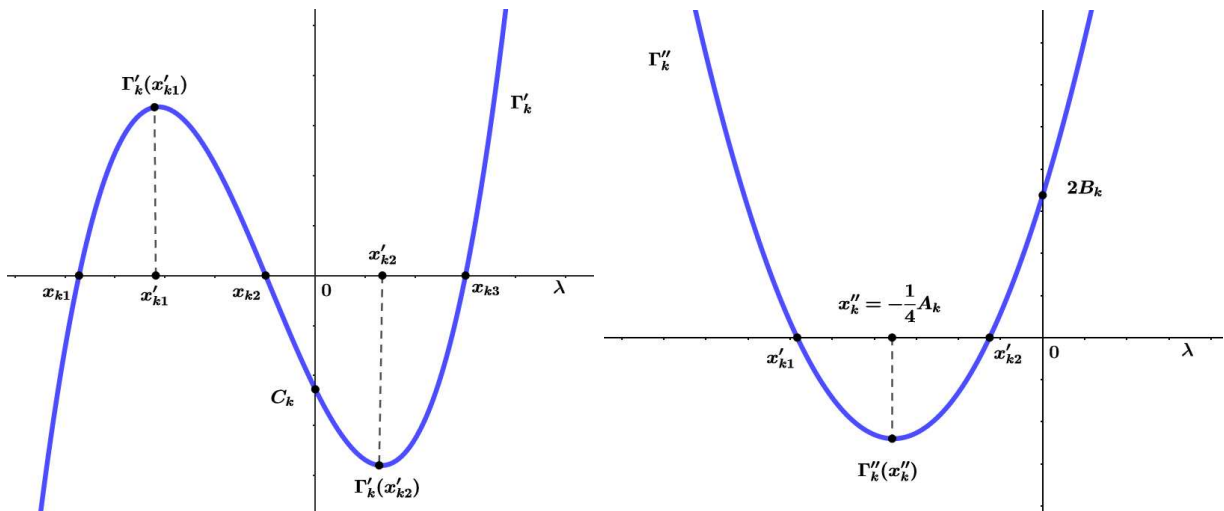


Figure 4.10: **Sub-case 2:** x'_{k1} is negative, x'_{k2} positive, and B_k negative.

To summarize, the saddle with one unstable direction corresponds to the cases where the vector sign $(\text{sg}(B_k), \text{sg}(C_k), \text{sg}(D_k))$ is $(+, +, -)$, $(+, -, -)$, and $(-, -, -)$ corresponding to the conditions (*unstab cond 1*), (*unstab cond 2*), and (*unstab cond 2*), respectively. The situation where the turning point of Γ_k'' is positive is simply impossible since A_k is positive, and the corresponding turning point is $x_k'' = -\frac{1}{4}A_k$.

Saddle with two unstable directions

According to Table 4.5, for having a saddle with two unstable directions, D_k must be positive. By using a similar analysis of the characteristic polynomial $\Gamma_k(\lambda)$ and its derivatives, like in the case of the saddle with one unstable direction 4.3.2, one obtains the scenarios where the vector $(\text{sg}(B_k), \text{sg}(C_k), \text{sg}(D_k))$ takes the combination of signs $(+, -, +)$, $(+, -, +)$, and $(+, +, +)$, respectively. These scenarios correspond respectively to the following set of conditions,

$$(\text{unstab cond 4}) \left\{ \begin{array}{l} B_k < 0 \\ C_k < 0 \\ D_k > 0 \\ \Gamma_k'(x_{k_1}') > 0 \\ \Gamma_k'(x_{k_2}') < 0 \\ \Gamma_k(x_{k_1}) < 0 \\ \Gamma_k(x_{k_2}) > 0 \\ \Gamma_k(x_{k_3}) < 0 \end{array} \right. , \quad (4.3.44)$$

$$(\text{unstab cond 5}) \left\{ \begin{array}{l} B_k > 0 \\ 3A_k^2 - 8B_k > 0 \\ C_k < 0 \\ D_k > 0 \\ \Gamma_k'(x_{k_1}') > 0 \\ \Gamma_k'(x_{k_2}') < 0 \\ \Gamma_k(x_{k_1}) < 0 \\ \Gamma_k(x_{k_2}) > 0 \\ \Gamma_k(x_{k_3}) < 0 \end{array} \right. , \quad (4.3.45)$$

and

$$(\text{unstab cond 6}) \left\{ \begin{array}{l} B_k > 0 \\ 3A_k^2 - 8B_k > 0 \\ C_k > 0 \\ D_k > 0 \\ \Gamma'_k(x'_{k_1}) > 0 \\ \Gamma'_k(x'_{k_2}) < 0 \\ \Gamma_k(x_{k_1}) < 0 \\ \Gamma_k(x_{k_2}) > 0 \\ \Gamma_k(x_{k_3}) < 0 \end{array} \right. \quad (4.3.46)$$

Saddle with three unstable directions

Table 4.5 shows that for having a saddle with three unstable directions, D_k must be negative. The same reasoning like for saddle with one unstable direction 4.3.2 leads to the scenario where the, vector sign $(\text{sg}(B_k), \text{sg}(C_k), \text{sg}(D_k))$ is $(-, +, -)$, corresponding to the following set of conditions,

$$(\text{unstab cond 7}) \left\{ \begin{array}{l} B_k < 0 \\ C_k > 0 \\ D_k < 0 \\ \Gamma'_k(x'_{k_1}) > 0 \\ \Gamma'_k(x'_{k_2}) < 0 \\ \Gamma_k(x_{k_1}) < 0 \\ \Gamma_k(x_{k_2}) > 0 \\ \Gamma_k(x_{k_3}) < 0 \end{array} \right. \quad (4.3.47)$$

4.4 Summary of bi-stability conditions

For my model of FA metabolism (see Figure 4) to be a bi-stable system, the parameterization of the system must be such that the coefficients A_2 , B_2 , C_2 , and D_2 of the polynomial $P_2(S_3^*)$ representing the equation of the FA pool at the steady-state and its turning points x_1 and x_2 fulfill

the following necessary conditions:

$$(3 \text{ steady-state cond}) \quad \left\{ \begin{array}{l} B_2 > 0 \\ C_2 < 0 \\ B_2 > 3A_2C_2 \\ P_2(x_1) < 0 \\ P_2(x_2) > 0 \end{array} \right. . \quad (4.4.1)$$

Once (3 *steady-state cond*) is fulfilled, one would like to have S^*_1 and S^*_3 to be stable and S^*_2 unstable. To do so, the characteristic polynomials associated with the Jacobian matrices of S^*_1 and S^*_3 must fulfill (*stab cond*), and the one of S^*_2 must fulfill one among (*unstab cond 1*) to (*unstab cond 7*).

4.5 Discussion and conclusion

Fatty acids (FAs) play a crucial role in maintaining the body's energy balance. In the fed state, when carbohydrates are abundant, FAs are synthesized from acetyl-CoA, which results from the breakdown of carbohydrates. Conversely, in the fasted state, as the cell's energy status declines due to a scarcity of carbohydrates, FAs are degraded to compensate for the energy shortfall. Malonyl-CoA is pivotal in these processes, serving both as a substrate, an intermediate for FA synthesis, and an inhibitor for FA degradation. Acetyl-CoA occupies a central position in FA metabolism, acting as both the precursor for synthesis and the final product in degradation. The synthesized FAs are esterified into triglycerides (TGs) for storage and later mobilized in the fasted state. Furthermore, FAs self-regulate their synthesis by inhibiting the production of malonyl-CoA. This delineation underscores that FA metabolism operates across two regimes: the synthesis and storage of FAs and their degradation. Shi and Tu [172] posited that acetyl-CoA concentration in the cytosol dictates the metabolic regime (synthesis or degradation) a cell engages in. This hypothesis is explored through a simplified model of FA metabolism, which demonstrates that, alongside acetyl-CoA, FAs are critical for the bi-stability of FA metabolism. For the system to manifest as bi-stable, FAs must also be allocated for non-energetic functions, such as components in cellular membrane construction and signaling molecules. Analysis of various unstable steady-states indicates the impossibility of an unstable node, suggesting that not all metabolites can simultaneously deviate from their steady-state. The complexity of the system's mathematical framework and its extensive parameterization precluded a comprehensive examination of transitions between steady-states in every scenario. However, this exploration could illuminate disruptions in the system during FA oxidation disorders (FAODs), potentially guiding compensatory interventions. I developed a straightforward ordinary differential equation (ODE) model to capture the dynamics

of FA metabolism in the liver, incorporating key metabolites (acetyl-CoA, malonyl-CoA, FAs, and TGs) and focusing solely on the essential processes affecting FA dynamics: synthesis, degradation, and storage. Each process is modeled as a single enzymatic reaction, following either Michaelis-Menten kinetics or non-competitive inhibition. The model also accounts for the external influx and efflux associated with all metabolites, with the exception of malonyl-CoA. Upon constructing the model, a qualitative analysis was conducted to identify the sufficient and necessary conditions for FA metabolism to exhibit bi-stability. At steady-state, the equations governing the system's dynamics reveal that the polynomials for acetyl-CoA, malonyl-CoA, and TGs each have a singular positive root. However, the FA pool's polynomial is cubic, potentially yielding three positive roots under specific conditions. These roots represent possible steady-state values for the FA pool, allowing the system to exhibit bi-stability given additional conditions. The criteria for this polynomial to possess three positive roots were established using Descartes' rule of signs and by analyzing the polynomial's extrema. Stability analysis of the steady-states demonstrated that bi-stability is feasible only when two of the three steady-states are stable. Assuming the existing steady-states are hyperbolic, their stability or instability conditions were derived. Consequently, it is deduced that the model representing FA metabolism (Figure 4) constitutes a bi-stable system if: 1) three steady-states exist (*3 steady-state cond*); and 2) two of these steady-states are stable (*stab cond*), while the third meets one of the instability conditions (*unstab cond1* to *unstab cond7*). The model simplifies processes involving multiple reactions into a single reaction (lumping), raising questions about this approach given the complexity of enzymatic reactions involved. To address these concerns, one strategy might involve parameterizing the enzyme with the slowest kinetics to represent the overall kinetics of the lumped reaction or, alternatively, using the parameters of the first reaction in the pathway. The decision to model malonyl-CoA synthesis inhibition as non-competitive is based on findings that only long chains of fatty acids inhibit acetyl-CoA carboxylase (Brun et al. [174]), suggesting an allosteric mechanism rather than competitive inhibition. The inhibition of β -oxidation by malonyl-CoA, which competes with free carnitine rather than long-chain acyl-CoA, further supports the assumption of allosteric inhibition, with FAs considered the primary substrate for β -oxidation. Moreover, Fraser et al. [177] demonstrated that CPT1 inhibition by malonyl-CoA in the liver varies by mechanism, being competitive at mitochondrial contact sites and non-competitive elsewhere. Regarding the influxes and the outfluxes, for the sake of simplicity, I have represented them to be constant and proportional to the pool concentrations, respectively. However, the fluxes in and out of FA metabolism are highly subject to hormonal regulation. For instance, acetyl-CoA production from glucose occurs through a metabolic pathway strongly regulated by insulin, glucagon, and epinephrine. It is also the case for the influx of TGs. It would be interesting to represent acetyl-CoA and TGs' influxes as insulin and glucagon's increasing functions, respectively. At the same time, the two hormones would be described with opposite dynamics. In the formulation of the bi-stability conditions that I derived, it was impossible to express the steady-states vector S^*

as a strict function of the parameterization. Indeed, the conditions include the expression of the steady-state concentrations. Since one has a well-posed ODE system, the solutions depend only on time and parameterization once the initial values are specified. Thus, expressing the steady-state concentrations purely as a function of parameterization and bi-stability conditions is feasible, though finding suitable parameterization is computationally challenging with eighteen parameters. I recommend pre-fixing known parameters, such as those associated with malonyl-CoA synthesis, widely documented in the literature (see Table A2). Identifying the slowest reactions could further refine the approach to parameterizing the lumped reaction, with the parameterization of glycerol-3-phosphate-acyltransferase (GPAT) involved in the rate-limiting step of TG synthesis, serving as a model for the entire pathway ([178]). Sampling and rejection methods could then be employed to determine remaining parameters, sequentially verifying the (*3 steady-state cond*), (*stab cond*), and conditions from (*unstab cond 1*) through (*unstab cond 7*). My primary focus on qualitative system analysis precluded this step. Extending the model to incorporate citrate and its positive feed-forward activation of malonyl-CoA synthesis could unveil more complex dynamics, such as multi-stability and hysteresis cycles, offering further insights into FA metabolism's regulatory mechanisms.

Chapter 5

A semi mechanistic model of fatty acid *de novo* synthesis

Introduction

Short description of fatty acid *de novo* synthesis. In the introduction and Chapter 3, I briefly described the *de novo* synthesis of fatty acids from acetyl-CoA. This description shows that it takes place in the cytosol and is done in two phases, involving one enzyme each. The first phase synthesizes malonyl-CoA from acetyl-CoA, bicarbonate, and ATP. In contrast to the second phase, where several reactions occur, this phase catalyzed by the acetyl-CoA carboxylase (ACC) is less complex. In the second phase, known as the elongation phase, acetyl-CoA, malonyl-CoA, and NADPH are utilized to produce LCFAs, free CoA, and CO₂. This phase involves seven crucial reactions, each catalyzed at a distinct site on the Fatty Acid Synthase (FAS) enzyme (as detailed in Chapter 3 and Figure 5.1). To simplify, the entire elongation phase can be divided into three steps. The initialization stage activates the malonyl-acetyl transferase (MAT) site on the enzyme. The cyclic elongation stage makes use of the ketoacyl synthase (KS), ketoacyl reductase (KR), dehydratase (DH), and enoyl reductase (ER) sites on the enzyme. Finally, the termination stage utilizes the thioesterase site of the enzyme. The ACP site is responsible for transferring the intermediate from one site to another through the mechanism known as channeling. As highlighted in earlier studies on substrate channeling reactions by Ovádi [179], Spivey and Ovádi [180], and Ovádi et al. [181], the goal of channeling reactions whether between enzymes or within an enzyme's catalytic sites is not only to optimize fluxes but also to circumvent substrate competition with other pathways involving the same substrate(s). Indeed, channeling ensures that the intermediates are treated efficiently, rather than interacting with other enzymes resulting in the synthesis of unnecessary compounds [182]. Additionally, it limits the possibility of having unstable intermediates and reduces the transient time (the amount of time taken by an intermediate to reach the steady-state response after a change in substrate concentration) [180]. It is complex to study the kinetics of channeling reactions, either among enzymes of a pathway or within the sites of a particular enzyme.

The primary cause being the short life of the intermediates involved in the reactions, resulting in the difficulty of their quantification [183]. Secondly, the nature of the channeling mechanism can be very complex and may require tremendous experiments to be understood. To study the kinetic of channeling reactions besides experimental techniques such as isotope dilution and the measurement of transient times [180], stochastic simulation is the widely used theoretical framework. Among these methods, one can mention the queuing theory-based simulation, where the enzymes or the sites of an enzyme are considered to be connected via channels. The channel's characteristic defines the transition probability from one enzyme to another. The work of Tsitkov et al. [184] is an example of the use of queuing theory for modeling channeling cascade. Another approach would be to ignore channeling in the enzymatic mechanism and then assume that all enzyme-substrate complexes are in a steady-state (quasi-steady-state assumption) as in the case of the Michaelis-Menten Kinetics derivation. While this approach can offer a detailed and mechanistic model, it also introduces the challenge of dealing with numerous parameters. It is important to note that almost all the enzymatic sites of FAS follow a two-substrate ping pong mechanism. However, KR and ER are exceptions, as they follow the two-substrate, random sequential mechanism [185, 154]. Thus, such a model will contain at least 42 parameters if one further ignores the regulatory mechanisms. Cox and Hammes [36], after proposing a kinetic rate law for the elongation phase of FADNS until the production of palmitic acid, suggest this approach as a simplified mechanism for deriving kinetic rate laws. The proposed mechanism consists of two elementary reactions for the initialization phase, five elementary reactions for the cyclic elongation, and one for the termination (see Figure 5.1). Furthermore, the proposed mechanism ignores the regulation processes. In this work, I propose a further simplified mechanism that divides the pathway into three elementary reactions corresponding to the initialization, cyclic elongation, and termination.

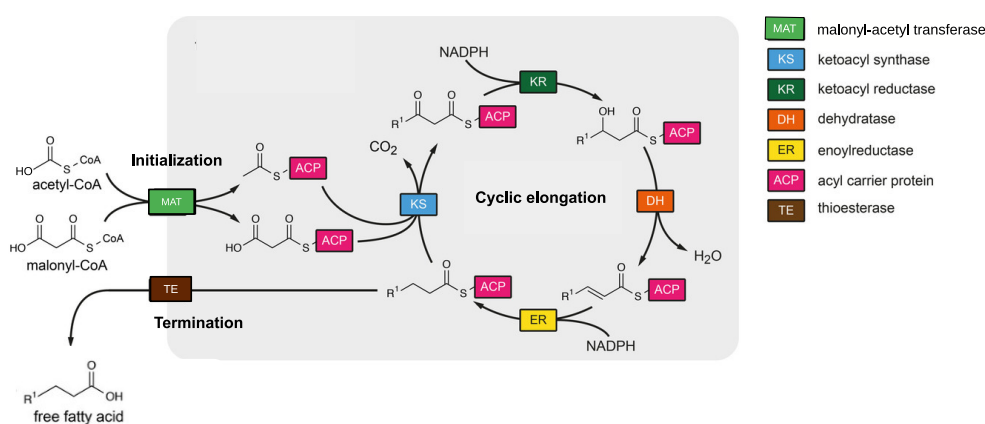


Figure 5.1: **Detailed reactions of FADNS:** The seven enzymatic site of FAS are represented, notably the malonyl-lacetyltransferase(MAT) (Reprinted (adapted) with permission from [186]. Copyright 2019 ChemBioChem)

Motivation and Objective. In a previous study by Martines [5], comparing the composition of TGs between knockout and wild-type adult mice fasted and refed and exposed to a temperature of 4 degrees observed a significant disturbance (see Figure 5.2). The suggested explanation is that the medium-chain FAs that are not degraded are exported from the mitochondria, modified by the microsomal pathway, and then stored as TGs. Even if this explanation is convincing, it would also be essential to question the impact of mFAODs on the FADNS. Furthermore, Tucci et al. [187] observed that VLCAD-deficient mice supplemented with medium-chain FAs were experiencing hepatic steatosis, although [188] later showed that this result was more pronounced in females. Earlier Mitchell et al. [189] have already demonstrated that the sequestration of free CoA by β -oxidation intermediates in mFAODs was the reason for the manifestation of metabolites syndromes. Given CoA's crucial role in the FA synthesis process, its sequestration will undoubtedly impact the synthesis and storage pathways. Indeed, CoA plays at least two roles in the synthesis of FAs. First, it serves as a substrate for activating FAs which microsomal synthesis pathways will modify. In the second place, it inhibits the phase of elongation of the FADNS. In order to better understand these lipid disturbances associated with FOADs, many computational models of β -oxidation have been developed. Noteworthy among these is the contribution by Modre-Osprian et al. [67], who delved into the kinetics of various mFAODs using a large model that comprised 64 reactions, 91 metabolites, and 301 parameters. Subsequent to this, there was a crescendo β -oxidation modeling endeavors, particularly in relation to MCAD deficiency. Esteemed works in this domain include those of van Eunen et al. [49], van Eunen et al. [190], Martines et al. [12], and Abegaz et al. [68], which inaugurated with a comprehensive model featuring 47 metabolites, 66 reactions, and 227 parameters. While these studies have significantly advanced our understanding of mFAODs, I believe that including the pathways of synthesis and storage could offer a more holistic perspective. This inclusion might provide a deeper insight into the cascade leading to hepatic steatosis in cases of mFAODs, the heterogeneity of symptoms, and the sexual dimorphism observed in specific conditions, such as MCADD and VLCAD deficiencies [63, 187]. Moreover, such a comprehensive model could be instrumental in evaluating diet-based solutions for mFAODs. This chapter introduces a semi-mechanistic model that captures an intricate aspect of FA synthesis, namely, the elongation phase of FADNS.

Existing models. In the literature, various studies have examined the kinetics of the elongation phase of the *de novo* synthesis of fatty acids. Among them, the work of Katiyar et al. [152] stands out, which delves into the kinetic mechanism of palmitate synthesis in pigeon liver. Upon determining the Michaelis-Menten constants for each of the three substrates, their research shifted to the competitive dynamics between acetyl-CoA and malonyl-CoA. They fitted the *in vitro* data to rate laws corresponding to competitive, uncompetitive, and non-competitive inhibition mechanisms. Finally, by considering the ping-pong mechanism inherent to the reactions of each enzymatic site of fatty acid synthase and employing the method of King and Altman [41], they established the rate

law for palmitate synthesis from acetyl-CoA, malonyl-CoA and NADPH. Likewise, Cox and Hammes [36] undertook a study on the kinetics of palmitate synthesis in chicken liver. They introduced a rate law encapsulating the competition between acetyl-CoA and malonyl-CoA. Further, they elucidated the dependence of the kinetic parameters on pH, specifically the turnover number (k_{cat}), the diverse Michaelis-Menten constants (K_m), and the inhibition constants (K_i). The proposed rate laws are detailed in the last row of Table A1.

Although these models are ingeniously designed and fit the *in vitro* data for palmitic acid synthesis, they do not address the synthesis of other long-chain fatty acids, notably 14:0 and 18:0, which are also products of this synthesis. Furthermore, the model by Katiyar et al. [152] is based on the enzymatic mechanism of each enzymatic site, making it intricate and parameter-rich, which complicates its utilization. My goal is therefore, to develop a simple, flexible model that describes the chain elongation phase of fatty acid *de novo* synthesis and the production of long-chain saturated fatty acids. Concurrently, I aim to design a model rooted in a minimalistic mechanism. This would involve, for instance, lumping the channeling reactions into a singular reaction and considering a minimal number of reversible reactions. This approach is influenced by the idea that channeling seeks to optimize reactions [183]. My model can be tailored to produce shorter chains of saturated FAs by adjusting the kinetic rate constant of termination k_{di} for the corresponding chains. For chains shorter than 14, the kinetic rate constants are presently set to 0.

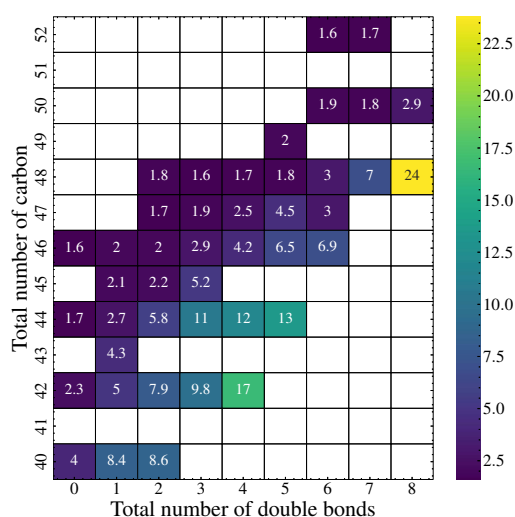


Figure 5.2: **Fold Changes in the TG Profile in MCAD Knockout and Wild-Type Mice:** The fold in this context is defined as the ratio between the mean TG concentration in MCAD knockout mice and that of the wild-type mice. A simple approach to describe the TG is by considering the total number of carbons and the number of double bonds in the FAs attached to the glycerol backbone. Using this description, I calculated the ratio between the means of each type of TG in MCAD knockout mice and the wild type. An overall increase in each type TG is noticeable. Moreover, these changes exhibit a positive correlation with the number of double bonds and a negative correlation with the number of carbons. It is notable that some TGs, such as 48:8 and 42:4, exhibit fold changes of 24 and 17, respectively. (The data were extracted from Chapter 4 [5].)

Why not a detailed approach? The enzymatic mechanisms of all the sites of FAS have been studied and are known to either follow the ping pong mechanism or the random sequential mechanism. A two-substrate ping pong mechanism includes 10 parameters. Hence, the most basic detailed model of FAS would contain at least 70 parameters if I assume the reactions are not substrate-specific, ignore the regulatory mechanisms, and presume each channeling by the ACP site follows the enzymatic mechanism and therefore the same rate law. The validation of such a model requires two distinct steps. The first step would involve validating the reactions of each enzymatic site, requiring at least ten parameters. In the second step, one would need to validate the overall kinetics of the pathway after combining these individual reactions. Given the limited knowledge about the kinetic parameters associated with the rate laws corresponding to the mechanism of each enzymatic site, it is not possible to consider the bottom-up approach. Additionally, such a detailed model would be intractable and, therefore, not practical for use. To address these challenges, I have opted for a simpler representation of the system, which will be described in the following section.

5.1 Model construction: hypotheses and dynamics

As mentioned in the previous paragraph, designing a detailed mechanistic model for such a complex enzymatic mechanism could quickly lead to an impasse as the model will enclose many reactions and parameters and therefore become tremendous to analyze. Instead, I consider a parsimonious approach that divides the elongation mechanism into essential processes. The initialization corresponds to the binding of acetyl-CoA to the free enzyme, the cyclic elongation of the enzyme-substrate complexes using malonyl-CoA and NADPH, and finally, the termination, which corresponds to the release of free FAs and the free enzyme. The three processes are modeled as a single reaction governed by the irreversible mass action kinetic rate laws. Thus, the initialization reaction that engages the MAT site of the enzyme binds acetyl-CoA to the enzyme to form the two-carbon enzyme-substrate complex $EC2$ and releases the free CoA. The reaction proceeds with the kinetic rate constant β . The cyclic elongations, which lengthen the intermediate enzyme-substrate complex (e.g., $EC2$ to $EC4$) by two carbons and release a molecule of the free CoA, include several intermediate reactions that are carried out by the MAT, KS, KR, and ER sites of the enzyme. I lumped all these reactions into a single reaction associated with the kinetic rate constant κ for all the chain elongations until the formation of the $EC16$ intermediate. I assume these reactions to be rapid binding, which allows having the quasi steady-state assumption for enzyme-substrates complexes during the initial phase kinetics. So their corresponding fluxes will be large compared to other reactions in the pathways. The last reaction of the cyclic elongation ($EC16$ to $EC18$) is associated with the kinetic rate constant δ , which is assumed to be smaller than κ . The consideration of a lower rate constant is justified by the fact that the KS site has limited space for growing

intermediates. When the chain exceeds 14 carbons, its ability to condense the malonyl-CoA with the growing intermediate reduces significantly as reported by Heil et al. [186]. The termination involves the TE site of the enzyme and produces FAs with chain lengths ranging from 4 to 18 and the free enzyme, E . Each release is associated with the kinetic rate constants k_{d_i} , ($i = 1, 2, \dots, 8$), for a fatty acid with $2i+2$ carbons. But to keep it simple for the version of the model I will present here, I only considered that 14:0, 16:0, and 18:0 are the only products of the pathways. Indeed, as shown by Topolska et al. [59], the pathway can produce shorter and longer chains, such as 20:0. However, their concentration is very low compared to those of 14:0, 16:0, and 18:0.

In the second model, I included the CoA inhibition that can highly impact the kinetics. Indeed, Cox and Hammes [36] in the *in vitro* experiment by variation of the concentration of free CoA from 0 to 120 μM with 10 μM of acetyl-CoA and 27 μM of malonyl-CoA, the overall elongation flux is reduced by 4-fold. I modeled the CoA inhibition as a reverse binding of free CoA to the MAT site of the free enzyme, thus preventing the initialization step from occurring. The associate rate kinetic follows the reversible mass action kinetics with kinetic rate constants $k_{f_{CoA}}$ and $k_{b_{CoA}}$ for the forward and backward reactions, respectively. In the forward reaction, free CoA bind to the enzyme to form $ECoA$ complex, whereas in the backward reaction, $ECoA$ dissociates into free enzyme E and free CoA. Despite that, the free CoA at low concentrations enhances the elongation flux. I decided not to include the activation, as it only modifies the overall elongation flux by a maximum of 15 % (see data in [36]). I assumed the concentration of enzyme species to be conserved in both models. The conservation relations are defined by the equations (5.1.1) for the model without CoA inhibition and (5.1.2) for the model with CoA inhibition.

$$E_t = E + \sum_{i=1}^9 EC2i \quad (5.1.1)$$

$$E_t = E + ECoA + \sum_{i=1}^9 EC2i \quad (5.1.2)$$

Given that I have data from *in vitro* experiments, in which the authors started with fixed concentrations of substrates, I will not include any influx or outflux in the system. One could question such a restriction as there are no isolated processes in the cell. However, the focus is to give a simplified kinetic mechanism to represent the elongation part of FADNS. Furthermore, the proposed models can be easily extended to an open system. To summarize the assumptions of models: Figure 5.3 and Figure 5.4 summarize the pathways scheme for the model with no CoA inhibition and with CoA inhibition, respectively. Table 5.1 summarizes all the compounds involved in the two models.

5.1.1 Summary of the assumptions

1. The model is a closed system with a fixed concentration of the enzyme (E_t) and the initial concentrations of the substrates (acetyl-CoA, malonyl-CoA, and NADPH) are constant

2. The complex mechanism of the elongation part of FADNS is divided into three reactions, namely initialization, cyclic elongation, and termination
3. The three reactions follow the irreversible mass action kinetic rate law
4. The cyclic elongation, corresponding to substrates binding to either the free enzyme or to enzyme-substrate complexes resulting in the formation of enzyme-substrate complexes $EC2i$ ($i = 1, 2, \dots, 9$), follows rapid binding mechanism for the formation $EC2$ to $EC16$, but exhibits slow binding for the production $EC18$
5. The rate law for the binding of CoA to the free enzyme to form the $ECoA$ complex, which inhibits the elongation, follows reversible mass action kinetics
6. I assume the conservation relationship on the enzyme (see equations 5.1.1 and 5.1.2)

5.1.2 Summary of the compounds in the models and their initial concentrations

Table 5.1 provides a summary of the variables and initial concentrations for the two models examined in this chapter.

5.1.3 Model schemes, ODEs and parameters

Model without inhibition

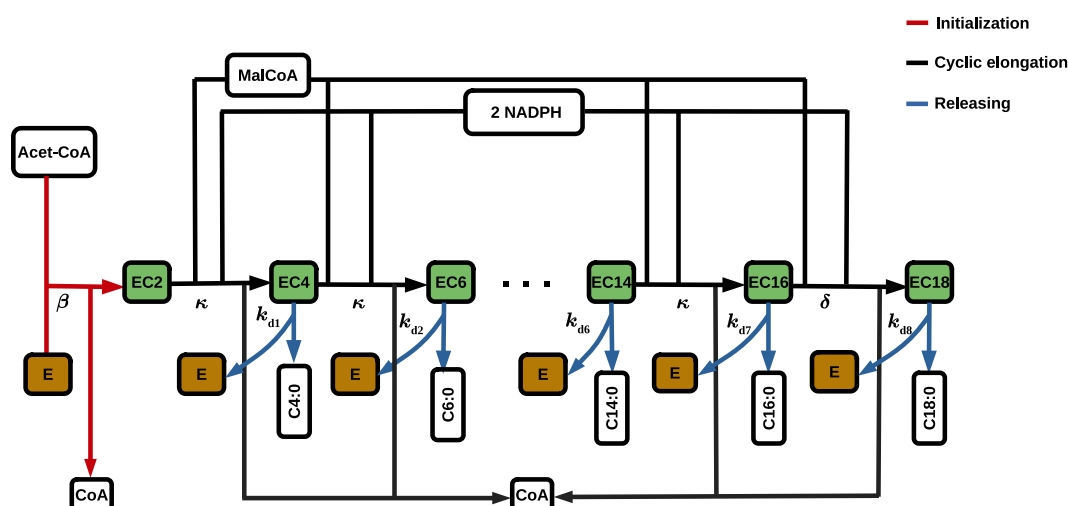


Figure 5.3: **Scheme of the model without CoA inhibition:** the reactions are color coded with red, black and blue, representing the initialization, the cyclic elongation, and termination steps, respectively.

Let x be an arbitrary compound in the system. We denote the rate of conversion of x to a compound y by $v_{x \rightarrow y}$. The rate of change of x over time, which represents the dynamics and

Table 5.1: Summary of the different compounds of the two models and their initial concentrations

Compound	Meaning	Initial concentration (μM)
<i>AcetCoA</i>	Acetyl-CoA	107.96
<i>MalCoA</i>	Malonyl-CoA	22.04
<i>NADPH</i>	Nicotinamide adenine dinucleotide phosphate	200
<i>E</i>	Free enzyme (fatty acid synthase)	
<i>EC2</i>	Complex enzyme substrates with two carbons	0
<i>EC4</i>	Complex enzyme substrates with four carbons	0
<i>EC6</i>	Complex enzyme substrates with six carbons	0
<i>EC8</i>	Complex enzyme substrates with eight carbons	0
<i>EC10</i>	Complex enzyme substrates with ten carbons	0
<i>EC12</i>	Complex enzyme substrates with twelve carbons	0
<i>EC14</i>	Complex enzyme substrates with fourteen carbons	0
<i>EC16</i>	Complex enzyme substrates with sixteen carbons	0
<i>EC18</i>	Complex enzyme substrates with eighteen carbons	0
<i>ECoA</i>	Complex enzyme-Coenzyme A	0
<i>C14:0</i>	Myristic acid	0
<i>C16:0</i>	Palmitic acid	0
<i>C18:0</i>	Stearic acid	0
<i>CoA</i>	Free Coenzyme A	0

is denoted by $\frac{dx}{dt}$, is equal to the sum of the rates of reactions that positively contribute to x 's pool minus those that contribute negatively. Hence, the dynamics of the system, excluding CoA inhibition, are represented by the following system of ODEs:

$$\frac{dAcetylCoA}{dt} = -V_{E \rightarrow EC2} \quad (5.1.3)$$

$$\frac{dMalCoA}{dt} = -\sum_{i=1}^8 V_{EC2i \rightarrow EC2i+2} \quad (5.1.4)$$

$$\frac{dNADPH}{dt} = -2 \sum_{i=1}^8 V_{EC2i \rightarrow EC2i+2} \quad (5.1.5)$$

$$\frac{dEC2}{dt} = V_{E \rightarrow EC2} - V_{EC2 \rightarrow EC4} \quad (5.1.6)$$

$$\frac{dEC2i}{dt} = V_{EC2i-2 \rightarrow EC2i} - V_{EC2i \rightarrow EC2i+2} \quad (2 \leq i \leq 6) \quad (5.1.7)$$

$$\frac{dEC14}{dt} = V_{EC12 \rightarrow EC14} - V_{EC14 \rightarrow EC16} - V_{EC14 \rightarrow C14:0} \quad (5.1.8)$$

$$\frac{dEC16}{dt} = V_{EC14 \rightarrow EC16} - V_{EC16 \rightarrow EC18} - V_{EC16 \rightarrow C16:0} \quad (5.1.9)$$

$$\frac{dEC18}{dt} = V_{EC16 \rightarrow EC18} - V_{EC18 \rightarrow C18:0} \quad (5.1.10)$$

$$\frac{dC14:0}{dt} = V_{EC14 \rightarrow C14:0} \quad (5.1.11)$$

$$\frac{dC16:0}{dt} = V_{EC16 \rightarrow C16:0} \quad (5.1.12)$$

$$\frac{dC18:0}{dt} = V_{EC18 \rightarrow C18:0} \quad (5.1.13)$$

$$E_{Total} = E + \sum_{i=1}^9 EC_{2i}, \quad (5.1.14)$$

where the different rate and the corresponding parameters and the parameters units are described by Table 5.2

Table 5.2: **Kinetic of each reaction of the FADNS for the model without inhibition:** The symbol $V_{x \rightarrow y}$ is the transformation rate from x to y . The mathematical formula describing the rate is in the column "**Expression**". The units of the parameters appearing in the mathematical formula of the rate are explained in the column "**Parameter units**".

Reaction	Rate law	Expression	Parameters	Parameter units
$V_{E \rightarrow EC2}$	Mass-action	$\beta \times E \times AcetCoA$	β	$\mu M^{-1} \times s^{-1}$
$V_{EC2i \rightarrow EC2i+2}$	Mass-action	$\kappa \times EC2i \times MalCoA \times NADPH$	κ or δ	$\mu M^{-2} \times s^{-1}$
$V_{EC2i+2 \rightarrow C2i+2:0}$	Mass-action	$k_{di} \times EC2i + 2$	k_{di}	s^{-1}

Model with inhibition by the free CoA

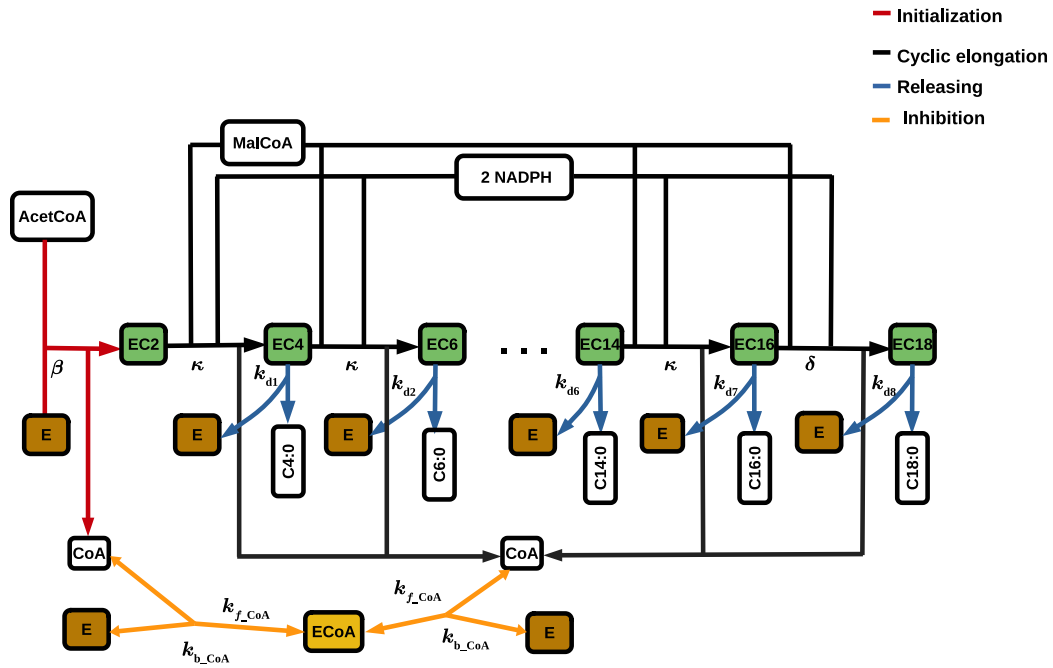


Figure 5.4: **Scheme of the model without CoA inhibition:** the reactions are color coded with red, black, blue, and orange representing the initialization, the cyclic elongation, termination steps, and the inhibition by the free CoA, respectively.

$$\frac{dAcetylCoA}{dt} = -V_{E \rightarrow EC2} \quad (5.1.15)$$

$$\frac{dMalCoA}{dt} = -\sum_{i=1}^8 V_{EC2i \rightarrow EC2i+2} \quad (5.1.16)$$

$$\frac{dNADPH}{dt} = -2 \sum_{i=1}^8 V_{EC2i \rightarrow EC2i+2} \quad (5.1.17)$$

$$\frac{dEC2}{dt} = V_{E \rightarrow EC2} - V_{EC2 \rightarrow EC4} \quad (5.1.18)$$

$$\frac{dEC2i}{dt} = V_{EC2i-2 \rightarrow EC2i} - V_{EC2i \rightarrow EC2i+2} \quad (2 \leq i \leq 6) \quad (5.1.19)$$

$$\frac{dEC14}{dt} = V_{EC12 \rightarrow EC14} - V_{EC14 \rightarrow EC16} - V_{EC14 \rightarrow C14:0} \quad (5.1.20)$$

$$\frac{dEC16}{dt} = V_{EC14 \rightarrow EC16} - V_{EC16 \rightarrow EC18} - V_{EC16 \rightarrow C16:0} \quad (5.1.21)$$

$$\frac{dEC18}{dt} = V_{EC16 \rightarrow EC18} - V_{EC18 \rightarrow C18:0} \quad (5.1.22)$$

$$\frac{dECoA}{dt} = V_{E \rightarrow ECoA} \quad (5.1.23)$$

$$\frac{dC14:0}{dt} = V_{EC14 \rightarrow C14:0} \quad (5.1.24)$$

$$\frac{dC16:0}{dt} = V_{EC16 \rightarrow C16:0} \quad (5.1.25)$$

$$\frac{dC18:0}{dt} = V_{EC18 \rightarrow C18:0} \quad (5.1.26)$$

$$\frac{dCoA}{dt} = -V_{E \rightarrow ECoA} + V_{E \rightarrow EC2} + \sum_{i=1}^8 V_{EC2i \rightarrow EC2i+2} \quad (5.1.27)$$

$$E_{Total} = E + ECoA + \sum_{i=1}^9 EC2i. \quad (5.1.28)$$

Table 5.3: **Kinetic of each reaction of the FADNS for the model with inhibition by the free CoA:** The symbol $V_{x \rightarrow y}$ is the transformation rate from x to y . The mathematical formula describing the rate is in the column "Expression". The units of the parameters appearing in the mathematical formula of the rate are explained in the column "Parameter units".

Reaction	Rate law	Expression	Parameters	Parameter units
$V_{E \rightarrow EC2}$	Mass-action	$\beta \times E \times AcetCoA$	β	$\mu M^{-1} \times s^{-1}$
$V_{EC2i \rightarrow EC2i+2}$	Mass-action	$\kappa \times EC2i \times MalCoA \times NADPH$	κ or δ	$\mu M^{-2} \times s^{-1}$
$V_{EC2i+2 \rightarrow C2i+2:0}$	Mass-action	$k_{di} \times EC2i + 2$	k_{di}	s^{-1}
$V_{E \rightarrow ECoA}$	Reversible mass-action	$k_{fCoA} \times E \times CoA - k_{bCoA} \times ECoA$	k_{fCoA}, k_{bCoA}	$\mu M^{-1} \times s^{-1} / s^{-1}$

Remark 5.1.4. Both models have the same dynamics, the only difference being from the CoA inhibition reaction, which can be represented by equation (5.1.27) and from the conservation of enzyme species (see (5.1.28))

5.1.5 Experimental data to support model validation

Experimental data from Topolska et al. [59] The authors designed mass spectrometry-based *in vitro* assays to measure the specific activity of FAS. They utilized ^{13}C -labeled malonyl-CoA, unlabeled acetyl-CoA, and NADPH as substrates, measuring the incorporation of ^{13}C into long-chain fatty acids (LCFAs) (C14:0, C16:0, and C18:0) during the initial phase. This phase is characterized by linear FA production over time, here specifically for 2 minutes (see Figure 5.5). Additionally, they provided time course data of total FAs for 90 minutes (see Figure 5.5). The experiment used 16.5 μg of purified FAS from cow mammary gland, conducted in a total volume of $V_T = 200 \mu L$ at 37° Celsius. The initial concentrations of substrates were 200 μM for NADPH, 50 μM for acetyl-CoA, and 80 μM . However, the authors noted contamination of malonyl-CoA due to its decarboxylation into acetyl-CoA. Using the initial phase data, I recalculated the initial concentrations (**Recalculated Initial Concentration**) of acetyl-CoA and malonyl-CoA to be 107.96 μM and 22.04 μM , respectively. I extracted the data from the publication using PlotDigitizer software, converted, and plotted the average of the replicates in the model's units.

Table 5.4: **Summary of experimental conditions from Topolska et al. [59] and recalculated initial conditions:** The column "Initial concentration" represents the concentrations prior the accounting for malonyl-CoA decarboxylation. The "Recalculated initial concentration" column reflects concentrations adjusted based on initial phase data analysis.

Compounds	Initial concentration	Recalculated initial concentration	Comments
NADPH	200 μM	200 μM	
Acetyl-CoA	50 μM	107.96 μM	The initial concentration was modified resulting from the decarboxylation of malonyl-CoA
Malonyl-CoA	80 μM	22.04 μM	The authors pointed out that the malonyl-CoA was decarboxylated into to acetyl-CoA. Based on the time course data and given that C16:0 is the major product of the pathway, I estimated the effective concentration of malonyl-CoA and therefore that of acetyl-CoA
Fatty acid synthase	0.153 μM	0.153 μM	The concentration of the enzyme is calculated from its mass in solution (16.5 μg). The molecular weight of FAS is 540 kDa as it consists of two polypeptide chains a 270 kDa each [191]

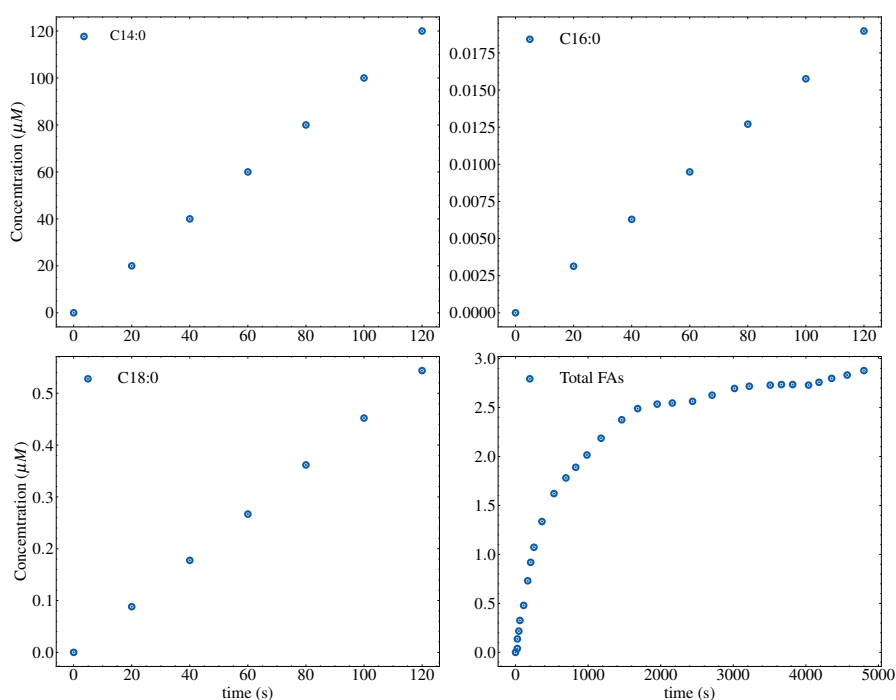


Figure 5.5: **Extracted data from the work by Topolska et al. [59]**

5.2 Results

In this section, I begin by introducing and subsequently discussing the main findings of this chapter, focusing on the development and performance of two models for the elongation phase of FADNS. The first model, known as the simple model, does not consider free CoA inhibition. In contrast, the second model includes this inhibition in the synthesis process. These results are presented in three stages:

1. Initially, I take a qualitative approach by choosing a suitable parameterization for the simple model and observing its behavior over three time scales. This process is essential to ensure that the model aligns with its foundational assumptions and to become familiar with its behavior, thereby identifying any unexpected dynamics. Although this initial analysis is confined to the simple model, I later illustrate that incorporating CoA inhibition enhances the model's qualitative dynamics. Additionally, I demonstrate that integrating CoA inhibition with appropriate rate kinetic constants for reversible mass action kinetics governing the inhibition process does not conflict with the rapid binding assumption.
2. Subsequently, I perform a global sensitivity analysis to assess the influence of each parameter on the model. This comprehensive analysis sheds light on the model's behavior across the entire parameter spectrum, highlighting any non-linearity and interactions among parameters. It aids in identifying the most crucial parameters for model fitting to experimental data.
3. Finally, I fit the model to data from Topolska et al. [59]. Given the sole data source, to evaluate the fitting accuracy, I generate artificial data from the model and fit it to Michaelis-Menten rate equations. The derived fitting parameters, especially the turnover number k_{cat} and the Michaelis-Menten constant K_m , are then compared with those reported in the literature.

5.2.1 Vanilla model

To perform a qualitative analysis of the model, I first choose a suitable parameterization consistent with the model's assumption, notably the rapid binding assumption. In the selected parameterization, I ensure that the rate of cyclic elongation at the initial phase is large compared to other rates. The chosen parameterization is summarized in Table 5.5.

Simulations for 200 milliseconds. To highlight the rapid binding, a crucial assumption of the model, I begin by simulating the model's dynamics for 200 milliseconds (see Figure 5.6 and Figure 5.7). It is noticeable that the fluxes of the cyclic elongations, associated with rapid binding, quickly reach their maxima before progressively moving toward steady-state. This rapid increase in flux is a key characteristic of rapid binding. In contrast, the flux of *EC18* formation, associated with

slow binding, reaches its maximum value later. Regarding the fluxes LCFAs production, the flux of $C16 : 0$ production is significantly higher compared to $C14 : 0$ and $C18 : 0$. Concerning the dynamics of the metabolites in the system, they follow the fluxes trends. Notably, the enzyme-substrate complexes with carbon numbers less or equal to 14 move toward the same equilibrium value, while $EC16$ is the dominant enzyme species. It is also evident that $C16 : 0$ is the main product of the pathway. Thus, I conclude that the model accurately reproduces rapid binding.

Table 5.5: Parameters for the vanilla models

Parameters	Value	Units
β	0.1	$\mu M^{-1} s^{-1}$
κ	0.1	$\mu M^{-2} s^{-1}$
δ	10^{-6}	$\mu M^{-2} s^{-1}$
k_{d6}	1	s^{-1}
k_{d7}	1	s^{-1}
k_{d8}	1	s^{-1}
k_{fCoA}	0.1	$\mu M^{-1} s^{-1}$
k_{bCoA}	5×10^{-4}	s^{-1}

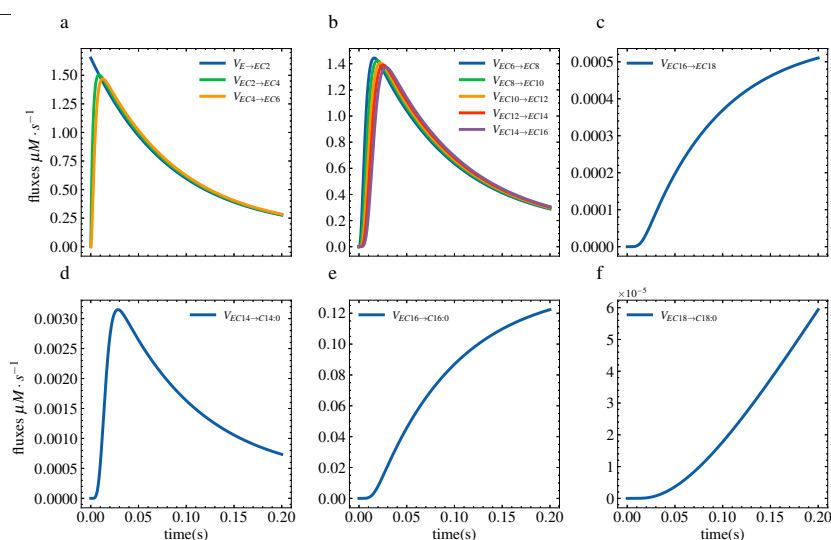


Figure 5.6: **Behavior of the fluxes of the vanilla model during the first 200 milliseconds:** in panels a and b, one can observe the effect of the rapid binding as the associated fluxes peak and decrease toward quasi-steady-state fluxes. Panel c shows the slow binding as the maximum production flux of *EC18* is lower than the other cyclic elongation fluxes. Panel d, the flux of production of *C14:0* increases rapidly and drops exponentially due to high flux toward the production *EC16*. Panels e and f show the rise in the production fluxes of *C16:0*, and *C18:0*, respectively.

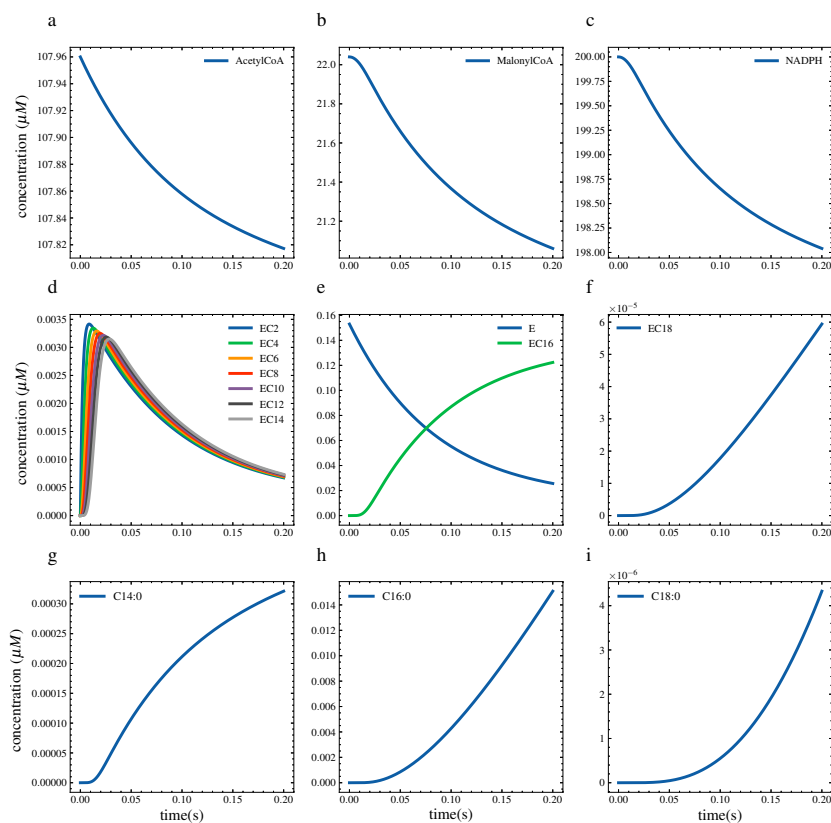


Figure 5.7: **Time course of the vanilla model during the first 200s milliseconds:** panels a, b, and c show the consumption of three substrates resulting from rapid binding. From panels d, e and f, it can be seen that almost all enzyme species are rapidly converted to *EC16*. *EC18* is the smallest enzyme species in the system. Panels g, h, and i show FADNS products. One can see that the *C16:0* is the main product of the channel.

Simulation for the Initial Phase. In order to assess the linear phase of the model dynamics (initial phase), I simulated the model for 5 seconds, as shown in Figure 5.8 and Figure 5.9. It can be observed that all fluxes, except those for the production of $EC18$ and $C18 : 0$, remain constant after a sharp increase followed by a sharp drop. The sharp increase corresponds to the initial formation of enzyme-substrate complexes via rapid binding. The sharp drop results from the partitioning of the enzyme according to the conservation relationship (see Equations 5.1.1 and 5.1.2). The fluxes associated with the cyclic elongation ($EC2$ to $EC16$) remain constant because the enzyme-substrate complexes are fully saturated. Regarding the fluxes for the formation of $EC18$ and $C18 : 0$, after reaching their maximum, they decrease progressively due to the slow conversion of $EC16$ to $EC18$.

The time course of substrate consumption and product formation is almost linear, except for the first few milliseconds, where a sharp drop in substrates is observed as a result of rapid binding. This sharp drop in substrates corresponds to the initial formation of enzyme-substrate complexes, as explained earlier (see Figure 5.6 and Figure 5.7). The linear time course for substrate consumption and product formation following the initial sharp drop is due to the fact that the enzyme-substrate complexes $EC2$ to $EC16$ remain constant. Notably, the concentration of $EC16$ is almost equal to the initial concentration of the free enzyme, suggesting that all enzyme species are converted via rapid binding into $EC16$, which remains quasi-constant during this kinetic phase. These observations support the use of the quasi-steady-state approximation in analyzing the model. As for the dynamics of $EC18$, it initially increases and then slowly decreases due to the combined effects of a decrease in flux from $EC16$ and the rapid formation of $C18$. In summary, the model exhibits the expected behavior in the initial phase.

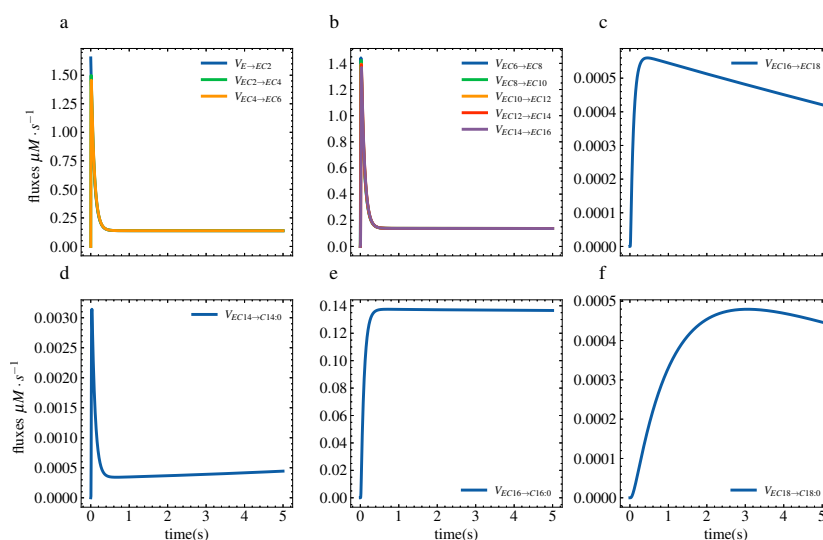


Figure 5.8: **Behavior of the fluxes of the vanilla model after 5 seconds** : The elongation fluxes associated with rapid binding reactions (panels a and b) are quasi-constant after half of a second, as well as the rate of production of $C14:0$ (panel d). The rate of production $C16:0$ (panel e) sharply increases and remains quasi-constant. The production rate of $C18:0$ has reached its maximum after 2.5 seconds and decreases due to slow production of $EC18$.

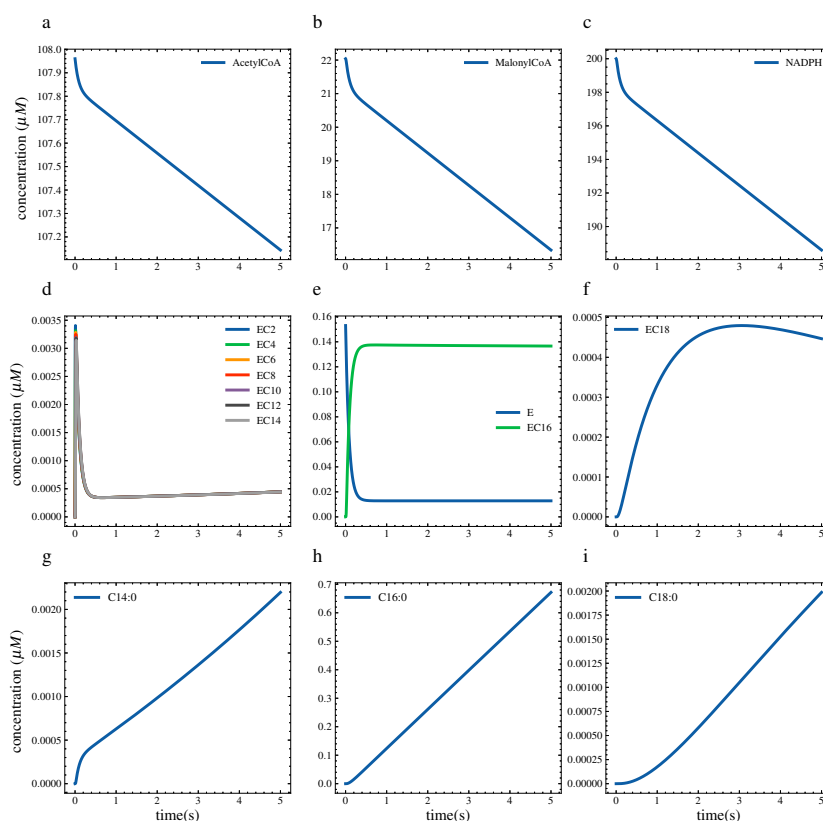


Figure 5.9: **Time course vanilla model after 5 seconds**: panels display the initial phase dynamics. Panels a, b, and c show the linear consumption of the substrate except for the sharp drop for the first milliseconds as a result of rapid binding. Panels d, e, and f show that almost all the enzyme species are converted to $EC16$ and are at quasi-steady-state except the $EC18$. Panels g, h, and i display the linear formation of the products, with $C16:0$ being the major one.

Simulation for the long-run. To evaluate the dynamics over the long-run and to highlight the transient phase, I simulated the model for 50 seconds, corresponding to the total depletion of malonyl-CoA. Figure 5.10 and Figure 5.11 display, respectively, the fluxes of production of the three types of FAs and the time course of the compounds of the model. For the flux of production of $C_{14}:0$ (panel a, Figure 5.10), one can observe a sharp initial peak between the first milliseconds resulting from the initial formation of EC_{14} (via rapid binding) from which $C_{14}:0$ is dissociated. Given that the rate of elongation of EC_{14} to EC_{16} is greater than the rate of production of $C_{14}:0$, the flux drops as almost all enzyme-substrate complexes are converted into EC_{16} , the latter which remains at a quasi-steady-states (see panels d and e, Figure 5.9). The subsequent increase is the result of a shortage in malonyl-CoA, which reduces the flux towards EC_{16} as EC_{14} is partitioned between its elongation into EC_{16} and the production of $C_{14}:0$. Once malonyl-CoA is fully depleted, the flux drops. Regarding the flux of production of $C_{16}:0$ (panel b, Figure 5.10), after a sharp increase as a result of rapid binding, it remains at quasi-steady states until the depletion of malonyl-CoA. For the flux of production of $C_{18}:0$ (panel c, Figure 5.10), after a sharp initial increase, it subsequently drops as a result of a large flux towards the production of $C_{16}:0$ and malonyl-CoA depletion.

By observing the time course of the metabolites in the system, one can observe that the substrates decay linearly until malonyl-CoA is fully depleted (panels a, b, and c of Figure 5.11). Furthermore, malonyl-CoA depletion (panel b of Figure 5.11) leads to an accumulation of enzyme-substrate complexes with carbon chain lengths smaller than 14 (panel d of Figure 5.11) as they cannot be further elongated. EC_{14} , EC_{16} , remain in a quasi-steady-state between 1 and around 20 seconds and drop suddenly with malonyl-CoA depletion. As for EC_{18} , one can observe a gradual decay after its initial formation over the first few milliseconds. This progressive decay of EC_{18} follows the dynamics of malonyl-CoA depletion, given that its formation occurs through slow binding. The dynamics of the three FAs can be directly inferred from the behaviors of their corresponding fluxes previously described. Notably, for $C_{14}:0$, after a short linear phase (between 1 and about 20 seconds) corresponding to the quasi-steady state, we observe a rapid increase until malonyl-CoA depletion. This second increase is due to the decrease of the flux from EC_{14} to EC_{16} . $C_{16}:0$ is built linearly until the malonyl-CoA is fully depleted. As for $C_{18}:0$ it follows the reverse dynamics of EC_{18} . This behavior reflects the linear dynamics of substrate consumption and product formation. For $C_{18}:0$, one can also observe that the dynamics of $C_{14}:0$ production are neither linear nor the expected trend. Indeed, after a short linear phase, it becomes exponential. This concavity change is consistent with the two peaks observed with the corresponding flux.

At this point, the model fails to capture the expected transient dynamics, as only a linear production of FAs is observed. Indeed, I would like the model to reproduce the long-run dynamics from the data of Topolska et al. [59] (see the bottom right panel of Figure 5.5). The model might not replicate the right dynamics because it may lack an important inhibition mechanism whose effect

could be significant in reproducing the transient kinetics observed in the data.

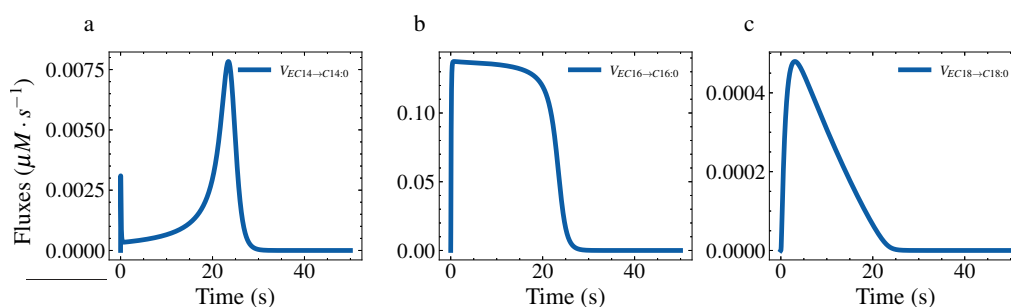


Figure 5.10: **Behavior of the fluxes of the vanilla model for long-run simulations:** Panel a displays the flux of production of $C14:0$. The first peak corresponds to the initial formation of the complex $EC14$, which then drops as a result of the large flux towards the production of $EC16$. The second peak occurs due to malonyl-CoA depletion, favoring the release of $C14:0$. Panel b shows a quasi-constant flux in the production of $C16:0$ after the initial formation of $EC16$, with the flux dropping upon malonyl-CoA depletion. Panel c illustrates the progressive decline in the production of $C18:0$ following the initial formation of $EC18$.

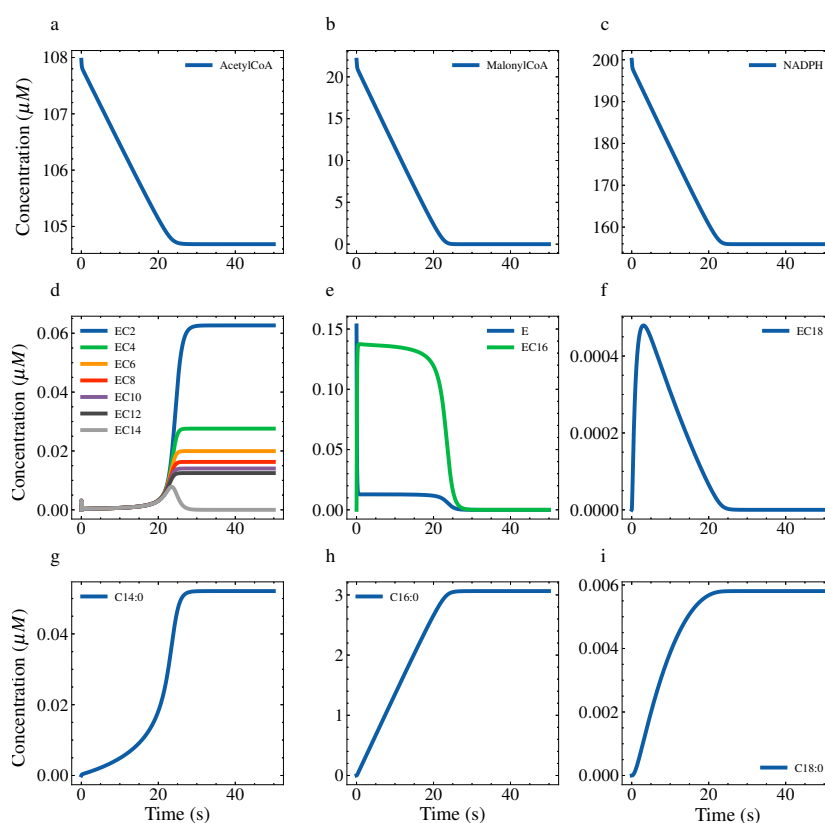


Figure 5.11: **Time course of the vanilla model for long-run simulation:** Panels a, b, c, h, and i display the linear consumption of substrates and the linear formation of products until malonyl-CoA depletion. After the total consumption of malonyl-CoA, occurring around 20 seconds, the concentration of the enzyme is distributed among enzyme-substrate complexes with chain lengths of 12 carbons or less (panel d). Panels e and f illustrate the dynamics of the $EC16$ and $EC18$ complexes. Notably, for $EC16$, a quasi-steady state is observed, followed by a drop due to malonyl-CoA depletion. $EC18$ is slowly converted into $C18:0$ as malonyl-CoA depletes. Panel g shows the dynamics of the production of $C14:0$.

Simulation for the long-run after CoA Inhibition being considered. To mitigate the persistent linear dynamics, I incorporated CoA inhibition following the insights from Cox and Hammes [36], who showed in an *in vitro* experiment that CoA significantly influences FA synthesis kinetics by inhibiting the pathway. Figures 5.12 and 5.13 depict the altered flux behaviors and the time courses of the compounds in the model, respectively. The initial rapid binding effect, consistent with earlier observations, is still observed in the first milliseconds (panels a, b, and d of Figure 5.12). Subsequently, as CoA accumulates, a noticeable decline in elongation and production fluxes is observed (panels a and b of Figure 5.12). This decline in elongation fluxes explains the resemblance of the time courses of FA production to that of the data. Specifically, the time course of the three FAs exhibits qualitatively the dynamics to those reported by Topolska et al. [59] (bottom right panel, Figure 5.5). This trend is attributed to the increasing CoA levels, which inhibit FA synthesis by occupying the binding site of the free enzyme. The flux of formation of the *EC_oA* complex displays two distinct peaks (panel c of Figure 5.12): The first peak corresponds to the initial binding of freshly produced CoA to the free enzyme, and the sharp drop follows due to the contribution of the backward reaction after the formation of the *EC_oA* complex. The second peak results from continuous CoA production. The latter escalates its inhibitory role, leading to extensive enzyme sequestration (panel e of Figure 5.13), indicative of CoA's competition with acetyl-CoA for the MAT site of the enzyme. This enzyme sequestration results in a non-linear decay of substrates and inversely affects CoA release (panels a, b, and c of Figure 5.13). Consequently, a non-linear FA production dynamic emerges, with *C16:0* as the predominant product. Overall, the dynamics of FA production and substrate consumption align qualitatively with the expected patterns, demonstrating the model's improved accuracy after CoA inhibition implementation.

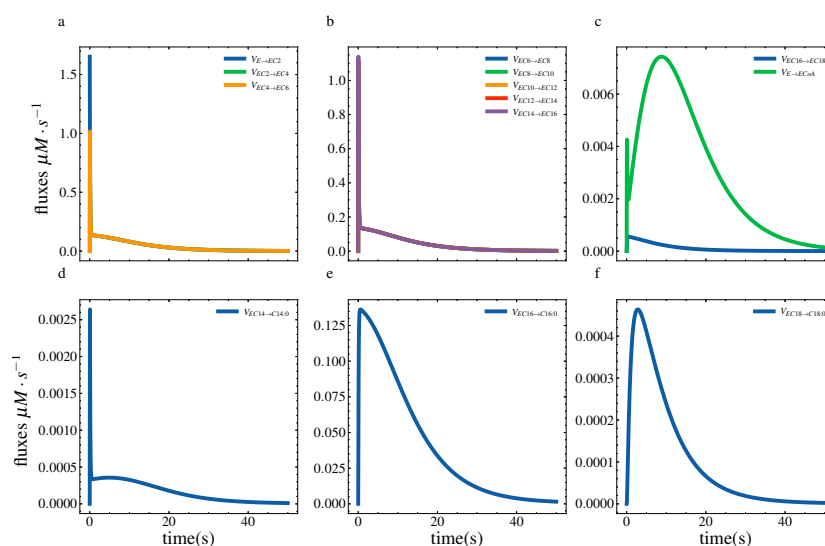


Figure 5.12: **Fluxes of the vanilla model after CoA inhibition being added** : Panel a and b show how the flux of cyclic elongation associated with the rapid binding display almost the same dynamics as in the case without CoA inhibition, but slightly less as result of the inhibition. Panel c shows the same trends as without inhibition for the flux $V_{EC16 \rightarrow EC18}$. One can observe the double peaks in the flux of *CoA* inhibition. The first peak corresponds to the first binding of the free *CoA* to the enzyme. The backward reaction could explain the drop after the first peak as the concentration of *CoA* is still low. The second increase following the drop results from the progressive production of the *CoA*. The *CoA* inhibition corrects the flux of production *C14:0* as one can observe only one peak instead of two as before the inclusion of the inhibition (panel d). The flux of production *C16:0* starts dropping earlier as compared to before I added the inhibition (panel e). This progressive drop can be explained by the progressive increase of the *ECoA*, resulting in a decrease of *EC16*. The flux of production of *C18:0* is almost unaffected by the inhibition.

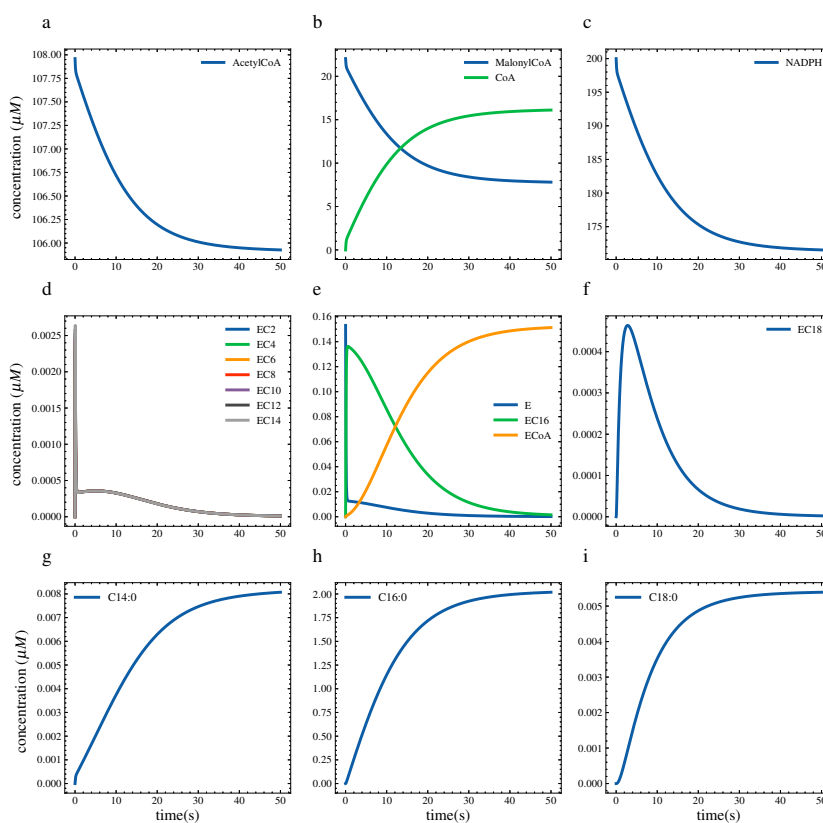


Figure 5.13: **Time course of vanilla model after CoA inhibition being added:** In panel a, b, and c, one can see that the consumption of substrates decay with time as the *CoA* becomes important in the system. The same trends can be observed with the production of *C14:0*, *C16:0* and *C18:0* in the panels g, h and i, respectively. Panels d, e, and f show progressive decay of the enzyme-substrate complexes as the *EC_{CoA}* complex takes over. The reaction becomes very slow once all the enzyme species are almost converted to *EC_{CoA}*.

After observing that the model almost displays the expected qualitative dynamics, the next step will be to fit the model to the available data. But before starting the fitting procedure, I would like to evaluate the importance of the parameters. In this way, I can prioritize some parameters over others. To do so, I use Sobol's sensitivity analysis, which measures each parameter's contribution to the output data (see Chapter 2).

5.2.2 Fitting the models to data

Determining the sample size for Sobol's sensitivity analysis. To effectively conduct a global sensitivity analysis of the models, determining an appropriate sample size for sampling the parameter vectors is critical. I performed sensitivity analyses on the model with inhibition, as it has a greater number of parameters, using a range of sample sizes from 0 to 20,000 in increments of 50. This method allowed me to observe how the sensitivity indices change with different sample sizes. The results are depicted in Figure 5.14, demonstrating the behavior of Sobol's first-order and total indices for each model output (*C14:0*, *C16:0*, and *C18:0*). Notably, for sample sizes larger than about 8,000, the indices show little variation, especially for *C16:0* (as seen in panels C and D of

Figure 5.14), which is the major product of the pathway. Given the computationally demanding nature of the method and its requirement for the sample size to be a power of 2, I opted for a sample size of 8,192 (2^{13}).

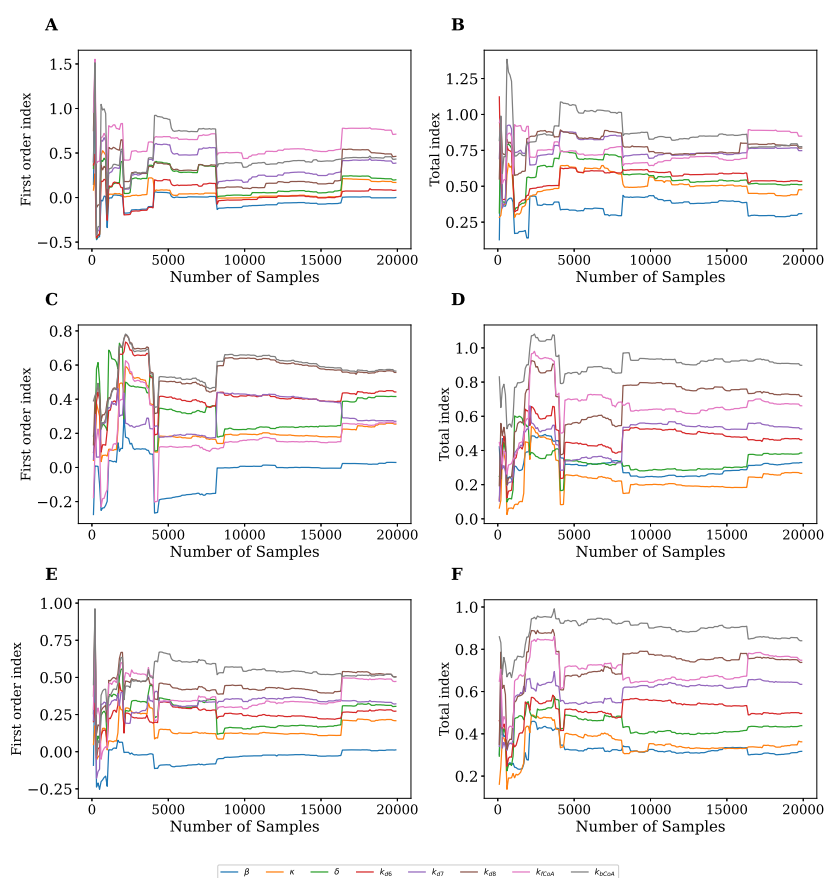


Figure 5.14: **Determination of sample size for Sobol's sensitivity analysis:** Panels A and B illustrate the variation of the first-order Sobol's indices and the total indices, respectively, with sample size for $C14:0$. Panels C and D show the variation of the first-order Sobol's indices and the total indices, respectively, with sample size for $C16:0$. Panels E and F depict the variation of the first-order Sobol's indices and the total indices, respectively, with sample size for $C18:0$.

Sensitivity of the model The models under consideration, one without inhibition and the other with CoA inhibition incorporate 6 and 8 parameters, respectively. A challenge I face in this context is the limited data availability, which hinders the estimation of reliable parameters. This issue is further compounded by the problem of parameter identifiability, where different sets of parameters can yield identical model performance. To address this, a global sensitivity analysis of the model is essential. This analysis will enable the identification of the most influential parameters for each model, thereby providing insights into what parameter to fit first.

The sensitivity analysis employed here relies on generating a Sobol sequence of size 4096 within a hypercube. The hypercube's dimensions are equivalent to the number of parameters, and each edge measures 100 units (reflecting the unit for each parameter). Essentially, this entails a sequence of

4096 parameter vectors, each parameter ranging from 0 to 100 units. Following this, I simulate the model, applying the initial conditions previously outlined for every parameter vector in the sequence. For each output of the model ($C14:0$, $C16:0$, and $C18:0$), I then gather a vector that depicts the time course (from 0 to 4800 seconds). Subsequently, for each model output, I normalize the entries of the corresponding vector by dividing them by its norm, followed by calculating the mean of these normalized vectors. This process yields 4096 values for each output, whose variance I analyze using Sobol's sensitivity analysis. In this way, I can access the first-order, second-order, and total indices. Further details on this methodology can be found in Chapter 2. The sensitivity analysis routine is executed using the *Python* library SAlib [192], as elaborated in Chapter 2.

Upon examining the first-order and total indices (refer to Figure 5.15 and Figure 5.17) of each model, it becomes apparent that the parameters κ and δ exert the most significant control on the model dynamics. This underlines the importance of choosing the kinetic rate constants for cyclic elongation in the parameterization of the models. Additionally, it is observed that k_{d6} and k_{d7} contribute less significantly than κ and δ . Specifically, the variations of k_{d6} slightly influence the time courses of $C14:0$ and $C18:0$, whereas variations in k_{d7} impact the time courses of $C16:0$ and $C18:0$. As expected, k_{d8} solely affects the output of $C18:0$, given that the flux towards the production of $C18:0$ faces no competition. Further, examining the second-order indices of the model with inhibition (see Figure 5.18) reveals the notable contributions of the inhibition reaction parameters k_{fCoA} and k_{bCoA} . They exhibit negative interactions with δ , particularly influencing the time course of $C16:0$. In contrast, such significant negative interactions of δ with other parameters were not observed in the model without inhibition (see Figure 5.16).

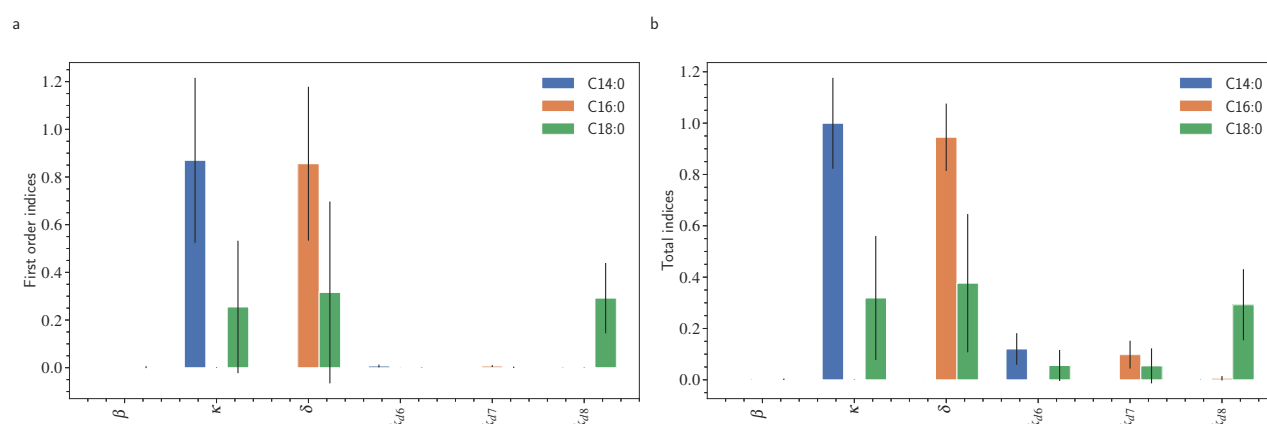


Figure 5.15: **First-Order and Total Indices for the model without inhibition:** The first-order and total Sobol's indices highlight the significant influence of the parameters κ and δ on the model's output. The total indices also reveal the relatively minor impacts of k_{d6} and k_{d7} . Notably, k_{d8} exclusively affects the dynamics of $C18:0$. The parameter β shows negligible influence on the model output.

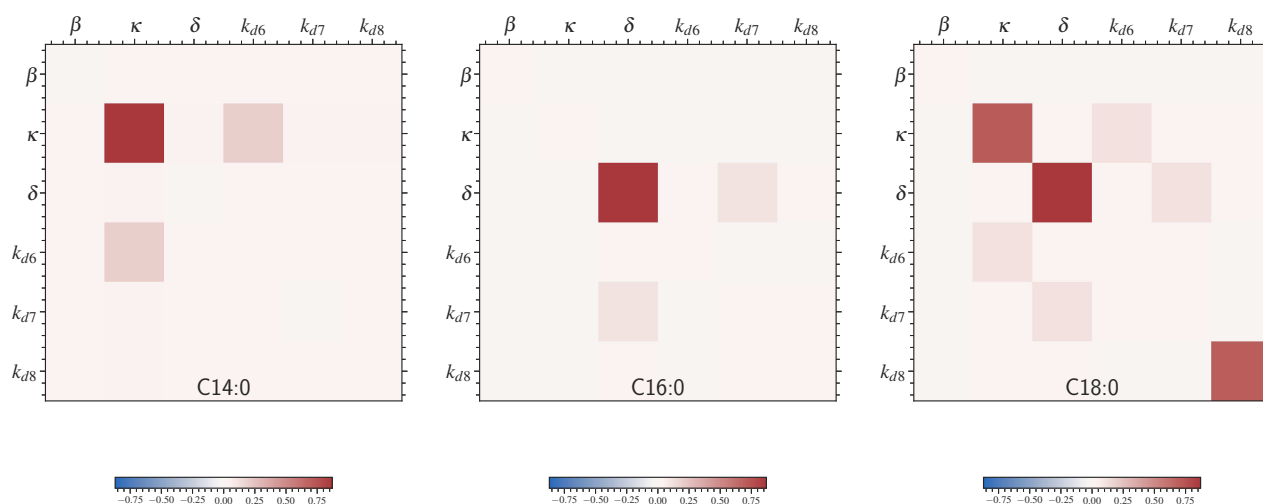


Figure 5.16: **Second order indices for the model without inhibition:** the interaction of κ and δ control the time course of the output of the model. One can see a slightly negative interaction of the couples (δ, k_{d6}) and (δ, k_{d8}) on the time course of $C16:0$

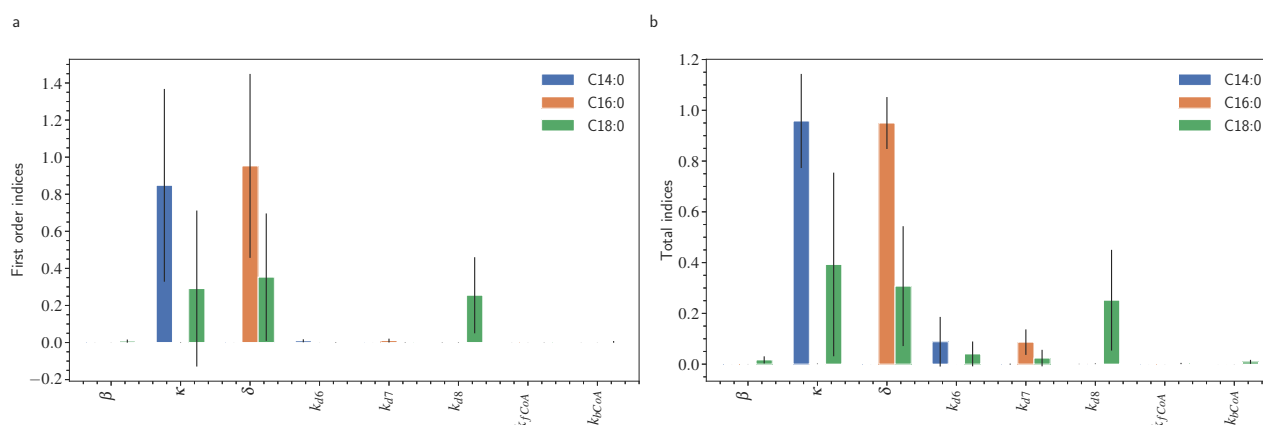


Figure 5.17: **First-order and total indices for the model with inhibition by CoA** : one can see the strong control of the parameters κ and δ on the model's output. The total indices show the minor influences of k_{d6} and k_{d7} . k_{d8} only control the dynamic of $C18:0$. β exerts a minor control on the model's output as well as k_{fCoA} and k_{bCoA} .

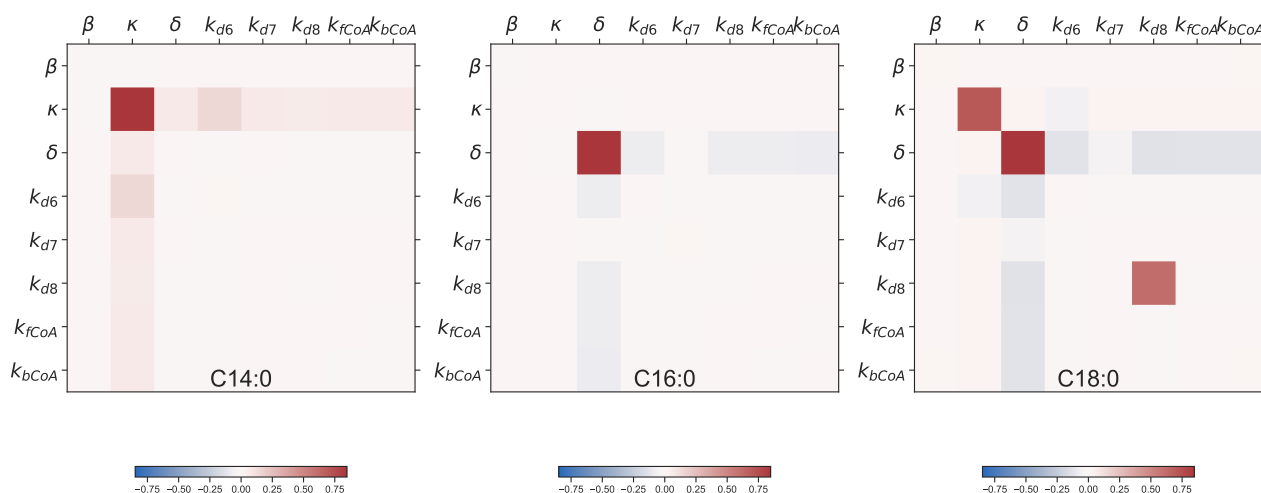


Figure 5.18: **Second order indices for the model without inhibition:** δ negatively interacts with k_{d6} , k_{d7} , k_{fCoA} , and k_{bCoA} to control the time courses of $C16:0$ and $C18:0$.

Estimation of the kinetic rate constant k_{d7} of release of $C16:0$. Given that I consider the rapid binding assumption, one can estimate the kinetic rate constant of the release of $C16:0$ (k_{d7}) from initial phase data by using the model without inhibition. The rapid binding assumption suggests that all free enzymes are instantaneously converted to an $EC16$ complex, which remains in a quasi-steady state until one substrate is fully consumed (refer to Figure 5.9, and Figure 5.11). It will later be seen that using the model with inhibition would have led to a similar result, as the $EC16$ complex almost maintains a quasi-steady state during the initial phase (see panel e, Figure 5.22). As the slope of the initial phase time course data corresponds to the rate of release of $C16:0$, one can estimate k_{d7} as follows:

$$k_{d7} = \frac{V_{EC16 \rightarrow C16:0}}{EC16}. \quad (5.2.1)$$

From the initial phase time course data, which is recorded for 120 seconds, the slope is given by

$$V_{EC16 \rightarrow C16:0} \simeq \frac{0.55 \mu M - 0 \mu M}{120 s - 0 s} = 0.0046 \mu M \cdot s^{-1}, \quad (5.2.2)$$

therefore

$$k_{d7} = 0.03 s^{-1}. \quad (5.2.3)$$

As k_{d7} is already estimated, it is essential to check the rapid binding assumption after estimating the other parameters from the data.

Fitting of the initial phase data. Since the value of k_{d7} was directly calculated from the initial phase time course data, I can now focus on estimating the remaining parameters. Priority should be given to δ and κ , as indicated by the results of the Sobol's sensitivity analysis. Once the values of

these parameters are determined, my attention will shift to k_{d6} , k_{d8} , and β . It is important to note that the parameters estimated or calculated from the model without inhibition will remain valid for the model with inhibition. This is because both models are nearly identical in the initial phase, as previously observed. Specifically, the introduction of inhibition by CoA does not significantly affect the initial phase but becomes crucial in the long-run when CoA levels rise. Regarding the parameters of the inhibition reaction by CoA (k_{fCoA} and k_{bCoA}) for the model with inhibition, they will be fitted later to the long-run time course data. This strategy will be applied to fit the model to the data from Topolska et al. [59], with the only difference being that for the model without inhibition, the parameters will be fitted simultaneously to both initial phase and long-run data. The parameter space has been limited to a hypercube whose edges measure 1 unit. This means that the fitted value of each parameter will be between 0 and 1 unit, the unit of each parameter being considered. The logic behind choosing the upper bound of the parameter space is explained below.

Considering the rapid binding associated with κ and the slow binding with δ and that the reactions associated with these parameters have the same substrates and follow the same pattern, one can conclude that κ will be strictly greater than δ . Therefore, an upper bound for κ will also be an upper bound for δ . Consequently, I will determine only the upper bound for κ . In order to determine the upper bound for κ , I use the kinetic parameters (k_{cat} and K_m) of the KR site of the enzymes for NADPH, as it has a faster rate [154]. The KR site uses a molecule of NADPH to reduce the enzyme-substrate complex bearing malonyl-CoA. Hence, for the considered reaction, one has

$$K_m^{\text{NADPH}} = \frac{k_b^{\text{NADPH}} + k_{cat}^{\text{NADPH}}}{k_f^{\text{NADPH}}}, \quad (5.2.4)$$

which implies

$$k_f^{\text{NADPH}} = \frac{k_b^{\text{NADPH}} + k_{cat}^{\text{NADPH}}}{K_m^{\text{NADPH}}}. \quad (5.2.5)$$

Given that, in my model, I have considered the reactions to be irreversible, this same consideration is applied to the reaction executed by the KR site (i.e., $k_b^{\text{NADPH}} \ll k_{cat}^{\text{NADPH}}$). Consequently, one will have:

$$k_f^{\text{NADPH}} \simeq \frac{k_{cat}^{\text{NADPH}}}{K_m^{\text{NADPH}}}. \quad (5.2.6)$$

The binding constant k_f^{NADPH} , representing the binding of NADPH to the enzyme-substrate complex, is proportional to κ , the binding constant of NADPH and malonyl-CoA to the enzyme-substrate complex. This proportionality assumes that the binding interactions in these complexes are similar. Hence, κ can be estimated from Equation (5.2.6) as follows:

$$\kappa \approx \frac{k_{cat}^{\text{NADPH}}}{K_m^{\text{NADPH}} \times MalCoA_0}, \quad (5.2.7)$$

where $MalCoA_0$ represents the initial concentration of malonyl-CoA in the system. The parameters k_{cat}^{NADPH} and K_m^{NADPH} are the turnover number and the Michaelis-Menten constant, respectively, of the KR site of the enzyme. These values are extracted from the work by Carlisle-Moore et al. [154], where they used a human enzyme *in vitro* (refer to Table A3). The values reported are $4 : s^{-1}$ and $4 : \mu M$ for k_{cat}^{NADPH} and K_m^{NADPH} , respectively. Thus, one can calculate κ as follows:

$$\kappa \approx \frac{4 s^{-1}}{4 \mu M \times 22.04 \mu M} \approx 0.04 \mu M^{-1} \times s^{-1}. \quad (5.2.8)$$

The rationale for choosing the KR site parameters for calculating the first estimates of κ is based on the fact that the KR site reaction exhibits the largest ratio of K_{cat}/K_m among the four cyclic elongation reactions. This significant ratio indicates a high enzymatic efficiency, making it a reliable reference point. Consequently, this initial estimate of κ will enable me to confidently set an upper bound for both κ and δ .

Applying the same reasoning to the MAT site of the enzyme, which involves acetyl-CoA, a preliminary estimate of β can be derived. This estimate utilizes the values extracted from Carlisle-Moore et al. [154]. The calculation is as follows:

$$\beta \approx \frac{k_{cat}^{Acet}}{K_m^{Acet}}, \quad (5.2.9)$$

where k_{cat}^{Acet} is the catalytic rate constant and K_m^{Acet} is the Michaelis-Menten constant for the MAT site involving acetyl-CoA. Consequently,

$$\beta = \frac{1.9 s^{-1}}{3.9 \mu M} \approx 0.5 \mu M^{-1} \times s^{-1}. \quad (5.2.10)$$

With these initial estimates of β , κ , and δ , I can confidently set the upper bounds of the parameter space for each parameter to 1.

As I already announced in Chapter 2, I use the Levenberg–Marquardt algorithm implemented in Python with `lmfit` package to solve the following optimization problem: Find θ_{min}

$$\theta_{min} = \operatorname{argmin} \mathcal{L}(\theta), \quad (5.2.11)$$

where

$$\mathcal{L}(\theta) = \frac{1}{2} \sum_{i=1}^n (f_i(\theta, \mathbf{x}(\theta)) - y_i)^2. \quad (5.2.12)$$

$f_i(\theta, \mathbf{x}(\theta))$ is the output of my model at times t_i of measurement of data y_i . θ is the vector of the parameters of my model. $\mathbf{x}(\theta)$ are the inputs of the model, which depend on the parameterization θ , in this case, the metabolites of the model.

Table 5.6: **Best parameters for the initial phase fit.**

Parameters	Values	Units
β	0.043	$\mu M^{-1} \times s^{-1}$
κ	0.12	$\mu M^{-2} \times s^{-1}$
δ	1.3×10^{-6}	$\mu M^{-2} \times s^{-1}$
k_{d6}	1.16	s^{-1}
k_{d7}	0.03	s^{-1}
k_{d8}	0.7	s^{-1}

To ensure the most accurate fit, I enhanced the selection of initial guesses for the parameter vector by generating 1024 initial guesses using Sobol sequences (Sobol sampling). I ran the optimization algorithm for each of these initial guesses, which yielded the best-estimated parameter vector alongside the corresponding Root Mean Square Errors (RMSEs). The results are summarized in the pair plot (Figure 5.19). It is noticeable that the distribution of the values for κ and δ , which correspond to the minimum RMSE (highlighted in blue), are narrowly concentrated around $0.12 \mu M^{-2} \times s^{-1}$ for κ and $1.3 \times 10^{-6} \mu M^{-2} \times s^{-1}$ for δ . In contrast, the values minimizing the RMSE for other parameters are more widely dispersed in the parameter space. Among the best parameter vectors, I selected the one with the smallest RMSE due to the presence of several local minima. The chosen parameters are detailed in Table 5.6. Figure 5.20 (left panel) illustrates that the model, with the selected parameter vector, fits the initial phase data well (RMSE = 0.013) but is inadequate for the long-run phase. However, attempting to fit both the initial and long-run phases simultaneously resulted in a significantly poorer fit. In fact, the model fails to represent either phase adequately, even after expanding the limits of the parameter space to infinity, as shown in the right panel of Figure 5.20.

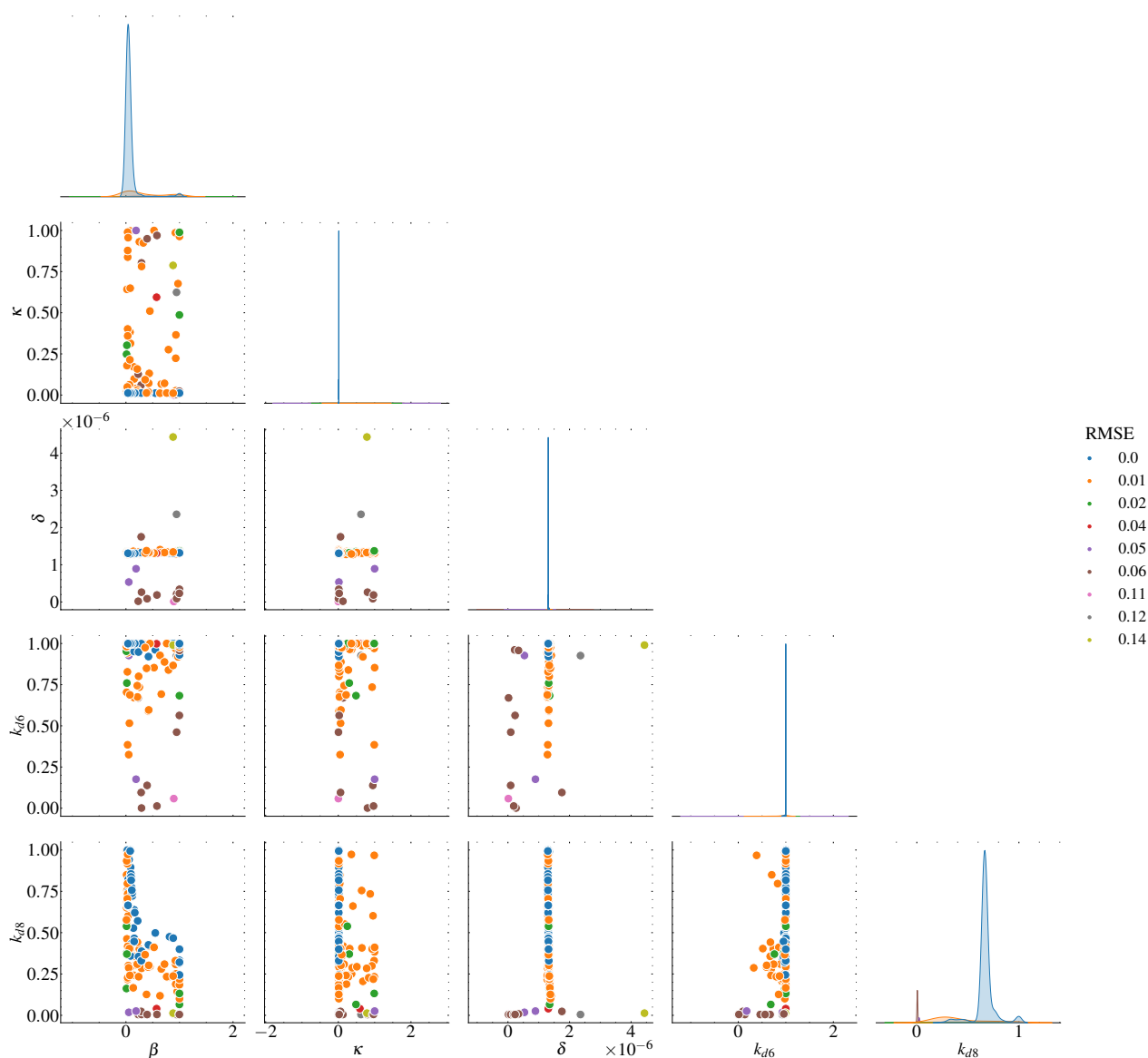


Figure 5.19: **Parameter distribution and the corresponding root-means-square for the model without inhibition:** The pair plots the distribution of parameter values, considering each pair of parameters. The distributions of each parameter taken individually are presented on the diagonal. The color coding corresponds to the value of the RRMSE. The values of κ and δ associated with the smallest RMSE (indicated by blue points and distributions) demonstrate a narrow distribution centered around $0.12 \mu M^{-2} \times s^{-1}$ for κ and $1.3 \times 10^{-6} \mu M^{-1} \times s^{-1}$ for δ . This narrow distribution suggests a higher level of certainty in these parameter estimates. In contrast, parameters such as β , k_{d6} , and k_{d8} exhibit wide distributions even at minimal RMSE, indicating greater variability and less certainty in their optimal values. The graph also reveals that various combinations of these parameters can lead to the same RMSE, highlighting the interdependence of its parameters.

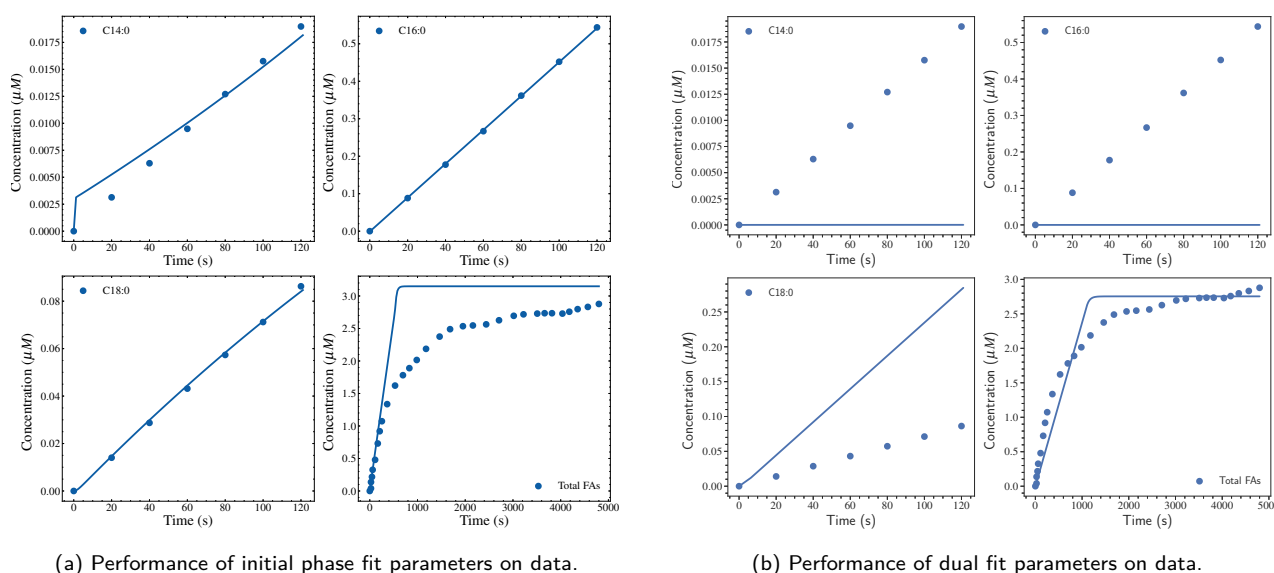


Figure 5.20: **Performance of the model without inhibition on data:** (a), I have a good fit of the initial phase but a poor of the long-run, notably the transient phase. (b), the model fails to reproduce both the initial phase and the long-run.

Fitting the model to Total Fatty acids production data. Given that the initial phase kinetics determine the overall time course, I fixed the parameters previously obtained from fitting the model without inhibition to the initial phase data. I only fitted the parameters k_{fCoA} and k_{bCoA} . I generated 1024 initial guesses using Sobol's sampling and proceeded as done previously in the case of the fit of the initial phase data. The only difference is that I fitted both the initial phase and the long-run data. Consequently, I obtained the values of $0.041 \mu M^{-1} \times s^{-1}$ for k_{fCoA} and $2.6 \times 10^{-4} s^{-1}$ for k_{bCoA} , with an RMSE of 0.521 (see Figure 5.21). Figures 5.22 and 5.23 demonstrate the model's performance in fitting the data from both the initial phase and the long-run, respectively, as well as the time course of the different metabolites in the system. The plots in Figures 5.22 and 5.23 show that the model reproduces quite well both the initial phase data and C16:0 and C18:0 (see panels b and c of Figure 5.22). Additionally, the model qualitatively follows the same dynamics as the long-run data from Topolska et al. [59] (see panels a, h, and i of Figure 5.23). However, the model fails to reproduce the kinetics of C14:0, as deviations from the data are observed. One reason for the observed rapid kinetics (compared to the data) in the first milliseconds (panel a of Figure 5.22) and during the long-run (panel g of Figure 5.23) might be that our model does not account for the production of shorter FA chains. *In vitro* experiments, such as those conducted by Carlisle-Moore et al. [154] and Topolska et al. [59], have shown that shorter chains can be produced in small quantities (about 4%). Considering the production of shorter chains may correct the observed deviation. I chose not to consider the production of shorter chains due to the lack of time course data about their production. Furthermore, including shorter chains would double the number of parameters in the model.

As mentioned earlier, it is also notable that, although inhibition by CoA is introduced, the quasi-

steady-state assumption is still fulfilled. All enzymes are converted to the $EC16$ complex, which remains almost at a quasi-steady state during the initial phase (see panels d, e, and f of Figure 5.22). A progressive accumulation of CoA in the system is also observed (see panel h of Figure 5.22 and panel f of Figure 5.23), gradually sequestering the enzyme (see panel c of Figure 5.23) and progressively reducing the rate of FA production. Overall, the time course of substrate consumption and product formation adequately reflects the dynamics of FA production as reported by Topolska et al. [59]. The parameters resulting from fitting the model to the data are summarized in Table 5.7.

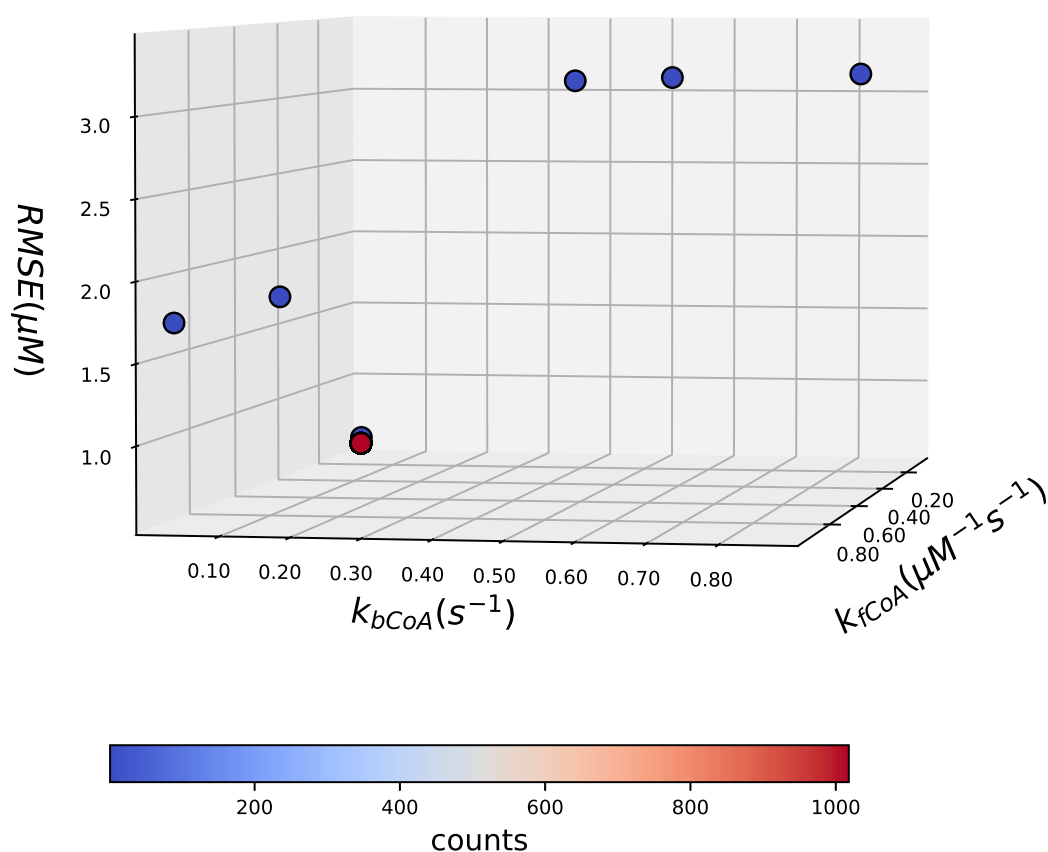


Figure 5.21: **RMSE as a function of k_{fCoA} and k_{bCoA}** : After conducting 1024 fits, approximately 7 local minima were identified based on their RMSE values, with the smallest RMSE being 0.521. The values of k_{fCoA} and k_{bCoA} corresponding to the smallest RMSE occurred more than 900 times (indicated by red points), whereas the other local minima appeared fewer than 10 times (indicated by blue points). The optimal parameter values associated with the smallest RMSE (0.521) are $0.041 \mu M^{-1} \times s^{-1}$ for k_{fCoA} and $2.6 \times 10^{-4} s^{-1}$ for k_{bCoA} .

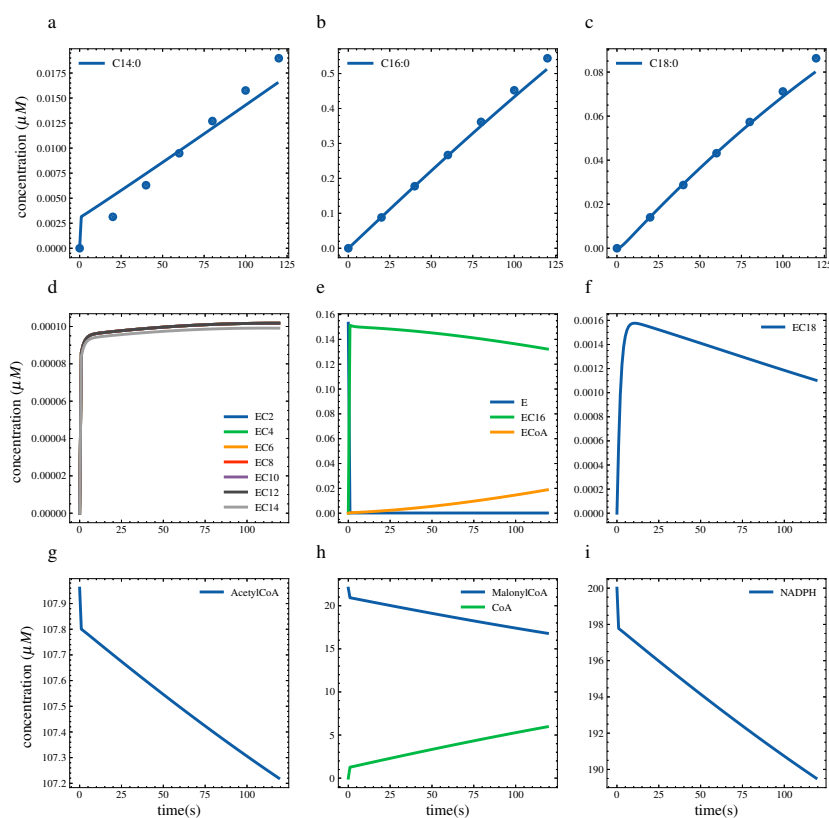


Figure 5.22: **Initial phase fit for the model with inhibition:** Panels a, b, and c show the fit of the initial phase data (RMSE = 0.521, indicative of the dual fitting's accuracy). Panels d, e, and f demonstrate that, despite a slight deviation during the first milliseconds from *C14:0*, the model's rapid binding assumption remains valid, as almost all the enzyme is converted into *EC16* complex during the initial phase. Panel e further illustrates the inhibition effect, revealing a progressive formation of the *ECoA* complex within the system. Panels g, h, and i display the substrates' linear consumption and *CoA* formation, with the rapid binding evidenced by the quick drop of substrates in the first milliseconds.

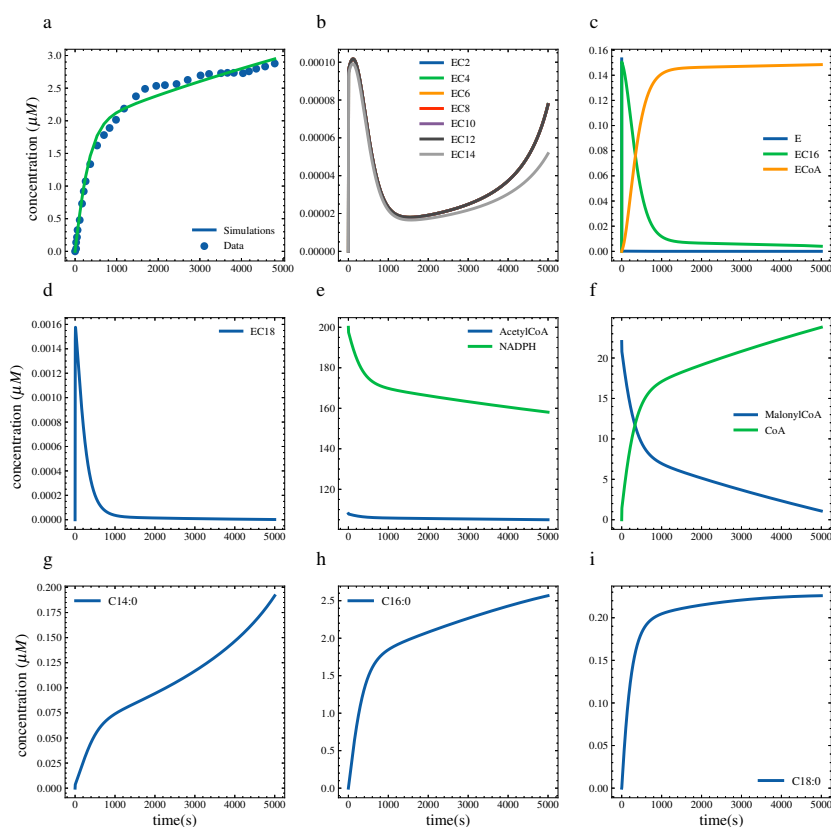


Figure 5.23: **Fitting the long-run simulation and dynamics of the compounds:** Panel a demonstrates that the model accurately fits the long-run experimental data, with an RMSE of 0.521. Panels b, c, and d illustrate CoA's progressive sequestration of the enzyme after the initial phase by forming the *ECoA* complex. Panels e and f reveal slower substrate consumption dynamics compared to the initial phase, highlighting the inhibition by CoA. This is further evidenced by a gradual increase in *CoA*, which exhibits dynamics opposite to malonyl-CoA consumption. Panels h and i display the production of *C16:0* and *C18:0*, both quantitatively and qualitatively, consistent with the total fatty acids (FAs) production data.

Table 5.7: **Summary of the parameters resulting from the fit of both initial phase and long-run data.**

Parameters	Values	Units
β	0.043	$\mu M^{-1} \times s^{-1}$
κ	0.12	$\mu M^{-2} \times s^{-1}$
δ	1.3×10^{-6}	$\mu M^{-2} \times s^{-1}$
k_{d6}	1.16	s^{-1}
k_{d7}	0.03	s^{-1}
k_{d8}	0.7	s^{-1}
k_{fCoA}	0.041	$\mu M^{-1} \times s^{-1}$
k_{bCoA}	2.6×10^{-4}	s^{-1}

Fitting the model to Michaelis-Menten rate equations and estimation of the corresponding parameters. Given that the model's parameters are not directly comparable to standard enzyme kinetic parameters found in the literature, notably k_{cat} and K_m , a strategy is required to evaluate the model effectively. This strategy involves generating synthetic time course data using the model parameters outlined in Table 5.7 and the experiment conditions by Carlisle-Moore et al. [154]. The initial rate is inferred from the generated data by varying the substrates, then fitting Michaelis-Menten rate laws, and corresponding k_{cat} and K_m for each substrate are recorded. These inferred values will subsequently be compared to those reported in the literature, especially the work of Carlisle-Moore et al. [154], where the kinetic parameters (k_{cat} and K_m) of the production of $C16:0$ using human FAS expressed in baculovirus, and Rangan and Smith [193], who study FAS purified from rat liver, are detailed. I chose the conditions of Carlisle-Moore et al. [154] for determining the kinetic parameters because this was the most recent study providing detailed data. Moreover, this work aims to offer insights specifically for human FAS, mirroring the focus of Carlisle-Moore et al. [154]. The conditions utilized to determine the kinetic parameters of the model are summarized in Table 5.8.

Table 5.8: **Summary of conditions for determining k_{cat} and K_m for each substrate.** I use the same conditions as in the experimental work of Carlisle-Moore et al. [154]. To determine the kinetics parameter of a given substrate, I first make sure that the others are in excess (saturation of the enzyme) and vary the value of the substrate of interest, the corresponding initial rate is recorded from time course.

Determination of parameters of acetyl-CoA		Determination of parameters of Malonyl-CoA	Determination of parameters of NADPH
Acetyl-CoA	0 - 50 μM	25 μM	25 μM
malonyl-CoA	100 μM	1-100 μM	100 μM
NADPH	100 μM	100 μM	5-100 μM
FAS	0.02 μM	0.02 μM	0.02 μM

To generate the kinetic rate curve (v) as a function of a specific substrate concentration, I adhere to the methodology described by Carlisle-Moore et al. [154] and Cox and Hammes [36], where the concentrations of the two non-focal substrates are fixed at saturating levels to ensure enzyme saturation. This setup allows for the isolated variation of the substrate of interest's concentration. For each concentration of this substrate, the initial rate v is determined by analyzing the linear segment of the time course, as depicted in Figure 5.24. Subsequently, I plot the rate v against the substrate concentration to visualize the relationship. The final step involves fitting these plotted data points to the Michaelis-Menten rate equations, enabling the extraction of the kinetic parameters k_{cat} and K_m .

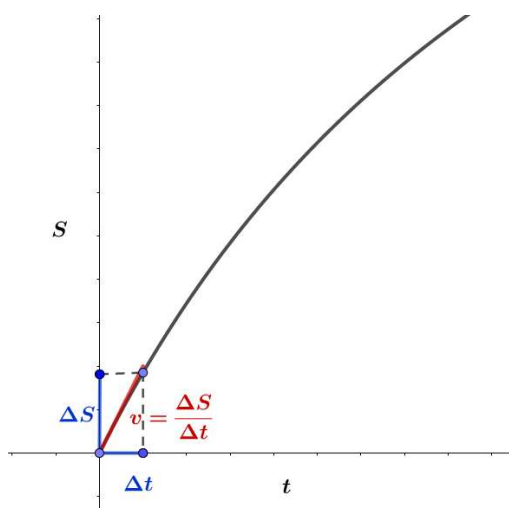


Figure 5.24: **Description of the initial rate of the reaction:** t stands for the time, S for the concentration of substrate, Δt time interval, ΔS the interval of variation, and v the initial rate.

My model successfully reproduces the Michaelis-Menten rate kinetics for the rate of formation of $C16:0$ across the three substrates, as evidenced in the middle panels of Figures 5.25, 5.26, and 5.27. Furthermore, it simulates Michaelis-Menten kinetics for the production rates of all three types of fatty acids (FAs) using acetyl-CoA as the substrate, despite some numerical artifacts observed in the rate of production for $C14:0$. However, the kinetic parameters derived from my model significantly deviate from those reported in the literature, specifically by Carlisle-Moore et al. [154] and Rangan and Smith [193]. Notably, the model indicates that the production rates of $C14:0$ and $C18:0$, as functions of malonyl-CoA or NADPH, do not conform to the Michaelis-Menten rate equations, as demonstrated in the left and right panels of Figures 5.26 and 5.27. The discrepancies and similarities between my model's predictions and established kinetic parameters are summarized in Table 5.9, highlighting the unique insights offered by my model into fatty acid synthesis kinetics.

Table 5.9: Comparison of the parameter of my model to enzyme kinetic parameters existing in the literature.

Origin of the purified enzyme	My model parameters		Parameters from the literature				Reference
	Bovine mammary gland		Rodent		Human		
Substrate/ product	$k_{cat}(s^{-1})$	$k_m(\mu M)$	$k_{cat}(s^{-1})$	$k_m(\mu M)$	$k_{cat}(s^{-1})$	$k_m(\mu M)$	
Acetyl-CoA/C14:0	0.00037	1.56					
Malonyl-CoA/C14:0	0.0012	3.3×10^{-11}					
NADPH/ C14:0	0.0012	2.2×10^{-11}					
Acetyl-CoA/C16:0	0.03	1.17	1.9 ± 0.06	3.9 ± 0.4	2.7 ± 0.2	7 ± 3	[193], [154]
Malonyl-CoA/C16:0	0.03	1.24	1.2 ± 0.008	1.9 ± 0.23	2.7 ± 0.2	6 ± 2	[193], [154]
NADPH/ C16:0	0.03	1.22			2.7 ± 0.2	5 ± 1	[193], [154]
Acetyl-CoA/C18:0	0.013	1.16					
Malonyl-CoA/C18:0	0.56	4443					
NADPH/ C18:0	0.75	6071					

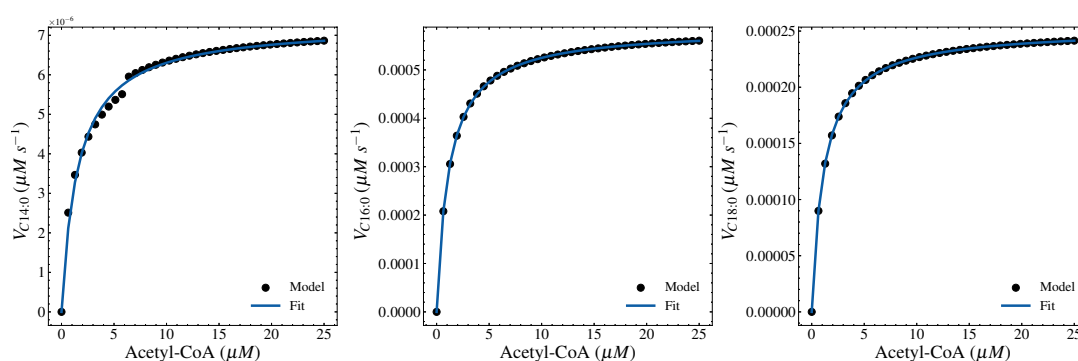


Figure 5.25: Fitting my model with Michaelis-Menten rate equations in order to estimate k_{cat} and k_m for acetyl-CoA: The rates of production of the three FAs as a function of acetyl-CoA by the model can be approximated with Michaelis-Menten rate equations.

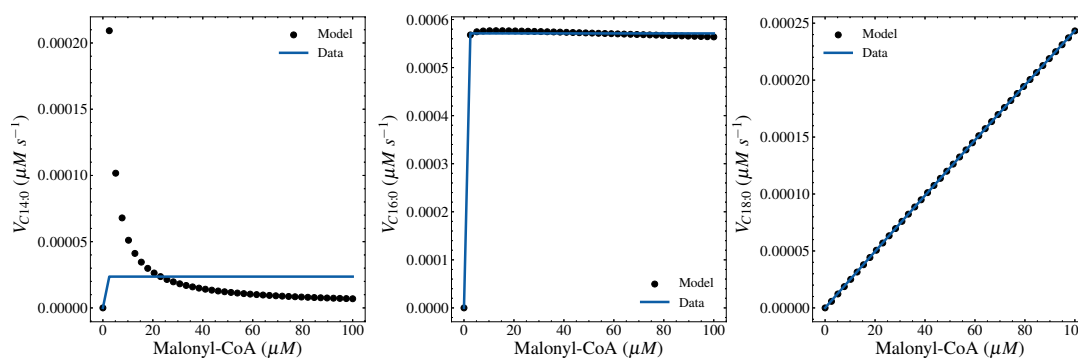


Figure 5.26: Fitting my model with Michaelis-Menten rate equations in order to estimate k_{cat} and k_m for malonyl-CoA: Only the rate of formation of C16:0 can be approximated with Michaelis-Menten rate equations

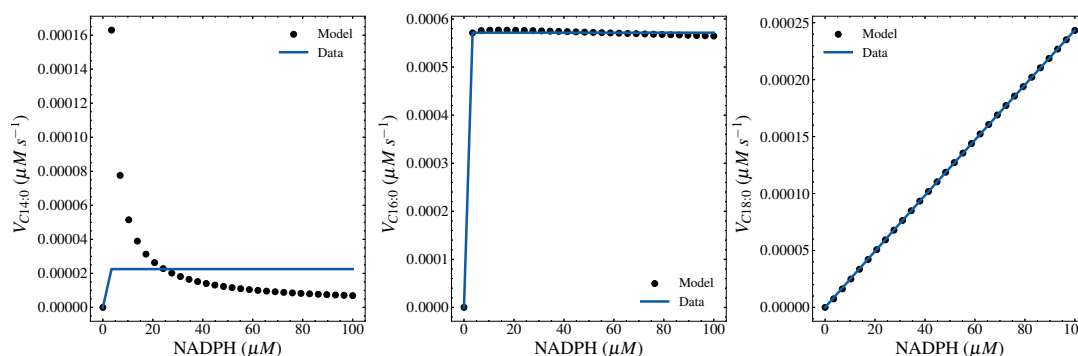


Figure 5.27: Fitting my model with Michaelis-Menten rate equations in order to estimate k_{cat} and k_m for NADPH: Only the rate of production of $C16:0$ can be approximated with Michaelis-Menten rate equations

5.3 Discussion and Conclusion

Fatty acid *de novo* synthesis (FADNS) relates carbohydrate metabolism to lipid metabolism. It uses acetyl-CoA as a precursor and produces LCFAs. This process is crucial both from an energetic and physiological point of view. It allows the storage of excess carbohydrates into fats for later use in case of long-time fasting. FADNS ensures the availability of FAs, which are building blocks for the formation of complex lipids such as phospholipids, the main constituents of cell and organelle membranes. Due to its association with cancer and metabolic syndromes such as insulin resistance, type 2 diabetes, and obesity, the FADN pathway is of significant medical interest. Therefore, modeling its dynamics could provide more insights that are beneficial for systems medicine and metabolic engineering. Specifically, in the case of mitochondrial fatty acid oxidation disorders (mFAODs), which is the motivation of this work, I presented a dynamical mathematical model of FADNS that can be combined with the existing mathematical models of FA oxidation to study mFAODs. A global approach combining FA oxidation, synthesis, and storage could provide insights into understanding the metabolic dysregulation observed in the case of certain mFAODs. FADNS occurs in two stages. The first is the synthesis of malonyl-CoA from acetyl-CoA, and the second is the elongation phase, which consists of synthesizing LCFAs from acetyl-CoA, malonyl-CoA, and NADPH. This second step was the subject of this chapter. The elongation phase of FADNS has a particularity in that it incorporates a series of cyclic reactions, and each cycle comprises several reactions catalyzed by the unique enzyme, FAS. Moreover, these reactions are complex as they are carried out through channeling, where one site of the enzyme passes the intermediates to the next one without formally releasing the product. In addition, the pathways produce different products depending on the number of cycles, notably $C14:0$, $C16:0$, and $C18:0$, which are the major products with $C16:0$ being around 90% of the production [36, 193, 154, 59]. These unique mechanisms make the pathway challenging to model using either detailed mechanistic modeling or coarse-grained approaches.

In this chapter, after briefly presenting existing models available in the literature, I proposed a semi-

mechanistic model of the elongation phase of FADNS. The model considers the critical processes involved in FADNS: initialization, chain cyclic elongation, and termination. I assume each of these processes to be elementary steps modeled as irreversible mass action rate laws, except for the competitive inhibition by CoA, which is considered to follow reversible mass action rate laws. Furthermore, as the channeling intends to optimize kinetic efficiency, I assume that the cyclic elongations are rapid binding except for the last elongation step where the affinity decreases [99]. Thus, I developed two models. The first does not include CoA inhibition, and the second considers CoA inhibition. As my goal is to construct a simplest while informative model that can reproduce the FADNS mechanism and given that I only have scarce *in vitro* data (closed system), I decided to consider the system to be closed. To validate, I use the data of the time course of FADNS extracted from the work of Topolska et al. [59], who developed a high-resolution mass spectrometry-based assay using the FAS purified from the cow mammary gland. They measured the initial phase of the time course of the formation of $C_{14}:0$, $C_{16}:0$, and $C_{18}:0$ (120 seconds). They also produced the temporal evolution of the concentration of all FAs (the sum of all FAs produced) for an hour and a half (long-run). After a global sensitivity analysis of the constructed model using the Sobol approach, I classified the parameters in order of importance. While fitting the model to the data, this classification is considered by prioritizing the parameters that exert greater control over the model outputs. My fitting approach minimizes the residual between the model and the data using the Levenberg–Marquardt algorithm. The quality of the fitting is evaluated by measuring the root-mean-square error (RMSE) between the model and the data.

If the model without inhibition reproduces the initial phase data, it fails to do so with the long-run data qualitatively and quantitatively. However, considering the competitive inhibition reaction by CoA allows fitting both the initial phase and the long-run data with a reasonable RMSE. I believe the CoA inhibition must still be incorporated even in the *in vivo* situation where the system is open, although other processes could use the freshly produced CoA. Indeed, CoA plays an essential role in regulating metabolism through feedback inhibition [194].

Finally, to compare my model with the existing parameters in the literature, I constructed from the model the production rates of the different products of the pathway ($C_{14}:0$, $C_{16}:0$, and $C_{18}:0$) as functions of each of the substrates of the pathway (acetyl-CoA, malonyl-CoA, and NADPH). I then fitted the Michaelis-Menten rate equation to each to extract the kinetic parameters. The conclusion is that the model produces all three types of FAs considered at rates similar to Michaelis-Menten rate laws when considering acetyl-CoA as a substrate (malonyl-CoA and NADPH kept constant at high concentrations). Additionally, for the rate of production of $C_{16}:0$ as a function of malonyl-CoA and NADPH, it can be assimilated to Michaelis-Menten rate law, but a fast kinetic rate as the 0 order kinetic is achieved almost instantly. However, the model cannot be approximated with Michaelis-Menten rate laws for the rate of production of $C_{14}:0$ with either malonyl-CoA or NADPH as substrates. Regarding the rate of production of $C_{18}:0$ with malonyl-CoA or NADPH

as substrates, the model can only agree with the linear part of the Michaelis-Menten rate laws. Besides, the parameters recorded deviate considerably from those in the literature, as k_{cat} values are 100 folds lower than those reported by Carlisle-Moore et al. [154] and Rangan and Smith [193]. Positively, the K_m values are in the same order of magnitude as those in the literature but lower.

One should notice that the sources of the enzymes in the works of Carlisle-Moore et al. [154] and Rangan and Smith [193] are humans and rats, respectively. For the model calibration, I used data that was measured with an assay using an enzyme from cow mammary glands. Indeed, in ruminants, the termination mechanism is different as it involves both MAT and TE sites of the enzyme, which is not the case in non-ruminants where only the TE site is responsible for termination [195, 186]. This may explain the enormous difference in k_{cat} . Additionally, with the data from Topolska et al. [59], I could not tell the effective concentration of malonyl-CoA participating in the reaction since the authors reported that there had been decarboxylation of malonyl-CoA into acetyl-CoA. I then assumed that decarboxylation happened before the sample was added to the assay. However, if the decarboxylation occurred during the reactions, my model does not fully represent the *in vitro* assay. Indeed, the decarboxylation reaction would be missing.

I also coarse-grained the elongation reactions as multi-substrate irreversible mass action kinetics. Notably, for the irreversibility of the formation of $EC2i$, $i = 1, 2 \dots 9$, this is only valid if the rate of the backward reaction is negligible compared to k_{cat} of each enzymatic site participating in the elongation steps. As I could not verify this assumption given that there is no reliable data, I consider it to be the case as the channeling intends to make the elongation process more efficient (presumably by lowering K_m). Moreover, when fitting the model to the data, I limited the parameterization space to the hypercube of edge 1 based on the ratio k_{cat}/K_m of enzymes coming from human and rat sources. It would be interesting to extend the parameterization space of the model despite the presence of many local minima. It will also be interesting further to investigate the dynamics of production of $C14:0$ produced by my model as it does not align with the dynamics of $C16:0$ and $C18:0$. It would also be interesting to include the competition of acetyl-CoA and malonyl-CoA for the MAT site of the enzyme.

General conclusion

Fatty acids (FA) constitute the cornerstone of cellular energy metabolism, playing a central role beyond simple energy storage. As fundamental components of complex lipids, they form the structural backbone of cell membranes and organelles, influencing membrane fluidity, signaling pathways, and cellular compartments' functional integrity. The synthesis of hormones and signaling molecules further highlights the versatility of FAs, illustrating their importance in maintaining physiological homeostasis and facilitating cellular communication. Recent scientific advances have shed light on the dual nature of FAs, highlighting their contribution to both health and disease. Notably, research has begun to elucidate the complex relationship between FAs and tumorigenesis, with evidence suggesting that alterations in fatty acid metabolism may promote cancer progression [196]. This growing area of study illustrates the critical balance maintained by FA metabolism in cellular processes and the potential consequences of its dysregulation.

Among the spectrum of metabolic disorders associated with FA metabolism, mitochondrial fatty acid oxidation disorders (mFAODs) represent a significant clinical challenge [9, 12, 14]. Characterized by an inability to oxidize fatty acids in mitochondria adequately, mFAODs disrupt the delicate balance of energy production and storage, leading to a range of pathological conditions. The manifestation of mFAODs, often observed in infants, can lead to severe outcomes, including metabolic crises and sudden infant death [24, 63, 22]. The heterogeneity of these disorders, as noted in seminal works by researchers such as Derks et al. [197], Sanders and Griffin [198], complicates the affected individuals' diagnosis, understanding, and treatment. Despite the heterogeneity in the specific case of medium-chain acyl-coenzyme A dehydrogenase (MCAD) deficiency, a typical pattern observed is the high increase of the liver triglycerides concentration [5]. This observation underlines the complexity of the pathophysiology of mFAODs and suggests considering both the synthesis and oxidation pathways while investigating them. Furthermore, innovative approaches are needed to decipher the intricate web of metabolic pathways involved. In this regard, mathematical modeling emerges as a powerful tool, enabling the exploration of metabolic interactions and responses to various perturbations that are challenging, if not impossible, to investigate experimentally. Through computational models, hypotheses can be rigorously tested, and underlying mechanisms of complex biochemical processes can be unveiled. This thesis, therefore, relies on mathematical modeling to

improve the understanding of FA metabolism in the liver, with the ultimate goal of elucidating and understanding the dynamics of mFAODs.

The research questions at the heart of this thesis aim to shed light on critical aspects of FA metabolism in the context of mFAODs:

1. Which metabolic routes lead to the disruption of triglyceride distribution in the liver in the context of MCAD deficiency?
2. What is the magnitude of the shift in steady-state concentration values of key metabolites (acetyl-CoA, malonyl-CoA, and FAs) in MCAD deficiency?

Addressing these questions represents a significant step towards a comprehensive understanding of FA metabolism's role in health and disease. By dissecting the metabolic routes implicated in mFAODs and quantifying shifts in key metabolite concentrations, this work seeks to contribute valuable insights into the mechanisms underlying these disorders and pave the way for novel therapeutic strategies.

Addressing the research questions

The core objective of this thesis was to delve into the complexities of FA metabolism, focusing on providing comprehensive tools to investigate mFAODs via mathematical modeling. This approach is a significant step towards addressing two pivotal research questions: what are the metabolic pathways that lead to the disruption of triglyceride distribution in the liver, particularly in the context of MCAD deficiency, and quantifying the shifts in the steady-state concentration values of key metabolites.

Development of mathematical models The first significant step towards answering these questions was the development of a minimal coarse-grained model of FA metabolism that includes the key involved metabolites, namely acetyl-CoA, malonyl-CoA, FAs, and triglycerides (see Chapter 4). The model is an ordinary differential equation model, where the rates of reactions are based on enzyme kinetic rate laws, notably Michaelis-Menten and non-competitive inhibition rate laws. The model qualitatively explores the synthesis and degradation of FA via bi-stability analysis. This model aims to understand how the transition between fatty acid synthesis and degradation occurs in the liver, thereby elucidating the metabolic flexibility required to maintain energy homeostasis. By establishing the necessary and sufficient conditions for the system to exhibit bi-stability and highlighting the crucial role FA pools play in guaranteeing bi-stability, the model provides a theoretical basis for the robustness of cellular metabolism in the face of fluctuations in energy demand and supply. Furthermore, the creation of a semi-mechanistic model for the elongation part of fatty acid *de novo* synthesis (FADNS) (see Chapter 5) marks a considerable contribution to the field.

This model simplifies the complex enzymatic processes involved in FADNS, reducing the complex mechanism to four processes: initiation, cyclic elongation, termination, and inhibition. Despite its simplified nature, the model reproduces the time course of FA synthesis and can be incorporated into a larger modeling framework to inform critical aspects of cellular metabolism that have been less explored in the context of mFAODs.

Insights Gained and Their Implications Through rigorous analysis, these models have provided valuable insights that can be used to understand metabolic disturbances associated with mFAODs. The bi-stability model, in particular, suggests that the liver possesses inherent mechanisms to switch between anabolic and catabolic states, a flexibility guaranteed by the use of FAs for non-energetic purposes. Furthermore, the analysis of unstable steady states showed that it is impossible to have an unstable node, suggesting that not all metabolites may be simultaneously out of steady state. This finding has profound implications for understanding the pathophysiology of mFAODs and suggests new avenues for therapeutic intervention.

The semi-mechanistic FADNS model further contributes globally in the field of lipid metabolism, as it can be used to assess how alterations in FADNS affects the overall dynamics of fatty acid synthesis. Moreover, its incorporation into a larger model of FA metabolism will help in answering the original research questions. By fitting the model to experimental data and comparing the parameters to literature values, I have begun to offer a tool to analyze and comprehend the shifts in metabolite concentrations that characterize MCAD deficiency.

In summary, the mathematical models developed in this thesis represent a significant step towards answering the research questions posed at the outset. By elucidating the conditions that lead to bi-stability in FA metabolism and modeling the complexities of FADNS, this work advances our theoretical understanding of FA metabolism's role in health and disease. These findings not only contribute to the scientific community's knowledge base but also open up new possibilities for diagnosing and treating mFAODs, moving us closer to the ultimate goal of mitigating the impact of these disorders on affected individuals.

Limitations of this work

Chapter 4's model, developed to elucidate aspects of FA metabolism through a coarse-grained approach, inherently simplifies the complex biochemical landscape of fatty acid metabolism. While this simplification facilitates analysis, it may also obscure critical enzymatic mechanisms and regulatory interactions integral to FA metabolism, such as feedforward and feedback loops. A notable omission is the model's disregard for the role of citrate, a known enhancer of acetyl-CoA carboxylase activity, which is pivotal in the synthesis of malonyl-CoA, a key intermediate in fatty acid synthesis. Including citrate could lead to more complex dynamics like limit cycles or hysteresis. Moreover, the

assumption of constant influxes and concentration-proportional effluxes oversimplifies the reality of hormonal regulation, which can significantly alter these rates in response to physiological needs. The qualitative nature of the model's analysis limits its ability to validate and accurately characterize the system's steady states, underscoring the need for quantitative analysis to understand FA metabolism dynamics better.

Regarding the semi-mechanistic model of FADNS (Chapter 5), it abstracts the complexity of fatty acid synthase (FAS) function, simplifying complex processes such as increases in binding affinity and substrate specificity. Critical aspects like the order in which substrates bind to each enzymatic site, ionization, and the mechanistic role of the acyl carrier protein (ACP), essential for channeling substrates through the enzymatic process, are not sufficiently accounted for by the model. This limitation is partly due to the lack of kinetic data on ACP and the challenge of over-parameterization, which could compromise the model's tractability and interpretability. The model does not faithfully reproduce the $C_{14}:0$ dynamics, suggesting that some assumptions deserve reevaluation. However, I believe this discrepancy might be due to the non-consideration of the production of shorter chains and their fluxes towards the production $C_{14}:0$, explaining the overshooting observed in the fitting. Discrepancies between the kinetic parameters derived from the model and those reported in the literature could be attributed to differences in enzyme sources (bovine vs. human/rat) and the uncertainty of the malonyl-CoA concentration from which the model parameterization is constructed. This last point highlights the critical need to develop an experimental pipeline that measures the kinetic parameters under various conditions while providing time-course data. A significant effort should also be put into measuring the kinetics of each enzymatic site of FAS, considering the detailed enzymatic mechanism.

Recommendations for future work

Enhancing model complexity and integrating regulatory networks Future research should focus on incorporating detailed enzymatic mechanisms and comprehensive regulatory networks into the models of FA metabolism. The bi-stability model entails integrating the role of citrate and other allosteric regulators that significantly influence enzyme activities, such as acetyl-CoA carboxylase. Expanding the model to include hormonal regulation of influxes and effluxes will provide a more physiologically relevant representation of FA metabolism dynamics. Similarly, the semi-mechanistic model of FADNS could be significantly improved by incorporating the specificity of fatty acid synthase (FAS) binding sites and the mechanism of the acyl carrier protein (ACP), despite the current limitations due to data scarcity.

Quantitative analysis and experimental validation Transitioning from qualitative to quantitative analysis is imperative for the bi-stability model to validate its predictions and accurately

characterize metabolic states. Establishing collaborations with experimental laboratories to gather comprehensive kinetic data and perform detailed validations of the models under various physiological and pathological conditions will enhance the models' applicability and reliability. For the semi-mechanistic model of FADNS, as mentioned before, developing experimental pipelines that measure kinetic parameters across different conditions, including time-course data, will address the current discrepancies in kinetic parameters and improve model fidelity.

Broadening the scope of models To address the limitations related to model scope and generalizability, future models should aim to cover a broader spectrum of FA metabolism, potentially including other metabolic pathways and tissue-specific metabolic processes. This expansion would provide a more holistic view of FA metabolism and cater to the diverse phenotypes observed in mFAODs. Developing models that can account for the variability in enzyme kinetics between different species and tissues (e.g., bovine versus human) will be crucial for understanding the species-specific aspects of FA metabolism.

The path forward for FA metabolism and mFAODs research is challenging and promising. By addressing the outlined limitations through enhanced model complexity, rigorous experimental validation, and interdisciplinary collaborations, future work can build on the foundational insights provided by this thesis. The ultimate goal is to develop predictive models that advance our understanding of FA metabolism's underlying mechanisms and contribute to developing novel therapeutic strategies for metabolic disorders.

Contributions of this work

Novel insights into bi-stability in FA metabolism in the liver One of the key contributions of this thesis is the development and analysis of a minimal model that highlights the bi-stability in FA metabolism. This model advances our understanding by proposing a theoretical framework for how the liver may switch between synthesis and degradation of FA. By identifying conditions under which bi-stability occurs, this work contributes a novel perspective on the metabolic flexibility required for energy homeostasis and its potential dysregulation in mFAODs. This insight opens new avenues for researching metabolic disorders, suggesting that targeting the mechanisms underlying metabolic switching could offer therapeutic potential.

Advancing the modeling of FADNS The semi-mechanistic model of the elongation part of fatty acid *de novo* synthesis (FADNS) represents another significant contribution of this thesis. Indeed, to my knowledge, this is the first detailed model of FADNS. By abstracting the complex enzymatic processes involved in FADNS into a more tractable form, this model provides valuable insights into the dynamics of FA synthesis. Despite simplifications, it offers a foundation for

understanding the elongation phase of FADNS. This contribution is particularly relevant for studying disorders like mFAODs, as it can be integrated into a detailed FA metabolism model.

Bridging theoretical modeling with experimental validation Although faced with limitations regarding experimental data availability and model simplifications, this thesis work has laid the groundwork for integrating theoretical models with experimental validation. By fitting the semi-mechanistic model of FADNS to available experimental data and discussing the discrepancies and challenges encountered, this work underscores the importance of a collaborative approach between computational and experimental researchers. This contribution highlights the potential for mathematical models to predict and interpret complex biological phenomena and the necessity for rigorous validation to refine these models further.

Implications for understanding and treating mFAODs By offering new theoretical tools to explore the metabolic underpinnings of these disorders, this work paves the way for future research to identify therapeutic targets and strategies to mitigate the effects of mFAODs on affected individuals.

In addition to the advancements made through mathematical modeling, a significant portion of my research entailed conducting a comprehensive review of the kinetics of enzymes involved in fatty acid synthesis. This review served a dual purpose: firstly, to consolidate the state of the art, providing a thorough overview of current understanding and methodologies in enzyme kinetics within FA metabolism, and secondly, to critically identify and highlight the gaps in the literature where data is sparse or conflicting. By mapping out these gaps, my work points to areas needing further experimental investigation and contextualizes the contributions of my modeling efforts against the backdrop of these identified gaps.

In conclusion, this thesis represents a meaningful advancement in the study of FA metabolism, providing novel theoretical insights and a platform for future experimental and computational research. The development of models that elucidate bi-stability in FA metabolism and the dynamics of FADNS offers new perspectives on regulating energy metabolism and its dysregulation in disease states. By bridging gaps in our current understanding and highlighting areas for further investigation, this work contributes significantly to metabolic research. It opens up new possibilities for understanding and treating metabolic disorders.

Appendix

Summary of the Kinetic of enzymes of FA synthesis

Table A1: Kinetic rate laws corresponding to the parameters reported in the Tables A2, A3, A6, A7, and A8.

Enzyme	Rate law	Formula	Parameters	Reference
ACC	Competitive inhibition and activation	$\frac{V_{max} \times S}{K_m \left(1 + \frac{I}{K_i}\right) + S \left(1 + \frac{K_a}{A}\right)}$	Table A2	[149]
ACC ELOVL Δ -9 Δ -5 Δ -6	Michaelis-Menten kinetics	$\frac{k_{cat} \times E_0 \times S}{K_m + S} = \frac{V_{max} \times S}{K_m + S}$	Table A2, A3, A6, A7, A8	[91], [143], [154], [193], [157], [118], [158], [167],[160], [161], [163], [166], [165]
FAS		$\frac{k_{cat} \times E_0}{1 + \frac{K_{M_{Mal}}}{Mal} \left(1 + \frac{Acet}{K_{I_{Acet}}}\right) + \frac{K_{M_{Acet}}}{Acet} \left(1 + \frac{Mal}{K_{I_{Mal}}}\right) + \frac{K_{M_{NADPH}}}{NADPH}}$	Table A3	[36]

Table A2: **Kinetic parameters of ACC iso-enzymes.** Cells are empty when the parameter values were either not measured or not considered in the rate laws. The meaning of each symbol is defined in the List of Symbols.

Acetyl-CoA carboxylase												
Organism /Source	Substrate	Activator	Inhibitor	K_m	k_{cat}	K_a	K_i	pH	Temperature	Measurement approach	Remarks	Reference
Rat hindlimb muscle	Acetyl-CoA	Citrate	Malonyl-CoA	$31.7 \pm 1.5 \mu M$		$2.13 \pm 0.05 mM$	$10.6 \pm 1 \mu M$	7.5	37°C	^{14}C -labeled $KHCO_3$ radioactivity-based assay; the kinetic parameters were measured by using the Lineweaver-Burk plot method	Purified enzyme Unknown isoform	[149]
	ATP		$57.6 \pm 0.9 \mu M$	$2.2 \pm 0.3 \mu M$								
	$KHCO_3$		$2.25 \pm 0.1 mM$									
Rat adipose tissue	Acetyl-CoA	Citrate		$21.5 \pm 1 \mu M$		$3.02 \pm 0.12 mM$		7.5	37°C			
	ATP			$106.5 \pm 2.6 \mu M$								
	$KHCO_3$			$2.73 \pm 0.29 mM$								
Human ACC1	Acetyl-CoA			$34 \pm 4 \mu M$	$10.1 \pm 1.2 s^{-1}$			7.5	37°C		Purified recombinant enzyme expressed in baculovirus; the ACC2 lacks the N-terminal 148 aa region; the malonyl-CoA exerts a competitive inhibition	[91]
	ATP			$161 \pm 31 \mu M$								
	$NaHCO_3$			$12.8 \pm 0.7 mM$								
Human ACC2	Acetyl-CoA			$58 \pm 17 \mu M$	$11.8 \pm 3.8 s^{-1}$			7.5	37°C	^{14}C -labeled $NaHCO_3$ radioactivity-based assay; the kinetic parameters were measured by non-linear regression fitting to Michaelis-Menten equations		
	ATP			$120 \pm 15 \mu M$								
	$NaHCO_3$			$3.0 \pm 0.8 mM$								
Rat ACC2	Acetyl-CoA			$37 \pm 12 \mu M$	$11.6 \pm 2.4 s^{-1}$			7.5	37°C			
	ATP			$147 \pm 13 \mu M$								
	$NaHCO_3$			$5.1 \pm 0.3 mM$								
Human ACC2 (27-2458)	Acetyl-CoA			$2 \pm 0.2 \mu M$	$11.5 \pm 2.0 min^{-1}$			7.5	25°C	^{14}C -labeled acetyl-CoA radioactivity-based assay; the kinetic parameters were measured by fitting data to Michaelis-Menten equation	The enzyme is expressed in the baculovirus; the ACC2 are truncated (lacking 1-148 aa), or N-terminal 275 aa is replaced with the ACC1 region (1-33 aa)	[143]
	ATP			$52.3 \pm 4.4 \mu M$	$9.3 \pm 2.0 min^{-1}$							
Human ACC2 (21-2458)	Acetyl-CoA			$2.6 \pm 0.8 \mu M$	$17.8 \pm 1.6 min^{-1}$			7.5	25°C			
	ATP			$43.7 \pm 3.5 \mu M$	$13.7 \pm 0.5 min^{-1}$							

Table A3: **Kinetic parameters of FAS.** Cells are empty when the parameter values were either not measured or not considered in the rate laws. The meaning of each symbol is defined in the List of Symbols.

FAS & Active sites																	
Organism/Source	Substrate	Activator	Inhibitor	K_m	k_{cat}	K_i	K_i	pH	Temperature	Measurement approach	Remarks	Reference					
Chicken Liver (full enzyme)	Acetyl-CoA	CoA	Malonyl-CoA	0.2 μM	$10.4 \pm 0.7 s^{-1}$		1.2 μM	5.90	25°C	Spectrophotometry-based assay by following the reduction of NADPH absorbance	Purified enzyme: although it was shown that the free CoA at low concentration activates the enzyme and at high concentration inhibits the enzyme, the value of the corresponding constants are not reported, the reported parameters correspond to the formation of 16:0	[36]					
	Malonyl-CoA		Acetyl-CoA	$1.7 \pm 0.3 \mu M$			$6.0 \pm 1.3 \mu M$										
	NADPH			$2.0 \pm 0.8 \mu M$													
	Acetyl-CoA		Malonyl-CoA	0.25	$10.4 \pm 0.7 s^{-1}$		1.9 μM	6.56									
	Malonyl-CoA		Acetyl-CoA	$1.6 \pm 0.4 \mu M$			$5.0 \pm 1.3 \mu M$										
	NADPH																
	Acetyl-CoA		Malonyl-CoA	0.72 ± 0.17	$23.0 \pm 0.7 s^{-1}$		$3.1 \pm 0.8 \mu M$	7.0									
	Malonyl-CoA		Acetyl-CoA	2.5 ± 0.8			$5.4 \pm 0.6 \mu M$										
	NADPH			$2.9 \pm 0.4 \mu M$													
	Acetyl-CoA		Malonyl-CoA	$0.85 \pm 0.27 \mu M$	$17.0 \pm 0.9 s^{-1}$		$4.0 \pm 0.4 \mu M$	7.49									
	Malonyl-CoA		Acetyl-CoA	$4.3 \pm 0.6 \mu M$			$10.4 \pm 1.5 \mu M$										
	NADPH																
	Acetyl-CoA		Malonyl-CoA	$1.9 \pm 0.5 \mu M$	$11.0 \pm 1.0 s^{-1}$		$16.3 \pm 11 \mu M$	8.0									
	Malonyl-CoA		Acetyl-CoA	$5.7 \pm 1.0 \mu M$			$16.9 \pm 3.2 \mu M$										
	NADPH			$3.5 \pm 0.8 \mu M$													
Acetyl-CoA	Malonyl-CoA	$2.9 \pm 0.4 \mu M$	$4.0 \pm 0.2 s^{-1}$		$60.0 \pm 30 \mu M$	8.60											
Malonyl-CoA	Acetyl-CoA	$5.5 \pm 0.9 \mu M$			$19.0 \pm 4.5 \mu M$												
NADPH		$5.0 \pm 0.6 \mu M$															
Human (full enzyme)	Acetyl-CoA			$7 \pm 3 \mu M$	$2.7 \pm 0.25 s^{-1}$			7.0	25°C	Spectrophotometry-based assay by following the reduction of NADPH absorbance	Purified enzyme expressed in the baculovirus	[154]					
	Malonyl-CoA			$6 \pm 2 \mu M$													
	NADPH			$5 \pm 1 \mu M$													
β -ketoacyl reductase site (human)	Acetoacetyl-CoA			$10 \pm 2 \mu M$	$4 \pm 0.2 s^{-1}$												
	NADPH			$4 \pm 2 \mu M$													
β -hydroxyacyl dehydratase site (human)	Crotonyl-CoA (4.0)			$7 \pm 5 \mu M$	$0.1 \pm 0.02 s^{-1}$												
Enoyl-reductase site (human)	Crotonyl-CoA (4.0)			$6 \pm 2 \mu M$	$0.3 \pm 0.03 s^{-1}$												
	NADPH			$3 \pm 2 \mu M$													
Enoyl-reductase site (human)	Octenoyl-CoA (8.0)				$0.05 \pm 0.02 s^{-1}$												
	NADPH			$100 \pm 70 \mu M$													
Enoyl-reductase site (human)	Dodecenoyl-CoA (12.0)			$7 \pm 1 \mu M$	$0.22 \pm 0.08 s^{-1}$												
	NADPH			$540 \pm 300 \mu M$													
Malonyl-acetyl-transferase site (human)	Acetyl-CoA			$3.9 \pm 0.4 \mu M$	$1.9 \pm 0.06 s^{-1}$								6.8	0°C	Radioactivity-based assay combined with liquid chromatography using either ^{14}C -labeled acetyl-CoA or malonyl-CoA	Purified enzyme expressed in <i>Escherichia coli</i>	[193]
Malonyl-acetyl-transferase site (rat liver)	Malonyl-CoA			$1.9 \pm 0.23 \mu M$	$1.2 \pm 0.008 s^{-1}$												

Table A4: **Summary on biochemistry of elongases.** The symbols "+" and "-" on top of tissues respectively mean highly expressed and poorly expressed in the corresponding tissue. If no sign is indicated, the information could not be retrieved from literature. All acronyms used here are listed in the Abbreviation subsection.

Enzyme	Tissue expression	Substrate type	Substrate chain length	References
ELOVL 1	almost all tissues	SFAs and MUFAs	18 - 26	[102], [111], [199], [200]
ELOVL 2	testis ⁺ , liver ⁺ , brain ⁻ , kidney ⁻ , WAT ⁻ , lung ⁻	essential PUFAs preference for non-essential FAs in mouse	20 - 22	[102], [199], [200], [115], [112]
ELOVL 3	skin sebaceous gland, hair follicles, BAT	SFAs, USFAs	16 - 22	[102], [200], [118], [199]
ELOVL 4	retina, brain, skin, testis ⁺ , prostate ⁺ , ovary, thymus ⁺ , small intestine ⁺	SFAs, ULCFAs	≥ 24	[102], [199]
ELOVL 5	almost all tissues	essential PUFAs	18 - 20	[102]
ELOVL 6	almost all tissues	12:0, 14:0, 16:0, 16:1n7, 18:1n9	12 - 18	[102], [115], [201], [117]
ELOVL 7	brain ⁻ , liver ⁻ , small intestine ⁻ , testis ⁻ , leukocytes ⁻ , placenta ⁻ , colon ⁺ , kidney ⁺ , prostate ⁺ , pancreas ⁺ , adrenal glands ⁺	16:0, 18:0, 20:0, 18:1n9, 18:3n6 preference for non-essential FAs	16 - 20	[102], [202], [118]

Table A5: **Summary on biochemistry of desaturases.** In the isoforms column, *m* and *h* mean present in mice and humans, respectively. In the substrates column, "*" indicates the preferred substrate, while "#" indicates a special case of desaturation. In the column tissue specificity, "+" and "-" indicate that the enzyme is highly or lowly expressed, respectively, while "±" means moderately expressed in the corresponding tissue. In the regulators column, "+" and "-" indicate enzyme activity increase and decrease, respectively. All acronyms used here are listed in the Abbreviation subsection.

Enzyme	Isoforms	Substrates	Tissue specificity	Regulators	Biological function	References
Δ9	SCD1 ^{m,h}	14:0, 16:0, 18:0 *	lipogenic tissues (e.g., liver and adipose tissues)	HCD ⁺ , SFAs ⁺ , insulin ⁺ , estrogen ⁺ , liver X receptors ⁺ PPARα ⁺ , glucagon ⁻ , PUFAs ⁻ , leptin ⁻	desaturate LCSFAs	[120], [123], [125], [129], [130], [131], [132], [133]
	SCD2 ^m		brain, pancreas			[120], [123], [125], [133]
	SCD3 ^m	harderian, sebocytes, preputial glands	[120], [123], [125], [134]			
	SCD4 ^m	heart	[120], [123], [125], [132]			
	SCD5 ^h	brain, pancreas	[120], [123], [125], [133]			
Δ6	FASD1	16:0#, 18:2n-6, 18:3n-3, 24:5n-3	skin ⁺ , liver ⁺ , brain ⁺ , heart [±] , lungs [±] , kidney ⁻ , spleen ⁻ , muscles ⁻	PUFAs ⁺	build HUFAs, build 16:1n7 found in human sebum	[103], [121], [21], [136]
Δ5	FASD2	20:3n-6, 20:4n-3	liver ⁺ , brain ⁺ , heart [±] , lungs [±] , kidney ⁻ , spleen ⁻ , muscles ⁻	PUFAs ⁺	build HUFAs	[103], [121], [21], [136]

Table A6: **Kinetic parameters of elongases.** It is important to recall that the purified microsomes are not the purified enzymes. They contain the four enzymes of the elongation cycle, together with other enzymes that could impact their kinetics. The concentration of each elongation enzyme therefore remains unknown. Cells are empty when the parameter values were either not measured or not considered in the rate laws. The meaning of each symbol is defined in the List of Symbols.

Elongation cycle/ ELOVLs													
Organism/Source	Substrate	Activator	Inhibitor	K_m	V_{max}	K_a	K_i	pH	Temperature	Measurement approach	Remarks	Reference	
Porcine purified microsomes	Malonyl-CoA			32.5 μM	1.6 $nmol \cdot h^{-1} \cdot mg^{-1}$			7.5		Radioactivity-based assay combined with ¹⁴ C labeled malonyl-CoA	Purified microsomes containing all the enzymes responsible for the elongation cycle	[157]	
	16:0-CoA												
	NADPH			9.1 μM	1.2 $nmol \cdot h^{-1} \cdot mg^{-1}$								
Porcine purified microsomes	Malonyl-CoA			12.9 μM	0.8 $nmol \cdot h^{-1} \cdot mg^{-1}$								
	20:0-CoA												
	NADPH			23.8 μM	0.67 $nmol \cdot h^{-1} \cdot mg^{-1}$								
ELOVL7 (human)	Malonyl-CoA			11.7 μM	0.31 $pmol \cdot min^{-1} \cdot \mu g^{-1}$			6.8	37°C	Radioactivity-based assay combined with ¹⁴ C labeled malonyl-CoA	Reconstituted purified enzyme using the proteoliposome-reconstitution system	[118]	
	18:3n-3-CoA			2.6 μM	0.33 $pmol \cdot min^{-1} \cdot \mu g^{-1}$								
ELOVL6 (human)	Malonyl-CoA			6.46 μM	1.03 $pmol \cdot min^{-1} \cdot \mu g^{-1}$			6.8	37°C	Radioactivity-based assay combined with ¹⁴ C labeled malonyl-CoA	Reconstituted purified enzyme using the proteoliposome-reconstitution system	[158]	
	16:0-CoA			1.22 μM	0.79 $pmol \cdot min^{-1} \cdot \mu g^{-1}$								

Table A7: **Kinetic parameters of $\Delta 9$ desaturases.** Cells are empty when the parameter values were either not measured or not considered in the rate laws. The meaning of each symbol is defined in the List of Symbols.

$\Delta 9$ desaturase													
Organism/Source	Substrate	Activator	Inhibitor	K_m	k_{cat}	K_a	K_i	pH	Temperature	Measurement approach	Remarks	Reference	
Rat liver microsomes	C18:0-CoA			10.5 μM				7.4	37°C	2H -labeled C18:0-CoA mass spectrometry approach (RF-MS), Lineweaver-Burk plot	Not the purified enzyme	[167]	
	NADH												
Bovine mammary microsomes	C18:0-CoA			25 μM				7.4	30°C	^{14}C -labeled C18:0-CoA radioactivity-based method, Lineweaver-Burk plot	Not the purified enzyme	[160]	
	NADH			3 μM									
Rat liver	14-19 carbon chain Acyl-CoAs			4.5 – 5 μM					25°C	Radioactivity-based assay using ^{14}C -labeled substrates	Purified enzyme; The exact names of the Acyl-CoAs are not specified	[161]	

Table A8: **Kinetic parameters of $\Delta 5$ and $\Delta 6$ desaturases.** Cells are empty when the parameter values were either not measured or not considered in the rate laws. The meaning of each symbol is defined in the List of Symbols.

$\Delta 5$ and $\Delta 6$ desaturases													
Organism/Source	Substrate	Activator	Inhibitor	K_m	V_{max}	K_a	K_i	pH	Temperature	Measurement approach	Remarks	Reference	
$\Delta 6$ Human fetal liver	18:2n-6-CoA			6.5 μM	7.5 $pmol \cdot min^{-1} \cdot mg^{-1}$			7.4	37° C	Radioactivity-based assay using ^{14}C -labeled substrates; Lineweaver-Burk plot	Not a purified enzyme; liver microsomes from human fetus	[166]	
	18:3n-3-CoA			24.5 μM	24.4 $pmol \cdot min^{-1} \cdot mg^{-1}$								
$\Delta 5$ Human fetal liver	20:3n-6-CoA			3.91 μM	9.5 $pmol \cdot min^{-1} \cdot mg^{-1}$			7.4	37° C	Radioactivity-based assay using ^{14}C -labeled substrates; Lineweaver-Burk plot	Not a purified enzyme; liver microsomes from human fetus	[166]	
$\Delta 5$ rat kidney	20:3n-6-CoA			56 μM	60 $pmol \cdot min^{-1} \cdot mg^{-1}$			7.0	36° C	Radioactivity-based assay using ^{14}C -labeled substrates; Lineweaver-Burk plot	Not a purified enzyme; rat kidney microsomes	[165]	
$\Delta 6$ rat liver	18:2n-6-CoA			45 μM	83 $nmol \cdot min^{-1} \cdot mg^{-1}$			7.2	30° C	Radioactivity-based assay using ^{14}C -labeled substrates; Lineweaver-Burk plot	Purified enzyme	[163]	

Thermodynamics of the reactions of FADNS estimate with eQuilibrator

Base on this calculations of the thermodynamic of the reactions of FADNS, it clearly shows that the overall reactions are thermodynamically favorable. This justify the choice of modeling this elongation reactions irreversible.

- Acetyl-CoA(aq) + 6 Malonyl-CoA(aq) + 12 NADH(aq) + H₂O(l) \rightleftharpoons 12 NAD(aq) + 7 CoA(aq) + Myristic acid(aq) + 6 CO₂(total)

$$\text{Estimated } \Delta_r G'^m = -519.1 \pm 27.9 [kJ/mol]$$

$$\text{Estimated } \Delta_r G'^\circ = -399.3 \pm 27.9 [kJ/mol]$$

$$K'_{eq} = 9.8 \times 10^{69}$$

$$pH = 7.5$$

$$pMg = 3.0$$

$$\text{Ionic strength} = 0.25M$$

- Acetyl-CoA(aq) + 7 Malonyl-CoA(aq) + 14 NADH(aq) + H₂O(l) \rightleftharpoons 14 NAD(aq) + 8

CoA(aq) + Palmitate(aq) + 7 CO₂(total)

Estimated $\Delta_r G'_m = -601.4 \pm 31.3 [kJ/mol]$

Estimated $\Delta_r G'^{\circ} = -464.4 \pm 31.3 [kJ/mol]$

$K'_{eq} = 2.6 \times 10^{81}$

pH = 7.5

pMg = 3.0

Ionic strength = 0.25M

List of figures

1.1	Summary of energy homeostasis of the body: The liver's vital function is emphasized, as it degrades internal and peripheral organ-derived molecules during fasting to supply other organs with the necessary nutrients. Conversely, during the fed state, the liver converts and stores macronutrients in the peripheral organs. . .	2
1.2	Example of structural formula of saturated and unsaturated FAs	5
1.3	Summary of mitochondrial β-oxidation reactions in rodents: the purple square boxes represent the enzymes of the carnitine shuttle system, while the green square boxes represent the enzymes of the β -oxidation cycle. (Adapted from [5]) .	6
1.4	Mechanism of Δ^3, Δ^2-enoyl-CoA Isomerase: The enzyme relocates the double bond from between carbons 3 and 4 to between carbons 2 and 3. (Adapted from https://www.slideserve.com/hang/lecture-notes-for-chapter-17-lipid-metabolism) .	7
2.1	Basic description of an enzyme (Adapted from "Enzymes, Substrates, and Inhibitors", by BioRender.com (2022). Retrieved from https://app.biorender.com/biorender-templates)	24
2.2	Michaelis-Menten kinetics curve	26
2.3	How to extract the parameter of Michaelis-Menten equation using Lineweaver-Burk plot	26
2.4	Different type of inhibition (Adapted from "Enzymes, Substrates, and Inhibitors", by BioRender.com (2022). Retrieved from https://app.biorender.com/biorender-templates)	27
2.5	Fitting result with <code>lmfit</code> library	34
2.6	Sobol sampling vs. random sampling: In the left panel, we have a Sobol sample of 256 points couples of points (θ_1, θ_2) between 0 and 1, and the right panel random sample of 256 couples of points (θ_1, θ_2) between 0 and 1. The Sobol sample is evenly distributed in the sample space, whereas the random sample does not uniformly cover the sample space uniformly.	41
2.7	Scheme and time course of a linear open system made of two compounds and three reactions	42

- 2.8 **Sobol's sensitivity analysis for the linear model with two compounds:** As expected, k_1 and k_2 are the only parameters controlling the variance of the compound A , whereas k_3 exclusively control the variance of B 42
- 2.9 **Scheme and time course of a branched open system made of four compounds and seven reactions** 43
- 2.10 **Sobol's sensitivity analysis for the branched open model with four compounds:** By looking at the total indices, one can note that k_1 has a substantial control on the concentrations of all compounds. The other parameters have less global influences, although their effect on the concentration of a particular compound can be more considerable, as shown by the first-order, second-order, and total indices. 43
- 3.1 **Schematic representation of the biochemistry of fatty acid biosynthesis.**
 The process is organized in two main parts. Enzymes involved in the fatty acid *de novo* synthesis (FAS and ACC1) are color-coded with a gray background. They are responsible for the production of long chain saturated fatty acids (LCSFAs). This process takes place in the cytoplasm. Enzymes involved in the microsomal modifications of fatty acids (ELOVLs, Δ -desaturases) are color-coded with a black background. They are responsible for elongating and desaturating long-chain fatty acids (LCFAs) and very long-chain fatty acids (VLCFAs). This process takes place in the endoplasmic reticulum (ER) where these enzymes are membrane-bound. In the ER, LCFAs and VLCFAs, represented in the figure, include long-chain saturated fatty acids (LCSFAs), mono-unsaturated FAs (MUFAs), and poly-unsaturated FAs (PUFAs). The β -oxidation that takes place in the mitochondria is not part of fatty acid synthesis. Still, it is represented because it influences the overall synthesis process. 45
- 4.1 **Illustration of interactions among key metabolites in lipid homeostasis:**
 Square boxes denote the concentrations of distinct metabolites of the system, while triangular-shaped arrows signify reaction fluxes. Reaction fluxes associated with FA synthesis are color-coded in blue, whereas those involved in FA degradation are depicted in black. Circular arrowheads do not represent fluxes but instead indicate inhibition of the target reaction by the originating metabolite. For instance, malonyl-CoA suppresses the flux from the FA pool to acetyl-CoA. V_{ini} and V_{outi} (where $i \in \{1, 2, 3\}$) signify the respective influxes and outfluxes of the attached metabolites. 59
- 4.2 Illustration of the scenario where one could have three positive values of S_3^* at the steady-state. 67
- 4.3 **Conditions for the Jacobian matrix J_k to have three negative eigenvalues.** 73

4.4	Analysis of the scenario where $\Gamma'_k(\lambda)$ has two turning points.	73
4.5	Illustration of the conditions for $\Gamma_k(\lambda)$ to have four roots.	77
4.6	Illustration of the case where $\Gamma_k(\lambda)$ has four distinct roots (three negative and one positive), and all its turning points are negative.	77
4.7	Illustration of the curves of the first (left) and second (right) derivatives ensuring that $\Gamma_k(\lambda)$ has four distinct roots (three negative and one positive), and all its turning points are negative.	78
4.8	Illustration of a case where $\Gamma_k(\lambda)$ has four distinct roots (including three negative ones). Among the three turning points, two are negative, and one is positive.	79
4.9	Sub-case 1: x'_{k_1} and x'_{k_2} are both negative and B_k is positive.	80
4.10	Sub-case 2: x'_{k_1} is negative, x'_{k_2} positive, and B_k negative.	81
5.1	Detailed reactions of FADNS: The seven enzymatic site of FAS are represented, notably the malonylacetyltransferase(MAT) (Reprinted (adapted) with permission from [186]. Copyright 2019 ChemBioChem)	88
5.2	Fold Changes in the TG Profile in MCAD Knockout and Wild-Type Mice: The fold in this context is defined as the ratio between the mean TG concentration in MCAD knockout mice and that of the wild-type mice. A simple approach to describe the TG is by considering the total number of carbons and the number of double bonds in the FAs attached to the glycerol backbone. Using this description, I calculated the ratio between the means of each type of TG in MCAD knockout mice and the wild type. An overall increase in each type TG is noticeable. Moreover, these changes exhibit a positive correlation with the number of double bonds and a negative correlation with the number of carbons. It is notable that some TGs, such as 48:8 and 42:4, exhibit fold changes of 24 and 17, respectively. (The data were extracted from Chapter 4 [5].)	90
5.3	Scheme of the model without CoA inhibition: the reactions are color coded with red, black and blue, representing the initialization, the cyclic elongation, and termination steps, respectively.	93
5.4	Scheme of the model without CoA inhibition: the reactions are color coded with red, black, blue, and orange representing the initialization, the cyclic elongation, termination steps, and the inhibition by the free CoA, respectively.	96
5.5	Extracted data from the work by Topolska et al. [59]	98

- 5.6 Behavior of the fluxes of the vanilla model during the first 200 milliseconds:** in panels a and b, one can observe the effect of the rapid binding as the associated fluxes peak and decrease toward quasi-steady-state fluxes. Panel c shows the slow binding as the maximum production flux of *EC18* is lower than the other cyclic elongation fluxes. Panel d, the flux of production of *C14:0* increases rapidly and drops exponentially due to high flux toward the production *EC16*. Panels e and f show the rise in the production fluxes of *C16:0*, and *C18:0*, respectively. 101
- 5.7 Time course of the vanilla model during the first 200s milliseconds:** panels a, b, and c show the consumption of three substrates resulting from rapid binding. From panels d, e and f, it can be seen that almost all enzyme species are rapidly converted to *EC16*. *EC18* is the smallest enzyme species in the system. Panels g, h, and i show FADNS products. One can see that the *C16:0* is the main product of the channel. 101
- 5.8 Behavior of the fluxes of the vanilla model after 5 seconds :** The elongation fluxes associated with rapid binding reactions (panels a and b) are quasi-constant after half of a second, as well as the rate of production of *C14:0* (panel d). The rate of production *C16:0* (panel e) sharply increases and remains quasi-constant. The production rate of *C18:0* has reached its maximum after 2.5 seconds and decreases due to slow production of *EC18*. 103
- 5.9 Time course vanilla model after 5 seconds:** panels display the initial phase dynamics. Panels a,b, and c show the linear consumption of the substrate except for the sharp drop for the first milliseconds as a result of rapid binding. Panels d, e, and f show that almost all the enzyme species are converted to *EC16* and are at quasi-steady-state except the *EC18*. Panels g, h, and i display the linear formation of the products, with *C16:0* being the major one. 103
- 5.10 Behavior of the fluxes of the vanilla model for long-run simulations:** Panel a displays the flux of production of *C14:0*. The first peak corresponds to the initial formation of the complex *EC14*, which then drops as a result of the large flux towards the production of *EC16*. The second peak occurs due to malonyl-CoA depletion, favoring the release of *C14:0*. Panel b shows a quasi-constant flux in the production of *C16:0* after the initial formation of *EC16*, with the flux dropping upon malonyl-CoA depletion. Panel c illustrates the progressive decline in the production of *C18:0* following the initial formation of *EC18*. 105

- 5.11 **Time course of the vanilla model for long-run simulation:** Panels a, b, c, h, and i display the linear consumption of substrates and the linear formation of products until malonyl-CoA depletion. After the total consumption of malonyl-CoA, occurring around 20 seconds, the concentration of the enzyme is distributed among enzyme-substrate complexes with chain lengths of 12 carbons or less (panel d). Panels e and f illustrate the dynamics of the $EC16$ and $EC18$ complexes. Notably, for $EC16$, a quasi-steady state is observed, followed by a drop due to malonyl-CoA depletion. $EC18$ is slowly converted into $C18:0$ as malonyl-CoA depletes. Panel g shows the dynamics of the production of $C14:0$ 105
- 5.12 **Fluxes of the vanilla model after CoA inhibition being added :** Panel a and b show how the flux of cyclic elongation associated with the rapid binding display almost the same dynamics as in the case without CoA inhibition, but slightly less as result of the inhibition. Panel c shows the same trends as without inhibition for the flux $V_{EC16 \rightarrow EC18}$. One can observe the double peaks in the flux of CoA inhibition. The first peak corresponds to the first binding of the free CoA to the enzyme. The backward reaction could explain the drop after the first peak as the concentration of CoA is still low. The second increase following the drop results from the progressive production of the CoA . The CoA inhibition corrects the flux of production $C14:0$ as one can observe only one peak instead of two as before the inclusion of the inhibition (panel d). The flux of production $C16:0$ starts dropping earlier as compared to before I added the inhibition (panel e). This progressive drop can be explained by the progressive increase of the $ECoA$, resulting in a decrease of $EC16$. The flux of production of $C18:0$ is almost unaffected by the inhibition. 107
- 5.13 **Time course of vanilla model after CoA inhibition being added:** In panel a, b, and c, one can see that the consumption of substrates decay with time as the CoA becomes important in the system. the same trends can be observed with the production of $C14:0$, $C16:0$ and $C18:0$ in the panels g, h and i, respectively. Panels d, e, and f show progressive decay of the enzyme-substrate complexes as the $ECoA$ complex takes over. The reaction becomes very slow once all the enzyme species are almost converted to $ECoA$ 108
- 5.14 **Determination of sample size for Sobol's sensitivity analysis:** Panels A and B illustrate the variation of the first-order Sobol's indices and the total indices, respectively, with sample size for $C14:0$. Panels C and D show the variation of the first-order Sobol's indices and the total indices, respectively, with sample size for $C16:0$. Panels E and F depict the variation of the first-order Sobol's indices and the total indices, respectively, with sample size for $C18:0$ 109

- 5.15 **First-Order and Total Indices for the model without inhibition:** The first-order and total Sobol's indices highlight the significant influence of the parameters κ and δ on the model's output. The total indices also reveal the relatively minor impacts of k_{d6} and k_{d7} . Notably, k_{d8} exclusively affects the dynamics of $C18:0$. The parameter β shows negligible influence on the model output. 110
- 5.16 **Second order indices for the model without inhibition:** the interaction of κ and δ control the time course of the output of the model. One can see a slightly negative interaction of the couples (δ, k_{d6}) and (δ, k_{d8}) on the time course of $C16:0$ 111
- 5.17 **First-order and total indices for the model with inhibition by C_{oA} :** one can see the strong control of the parameters κ and δ on the model's output. The total indices show the minor influences of k_{d6} and k_{d7} . k_{d8} only control the dynamic of $C18:0$. β exerts a minor control on the model's output as well as $k_{fC_{oA}}$ and $k_{bC_{oA}}$. 111
- 5.18 **Second order indices for the model without inhibition:** δ negatively interacts with k_{d6} , k_{d6} , $k_{fC_{oA}}$, and $k_{bC_{oA}}$ to control the time courses of $C16:0$ and $C18:0$. 112
- 5.19 **Parameter distribution and the corresponding root-means-square for the model without inhibition:** The pair plots the distribution of parameter values, considering each pair of parameters. The distributions of each parameter taken individually are presented on the diagonal. The color coding corresponds to the value of the RRMSE. The values of κ and δ associated with the smallest RMSE (indicated by blue points and distributions) demonstrate a narrow distribution centered around $0.12 \mu M^{-2} \times s^{-1}$ for κ and $1.3 \times 10^{-6} \mu M^{-1} \times s^{-1}$ for δ . This narrow distribution suggests a higher level of certainty in these parameter estimates. In contrast, parameters such as β , k_{d6} , and k_{d8} exhibit wide distributions even at minimal RMSE, indicating greater variability and less certainty in their optimal values. The graph also reveals that various combinations of these parameters can lead to the same RMSE, highlighting the interdependence of its parameters. 116
- 5.20 **Performance of the model without inhibition on data:** (a), I have a good fit of the initial phase but a poor of the long-run, notably the transient phase. (b), the model fails to reproduce both the initial phase and the long-run. 117
- 5.21 **RMSE as a function of $k_{fC_{oA}}$ and $k_{bC_{oA}}$:** After conducting 1024 fits, approximately 7 local minima were identified based on their RMSE values, with the smallest RMSE being 0.521. The values of $k_{fC_{oA}}$ and $k_{bC_{oA}}$ corresponding to the smallest RMSE occurred more than 900 times (indicated by red points), whereas the other local minima appeared fewer than 10 times (indicated by blue points). The optimal parameter values associated with the smallest RMSE (0.521) are $0.041 \mu M^{-1} \times s^{-1}$ for $k_{fC_{oA}}$ and $2.6 \times 10^{-4} s^{-1}$ for $k_{bC_{oA}}$ 118

- 5.22 **Initial phase fit for the model with inhibition:** Panels a, b, and c show the fit of the initial phase data (RMSE = 0.521, indicative of the dual fitting's accuracy). Panels d, e, and f demonstrate that, despite a slight deviation during the first milliseconds from $C14:0$, the model's rapid binding assumption remains valid, as almost all the enzyme is converted into $EC16$ complex during the initial phase. Panel e further illustrates the inhibition effect, revealing a progressive formation of the $ECoA$ complex within the system. Panels g, h, and i display the substrates' linear consumption and CoA formation, with the rapid binding evidenced by the quick drop of substrates in the first milliseconds. 119
- 5.23 **Fitting the long-run simulation and dynamics of the compounds:** Panel a demonstrates that the model accurately fits the long-run experimental data, with an RMSE of 0.521. Panels b, c, and d illustrate CoA 's progressive sequestration of the enzyme after the initial phase by forming the $ECoA$ complex. Panels e and f reveal slower substrate consumption dynamics compared to the initial phase, highlighting the inhibition by CoA . This is further evidenced by a gradual increase in CoA , which exhibits dynamics opposite to malonyl- CoA consumption. Panels h and i display the production of $C16:0$ and $C18:0$, both quantitatively and qualitatively, consistent with the total fatty acids (FAs) production data. 120
- 5.24 **Description of the initial rate of the reaction:** t stands for the time, S for the concentration of substrate, Δt time interval, ΔS the interval of variation, and v the initial rate. 122
- 5.25 **Fitting my model with Michaelis-Menten rate equations in order to estimate k_{cat} and k_m for acetyl-CoA:** The rates of production of the three FAs as a function of acetyl- CoA by the model can be approximated with Michaelis-Menten rate equations. 123
- 5.26 **Fitting my model with Michaelis-Menten rate equations in order to estimate k_{cat} and k_m for malonyl-CoA:** Only the rate of formation of $C16:0$ can be approximated with Michaelis-Menten rate equations 123
- 5.27 **Fitting my model with Michaelis-Menten rate equations in order to estimate k_{cat} and k_m for NADPH:** Only the rate of production of $C16:0$ can be approximated with Michaelis-Menten rate equations 124

List of tables

4.1	Rate laws with the corresponding parameters: the k_i , $i = 1, 2, 3$ are constants and with the dimension of a rate. α , β , and γ are first order rate kinetic constants. V_i , $i = 1, 2, 3, 4, 5$ are the maximum rate of each reaction. K_{mi} , $i = 1, 2, 3, 4, 5$ are the Michaelis-Menten constants. q_1 and q_4 are the inverse of the inhibition constants. S_i , $i = 1, 2, 3, 4$ are the metabolites of the system.	61
4.2	Summary of the possible number of roots for $P_2(S_3)$ by applying Descartes' rule of signs for positive roots: the highlighted row represents the case where one can have either one positive root or three positive roots. $V_p(P_2)$ is the number of sign-changes in the polynomial $P_2(S_3)$ and $N_p(P_2)$ is the corresponding number of positive roots.	65
4.3	The possible number of negative roots of $\Gamma_k(\lambda)$ by applying Descartes' rule of signs for negative roots: the highlighted represents the scenario of interest. $V_n(\Gamma_k)$ is the number of sign-changes in the polynomial $\Gamma_k(-\lambda)$ and $N_n(\Gamma_k)$ is the corresponding number of negative roots.	72
4.4	The possible number of positive roots of $\Gamma_k(\lambda)$ by applying Descartes' rule of signs for positive roots.	75
4.5	The possible number of positive and negative roots $\Gamma_k(\lambda)$ by applying Descartes' rule of signs	76
5.1	Summary of the different compounds of the two models and their initial concentrations	94
5.2	Kinetic of each reaction of the FADNS for the model without inhibition: The symbol $V_{x \rightarrow y}$ is the transformation rate from x to y . The mathematical formula describing the rate is in the column " Expression ". The units of the parameters appearing in the mathematical formula of the rate are explained in the column " Parameter units ".	95

5.3	Kinetic of each reaction of the FADNS for the model with inhibition by the free CoA: The symbol $V_{x \rightarrow y}$ is the transformation rate from x to y . The mathematical formula describing the rate is in the column " Expression ". The units of the parameters appearing in the mathematical formula of the rate are explained in the column " Parameter units ".	97
5.4	Summary of experimental conditions from Topolska et al. [59] and recalculated initial conditions: The column " Initial concentration " represents the concentrations prior the accounting for malonyl-CoA decarboxylation. The " Recalculated initial concentration " column reflects concentrations adjusted based on initial phase data analysis.	98
5.5	Parameters for the vanilla models	100
5.6	Best parameters for the initial phase fit.	115
5.7	Summary of the parameters resulting from the fit of both initial phase and long-run data.	120
5.8	Summary of conditions for determining k_{cat} and K_m for each substrate. I use the same conditions as in the experimental work of Carlisle-Moore et al. [154]. To determine the kinetics parameter of a given substrate, I first make sure that the others are in excess (saturation of the enzyme) and vary the value of the substrate of interest, the corresponding initial rate is recorded from time course.	121
5.9	Comparison of the parameter of my model to enzyme kinetic parameters existing in the literature.	123
A1	Kinetic rate laws corresponding to the parameters reported in the Tables A2, A3, A6, A7, and A8.	133
A2	Kinetic parameters of ACC iso-enzymes. Cells are empty when the parameter values were either not measured or not considered in the rate laws. The meaning of each symbol is defined in the List of Symbols.	134
A3	Kinetic parameters of FAS. Cells are empty when the parameter values were either not measured or not considered in the rate laws. The meaning of each symbol is defined in the List of Symbols.	135
A4	Summary on biochemistry of elongases. The symbols "+" and "-" on top of tissues respectively mean highly expressed and poorly expressed in the corresponding tissue. If no sign is indicated, the information could not be retrieved from literature. All acronyms used here are listed in the Abbreviation subsection.	136

- A5 **Summary on biochemistry of desaturases.** In the isoforms column, *m* and *h* mean present in mice and humans, respectively. In the substrates column, "*" indicates the preferred substrate, while "#" indicates a special case of desaturation. In the column tissue specificity, "+" and "-" indicate that the enzyme is highly or lowly expressed, respectively, while "±" means moderately expressed in the corresponding tissue. In the regulators column, "+" and "-" indicate enzyme activity increase and decrease, respectively. All acronyms used here are listed in the Abbreviation subsection. 137
- A6 **Kinetic parameters of elongases.** It is important to recall that the purified microsomes are not the purified enzymes. They contain the four enzymes of the elongation cycle, together with other enzymes that could impact their kinetics. The concentration of each elongation enzyme therefore remains unknown. Cells are empty when the parameter values were either not measured or not considered in the rate laws. The meaning of each symbol is defined in the List of Symbols. . . . 137
- A7 **Kinetic parameters of Δ^9 desaturases.** Cells are empty when the parameter values were either not measured or not considered in the rate laws. The meaning of each symbol is defined in the List of Symbols. 138
- A8 **Kinetic parameters of Δ^5 and Δ^6 desaturases.** Cells are empty when the parameter values were either not measured or not considered in the rate laws. The meaning of each symbol is defined in the List of Symbols. 138

References

- [1] John L Tymoczko, Jeremy M Berg, and Lubert Stryer. *Biochemistry: a short course*. Macmillan, 2011.
- [2] Robert C Nordlie, James D Foster, and Alex J Lange. Regulation of glucose production by the liver. *Annual review of nutrition*, 19:379, 1999.
- [3] Hye-Sook Han, Geon Kang, Jun Seok Kim, Byeong Hoon Choi, and Seung-Hoi Koo. Regulation of glucose metabolism from a liver-centric perspective. *Experimental & molecular medicine*, 48(3):e218–e218, 2016.
- [4] Henri A Favre and Warren H Powell. *Nomenclature of organic chemistry: IUPAC recommendations and preferred names 2013*. Royal Society of Chemistry, 2013.
- [5] Anne-Claire Martines. *Exploring the mechanisms underlying the phenotype of MCAD deficiency with Systems Medicine: from computational model to mice to man*. Phd dissertation, University of Groningen, 2019.
- [6] Marc Fransen, Celien Lismont, and Paul Walton. The peroxisome-mitochondria connection: how and why? *International Journal of Molecular Sciences*, 18(6):1126, 2017.
- [7] Eric Soupene and Frans A Kuypers. Mammalian long-chain acyl-coa synthetases. *Experimental biology and medicine*, 233(5):507–521, 2008.
- [8] Peter Schönfeld, Mariusz R Więckowski, Magdalena Lebedzińska, and Lech Wojtczak. Mitochondrial fatty acid oxidation and oxidative stress: lack of reverse electron transfer-associated production of reactive oxygen species. *Biochimica et Biophysica Acta (BBA)-Bioenergetics*, 1797(6-7):929–938, 2010.
- [9] Bernard Fromenty and Dominique Pessayre. Inhibition of mitochondrial beta-oxidation as a mechanism of hepatotoxicity. *Pharmacology & therapeutics*, 67(1):101–154, 1995.
- [10] Johanna M Kilponen and J Kalervo Hiltunen. β -oxidation of unsaturated fatty acids in humans isoforms of $\delta 3$, $\delta 2$ -enoyl-coa isomerase. *FEBS letters*, 322(3):299–303, 1993.
- [11] Simon Eaton. Control of mitochondrial β -oxidation flux. *Progress in lipid research*, 41(3): 197–239, 2002.
- [12] Anne-Claire MF Martines, Karen Van Eunen, Dirk-Jan Reijngoud, and Barbara M Bakker. The promiscuous enzyme medium-chain 3-keto-acyl-coa thiolase triggers a vicious cycle in fatty-acid beta-oxidation. *PLoS computational biology*, 13(4):e1005461, 2017.

- [13] Lutfi Abu-Elheiga, William R Brinkley, Ling Zhong, Subrahmanyam S Chirala, Gebretateos Woldegiorgis, and Salih J Wakil. The subcellular localization of acetyl-coa carboxylase 2. *Proceedings of the National Academy of Sciences*, 97(4):1444–1449, 2000.
- [14] Carlos R Ferreira and Clara DM van Karnebeek. Inborn errors of metabolism. *Handbook of clinical neurology*, 162:449–481, 2019.
- [15] Philippe M Campeau, Charles R Scriver, and John J Mitchell. A 25-year longitudinal analysis of treatment efficacy in inborn errors of metabolism. *Molecular genetics and metabolism*, 95(1-2):11–16, 2008.
- [16] Michelle Kompare and William B Rizzo. Mitochondrial fatty-acid oxidation disorders. In *Seminars in pediatric neurology*, volume 15, pages 140–149. Elsevier, 2008.
- [17] Il J Lawrence Merritt, Marie Norris, and Shibani Kanungo. Fatty acid oxidation disorders. *Annals of translational medicine*, 6(24), 2018.
- [18] Charles A Stanley, Susan DeLeeuw, Paul M Coates, Christine Vianey-Liaud, Priscille Divry, Jean-Paul Bonnefont, Jean-Marie Saudubray, Morey Haymond, Friedrich K Trefz, Galen N Breningstall, et al. Chronic cardiomyopathy and weakness or acute coma in children with a defect in carnitine uptake. *Annals of Neurology: Official Journal of the American Neurological Association and the Child Neurology Society*, 30(5):709–716, 1991.
- [19] Charles A Stanley, Michael J Bennett, and Ertan Mayatepek. Disorders of mitochondrial fatty acid oxidation and related metabolic pathways. In *Inborn metabolic diseases*, pages 175–190. Springer, 2006.
- [20] Nicola Longo, Cristina Amat di San Filippo, and Marzia Pasquali. Disorders of carnitine transport and the carnitine cycle. *American Journal of Medical Genetics Part C: Seminars in Medical Genetics*, 142C(2):77–85, 2006. doi: <https://doi.org/10.1002/ajmg.c.30087>. URL <https://onlinelibrary.wiley.com/doi/abs/10.1002/ajmg.c.30087>.
- [21] Hyekyung P Cho, Manabu Nakamura, and Steven D Clarke. Cloning, expression, and fatty acid regulation of the human δ -5 desaturase. *Journal of Biological Chemistry*, 274(52): 37335–37339, 1999.
- [22] J Lawrence Merritt 2nd and Irene J Chang. Medium-chain acyl-coenzyme a dehydrogenase deficiency. *GeneReviews®[Internet]*, 2019.
- [23] Moseley Waite and Salih J Wakil. Studies on the mechanism of fatty acid synthesis: Xii. acetyl coenzyme a carboxylase. *Journal of Biological Chemistry*, 237(9):2750–2757, 1962.

- [24] Nicol C Voermans, Baziel G van Engelen, Leo A Kluijtmans, Nike M Stikkelbroeck, and Ad R Hermus. Rhabdomyolysis caused by an inherited metabolic disease: very long-chain acyl-coa dehydrogenase deficiency. *The American journal of medicine*, 119(2):176–179, 2006.
- [25] Scott D Grosse, Muin J Khoury, Carol L Greene, Krista S Crider, and Rodney J Pollitt. The epidemiology of medium chain acyl-coa dehydrogenase deficiency: an update. *Genetics in Medicine*, 8(4):205–212, 2006.
- [26] Hans Peter Fischer. Mathematical modeling of complex biological systems: from parts lists to understanding systems behavior. *Alcohol Research & Health*, 31(1):49, 2008.
- [27] EO Voit. A first course in systems biology. new york: Garland science, 2012.
- [28] Santo Motta and Francesco Pappalardo. Mathematical modeling of biological systems. *Briefings in Bioinformatics*, 14(4):411–422, 2013.
- [29] Osvaldo D Kim, Miguel Rocha, and Paulo Maia. A review of dynamic modeling approaches and their application in computational strain optimization for metabolic engineering. *Frontiers in microbiology*, 9:1690, 2018.
- [30] Adam M Feist and Bernhard O Palsson. The biomass objective function. *Current opinion in microbiology*, 13(3):344–349, 2010.
- [31] Pedro A Saa and Lars K Nielsen. Formulation, construction and analysis of kinetic models of metabolism: A review of modelling frameworks. *Biotechnology advances*, 35(8):981–1003, 2017.
- [32] Jon-Marc G Rodriguez, Nicholas P Hux, Sven J Philips, and Marcy H Towns. Michaelis–menten graphs, lineweaver–burk plots, and reaction schemes: investigating introductory biochemistry students' conceptions of representations in enzyme kinetics. *Journal of Chemical Education*, 96(9):1833–1845, 2019.
- [33] AA Saboury. Enzyme inhibition and activation: a general theory. *Journal of the Iranian Chemical Society*, 6(2):219–229, 2009.
- [34] Grover L Waldrop. A qualitative approach to enzyme inhibition. *Biochemistry and Molecular Biology Education*, 37(1):11–15, 2009.
- [35] Alexander Rittner, Karthik S Paithankar, Khanh Vu Huu, and Martin Grninger. Characterization of the polyspecific transferase of murine type i fatty acid synthase (fas) and implications for polyketide synthase (pks) engineering. *ACS chemical biology*, 13(3):723–732, 2018.
- [36] Brian G Cox and Gordon G Hammes. Steady-state kinetic study of fatty acid synthase from chicken liver. *Proceedings of the National Academy of Sciences*, 80(14):4233–4237, 1983.

- [37] Wolfram Liebermeister and Edda Klipp. Bringing metabolic networks to life: convenience rate law and thermodynamic constraints. *Theoretical Biology and Medical Modelling*, 3(1): 1–13, 2006.
- [38] Leonor Michaelis, Maud L Menten, et al. Die kinetik der invertinwirkung. *Biochem. z*, 49 (333-369):352, 1913.
- [39] WW Cleland. the kinetics of enzyme-catalyzed reaction with two or more substrates or products. i. nomenclature and rate equations. *biochem. biophys. acta* 67, 1963.
- [40] Johann M Rohwer, Arno J Hanekom, and Jan-Hendrik S Hofmeyr. A universal rate equation for systems biology. In *Experimental standard conditions of enzyme characterizations. Proceedings of the 2nd International Beilstein Workshop*, pages 175–187. Beilstein-Institut zur Förderung der Chemischen Wissenschaften Frankfurt, 2007.
- [41] Edward L King and Carl Altman. A schematic method of deriving the rate laws for enzyme-catalyzed reactions. *The Journal of physical chemistry*, 60(10):1375–1378, 1956.
- [42] John Happel and Peter H Sellers. New perspective on the kinetics of enzyme catalysis. *The Journal of Physical Chemistry*, 99(17):6595–6600, 1995.
- [43] John Happel and Peter H Sellers. Systemization for the king-altman-hill diagram method in chemical kinetics. *The Journal of Physical Chemistry*, 96(6):2593–2597, 1992.
- [44] Nuriye Nuray Ulusu. Evolution of enzyme kinetic mechanisms. *Journal of molecular evolution*, 80(5):251–257, 2015.
- [45] Oliver Ebenhöh, Marvin van Aalst, Nima P Saadat, Tim Nies, and Anna Matuszyńska. Building mathematical models of biological systems with modelbase. *Journal of Open Research Software*, 6(1), 2018.
- [46] Stefan Hoops, Sven Sahle, Ralph Gauges, Christine Lee, Jürgen Pahle, Natalia Simus, Mudita Singhal, Liang Xu, Pedro Mendes, and Ursula Kummer. Copasi—a complex pathway simulator. *Bioinformatics*, 22(24):3067–3074, 2006.
- [47] Brett G Olivier, Johann M Rohwer, and Jan-Hendrik S Hofmeyr. Modelling cellular systems with pysces. *Bioinformatics*, 21(4):560–561, 2005.
- [48] Frank V Marcoline, John Furth, Smita Nayak, Michael Grabe, and Robert I Macey. Berkeley madonna version 10—a simulation package for solving mathematical models. *CPT: pharmacometrics & systems pharmacology*, 11(3):290–301, 2022.

- [49] Karen van Eunen, Sereh MJ Simons, Albert Gerding, Aycha Bleeker, Gijs den Besten, Catharina ML Touw, Sander M Houten, Bert K Groen, Klaas Krab, Dirk-Jan Reijngoud, et al. Biochemical competition makes fatty-acid β -oxidation vulnerable to substrate overload. *PLoS computational biology*, 9(8):e1003186, 2013.
- [50] Aarash Bordbar, Douglas McCloskey, Daniel C Zielinski, Nikolaus Sonnenschein, Neema Jamshidi, and Bernhard O Palsson. Personalized whole-cell kinetic models of metabolism for discovery in genomics and pharmacodynamics. *Cell systems*, 1(4):283–292, 2015.
- [51] Jurgen R Haanstra, Albert Gerding, Amalia M Dolga, Freek JH Sorgdrager, Manon Buist-Homan, Francois Du Toit, Klaas Nico Faber, Hermann-Georg Holzhütter, Balázs Szöör, Keith R Matthews, et al. Targeting pathogen metabolism without collateral damage to the host. *Scientific reports*, 7(1):1–15, 2017.
- [52] Claudio R Santos and Almut Schulze. Lipid metabolism in cancer. *The FEBS journal*, 279(15):2610–2623, 2012.
- [53] Marta Gómez de Cedrón and Ana Ramírez de Molina. Precision nutrition to target lipid metabolism alterations in cancer. In *Precision medicine for investigators, practitioners and providers*, pages 291–299. Elsevier, 2020.
- [54] C Lelliott and AJ Vidal-Puig. Lipotoxicity, an imbalance between lipogenesis de novo and fatty acid oxidation. *International journal of obesity*, 28(4):S22–S28, 2004.
- [55] Ida Schomburg, Antje Chang, Christian Ebeling, Marion Gremse, Christian Heldt, Gregor Huhn, and Dietmar Schomburg. Brenda, the enzyme database: updates and major new developments. *Nucleic acids research*, 32(suppl_1):D431–D433, 2004.
- [56] Ulrike Wittig, Renate Kania, Martin Golebiewski, Maja Rey, Lei Shi, Lenneke Jong, Enkhjargal Algaa, Andreas Weidemann, Heidrun Sauer-Danzwith, Saqib Mir, et al. Sabio-rk—database for biochemical reaction kinetics. *Nucleic acids research*, 40(D1):D790–D796, 2012.
- [57] Polina Lakrisenko and Daniel Weindl. Dynamic models for metabolomics data integration. *Current Opinion in Systems Biology*, 28:100358, 2021.
- [58] Ilya R Bederman, Takhar Kasumov, Aneta E Reszko, France David, Henri Brunengraber, and Joanne K Kelleher. In vitro modeling of fatty acid synthesis under conditions simulating the zonation of lipogenic [^{13}C] acetyl-coa enrichment in the liver. *Journal of Biological Chemistry*, 279(41):43217–43226, 2004.

- [59] Magdalena Topolska, Fernando Martínez-Montañés, and Christer S Ejsing. A simple and direct assay for monitoring fatty acid synthase activity and product-specificity by high-resolution mass spectrometry. *Biomolecules*, 10(1):118, 2020.
- [60] Hyuntae Yoo, Gregory Stephanopoulos, and Joanne K Kelleher. Quantifying carbon sources for de novo lipogenesis in wild-type and *irs-1* knockout brown adipocytes. *Journal of lipid research*, 45(7):1324–1332, 2004.
- [61] Caroline H Johnson, Julijana Ivanisevic, and Gary Siuzdak. Metabolomics: beyond biomarkers and towards mechanisms. *Nature reviews Molecular cell biology*, 17(7):451–459, 2016.
- [62] Shodhan Rao, Arjan van der Schaft, Karen van Eunen, Barbara M Bakker, and Bayu Jayawardhana. A model reduction method for biochemical reaction networks. *BMC systems biology*, 8(1):1–17, 2014.
- [63] Kristi Bentler, Shaohui Zhai, Sara A. Elsbecker, Georgianne L. Arnold, Barbara K. Burton, Jerry Vockley, Cynthia A. Cameron, Sally J. Hiner, Mathew J. Edick, Susan A. Berry, Janet Thomas, Melinda Dodge, Rani Singh, Sangeetha Lakshman, Katie Coakley, Adrya Stembridge, Alvaro Serrano Russi, Emily Phillips, Barbara Burton, Clare Edano, Sheela Shrestha, George Hoganson, Lauren Dwyer, Bryan Hainline, Susan Romie, Sarah Hainline, Alexander Asamoah, Kara Goodin, Cecilia Rajakaruna, Kelly Jackson, Ada Hamosh, Hilary Vernon, Nancy Smith, Ayesha Ahmad, Sue Lipinski, Gerald Feldman, Susan Berry, Sara Elsbecker, Kristi Bentler, Esperanza Font-Montgomery, Dawn Peck, Loren D.M. Pena, Dwight D. Koeberl, Yong hui Jiang, Priya S. Kishnani, William Rizzo, Mabelle Dawson, Nancy Ambrose, Paul Levy, David Kronn, Chin to Fong, Kristin D’Aco, Theresa Hart, Richard Erbe, Melissa Samons, Nancy Leslie, Racheal Powers, Dennis Bartholomew, Melanie Goff, Sandy vanCalcar, Joyanna Hansen, Georgianne Arnold, Jerry Vockley, Cate Walsh-Vockley, William Rhead, David Dimmock, Paula Engelking, Cassie Bird, Ashley Swan, Jessica Scott Schwoerer, Sonja Henry, TaraChandra Narumanchi, Marybeth Hummel, Jennie Wilkins, Laura Davis-Keppen, Quinn Stein, Rebecca Loman, Cynthia Cameron, Mathew J. Edick, Sally J. Hiner, Kaitlin Justice, and Shaohui Zhai. 221 newborn-screened neonates with medium-chain acyl-coenzyme a dehydrogenase deficiency: Findings from the inborn errors of metabolism collaborative. *Molecular Genetics and Metabolism*, 119(1):75–82, 2016. ISSN 1096-7192. doi: <https://doi.org/10.1016/j.ymgme.2016.07.002>. URL <https://www.sciencedirect.com/science/article/pii/S109671921630124X>.
- [64] Anne Claire M.F. Martines, Albert Gerding, Sarah Stolle, Marcel A. Vieira-Lara, Justina C. Wolters, Angelika Jurdzinski, Laura Bongiovanni, Alain de Bruin, Pieter van der Vlies, Gerben van der Vries, Vincent W. Bloks, Terry G.J. Derks, Dirk Jan Reijngoud, and Barbara M. Bakker. Transcriptome analysis suggests a compensatory role of the cofactors coenzyme

- a and nad⁺ in medium-chain acyl-coa dehydrogenase knockout mice. *Scientific Reports* 2019 9:1, 9:1–11, 10 2019. ISSN 2045-2322. doi: 10.1038/s41598-019-50758-0. URL <https://www.nature.com/articles/s41598-019-50758-0>.
- [65] Sara Tucci, Sidney Behringer, and Ute Spiekerkoetter. De novo fatty acid biosynthesis and elongation in very long-chain acyl-coa dehydrogenase-deficient mice supplemented with odd or even medium-chain fatty acids. *The FEBS journal*, 282(21):4242–4253, 2015.
- [66] Sylvia Stockler-Ipsiroglu, Beth K. Potter, Nataliya Yuskiv, Kylie Tingley, Marc Patterson, and Clara van Karnebeek. Developments in evidence creation for treatments of inborn errors of metabolism. *Journal of Inherited Metabolic Disease*, 44(1):88–98, 2021. doi: <https://doi.org/10.1002/jimd.12315>. URL <https://onlinelibrary.wiley.com/doi/abs/10.1002/jimd.12315>.
- [67] Robert Modre-Osprian, Ingrid Osprian, Bernhard Tilg, Günter Schreier, Klaus M. Weinberger, and Armin Graber. Dynamic simulations on the mitochondrial fatty acid beta-oxidation network. *BMC Systems Biology*, 3:1–15, 2009. ISSN 17520509. doi: 10.1186/1752-0509-3-2.
- [68] Fentaw Abegaz, Anne-Claire MF Martines, Marcel A Vieira-Lara, Melany Rios-Morales, Dirk-Jan Reijngoud, Ernst C Wit, and Barbara M Bakker. Bistability in fatty-acid oxidation resulting from substrate inhibition. *PLoS computational biology*, 17(8):e1009259, 2021.
- [69] Bruce Anderson, Jeffrey Jackson, and Meera Sitharam. Descartes’ rule of signs revisited. *The American Mathematical Monthly*, 105(5):447–451, 1998.
- [70] Aleksandr Mikhailovich Lyapunov. The general problem of the stability of motion. *International journal of control*, 55(3):531–534, 1992.
- [71] George Edward Briggs and John Burdon Sanderson Haldane. A note on the kinetics of enzyme action. *Biochemical journal*, 19(2):338, 1925.
- [72] Jorge Nocedal and Stephen J Wright. *Numerical optimization*. Springer, 1999.
- [73] Stephen Boyd, Stephen P Boyd, and Lieven Vandenberghe. *Convex optimization*. Cambridge university press, 2004.
- [74] Matthew Newville, Till Stensitzki, Daniel B Allen, Michal Rawlik, Antonino Ingargiola, and Andrew Nelson. Lmfit: Non-linear least-square minimization and curve-fitting for python. *Astrophysics Source Code Library*, pages ascl–1606, 2016.
- [75] Max D Morris. Factorial sampling plans for preliminary computational experiments. *Technometrics*, 33(2):161–174, 1991.

- [76] Andrea Saltelli, Stefano Tarantola, and Francesca Campolongo. Sensitivity analysis as an ingredient of modeling. *Statistical Science*, pages 377–395, 2000.
- [77] Reinhart Heinrich and Stefan Schuster. Metabolic control analysis. In *The Regulation of Cellular Systems*, pages 138–291. Springer, 1996.
- [78] Bruno Sudret. Global sensitivity analysis using polynomial chaos expansions. *Reliability engineering & system safety*, 93(7):964–979, 2008.
- [79] Il'ya Meerovich Sobol. On sensitivity estimation for nonlinear mathematical models. *Matematicheskoe modelirovanie*, 2(1):112–118, 1990.
- [80] Sebastian Burhenne, Dirk Jacob, Gregor P Henze, et al. Sampling based on sobol'sequences for monte carlo techniques applied to building simulations. In *Proc. Int. Conf. Build. Simulat*, pages 1816–1823, 2011.
- [81] Marissa Renardy, Louis R Joslyn, Jess A Millar, and Denise E Kirschner. To sobol or not to sobol? the effects of sampling schemes in systems biology applications. *Mathematical biosciences*, 337:108593, 2021.
- [82] Heinz Johs Max Hansen, EM Carey, and R Dils. Fatty acid biosynthesis vii. substrate control of chain-length of products synthesised by rat liver fatty acid synthetase. *Biochimica et Biophysica Acta (BBA)-Lipids and Lipid Metabolism*, 210(3):400–410, 1970.
- [83] EM Carey, R Dils, and Heinz Johs Max Hansen. Chain-length specificity for termination of fatty acid biosynthesis by fatty acid synthetase complexes from lactating rabbit mammary gland and rat liver. *Biochemical Journal*, 117(3):633–635, 1970.
- [84] Morgan D Fullerton, Sandra Galic, Katarina Marcinko, Sarah Sikkema, Thomas Pulinilkunnil, Zhi-Ping Chen, Hayley M O'neill, Rebecca J Ford, Rengasamy Palanivel, Matthew O'brien, et al. Single phosphorylation sites in acc1 and acc2 regulate lipid homeostasis and the insulin-sensitizing effects of metformin. *Nature medicine*, 19(12):1649–1654, 2013.
- [85] Salih J Wakil and Lutfi A Abu-Elheiga. Fatty acid metabolism: target for metabolic syndrome. *Journal of lipid research*, 50:S138–S143, 2009.
- [86] Lutfi Abu-Elheiga, Deysee B Almarza-Ortega, Antonio Baldini, and Salih J Wakil. Human acetyl-coa carboxylase 2: molecular cloning, characterization, chromosomal mapping, and evidence for two isoforms. *Journal of Biological Chemistry*, 272(16):10669–10677, 1997.
- [87] Lutfi Abu-Elheiga, Martin M Matzuk, Khaled AH Abo-Hashema, and Salih J Wakil. Continuous fatty acid oxidation and reduced fat storage in mice lacking acetyl-coa carboxylase 2. *Science*, 291(5513):2613–2616, 2001.

- [88] Lutfi Abu-Elheiga, Wonkeun Oh, Parichher Kordari, and Salih J Wakil. Acetyl-coa carboxylase 2 mutant mice are protected against obesity and diabetes induced by high-fat/high-carbohydrate diets. *Proceedings of the National Academy of Sciences*, 100(18):10207–10212, 2003.
- [89] Michael R Munday and Cheryl J Hemingway. The regulation of acetyl-coa carboxylase—a potential target for the action of hypolipidemic agents. *Advances in enzyme regulation*, 39: 205–234, 1999.
- [90] Daniel W Foster et al. Malonyl-coa: the regulator of fatty acid synthesis and oxidation. *The Journal of clinical investigation*, 122(6):1958–1959, 2012.
- [91] Dong Cheng, Ching-Hsuen Chu, Luping Chen, John N Feder, Gabe A Mintier, Yuli Wu, Joseph W Cook, Mark R Harpel, Gregory A Locke, Yongmi An, et al. Expression, purification, and characterization of human and rat acetyl cenzyme a carboxylase (acc) isozymes. *Protein expression and purification*, 51(1):11–21, 2007.
- [92] Hideo Ogiwara, Tadashi TANABE, Jun-ichi NIKAWA, and Shosaku NUMA. Inhibition of rat-liver acetyl-coenzyme-a carboxylase by palmitoyl-coenzyme a: Formation of equimolar enzyme-inhibitor complex. *European journal of biochemistry*, 89(1):33–41, 1978.
- [93] S Kelly Moule, Nigel J Edgell, Andrew C Borthwick, and Richard M Denton. Coenzyme a is a potent inhibitor of acetyl-coa carboxylase from rat epididymal fat-pads. *Biochemical Journal*, 283(1):35–38, 1992.
- [94] MR Munday. Regulation of mammalian acetyl-coa carboxylase. *Biochemical Society Transactions*, 30(6):1059–1064, 2002.
- [95] Alan G Goodridge. Regulation of the activity of acetyl coenzyme a carboxylase by palmitoyl coenzyme a and citrate. *Journal of Biological Chemistry*, 247(21):6946–6952, 1972.
- [96] Salih J Wakil, EL Pugh, and F Sauer. The mechanism of fatty acid synthesis. *Proceedings of the National Academy of Sciences of the United States of America*, 52(1):106, 1964.
- [97] Philip W Majerus, Alfred W Alberts, and P Roy Vagelos. The acyl carrier protein of fatty acid synthesis: purification, physical properties, and substrate binding site. *Proceedings of the National Academy of Sciences of the United States of America*, 51(6):1231, 1964.
- [98] Pedro Paiva, Fabiola E Medina, Matilde Viegas, Pedro Ferreira, Rui PP Neves, João PM Sousa, Maria J Ramos, and Pedro A Fernandes. Animal fatty acid synthase: A chemical nanofactory. *Chemical Reviews*, 2021.

- [99] Bornali Chakravarty, Ziwei Gu, Subrahmanyam S Chirala, Salih J Wakil, and Florante A Quioco. Human fatty acid synthase: structure and substrate selectivity of the thioesterase domain. *Proceedings of the National Academy of Sciences*, 101(44):15567–15572, 2004.
- [100] William E Connor. Importance of n-3 fatty acids in health and disease. *The American journal of clinical nutrition*, 71(1):171S–175S, 2000.
- [101] Katalin Nagy and Ioana-Daria Tiuca. Importance of fatty acids in physiopathology of human body. In *Fatty acids*. IntechOpen, 2017.
- [102] Yusuke Ohno, Shota Suto, Masao Yamanaka, Yukiko Mizutani, Susumu Mitsutake, Yasuyuki Igarashi, Takayuki Sassa, and Akio Kihara. Elovl1 production of c24 acyl-coas is linked to c24 sphingolipid synthesis. *Proceedings of the National Academy of Sciences*, 107(43):18439–18444, 2010.
- [103] Manabu T Nakamura and Takayuki Y Nara. Structure, function, and dietary regulation of $\delta 6$, $\delta 5$, and $\delta 9$ desaturases. *Annu. Rev. Nutr.*, 24:345–376, 2004.
- [104] Xiaoguang Yang, Wenwen Sheng, Grace Y Sun, and James C-M Lee. Effects of fatty acid unsaturation numbers on membrane fluidity and α -secretase-dependent amyloid precursor protein processing. *Neurochemistry international*, 58(3):321–329, 2011.
- [105] Donald B Jump. Mammalian fatty acid elongases. In *Lipidomics*, pages 375–389. Springer, 2009.
- [106] Akio Kihara. Very long-chain fatty acids: elongation, physiology and related disorders. *The journal of biochemistry*, 152(5):387–395, 2012.
- [107] Andreas Jakobsson, Rolf Westerberg, and Anders Jacobsson. Fatty acid elongases in mammals: their regulation and roles in metabolism. *Progress in lipid research*, 45(3):237–249, 2006.
- [108] Christopher D Green, Cansel G Ozguden-Akkoc, Yun Wang, Donald B Jump, and L Karl Olson. Role of fatty acid elongases in determination of de novo synthesized monounsaturated fatty acid species [s]. *Journal of lipid research*, 51(7):1871–1877, 2010.
- [109] Hervé Guillou, Damir Zdravec, Pascal GP Martin, and Anders Jacobsson. The key roles of elongases and desaturases in mammalian fatty acid metabolism: Insights from transgenic mice. *Progress in lipid research*, 49(2):186–199, 2010.
- [110] Takayuki Sassa, Yusuke Ohno, Shotaro Suzuki, Toshifumi Nomura, Chieko Nishioka, Toshiki Kashiwagi, Taisuke Hirayama, Masashi Akiyama, Ryo Taguchi, Hiroshi Shimizu, et al. Impaired epidermal permeability barrier in mice lacking elovl1, the gene responsible for very-long-chain fatty acid production. *Molecular and cellular biology*, 33(14):2787–2796, 2013.

- [111] Petr Tvrdik, Rolf Westerberg, Sandra Silve, Abolfazl Asadi, Andreas Jakobsson, Barbara Cannon, Gerard Loison, and Anders Jacobsson. Role of a new mammalian gene family in the biosynthesis of very long chain fatty acids and sphingolipids. *The Journal of cell biology*, 149(3):707–718, 2000.
- [112] Damir Zadavec, Petr Tvrdik, Hervé Guillou, Richard Haslam, Tsutomu Kobayashi, Johnathan A Napier, Mario R Capecchi, and Anders Jacobsson. Elovl2 controls the level of n-6 28: 5 and 30: 5 fatty acids in testis, a prerequisite for male fertility and sperm maturation in mice. *Journal of lipid research*, 52(2):245–255, 2011.
- [113] Petr Tvrdik, Abolfazl Asadi, Leslie P Kozak, Jan Nedergaard, Barbara Cannon, and Anders Jacobsson. Cig30, a mouse member of a novel membrane protein gene family, is involved in the recruitment of brown adipose tissue. *Journal of Biological Chemistry*, 272(50):31738–31746, 1997.
- [114] Amanda E LEONARD, Emil G BOBIK, Joseph DORADO, Paul E KROEGER, Lu-Te CHUANG, Jennifer M THURMOND, Jennifer M PARKER-BARNES, Tapas DAS, Yung-Sheng HUANG, and Pradip MUKERJI. Cloning of a human cDNA encoding a novel enzyme involved in the elongation of long-chain polyunsaturated fatty acids. *Biochemical Journal*, 350(3):765–770, 2000.
- [115] Young-Ah Moon, Nila A Shah, Suchismita Mohapatra, Janet A Warrington, and Jay D Horton. Identification of a mammalian long chain fatty acyl elongase regulated by sterol regulatory element-binding proteins. *Journal of Biological Chemistry*, 276(48):45358–45366, 2001.
- [116] Takashi Matsuzaka, Hitoshi Shimano, Naoya Yahagi, Tomohiro Yoshikawa, Michiyo Amemiya-Kudo, Alyssa H Hasty, Hiroaki Okazaki, Yoshiaki Tamura, Yoko Iizuka, Ken Ohashi, et al. Cloning and characterization of a mammalian fatty acyl-coa elongase as a lipogenic enzyme regulated by srebps. *Journal of lipid research*, 43(6):911–920, 2002.
- [117] Takashi Matsuzaka, Hitoshi Shimano, Naoya Yahagi, Toyonori Kato, Ayaka Atsumi, Takashi Yamamoto, Noriyuki Inoue, Mayumi Ishikawa, Sumiyo Okada, Naomi Ishigaki, et al. Crucial role of a long-chain fatty acid elongase, elovl6, in obesity-induced insulin resistance. *Nature medicine*, 13(10):1193–1202, 2007.
- [118] Tatsuro Naganuma, Yuichiro Sato, Takayuki Sassa, Yusuke Ohno, and Akio Kihara. Biochemical characterization of the very long-chain fatty acid elongase elovl7. *FEBS letters*, 585(20):3337–3341, 2011.

- [119] Harold W Cook and Christopher R McMaster. Fatty acid desaturation and chain elongation in eukaryotes. In *New comprehensive biochemistry*, volume 36, pages 181–204. Elsevier, 2002.
- [120] James M Ntambi. Regulation of stearoyl-coa desaturase by polyunsaturated fatty acids and cholesterol. *Journal of lipid research*, 40(9):1549–1558, 1999.
- [121] Hyekyung P Cho, Manabu T Nakamura, and Steven D Clarke. Cloning, expression, and nutritional regulation of the mammalian δ -6 desaturase. *Journal of Biological Chemistry*, 274(1):471–477, 1999.
- [122] James M Ntambi and Makoto Miyazaki. Regulation of stearoyl-coa desaturases and role in metabolism. *Progress in lipid research*, 43(2):91–104, 2004.
- [123] James M Ntambi and Makoto Miyazaki. Recent insights into stearoyl-coa desaturase-1. *Current opinion in lipidology*, 14(3):255–261, 2003.
- [124] Matthew T Flowers and James M Ntambi. Role of stearoyl-coenzyme a desaturase in regulating lipid metabolism. *Current opinion in lipidology*, 19(3):248, 2008.
- [125] HARRY G Enoch, A Catala, and P Strittmatter. Mechanism of rat liver microsomal stearyl-coa desaturase. studies of the substrate specificity, enzyme-substrate interactions, and the function of lipid. *Journal of Biological Chemistry*, 251(16):5095–5103, 1976.
- [126] James M Ntambi, Makoto Miyazaki, Jonathan P Stoehr, Hong Lan, Christina M Kendziorski, Brian S Yandell, Yang Song, Paul Cohen, Jeffrey M Friedman, and Alan D Attie. Loss of stearoyl-coa desaturase-1 function protects mice against adiposity. *Proceedings of the National Academy of Sciences*, 99(17):11482–11486, 2002.
- [127] Makoto Miyazaki, Harini Sampath, Xueqing Liu, Matthew T Flowers, Kiki Chu, Agnieszka Dobrzyn, and James M Ntambi. Stearoyl-coa desaturase-1 deficiency attenuates obesity and insulin resistance in leptin-resistant obese mice. *Biochemical and biophysical research communications*, 380(4):818–822, 2009.
- [128] Klaus H Kaestner, JM Ntambi, TJ Kelly Jr, and MD Lane. Differentiation-induced gene expression in 3t3-l1 preadipocytes: a second differentially expressed gene encoding stearoyl-coa desaturase. *Journal of Biological Chemistry*, 264(25):14755–14761, 1989.
- [129] Ying Zheng, Stephen M Prouty, Alex Harmon, John P Sundberg, Kurt S Stenn, and Satish Parimoo. Scd3—a novel gene of the stearoyl-coa desaturase family with restricted expression in skin. *Genomics*, 71(2):182–191, 2001.

- [130] Lin ZHANG, Lan GE, Satish PARIMOO, Kurt STENN, and Stephen M PROUTY. Human stearoyl-coa desaturase: alternative transcripts generated from a single gene by usage of tandem polyadenylation sites. *Biochemical Journal*, 340(1):255–264, 1999.
- [131] Jian Wang, Lan Yu, Robert E Schmidt, Chen Su, Xiaodi Huang, Kenneth Gould, and Guoqing Cao. Characterization of hscd5, a novel human stearoyl-coa desaturase unique to primates. *Biochemical and biophysical research communications*, 332(3):735–742, 2005.
- [132] Makoto Miyazaki, Mark J Jacobson, Weng Chi Man, Paul Cohen, Esra Asilmaz, Jeffrey M Friedman, and James M Ntambi. Identification and characterization of murine scd4, a novel heart-specific stearoyl-coa desaturase isoform regulated by leptin and dietary factors. *Journal of Biological Chemistry*, 278(36):33904–33911, 2003.
- [133] Makoto Miyazaki, Sean M Bruggink, and James M Ntambi. Identification of mouse palmitoyl-coenzyme a $\delta 9$ -desaturase. *Journal of lipid research*, 47(4):700–704, 2006.
- [134] Seong-Ho Lee, Agnieszka Dobrzyn, Pawel Dobrzyn, Shaikh Mizanoor Rahman, Makoto Miyazaki, and James M Ntambi. Lack of stearoyl-coa desaturase 1 upregulates basal thermogenesis but causes hypothermia in a cold environment. *Journal of lipid research*, 45(9):1674–1682, 2004.
- [135] Shaobo Zhang, Yanzhu Yang, and Yuguang Shi. Characterization of human scd2, an oligomeric desaturase with improved stability and enzyme activity by cross-linking in intact cells. *Biochemical Journal*, 388(1):135–142, 2005.
- [136] Lan Ge, Joel S Gordon, Charleen Hsuan, Kurt Stenn, and Stephen M Prouty. Identification of the δ -6 desaturase of human sebaceous glands: expression and enzyme activity. *Journal of Investigative Dermatology*, 120(5):707–714, 2003.
- [137] Nestor V Torres and Guido Santos. The (mathematical) modeling process in biosciences. *Frontiers in Genetics*, 6:354, 2015.
- [138] Abdelghani Bellouquid and Marcello Delitala. *Mathematical modeling of complex biological systems*. Springer, 2006.
- [139] Juan Zhang, Defeng Li, Xiquan Yue, Meiling Zhang, Ping Liu, and Genxi Li. Colorimetric in situ assay of membrane-bound enzyme based on lipid bilayer inhibition of ion transport. *Theranostics*, 8(12):3275, 2018.
- [140] Arumugam Jayakumar, Ming-Hong Tai, Wei-Yong Huang, Walid Al-Feel, Matthew Hsu, Lutfi Abu-Elheiga, Subrahmanyam S Chirala, and Salih J Wakil. Human fatty acid synthase: properties and molecular cloning. *Proceedings of the National Academy of Sciences*, 92(19):8695–8699, 1995.

- [141] TC Wright, JP Cant, JT Brenna, and BW McBride. Acetyl coa carboxylase shares control of fatty acid synthesis with fatty acid synthase in bovine mammary homogenate. *Journal of dairy science*, 89(7):2552–2558, 2006.
- [142] Shosaku Numa, Wlater M Bortz, and Feodor Lynen. Regulation of fatty acid synthesis at the acetyl-coa carboxylation step. *Advances in enzyme regulation*, 3:407–423, 1965.
- [143] Ki Won Kim, Harvey Yamane, James Zondlo, James Busby, and Minghan Wang. Expression, purification, and characterization of human acetyl-coa carboxylase 2. *Protein expression and purification*, 53(1):16–23, 2007.
- [144] Shosaku Numa and Tadashi Tanabe. Acetyl-coenzyme a carboxylase and its regulation. In *New comprehensive biochemistry*, volume 7, pages 1–27. Elsevier, 1984.
- [145] Takashi Hashimoto, Hiroshi Isano, Nobuko Iritani, and Shosaku Numa. Liver acetyl-coenzyme-a carboxylase: Studies on kynurenate inhibition, isotope exchange and interaction of the uncarboxylated enzyme with citrate. *European journal of biochemistry*, 24(1):128–139, 1971.
- [146] Tkashi Hashimoto and Shosaku Numa. kinetic studies on the reaction mechanism and the citrate activation or liver acetyl coenzyme a carboxylase. *European journal of biochemistry*, 18(3):319–331, 1971.
- [147] NB Beaty and M Daniel Lane. Acetyl coenzyme a carboxylase. rapid purification of the chick liver enzyme and steady state kinetic analysis of the carboxylase-catalyzed reaction. *Journal of Biological Chemistry*, 257(2):924–929, 1982.
- [148] Virendar K Kaushik, Michael Kavana, Jessica M Volz, Stephen C Weldon, Susan Hanrahan, Jian Xu, Shari L Caplan, and Brian K Hubbard. Characterization of recombinant human acetyl-coa carboxylase-2 steady-state kinetics. *Biochimica et Biophysica Acta (BBA)-Proteins and Proteomics*, 1794(6):961–967, 2009.
- [149] Garrett E Trumble, Marvin A Smith, and William W Winder. Purification and characterization of rat skeletal muscle acetyl-coa carboxylase. *European journal of biochemistry*, 231(1):192–198, 1995.
- [150] Tadashi Tanabe, Shigetada Nakanishi, Takashi Hashimoto, Hideo Ogiwara, Jun-ichi Nikawa, and Shosaku Numa. [1] acetyl-coa carboxylase from rat liver: Ec 6.4. 1.2 acetyl-coa: Carbon-dioxide ligase (adp-forming). In *Methods in enzymology*, volume 71, pages 5–16. Elsevier, 1981.
- [151] Salih J Wakil. Fatty acid synthase, a proficient multifunctional enzyme. *Biochemistry*, 28(11):4523–4530, 1989.

- [152] SS Katiyar, WW Cleland, and JOHN W Porter. Fatty acid synthetase. a steady state kinetic analysis of the reaction catalyzed by the enzyme from pigeon liver. *Journal of Biological Chemistry*, 250(7):2709–2717, 1975.
- [153] Simon A Aprahamian, Michael J Arslanian, and Salih J Wakil. Comparative studies on the kinetic parameters and product analyses of chicken and rat liver and yeast fatty acid synthetase. *Comparative biochemistry and physiology. B, Comparative biochemistry*, 71(4): 577–582, 1982.
- [154] Loretha Carlisle-Moore, Chris R Gordon, Carl A Machutta, W Todd Miller, and Peter J Tonge. Substrate recognition by the human fatty-acid synthase. *Journal of Biological Chemistry*, 280(52):42612–42618, 2005.
- [155] Kazumasa OHASHI, Hideaki OTSUKA, and Yousuke SEYAMA. Assay of fatty acid synthetase by mass fragmentography using [13c] malonyl-coa. *The Journal of Biochemistry*, 97 (3):867–875, 1985.
- [156] DH Nugteren. The enzymic chain elongation of fatty acids by rat-liver microsomes. *Biochimica et Biophysica Acta (BBA)-Lipids and Lipid Metabolism*, 106(2):280–290, 1965.
- [157] Mari Kugi, Satoshi Yoshida, and Masazumi Takeshita. Characterization of fatty acid elongation system in porcine neutrophil microsomes. *Biochimica et Biophysica Acta (BBA)-Lipids and Lipid Metabolism*, 1043(1):83–90, 1990.
- [158] Tatsuro Naganuma and Akio Kihara. Two modes of regulation of the fatty acid elongase elovl6 by the 3-ketoacyl-coa reductase kar in the fatty acid elongation cycle. *PLoS One*, 9 (7):e101823, 2014.
- [159] Scott G Harroun, Dominic Lauzon, Maximilian CCJC Ebert, Arnaud Desrosiers, Xiaomeng Wang, and Alexis Vallée-Bélisle. Monitoring protein conformational changes using fluorescent nanoantennas. *Nature Methods*, 19(1):71–80, 2022.
- [160] TM McDonald and JE Kinsella. Stearyl-coa desaturase of bovine mammary microsomes. *Archives of biochemistry and biophysics*, 156(1):223–231, 1973.
- [161] Philipp Strittmatter and Harry G Enoch. [18] purification of stearyl-coa desaturase from liver. In *Methods in enzymology*, volume 52, pages 188–193. Elsevier, 1978.
- [162] Denis Ravel, Jean Chambaz, Dominique Pepin, Marie-Christine Manier, and Gilbert Bereziat. Essential fatty acid interconversion during gestation in the rat. *Biochimica et Biophysica Acta (BBA)-Lipids and Lipid Metabolism*, 833(1):161–164, 1985.

- [163] Takako Okayasu, Masaki Nagao, Teruo Ishibashi, and Yoh Imai. Purification and partial characterization of linoleoyl-coa desaturase from rat liver microsomes. *Archives of biochemistry and biophysics*, 206(1):21–28, 1981.
- [164] Jean-Pierre Poisson, Renée-Pierre Dupuy, Pierre Sarda, Bernard Descomps, Michel Narce, Daniel Rieu, and A Crastes de Paulet. Evidence that liver microsomes of human neonates desaturate essential fatty acids. *Biochimica et Biophysica Acta (BBA)-Lipids and Lipid Metabolism*, 1167(2):109–113, 1993.
- [165] Carlos E Irazú, Susana González-Rodríguez, and Rodolfo R Brenner. $\delta 5$ desaturase activity in rat kidney microsomes. *Molecular and cellular biochemistry*, 129(1):31–37, 1993.
- [166] Annie Rodriguez, Pierre Sarda, Catherine Nessmann, Pierre Boulot, Claude Louis Leger, and Bernard Descomps. $\delta 6$ -and $\delta 5$ -desaturase activities in the human fetal liver: kinetic aspects. *Journal of lipid research*, 39(9):1825–1832, 1998.
- [167] Patricia Soulard, Meg McLaughlin, Jessica Stevens, Brendan Connolly, Rocco Coli, Leyu Wang, Jennifer Moore, Ming-Shang T Kuo, William A LaMarr, Can C Ozbal, et al. Development of a high-throughput screening assay for stearoyl-coa desaturase using rat liver microsomes, deuterium labeled stearoyl-coa and mass spectrometry. *Analytica chimica acta*, 627(1):105–111, 2008.
- [168] Vijayakumar Natesan and Sung-Jin Kim. Lipid metabolism, disorders and therapeutic drugs—review. *Biomolecules & therapeutics*, 29(6):596, 2021.
- [169] Kalpana Shanmugarajah, Nicole Linka, Katharina Gräfe, Sander HJ Smits, Andreas PM Weber, Jürgen Zeier, and Lutz Schmitt. Abcg1 contributes to suberin formation in arabidopsis thaliana roots. *Scientific reports*, 9(1):1–12, 2019.
- [170] Mi Jang, Pavel Neuzil, Thomas Volk, Andreas Manz, and Astrid Kleber. On-chip three-dimensional cell culture in phaseguides improves hepatocyte functions in vitro. *Biomicrofluidics*, 9(3):034113, 2015.
- [171] Boyang Zhang, Anastasia Korolj, Benjamin Fook Lun Lai, and Milica Radisic. Advances in organ-on-a-chip engineering. *Nature Reviews Materials*, 3(8):257–278, 2018.
- [172] Lei Shi and Benjamin P Tu. Acetyl-coa and the regulation of metabolism: mechanisms and consequences. *Current opinion in cell biology*, 33:125–131, 2015.
- [173] Michele Alves-Bezerra and David E Cohen. Triglyceride metabolism in the liver. *Comprehensive Physiology*, 8(1):1, 2017.

- [174] Thierry Brun, Franhise Assimacopoulos-Jeannet, Barbara E Corkey, and Marc Prentki. Long-chain fatty acids inhibit acetyl-coa carboxylase gene expression in the pancreatic β -cell line ins-1. *Diabetes*, 46(3):393–400, 1997.
- [175] Manfred Sumper. Control of fatty-acid biosynthesis by long-chain acyl coas and by lipid membranes. *European Journal of Biochemistry*, 49(2):469–475, 1974.
- [176] Joris Beld, D John Lee, and Michael D Burkart. Fatty acid biosynthesis revisited: structure elucidation and metabolic engineering. *Molecular BioSystems*, 11(1):38–59, 2015.
- [177] Fiona Fraser, Renato Padovese, and Victor A Zammit. Distinct kinetics of carnitine palmitoyltransferase i in contact sites and outer membranes of rat liver mitochondria. *Journal of Biological Chemistry*, 276(23):20182–20185, 2001.
- [178] Angela A Wendel, Tal M Lewin, and Rosalind A Coleman. Glycerol-3-phosphate acyltransferases: rate limiting enzymes of triacylglycerol biosynthesis. *Biochimica et Biophysica Acta (BBA)-Molecular and Cell Biology of Lipids*, 1791(6):501–506, 2009.
- [179] Judit Ovadi. Physiological significance of metabolic channelling. *Journal of theoretical biology*, 152(1):1–22, 1991.
- [180] H Olin Spivey and Judit Ovadi. Substrate channeling. *Methods*, 19(2):306–321, 1999.
- [181] J Ovadi, P Tompa, B Vertessy, F Orosz, T Keleti, and GR Welch. Transient-time analysis of substrate-channelling in interacting enzyme systems. *Biochemical Journal*, 257(1):187–190, 1989.
- [182] Zhen Chen and Dehua Liu. Toward glycerol biorefinery: metabolic engineering for the production of biofuels and chemicals from glycerol. *Biotechnology for biofuels*, 9(1):1–15, 2016.
- [183] Edith Wilson Miles. Tryptophan synthase: a multienzyme complex with an intramolecular tunnel. *The Chemical Record*, 1(2):140–151, 2001.
- [184] Stanislav Tsitkov, Theo Pesenti, Henri Palacci, Jose Blanchet, and Henry Hess. Queueing theory-based perspective of the kinetics of “channeled” enzyme cascade reactions. *ACS Catalysis*, 8(11):10721–10731, 2018.
- [185] Sarvagya S Katiyar and John W Porter. Substrate inhibition of pigeon liver fatty acid synthetase and optimum assay conditions for over-all synthetase activity. *Archives of biochemistry and biophysics*, 163(1):324–331, 1974.
- [186] Christina S. Heil, S. Sophia Wehrheim, Karthik S. Paithankar, and Martin Grininger. Fatty acid biosynthesis: Chain-length regulation and control. *ChemBioChem*, 20(18):2298–2321,

2019. doi: <https://doi.org/10.1002/cbic.201800809>. URL <https://chemistry-europe.onlinelibrary.wiley.com/doi/abs/10.1002/cbic.201800809>.

- [187] Sara Tucci, Sonja Primassin, Frank Ter Veld, and Ute Spiekerkoetter. Medium-chain triglycerides impair lipid metabolism and induce hepatic steatosis in very long-chain acyl-coa dehydrogenase (vlcad)-deficient mice. *Molecular genetics and metabolism*, 101(1):40–47, 2010.
- [188] Zeinab Wehbe, Khaled Alatibi, Julia Jellusova, Ute Spiekerkoetter, and Sara Tucci. The fate of medium-chain fatty acids in very long-chain acyl-coa dehydrogenase deficiency (vlcadd): A matter of sex? *Biochimica et Biophysica Acta (BBA)-Molecular and Cell Biology of Lipids*, 1864(11):1591–1605, 2019.
- [189] Grant A Mitchell, Nicolas Gauthier, Alain Lesimple, Shu Pei Wang, Orval Mamer, and Ijaz Qureshi. Hereditary and acquired diseases of acyl-coenzyme a metabolism. *Molecular genetics and metabolism*, 94(1):4–15, 2008.
- [190] Karen van Eunen, Catharina ML Volker-Touw, Albert Gerding, Aycha Bleeker, Justina C Wolters, Willemijn J van Rijt, Anne-Claire MF Martines, Klary E Niezen-Koning, Rebecca M Heiner, Hjalmar Permentier, et al. Living on the edge: substrate competition explains loss of robustness in mitochondrial fatty-acid oxidation disorders. *BMC biology*, 14(1):1–15, 2016.
- [191] Stuart Smith, Andrzej Witkowski, and Anil K Joshi. Structural and functional organization of the animal fatty acid synthase. *Progress in lipid research*, 42(4):289–317, 2003.
- [192] Jon Herman and Will Usher. Salib: An open-source python library for sensitivity analysis. *The Journal of Open Source Software*, 2, 01 2017. doi: 10.21105/joss.00097.
- [193] Vangipuram S Rangan and Stuart Smith. Alteration of the substrate specificity of the malonyl-coa/acetyl-coa: Acyl carrier proteins-acyltransferase domain of the multifunctional fatty acid synthase by mutation of a single arginine residue. *Journal of Biological Chemistry*, 272(18):11975–11978, 1997.
- [194] Philippe Naquet, Evan W Kerr, Schuyler D Vickers, and Roberta Leonardi. Regulation of coenzyme a levels by degradation: the ‘ins and outs’. *Progress in lipid research*, 78:101028, 2020.
- [195] Jiangjiang Zhu and Jun Luo. The synthesis of milk medium-chain fatty acids in mammary gland. In *Fatty Acids*, pages 200–207. IntechOpen, 2017.
- [196] Nikos Koundouros and George Poulogiannis. Reprogramming of fatty acid metabolism in cancer. *British journal of cancer*, 122(1):4–22, 2020.

- [197] Terry G J Derks, Marinus Duran, Hans R Waterham, Dirk-Jan Reijngoud, Leo P ten Kate, and G Peter A Smit. The difference between observed and expected prevalence of mcad deficiency in the netherlands: a genetic epidemiological study. *European Journal of Human Genetics*, 13(8):947–952, May 2005. ISSN 1476-5438. doi: 10.1038/sj.ejhg.5201428. URL <http://dx.doi.org/10.1038/sj.ejhg.5201428>.
- [198] Francis WB Sanders and Julian L Griffin. De novo lipogenesis in the liver in health and disease: more than just a shunting yard for glucose. *Biological Reviews*, 91(2):452–468, 2016.
- [199] Takayuki Sassa and Akio Kihara. Metabolism of very long-chain fatty acids: genes and pathophysiology. *Biomolecules & therapeutics*, 22(2):83, 2014.
- [200] Hidefumi Kitazawa, Yasuhisa Miyamoto, Ken Shimamura, Akira Nagumo, and Shigeru Tokita. Development of a high-density assay for long-chain fatty acyl-coa elongases. *Lipids*, 44(8):765–773, 2009.
- [201] Takashi Matsuzaka and Hitoshi Shimano. Elovl6: a new player in fatty acid metabolism and insulin sensitivity. *Journal of molecular medicine*, 87(4):379–384, 2009.
- [202] Kenji Tamura, Asami Makino, Françoise Hullin-Matsuda, Toshihide Kobayashi, Mutsuo Furihata, Suyoun Chung, Shingo Ashida, Tsuneharu Miki, Tomoaki Fujioka, Taro Shuin, et al. Novel lipogenic enzyme elovl7 is involved in prostate cancer growth through saturated long-chain fatty acid metabolism. *Cancer research*, 69(20):8133–8140, 2009.

Acknowledgements

This project is supported by European Union's Horizon 2020 research and innovation program under the Marie Skłodowska-Curie Actions Grant Agreement PoLiMeR, No 812616.

I am highly thankful to my supervisor Prof. Dr. Oliver Ebenhöf, head of the Institute for Quantitative and Theoretical Biology (QTB), for giving me the opportunity to embark on this incredible research adventure. I would also like to thank him for his noble guidance and support with full encouragement and enthusiasm. I am grateful to Prof. Dr. Barbara Bakker, professor of medical systems biology at the University Medical Centre Groningen (UMCG) and coordinator of the PoLiMeR project, for her valuable suggestions and motivating guidance. I express my full gratitude to Dr. Adélaïde Raguin for her daily co-supervision, scientific guidance, remarkable commitment, and mentoring on career development.

Very special thanks to the QTB team, notably Dr. Janina Maß and Mrs. Mara Schuff, for their guidance on administrative and logistic issues and for ensuring that I work in a comfortable environment. Marvin van Aalst, a big thanks for your support, sharing thoughts, help with coding, and being a wonderful friend. Thanks to Dr. St. Elmo Wilken for the discussions and collaboration for side projects. Thanks to Yvan Rousset, Hettie Chapman Nima Saadat, Dr. Ovidiu Popa, Tim Nies, Ellen Oldenburg, Thomas Wenske, and Davis Mathieu for being wonderful colleagues and for their support throughout this adventure.

Thank you to the PoLiMeR consortium for making this Ph.D. possible. In particular, I am thankful for all the training, networking, extracurricular activities and the exceptional research environment with wonderful people. Special thanks to all PoLiMeR students for our enjoyable discussions, meetings, and events.

I would also like to thank Prof. Dirk-Jan Reijngoud from UMCG for his enriching contributions to my work.

Thank you to Robin Denley Bowers, Katharine Hildago, Helena Hildago, and Juan Hildago for editing my work and for your emotional support.

Thanks to my dear and lovely Laura Lehoczky for the emotional support, advice, and help with editing.

A special thank you to you, Frances Pairaudeau, for your encouragement, support, and advice. Without you, none of this would have been possible.

Thank you to all my friends, notably Boris Njike, William Sangang, Eitel Kamgaing, Laura Randarevitch, Jasmin Theilmann, Diane Betoune-Moto, Hadrien Fogue, Swastik Mishra and all those not mentioned here.

Last but not least, I would also like to thank all of my family for encouraging and supporting me whenever I needed them.

Dedication

I dedicate this piece of work to Frances Pairaudeau

Portfolio

iGRAD Training

Description	Date	Loads
Good Scientific Practice for Doctoral Researchers	Feb 2020	5.25 hours
Advanced Workshop on AI and Data Science for Doctoral Researchers in Medicine and Biology	Dec 2021	8 hours
Optimizing Writing Strategies and Publishing Research in English	Dec 2021	12 hours

PoLiMeR Training

Description	Date	ECTS
Introduction to System Medicine and FAIR data management	November 2019	3
Pathway dynamics and Scientific Integrity and Ethics	November 2019	3
Course on Metabolism	Jun 2020	5
Combinatorial Explosion of Molecular Species and Enzyme Catalysis at the Polymer Surface IPR and Entrepreneurship	Nov 2020	3
Spatial and Hierarchical Regulation and Cognitive Flexibility	Jun 2021	3
	Dec 2021	3

Optimizing Writing Strategies and Publishing Research in English	Dec 2021	3
--	----------	---

Conferences and Symposia

Description	Role	Location	Date
International Study Group for Systems Biology (ISGSB)	Poster presentation	Innsbruck	Sept. 2020
Metabolic Pathway Analysis (MPA)	Participant	knoxville	Aug. 2021
PoLiMeR Final Symposium	Talk	Düsseldorf	Mar. 2022
8th Conference on Systems Biology of Mammalian Cells(SBMC)	Poster presentation	Heidelberg	Sept. 2022

List of publications

Wilken SE, Besançon M, Kratochvíl M, **Foko Kuate CA**, Trefois C, Gu W, Ebenhöf O. Interrogating the effect of enzyme kinetics on metabolism using differentiable constraint-based models. *Metab Eng.* 2022 Nov;74:72-82. doi: [10.1016/j.ymben.2022.09.002](https://doi.org/10.1016/j.ymben.2022.09.002). Epub 2022 Sep 21.

Foko Kuate CA, Ebenhöf O, Bakker BM, Raguin A. Kinetic data for modeling the dynamics of the enzymes involved in animal fatty acid synthesis. *Biosci Rep.* 2023 Jul 26;43(7):BSR20222496. DOI: [10.1042/BSR20222496](https://doi.org/10.1042/BSR20222496)